

Predictive health monitoring of wind turbine blades



Preface

This is a final report to EUDP project “Predictive health monitoring of wind turbine blade”. The project was conducted in cooperation between Vattenfall, Technical University of Denmark, Bladena and Total Wind and lead by Brüel & Kjær SVM.

Table of Contents

PREFACE	2
TABLE OF CONTENTS	4
PROJECT DETAILS	6
SHORT DESCRIPTION OF PROJECT OBJECTIVE AND RESULTS	7
EXECUTIVE SUMMARY	8
POTENTIAL CUSTOMER BENEFITS AND PROJECT UTILIZATION.....	8
SUMMARY OF THE PROJECT RESULTS	9
IP SITUATION	9
PROJECT DEVELOPMENT	10
PROJECT OBJECTIVES.....	10
PROJECT CONSORTIUM EVOLVEMENT	10
PROJECT EVOLVEMENT	10
POTENTIAL RISK	11
UNEXPECTED PROBLEM	11
DELAYS	11
RESULTS.....	11
PROJECT RESULTS AND DISSEMINATION OF RESULTS	12
MAIN ACTIVITIES DURING THE PROJECT RUN	12
<i>Work Package 1 (B&K)</i>	12
<i>Work Package 2A (Bladena)</i>	13
<i>Work Package 2B (DTU Wind)</i>	14
<i>Work Package 2C (DTU Wind)</i>	14
<i>Work Package 3 (DTU Wind)</i>	15
<i>Work Package 4 (DTU Compute)</i>	16
<i>Work Package 5 (B&K)</i>	16
<i>Work Package 6 (Bladena)</i>	17
SUMMARY OF THE PROJECT RESULTS	18
SHM SYSTEM PROTOTYPE: TECHNICAL INSIGHT	18
<i>Rationale for the method</i>	18
<i>Damage detection algorithm</i>	19
<i>Technical implementation of the system</i>	20
EVIDENCE OF EFFICIENCY	21
<i>34 m long SSP blade mounted on a test rig</i>	21
<i>Experiment on a small blade</i>	22
<i>Experiment on Vestas V27 operating wind turbine</i>	22
TYPES OF DAMAGE	23
DAMAGE / DEFECT MANAGEMENT	23
<i>Concept and proposed framework</i>	24
IP PROTECTION.....	25
STATEMENT FROM VATTENFALL	25
COMMERCIAL RESULTS	26
DISSEMINATION.....	26
UTILIZATION OF PROJECT RESULTS	28
RESULTS OF DISSEMINATION.....	28

PROJECT RESULT UTILIZATION	28
PATENT.....	28
USE FOR EDUCATION	28
COMMERCIAL PLAN	29
PROJECT CONCLUSION AND PERSPECTIVE.....	30
COMMERCIALIZATION OF THE DEVELOPED SOLUTION.....	30
PERSPECTIVES FROM MODELLING VIEWPOINT (WP2).....	30
PERSPECTIVES FROM MATERIAL DEVELOPMENT VIEWPOINT (WP3).....	31
PERSPECTIVES FROM DECISION-MAKING ALGORITHMS DEVELOPMENT (WP4).....	31
PUBLISHED PAPERS	32
ANNEX.....	34

Project details

Table 1. Project details

Project title	Predictive Health Monitoring of Wind Turbines based on Dynamic Characterization
Project identification (program abbrev. and file)	64011-0084
Name of the programme which has funded the project	EUDP
Project managing company/institution (name and address)	Brüel & Kjær Sound and Vibration Measurement A/S, Skodsborgvej 307, 2850 Nærum
Project partners	DTU: DTU Wind Energy, DTU Compute; Vattenfall; Bladena; Total Wind Blades
CVR (central business register)	DK23958414
Date for submission	03-Mar-2011

Short description of project objective and results

The main objective of the project was to develop a smart predictive health monitoring (PHM) solution, which will complete the detection of structural failures with effective follow up procedure thus helping wind turbine owner/operator making cost-effective decisions on wind turbine maintenance. The focus of the project is the predictive monitoring of blades, as they are the most expensive structural parts of a WT.

During the project, we developed such a system and demonstrated its efficiency on a prototype installed on an operating wind turbine. The developed system proved detecting structural damages like cracks, delamination, delamination due to wrinkles and blade edge openings without a need to stop the turbine. The system provides information about the damage area location and damage progression. The predictive capabilities of the system, however, were not possible to fulfil.

In the further development and commercialization of the system, we will focus on its detection and localization capabilities. We will temporarily leave the prognostic capabilities out of our scope until the research in this field reaches the adequate level.

Projektets formål var at udvikle en smart løsning til at forudsige sundhedstilstanden af vindmøllevinger. Løsningen skulle både detektere strukturfejl og hjælpe til at beslutte modforanstaltninger, og herved hjælpe vindmølleejere / -operatører til at træffe optimale beslutninger angående vindmøllevedligehold. Projektets fokus har været selve vingerne, da de er den dyreste del af vindmøllen.

I projektet blev sådan et system udviklet, installeret og testet på en kørende mølle. Det udviklede system viste sig i stand til at detektere strukturskader såsom: revner, delaminering forårsaget af slag, delaminering forårsaget af produktionsfejl (rynker) samt vingekantåbninger, uden det var nødvendigt at stoppe vindmøllen. Systemet giver viden om, hvor på vingen skaden er opstået, og hvordan den udvikler sig. Men det har ikke været muligt at opfylde målet om at kunne forudsige, hvordan en skade vil udvikle sig.

I den videre udvikling og kommercialisering af systemet vil vi fokusere på detektering og lokalisering af skader. For nu vil vi vente med at implementere funktionalitet til at forudsige udvikling af skader indtil forskning inden for dette felt når det nødvendige niveau.

Executive summary

This section provides a brief summary of the project and its results and expected utilization of project results.

Potential customer benefits and project utilization

The approach worked out during the project contributes to reduction of Operation and Maintenance (O&M) costs associated with wind turbines rotor blades maintenance. Namely, the proposed approach suggests replacing the blade inspections by blade monitoring.

The today's approach to blade maintenance is based on periodic visual inspections, provided by teams of highly skilled professionals, which operate from ropes or specially installed equipment (e.g. Sky Climber).

The proposed approach suggests replacing the visual inspections by permanent unmanned monitoring of blades using the proposed SHM system.

"It all starts with a small crack..." (**Figure 1**). The cost of repair grows significantly with the amount of blade damage. The main advantage of the blade monitoring is that blade damage can be detected in very early stages, when its repair cost is small. Taking an offshore 8MW Vestas V164 as an example, we can show that the wind turbine owner can save up to **32kEUR per wind turbine per year**, if SHM concept "don't let a failure grow above Category 3" is in place.

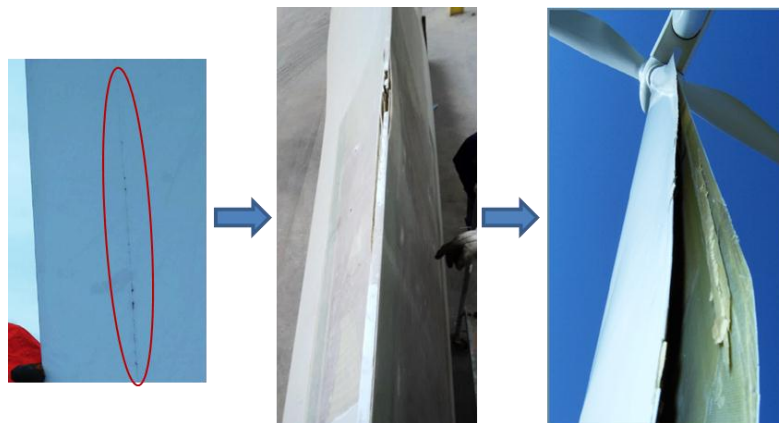


Figure 1. Blade failure development: from small crack (left) to catastrophic trailing edge opening (right) (the figure provided by *Bladena*)

Table 2 further compares the current and the suggested approaches:

Table 2. Comparison between the current and suggested blade maintenance techniques.

Current approach: via inspections	Proposed approach: via monitoring
Downtime issue: the wind turbine should be stopped for installation of ropes/platform and the inspection.	Monitoring takes place when the wind turbine is operating.
Due to weather conditions, the availability window for such inspections is quite limited, especially for offshore wind turbines	Monitoring does not depend on weather
The visual inspection (or even blade tapping) cannot reliably detect damages of the inner blade structures	Monitoring can detect even if the inner parts of the blade are damaged

Such inspections are typically conducted once in two years, thus the owner is unaware about the states of the blades	Monitoring is continuous, that is, the owner is constantly aware of the blades state and will be notified as soon as the fault appears.
Due to seldom inspection, the owner is unaware about damage progression, and faces difficulty developing an effective maintenance strategy.	Monitoring is continuous, which allows the owner observe damage progression. This makes possible to develop a more efficient maintenance program.
The inspections require highly skilled professionals working in dangerous conditions.	In special rear cases, a blade specialist will require looking into the data but it will happen remotely, in safe office environments.

The potential customer of such a system will receive the constantly updating information regarding the health of the blades of the entire fleet. The combination of the fleet health overview and the ability to follow damage progression is a valuable tool for O&M optimization.

Summary of the project results

During the project, we developed a blade structural health monitoring system, which:

- provides continuous remote monitoring of blades' structural health
- does not require the wind turbine to be stopped
- does not require any use of ropes/platforms
- ensures detecting structural defects like
 - o cracks
 - o delamination
 - o delamination due to wrinkles
 - o tip/edge openings due to e.g. lightning
- ensures detecting of inner damages (not visible from the outside)
- has low false alarms rate
- provides approximate damage localization and
- indication of damage progression.

The proposed technology cannot:

- detect not-structural damages, e.g. coating damages due to erosion

IP situation

The method is patent pending.

Project development

This section describes the project objectives, evolution and the implementation of the project, including the risks associated with the project.

Project objectives

As stated in the project application, the main objective of the project was to develop a smart predictive health monitoring (PHM) solution, which will complete the detection of structural failures with effective follow up procedure thus helping wind turbine owner/operator making cost-effective decisions on wind turbine maintenance. The focus of the project is the predictive monitoring of blades, as they are the most expensive structural parts of a WT.

Project consortium evolution

The initial project objectives (see Section 0) defined the project consortium. Originally, it was:

Brüel and Kjær SVM as the project integrator and project leader.

Vestas representing a potential customer

DTU (DTU Wind and DTU Compute) as research institutes.

However, six months after the project started, Vestas decided to pull itself out from the project. At the Extraordinary meeting that took place in Mar 2012, it was decided not to stop the project, but find new partners to replace Vestas. New partners became:

Vattenfall as a potential customer.

Bladena as a blade specialist company.

Total Wind as a company providing technical services when working with wind turbine blades.

With the new partners, the work packages were slightly redefined while the objectives of the project left unchanged.

Project evolution

After Vestas left the project, it evolved very much along the defined work packages and milestones. The work packages are listed in the **Table 3**.

Table 3. Project Work Packages

No.	Title	Responsible
WP0	Overall project management	B&K
WP1	Development of experimental MA technology for WTs	B&K
WP2A	Damage Library	Bladena
WP2B	Sensitivity analysis of modal parameters as detection features	DTU Wind
WP2C	Experimental verification of damage modelling by full scale test of SSP34m blade	DTU Wind
WP3	Development of damage progression model	DTU Wind
WP4	Development and test of a Decision Making Algorithm	DTU Compute
WP5	Development of prototype	B&K
WP6	Field test	Bladena

Potential risk

The initially foreknown risk was that the main tool, considered for enabling blade SHM system, was not sufficiently sensitive to detect small amount of damage. Therefore, the WP1, WP2A, WP2B and WP2C work packages were set up to investigate this risk.

The main tool, which we originally considered to utilize for the SHM system, is operational modal analysis (OMA). Via modal analysis, one performs dynamic system characterization, which results in modal parameters; the latter will vary depending on system's structural health. The original idea was to permanently monitor rotor modal parameters and, if they significantly deviate from "normal", raise a flag indicating blade damage.

During the above-mentioned work packages, we found out that indeed, the modal parameters and OMA as a tool for their extraction are not suitable for creating a robust blade SHM system according to the specifications.

In October 2013, we had a **Critical Design Review** meeting where we decided to stop using modal parameters as a key element of the SHM system and fully focus on a vibration-based system with an actuator. The content of the WP4-6 was reformulated to reflect the decision.

Unexpected problem

During 2014, the prototype of the new system was developed and ready for field test (WP6). The testing was supposed to take place on a Vestas V80 wind turbine, provided by Vattenfall. During the experiment, we planned to introduce damage into one of the blades. However, we run into an unexpected insurance issue: it was not possible to find an insurance company who agreed to offer the insurance covering artificial blade damage. Without the insurance, Vattenfall refused to conduct the experiment.

The problem was solved by using a wind turbine that belongs to DTU Wind. It was not a modern wind turbine as V80 but a much older Vestas V27. However, V27 has many features common for modern wind turbines, and the substitute was accepted.

Delays

The project experienced to delays, thus lasted 9 months longer than originally planned. The first delays happen due to Vestas left the consortium, and we used 6 months to find new partners and work out all the official documents, re-submitted to EUDP. The second delay happened due to the unforeseen insurance problem: it took three additional months in attempt to find an insurance company ready to cover the potential risk of introducing a damage to the blade.

Results

Anyway, despite the foreseen and unforeseen risks, the project objectives were accomplished, and the project resulted in a technology, which can detect and localize damage and follow damage progression. The only objective, which was not accomplished, is the predictive capability of the system. However, it is believed, that with the "follow damage progression" capability, the system is still attractive for potential customers.

Project results and dissemination of results

Main activities during the project run

This section describes the main activities performed by the partners during the project run.

The main activities in the frame of the project were defined as *tasks* specific for each work package (see Table 3). The timeframe for each task and their interdependencies were described in the Gantt diagram. The project mainly followed the work packages and tasks. Each work package was concluded with a milestone, representing a significant contribution into the project overall goal.

Work Package 1 (B&K)

WP1 Objectives

This work package was set up to develop the technical and algorithmic tools enabling extracting modal parameters of an operating wind turbine.

WP1 Activities

The WP had two folds:

1. To demonstrate technical feasibility of measuring vibrations on wind turbine blade, while the wind turbine is operating, during monitoring period (several months);
2. To demonstrate a feasible technique for extracting modal parameters from the measured data.

Below are the detailed description of the activities taken in the two directions.

1. During this WP, we demonstrated the technical feasibility of getting measurements from blades of an operating wind turbine. The main challenges in the practical implementation of the measurement system are
 - a. Data acquisition system inside the rotor, thus rotating with the rotor;
 - b. Vibration data transfer from the rotating rotor to the ground;
 - c. Synchronization of the data streams from the rotating rotor and not rotating nacelle.

In order to perform this task, Vestas V27 wind turbine was instrumented for measuring blade vibrations. The hardware and the measurement procedure was described in details in [1]. The measurement campaign took place from Nov-2013 until May-2014 (7 months). This task created unique datasets allowing testing different modal analysis algorithms on real measured data.

2. Even with the measurement data in hand, the modal analysis of an operating wind turbine remains challenging. The problem is that the operating wind turbine contains rotating parts while the classical modal analysis requires the object under test is not changing in time (so-called, time invariant). Two existing approaches addressing the problem were tested: multiblade coordinate transformation (MBC) and angular resampling approach. The results were published in [2], [6] and [9]. Though the results were acceptable for some particular cases, they were not good enough for robust modal analysis and a need in more advanced method was clearly identified. Such a method was developed based on Harmonic Power Spectrum method and published in [7] and [8].

WP1 Results

The main result of WP1 is a full methodology for estimating modal parameters of operating wind turbine, which includes its practical implementation and the algorithms. The methodology was successfully tested on vibration data obtained from the operating V27 wind turbine and on datasets produced by simulation software HAWC2.

Work Package 2A (Bladena)

WP2A Objectives.

In order to understand typical damages of wind turbine blade, it was decided to create a damage library, where Bladena has collected and organized the information in the form of easy to use product available to wind turbine operator companies.

WP2A Activities

A comprehensive dossier of various structural damages and variations seen on blades in service has been made. Bladena has been responsible for organizing the gathering of data, with specific input from Vattenfall and the support of company specialized in the maintenance and repair of blades (Total Wind Blades).

A database tool named Guide2Defect or G2D has been developed in this task (Figure 2). The main purpose of this G2D-database was to make a tool, which can categorize damages in wind turbine blades. The aim was to have a database where statically data about different damages can be analyzed by the occurrences and observe whether there is any relation to size of the blade, site or other parameters. The tool has been programmed and the data has started to be filled in, see [15]. An effort has been made to establish the input. Meetings with Bladena's service partners (Total Wind Blades, Broadwind and RopePartner) have been held, where they have agreed to use this tool in the future when the "final" version is released. This means that during the coming years more and more data will be included in the database, so the statistic population will be more reliable and not only represent one blade type placed on one specific site, etc.

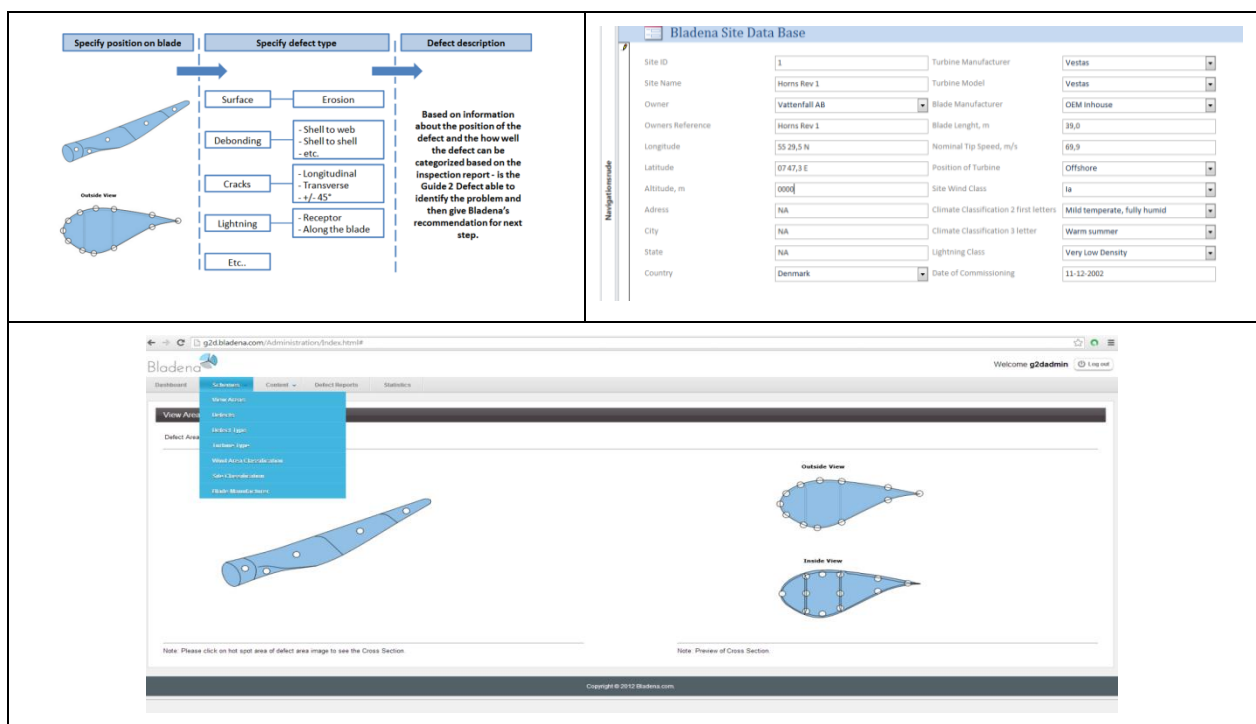


Figure 2. G2D database user interface.

Part of this WP2A is that Bladena had the task to arrange workshops where both industry and university present in order try to close the gap between the industry and research. The intension of the workshops were to "solve" practical problems, update researchers on the most pressing issues form the Industry, and present applied research which is ready to be implemented in industrial applications.

In collaboration with DTU Wind Energy, Bladena has arranged a workshop at Risø DTU in June 2013. The workshop was focused on issues related to blade failures and the challenges the industry is facing when wind turbine blades grow larger and when the wind turbines are placed offshore. In order to get inspiration from another

industry dealing with “Damage simulation in composite materials” was a simulation expert from Canadian company Lifetime Prediction (LPTI) invited to give a presentation and join the panel discussions, additionally representatives from the end users (wind turbine owners) participated in the panel discussions. 32 participants joined, and the feedback from both industry and university has been very positive.

Furthermore, because the G2D requires time to be able to produce reliable statistics, Bladena has created a document called *Blade Failure Catalog* where the damages found during inspections are presented. The aim of this document was to present to 3rd parties the damages found in the field. The Blade Failure Catalog is attached as an appendix.

WP2A Results.

The G2D product has been released and tested with big wind turbine operator companies. A comprehensive catalogue where the damages found in wind turbines has been created and is available.

Work Package 2B (DTU Wind)

WP2B Objectives

Knowing the typical damages and having the necessary analysis tools, one would need to check if the damages of interest could cause significant change of modal parameters, and thus could be detected. This work package was set for this task.

WP2B Activities

A very detailed finite element model of a 34 meters SSP (SSP34m) blade was set up, and damages from the damage library were introduced into the model. With eigenvalue analysis, it was shown that even a big blade damage does not significantly affect natural frequencies but has some effect on the mode shapes. The results of the study were published in [4].

WP2B Side development

During WP1, it was noticed that damage of one blade causes rotor anisotropy, and this can be detected as symmetry loss of the rotor mode shapes. This hypothesis was tested on a simplified three bladed rotor model via simulations, and showed promising results (published in [3]). The method was also tested using realistic simulations utilizing nonlinear aeroelastic code HAWC2 developed by DTU Wind Energy on a generic 10MW wind turbine with realistic damage. Unfortunately, the method did not demonstrate the expected sensitivity to blade damage.

WP2B Results

Based on numerical modelling, the work package demonstrated that a typical damage may have an effect on modal parameters but the effect is not significant.

Work Package 2C (DTU Wind)

WP2C Objectives

This work package is a natural extension of WP2B, where the findings from the numerical analysis to be confirmed by experimental work [4].

WP2C Activities

An extensive measurement campaign was conducted on an SSP34m blade mounted on a test rig inside DTU Wind Energy facilities, during summer 2013. The blade was instrumented with about 30 accelerometers, totaling 90 measurement channels. Artificial damage was introduced into the blade: a trailing edge opening, starting with a length of 20 cm and was then gradually extended to 120 cm and then repaired. Operational Modal Analysis (OMA) was conducted on all states, including the undamaged, damaged for all damage states and repaired blade; also the statistics for evaluating confidence interval of the obtained modal parameters, were collected. The results of the study were published in [4].

The experiments demonstrated that the predicted changes in modal parameters could not be detected experimentally: the measurement noise prevents catching the subtle changes in the mode shapes caused even by the biggest damage. In addition, the feasible density of the sensor network does not allow catching the mode shapes with the resolution sufficient for damage detection and localization, even when using dedicated magnification techniques like those that wavelets transform (presented in [5]).

WP2C Side development

During the campaign, the actuator-based method was suggested and initially tested. Later, the project mainly focused on this method.

WP2C Results

The work package clearly demonstrated that the subtle changes of the blade modal characteristics caused by damage could not be captured by OMA even with quite dense sensor grid. Nevertheless, the biggest achievement of this work package was the introduction and the initial test of the actuator-based method, which became the key element of the following work packages.

Critical Design Review

The Critical Design Review meeting took place in Oct-2013, after the WP1, WP2A-WP2C were finalized.

The results of the work packages WP1, WP2A, WP2B and WP2C allowed us to conclude that the originally considered approach, namely using modal parameters as damage indicator, is not suitable for robust blade SHM system enabling detection of typical blade damages. This became a turning point of the project, where we started looking for another, more sensitive technique.

The Critical Design Review meeting approved the alternative technique involving a mechanical actuator, which was initially tested in WP2C. It was decided to abandon the modal analysis-based approaches and fully focus on the new technique.

Work Package 3 (DTU Wind)

WP3 Objectives

Develop a damage progression approach based on measured material properties that can provide information about the severity and criticality of specific identified damages.

WP3 Activities

This Work package involved combining the inputs from Industrial partners, Research specialists, and Sensor suppliers to discuss the wind turbine blade structure and operational loading, the material properties and damage tolerance capacities, the damage/defect observations in-service, and the technologies available to update damage inspection reports with the detailed measurements necessary for accurate prognosis.

A series of technical meetings on this topic allowed agreement on the approach necessary at the research level, the industrial level, and the project level. This recognised the extensive International research effort still required to complete an understanding of (damaged) material behaviour and integrate this within design and operational guidelines for wind turbine blades. But also proposed an industrial target of “safe flight” for the most critical identified damages as well as known propagation rates under controlled dynamic loads. Finally a specific example of adhesive bondline failure (trailing edge) was chosen to make it possible for the project to demonstrate the general approach.

However, the composition of the consortium changed during the project duration and this had a significant effect on the content of Work Package 3. The scheduled mechanical testing of specimens to provide material level data to damage progression models was changed to an approach where structure level analysis was confirmed by direct measurements from a blade test (see WP2B and WP2C).

Instead an effort was made to address the WP3 issue by arranging a Workshop on damage and wind turbine blades, and then proposing a methodology for integrating the emerging research in a way that Industry can adopt.

WP3 Results

Using the input from the consortium experts (and the International Workshop) to address the challenges of integrating material damage models within structural response calculations has led to new synergies between the DTU capabilities focussing on fabrication, test, and measurement with respect to Wind Turbine Blades. Early Stage Researchers have been employed with the specific intention of developing the “smart structure” / damage detection capabilities described by the consortium. International collaboration on EU funded projects has been initiated with both research and Industry partners.

An overview of WP3 is reported in (DTU Wind Energy E; No. xxxx(EN) “Predictive Health Monitoring – EUDPnr.64011-0084, WP3: Investigating Material Damage Propagation in Wind Turbine Blades” May 2015.

A methodology for reliable design and maintenance of wind turbine blades by integrating improved damaged material models with a damage tolerant structural design is described by McGugan et. al. in [10].

Work Package 4 (DTU Compute)

WP4 Objectives

The SHM systems needs a robust decision making algorithm to be able provide warning about damages and avoid or minimize the false alarms. This WP concentrates on this problem.

WP4 Activities

The decision-making algorithm was developed in an iterative process governed by the data becoming available. An initial data analysis pipeline was implemented for ambient vibrations for an experiment on a slender composite beam as well as data from WP1 activities.

With the revised focus on the actuator-based system the main damage detection algorithm was developed. The algorithm was optimized to detect damages based on data from WP2C as well as a 50 cm blade, which made it possible to evaluate detection performance for different locations of damages. The resulting algorithm is described in [11]. The robustness of the algorithm was tested using WP2C data corrupted by additive noise acquired from the V27 measurements from WP1. These results are also reported in [11].

Finally, the decision-making algorithm method was applied to the data from WP6. The method was evaluated under the varying environmental and operational conditions. The tests revealed the need for an extended detection algorithm that takes advantage of the knowledge of these conditions.

WP4 Results

With the new approach, involving the actuator, such an algorithm was created and tested on a number of scenarios. The algorithm demonstrated an excellent detection rate and low level of the false alarms. The details of the algorithm can be found in [11].

Work Package 5 (B&K)

WP5 Objectives

In order to validate the system prototype tested in the lab during WP2C, a prototype enable to perform on an operating wind turbine needs to be developed. This WP focused on this task.

WP5 Activities

The experience gained during WP1, WP2C and WP4 was widely used for creating the prototype. The suggested SHM system consists of two main parts: actuator and data acquisition system. The actuator designed for WP2C was significantly enhanced: it became waterproof; its mechanical part was improved in order to operate under severe gravitational and centrifugal loads of operating wind turbine; its electrical part was redesigned to support the voltage supply available in the rotor (24V).

For data acquisition system, the experience gained during WP1 was used. The resulting system was a simplified version of the system used in WP1, where the parts proved functional during the 7 months long measurement campaign of WP1, were reused.

WP5 Results

The WP resulted in a prototype (hardware and software) ready to be installed on a wind turbine.

Work Package 6 (Bladena)

WP6 Objectives

The objective of this final work package was to demonstrate the SHM prototype on an operating wind turbine, the so-called field test.

WP6 Activities

The WP suggests installation of the SHM system prototype on an operational wind turbine and testing its detecting capabilities on artificial blade damage.

There are two groups of activities in this WP:

1. Collecting data from operating wind turbine in undamaged and damaged states;
2. Application of the damage detection algorithms developed in WP4 to the data, and the assessment of the overall system.

Below is the description of the activities.

In the steering group meeting, we decided to make a FEM-model of a Vestas 39m blade instead of the old well-known 34m blade from SSP-Technology. It was expected that this would add a value to the project, since the field test was supposed to be performed on a Vestas V80-turbine with these blades. Bladena had to put a great amount of efforts in order to make this model since the project had no drawings of the design of the blade. A 39m Vestas blade was accessible (belong to Total Wind), where geometry, thicknesses, layup, etc. has been measured during several field measurement trips and used as an input for the FEM-model.

However, we could not get a permission to introduce artificial damage to a blade of Vattenfall's V80 wind turbine, as it was originally planned. Instead, an older Vestas V27 wind turbine, which belong to DTU Wind, was used. Under some security prerequisites, we were granted a permission to introduce blade damage: trailing edge opening.

The SHM system prototype was installed on the wind turbine during Oct 2014, and the wind turbine was set to operation. The first damage stage, a 15 cm trailing edge opening, was introduced in 09 Dec 2015. Then the wind turbine was set to operation again, with the security precautions preventing any human risks in the case the blade gets broken due to the introduced artificial damage. After one week of operation, 15-Dec-2014, the damage was extended to 30 cm, and the wind turbine was set to operation again. On 04-Jan, the damage was extended until 45 cm, and the turbine was set to operation. Finally, 19-Jan the damage was repaired. Until 12-Mar, the acquisition system was in place generating data for the repaired state. Thus, during the measurement campaign, we collected data from five different states: "undamaged", "15 cm damage", "30 cm damage", "45 cm damage" and "repaired" for the wind turbine under a wide range of operating conditions.

Collected during the measurement campaign data was analyzed by different algorithms developed in the frame of WP4. The complete analysis is not yet finished but it is already now obvious that even the smallest damage (15cm) can be detected when the wind turbine is operating. Currently we are preparing a conference paper where some of the results will be reported [17].

This is the main achievement of the project proving its success.

WP6 Results

It was demonstrated that the system is capable detecting a typical blade damage on operating wind turbine (i.e. not requiring the turbine to be stopped). This proves the entire approach and thus demonstrates the success of the project.

Summary of the project results

The project involved many partners who during the project achieved many common and independent goals. This section briefly lists all the results achieved during the project.

1. A data acquisition system capable to measure blades vibration on the rotating rotor and providing a sample wise synchronization with turbine's not rotating parts has been developed and demonstrated during a six months measurement campaign.
2. The extension of operational modal analysis (OMA) to structures with rotating elements was developed.
3. Guide2Defect, an easy to use tool for collecting and organizing information about blade damages was developed, distributed among wind turbine operators, and the blade damage database is being filled now.
4. Sensitivity of modal parameters to typical blade damage was investigated. Based on this, we proved that the modal parameters are not sensitive enough and cannot be used as a key element for a robust SHM system.
5. Using the input from the consortium experts and the International Workshop, has led to new synergies between the DTU capabilities focusing on fabrication, test, and measurement with respect to Wind Turbine Blades.
6. Another approach to blade SHM system was suggested. The approach is based on using mechanical actuator and dedicated signal processing.
7. By testing the approach on two different setups, we demonstrated its applicability to SHM system.
8. A decision-making algorithm capable of detecting a damage with excellent detection rate and very low false alarm rate was developed and tested on the two setups.
9. A prototype of SHM system, combining the hardware and the decision-making algorithm, was developed and installed on a wind turbine. The prototype was validated during 4 months test campaign and proved effective.

SHM system prototype: technical insight

This section provides a technical insight into the rationale behind the proposed method, the implementation of the SHM system prototype and the brief description of the algorithm used for damage detection. The detailed explanation of the algorithms can be found in the papers published during the run.

Rationale for the method

The proposed approach is vibration-based: it utilizes vibration signals measured by a number of sensors (accelerometers) mounted on the blade. It also involves an "actuator", an electro-mechanical device introducing mechanical energy to the blade structure. The actuator is a kind of automatic "hammer" which hits the blade, thus introducing mechanical energy into the blade. The energy propagates along the blade as mechanical waves; the waves manifest themselves as mechanical vibrations, which can be sensed on the blade surface using vibration sensors, e.g. accelerometers.

The novelty of the method is in the frequency range of the excited vibrations: it is a compromise between the low frequency (long) waves, which can propagate long distances but have low sensitivity to small amount of damage and the high (ultrasound) frequencies, which have excellent sensitivity but cannot propagate long distances. The waves in the suggested frequency range (around 1kHz) can propagate 30-40 meters of composite blade structure without significant dissipation, while the wavelength (0.5-0.8 m) provides the damage detection resolution ($\frac{1}{2}$ of wavelength), which is sufficient for detecting amount of damage before it becomes critical for blades' structural integrity.

Applying a short mechanical impulse to the structure, the actuator excites a plurality of different waves at different frequencies, thus the detection capabilities of the system are actually quite high.

The structural health is evaluated as a change in the vibration pattern excited by the actuator: due to damage, the vibration pattern is being distorted. The vibrations are measured by a grid of vibration sensors (we used accelerometers). The distortion, in both magnitude and phase, is being detected and evaluated by a classification algorithm. **Figure 3** explains the rationale behind the method.

Use of advanced machine learning algorithms based on statistics, ensures low false alarms rate and secure robust result interpretation.

Damage detection algorithm

The damage detection algorithm utilized in the proposed SHM system consists of several steps:

1. Calculation of damage feature and dimensionality reduction
2. Statistical modelling of the reference state
3. Calculation of the threshold value
4. Calculation of the distance between the new data sample and the reference state (defined by the reference state model) and comparison of the distance with the threshold.
5. Post analysis of the time history of the distances, calculated at step 4.
6. Decision (damage detected) based on results of step 5.

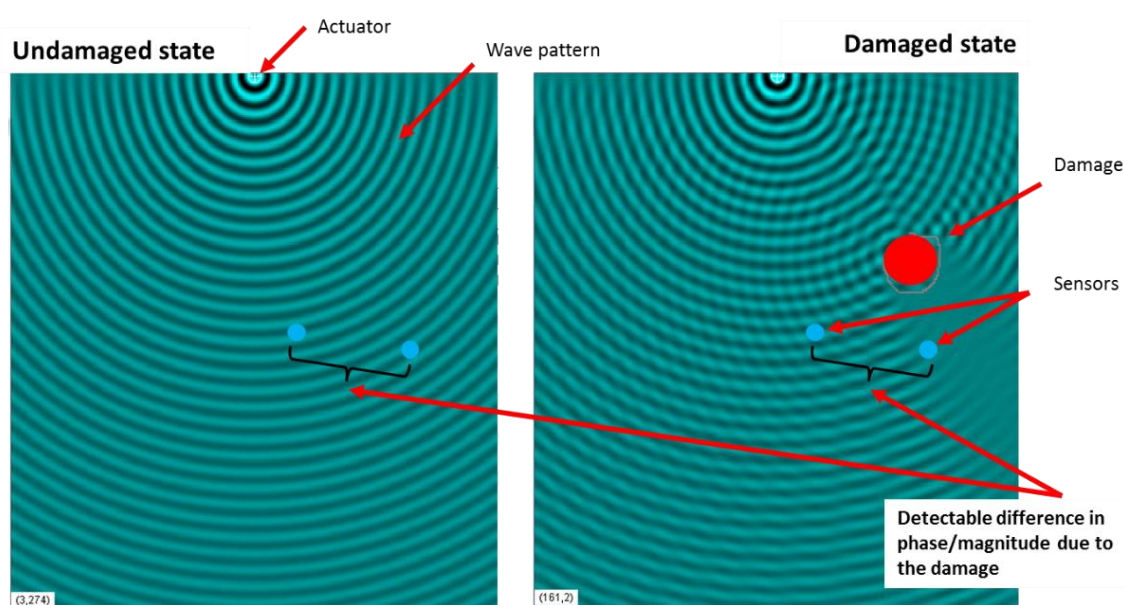


Figure 3. Vibration pattern due to actuator hit. Left: undamaged structure, right: the structure with a defect.

As a damage index, we use covariance between measured response signals, after some pre-processing (e.g. framing, band-pass filtering, and noise removal by e.g. signal enhancement or more advanced filtering). A simple Gaussian model turned to be sufficient for the reference state modeling. Principal component decomposition was used for dimensionality reduction, and Mahalanobis distance was used as a distance measure between the new sample and the reference state model. The details regarding the algorithm are given in [11].

Technical implementation of the system

From hardware point of view, the system consists of an actuator (one or several) and vibration sensors. Figure 4 shows the actuator design and typical placement of the actuator inside the blade (as on the SSP34m blade, Figure 4b). However, there is no access to blade inside for the older V27, therefore the actuator was mounted outside, Figure 4 c,d).

The actuator consists of a coil, which due to an electrical impulse, shots a plunger towards the blade. Then, the plunger is being returned to its original position by a spring.

The coil is mounted on plate, which is being attached to the surface of the blade by means of four feet. The feet are glued to the blade surface. Controlling the length of the feet, one can control the distance between the plunger and the blade surface, and thus, the strength of the hit. Controllable duration and magnitude of the electrical pulse can be used to tune characteristics of the mechanical impulse.

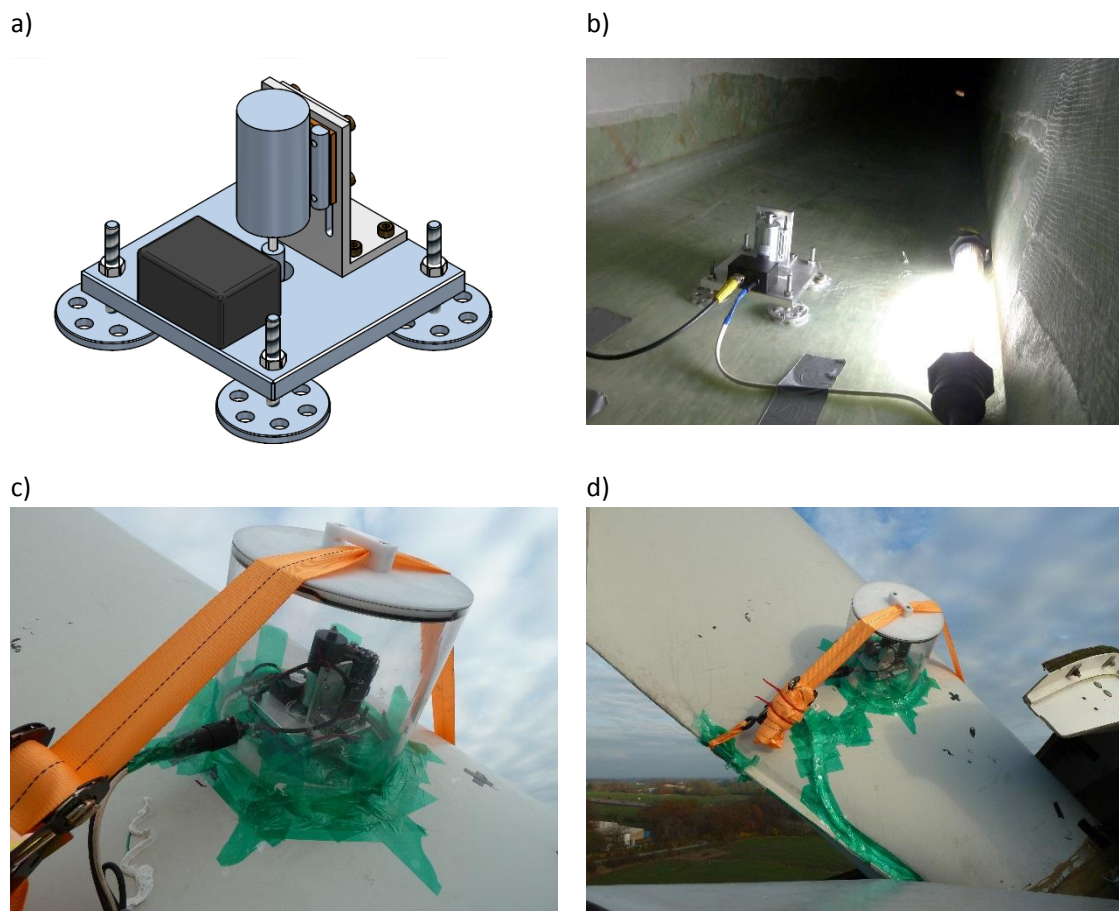


Figure 4. Actuator design and placement of the actuator inside the blade (SSP34m blade) and outside of the blade (V27) since no access to blade's inside due to the blade size

Hitting the structure, the actuator initiates mechanical waves of different nature (longitudinal, transversal, Lamb waves). The waves propagate along the structure, and they can be measured by vibration sensors. For the SHM system prototype, we used accelerometers, though other types of sensors (e.g. strain gauges) are also possible. The photos on Figure 5 show the implementation of the vibration sensors on the SPP34m blade (test rig) and V27 blade (operating wind turbine).

The next important part of the SHM system is a data acquisition unit. The data acquisition unit collects the vibration data from accelerometers and other important metadata (e.g. rotor azimuth, pitch angle, rotor speed, etc.) and transmits it to the analysis unit or some storage. Figure 6 shows the data acquisition unit mounted in a waterproof box inside the spinner of the V27 wind turbine.

Finally, the data was collected and stored on a computer located in the 4m platform of the tower. By means of a modem, it was possible to have access to the computer.

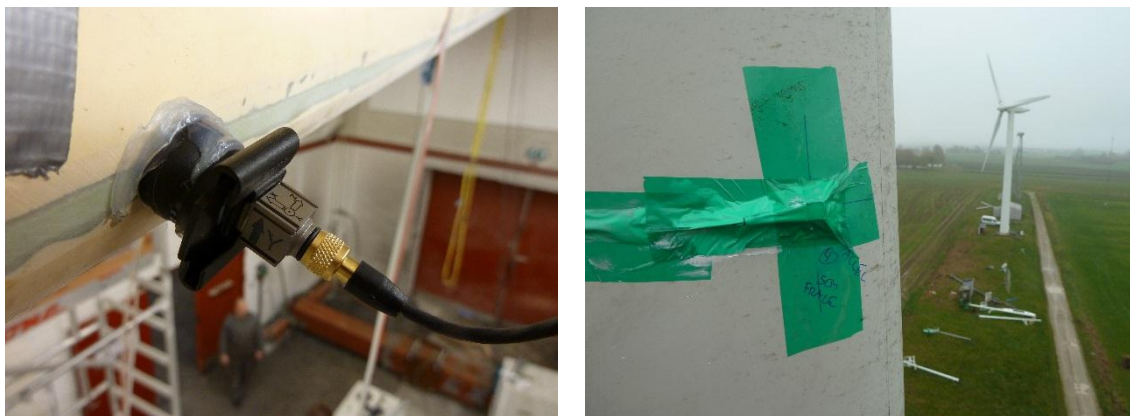


Figure 5. Left: B&K triaxial accelerometer mounted on the leading edge of the SSP34m blade. Right: monoaxial B&K accelerometer mounted 5cm from the leading edge on the blade of V27.



Figure 6. B&K data acquisition unit inside a waterproof box, mounted inside the spinner of V27 wind turbine. The unit accompanied by Cisco access point for wireless data transfer to the nacelle.

Evidence of efficiency

This section describes the experiments, which were conducted to prove the efficiency of the suggested method

To prove the method efficiency, several experiments were conducted.

34 m long SSP blade mounted on a test rig

During WP2C the approach was initially tested on an SSP34m blade mounted on a test rig (Figure 7a). Damage was introduced as a trailing edge opening (Figure 7b), which is one of the typical blade damages. The SHM system was able to detect a 20 cm long crack and detect the further development of the damage from 20 to 120 cm.

This experiment confirmed the feasibility of the active vibration-based approach on a modern blade manufactured from composite materials. The detailed description of the experiment is published in [4]. During the data processing, some attempts were made to model the noise that is unavoidable in case of real life measurement. Though the algorithm proved to be efficient in cases with modelled noise, we could not prove if the method works on real operating wind turbine or not. This was later demonstrated during the field test, WP6.



Figure 7. Left: SSP34m blade on a test rig. Right: an artificially introduced trailing edge crack.

Experiment on a small blade

Full-scale experiments involving a real wind turbine blade and introducing damage into it are obviously very time consuming and expensive. In order to simplify experiments, a smaller test object is much more convenient. A small 80 cm blade from DTU Wind Racer car project was acquired and converted to a test object (**Figure 8**). The two halves (shells) of the blades were connected by means of many small bolts located 20mm from each other. Loosening the bolts, it was possible to model a trailing or leading edge opening of any size and located at any place of the blade.



Figure 8. A 80cm blade from DTU Wind Racer project as a test object: left two halves; right – with mounted actuator and accelerometers

The experiments involving three damage scenarios were documented in a form of a video. The video is available on YouTube (<https://www.youtube.com/watch?v=A7UYwV-bc2w&feature=youtu.be>).

The video is also supposed to use for project results dissemination: in a simple way, it demonstrates the principle of the SHM system and the output of the damage detection and localization algorithms. The data collected during the experiment was used for testing alternative damage localization algorithms, [12] and [13].

Experiment on Vestas V27 operating wind turbine

This experiment was set up as a final field test with the goal to confirm the feasibility of the suggested SHM system in real life conditions.

One blade of Vestas V27 wind turbine (225kW rated power, rotor diameter 27m) was equipped with the system and a four-months monitoring campaign was conducted (**Figure 9**). During the campaign, the wind turbine was operational. Damage was artificially introduced into the blade (trailing edge crack): started with 15cm long, it was gradually extended to 45cm.



Figure 9. Left: Vestas V27 equipped with the blade SHM system. Right: the artificial 15cm trailing edge opening, which was successfully detected by the system.

The experiment confirmed that the damage could be detected without stopping the wind turbine. In addition, it confirmed the ability to monitor the damage progression (15cm-30cm-45cm).

Types of damage

The experiments conformed that the trailing edge cracks can be detected. We did not test for other types of damages due to reparation difficulty. However, the physics behind the method ensures detection of any kind of damage, which affect the blade structural integrity.

Damage / Defect management

In this section the vision of predictive capabilities of the system is presented and the requirement for developing the technological tools available as well as deepening the understanding of the fundamental physical modelling defined.

In engineering, the reliability of a system is always crucial. This is the ability to perform and maintain functions under normal operating circumstances for a defined period of time, as well as a robust resistance to hostile or unexpected circumstances.

A damage or defect within the structure of a wind turbine blade is a potential weak point that could lead to reduction in the efficiency of the system, shortening of the service life of the blade, the development of damage in other components, or even a sudden and catastrophic failure.

However to conclude whether a particular damage is critical requires technical tools based on a solid framework of knowledge regarding the location and nature of the defect, the local structural stress state, and material properties. If such a framework is not present then the correct response to any problems arising in an operating blade will not be clear.

In the EUDP PHM consortium a multiscale understanding of materials was to be used in the structural management of wind turbine blades. By developing a solid understanding of the material processes involved in defect/damage progression, along with the techniques to investigate structural health of a particular blade, we can provide deterministic criteria for the quality control requirement during manufacturing, the maintenance effort in operation, and correct decision towards the end of service life (reinsure, refit, repower, or recycle).

Concept and proposed framework

Figure 10 shows the proposed sequence of events for maintaining the condition (health) of an operating wind turbine blade. A surveillance operation is in place for each structure that could be an embedded sensor system that can remotely and automatically give an early warning of potential problems, or an alert could also be raised following a standard on-site inspection/observation. In either case it is considered unlikely that the initial information regarding a problem (exception) for a particular blade would be sufficient to decide the correct response. A more detailed investigation using Non-Destructive Inspection technology would reveal the precise location and extent of the damage and characterise the parameters that allow physical modelling of the local structure.

Figure 11 shows the step-by-step approach for combining structural dynamic response with known damage/defects in the structure to generate a prognosis under forecast operating conditions.

A first step is to determine the dynamic stresses and strains on the blade structure using aeroelastic models. This three dimensional Finite Element Model (FEM) calculates the combined effect of aerodynamic and gravitational loads applied during operation. The effect of various extreme wind loading and turbulent flow conditions can also be modelled at this stage.

This modelling provides details of the stresses and strains fluctuating around the local (sub-component) blade section where the characterised damage/defect exists. This local model uses material process (fracture mechanics) modelling to determine if normal operating conditions will result in damage propagation at this location; and if so to what extent and at what rate. If damage propagation is predicted to occur then these local models can also be used to calculate if the damage propagation rate can be reduced (perhaps to zero) by avoiding high aerodynamic (structural) loading occurring at higher wind speeds.

An integrated model that runs both the structural deflection at the global scale as well as including the local sub-models of known damages distributed throughout the structure is the ambition at this stage. This model should also accommodate any interactions between the damages and the effect on global response to any local non-linearity predicted by the sub-component model.

The prognosis for any damage constellation must then be evaluated according to a criterion for “severity” that will of course include the propagation rate for known damages, but also other factors such as weather forecasts, seasonality, available maintenance resource, energy prices, repair options, sensor response, etc., as well as various sources of empirical data. This evaluation is to be the subject of a decision making process (WP4).

If non-critical the turbine will continue normal operation with the known damage information being stored as “mark and monitor” for future evaluations following information updates. If action on the current damage state is required this could be:-

- to modify the operation of the turbine and avoid loading levels that will cause damage development

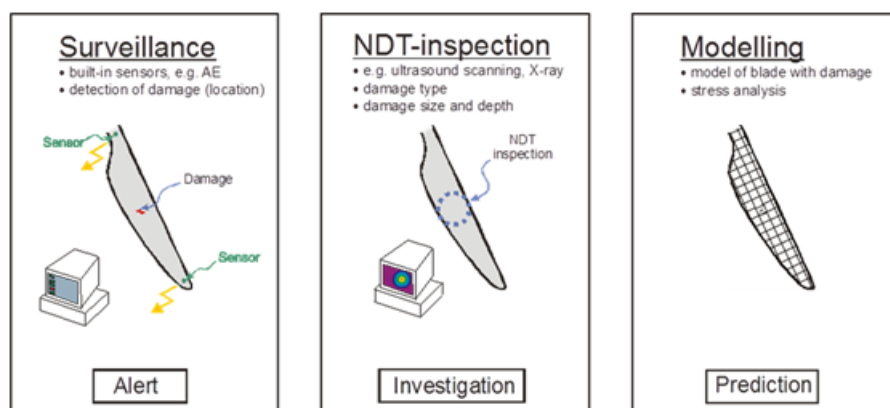


Figure 10. Overview of the detection – inspection – prediction sequence for blade maintenance

- to design and schedule a repair procedure in the near future
- or even to stop operation and either replace or re-fit the current structure.

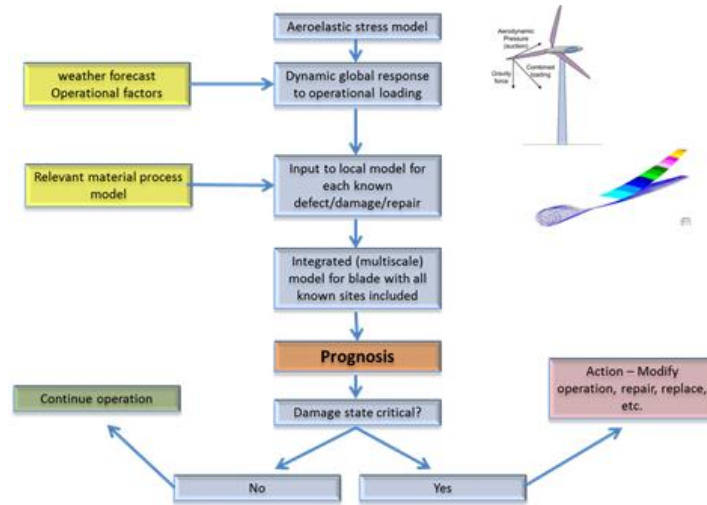


Figure 11. Block diagram showing the steps in producing a prognosis for a known damage condition in a particular wind turbine blade structure

IP protection

The key elements of the actuator-based vibration SHM system were identified as patentable, and a patent application was filled.

Statement from Vattenfall

During the project, Vattenfall represented the potential future customer. Evaluating the project results, Vattenfall's blade specialist Rikke Balle (RikkeJuul.Balle@vattenfall.com) made the following statement:

Blade damages and failures are not a new phenomenon and the impact is increasingly relevant. The continuing downward pressure on reducing the cost of energy is playing an important role. Based on above it is important to know the condition of the blades and being able to act when a damage occur.

The current approach is to stop the turbines once every 2nd year and do an external blades inspection by rope/high resolution camera/drones. These inspection methods all provide a contemporary status of the blade condition and they are not able to detect damages of the inner blade structure. Combining this with the fact that not all blades in a site is being inspected every 2nd year (maybe only 20%/year) it result in owners unaware of the states of the blades. This result in a risk of small insignificant damages growing into huge damages or even blade failures.

By mounting a monitoring system the monitoring takes place when turbines are operating, it is not dependent on weather conditions, and owners will be provided a "continuously inspection" status. Only the blades where defects are observed will need inspection/repair.

By replacing inspections with monitoring systems there is a huge cost saving potential (inspections and repairs) and it will minimize the risk of having blade failures in the future. These were the main drivers for Vattenfall getting involved in this project.

The project achieved impressive results. Implementation of such a system promises to significantly reduce the costs of the blade O&M, and therefore reduce the CoE and minimize the risk of having blade failures.

Commercial results

Now, the SHM system exists as a prototype, and it is recognized that there is a long way to raise its Technology Readiness Level (TRL) to the level of a commercial product.

We identified two groups of potential customers for such a system:

1. Wind turbine owners (energy operator companies which perform O&M work themselves)
2. Wind turbine manufactures, which may have some identified “issues” with their blades; such customers might be interested in monitoring these issues on the existing fleet.

In order to make the potential customers interested in the SHM system, it is important to provide a “business case” showing the economic benefits of installing such systems on the fleet.

We identified several scenarios utilizing the SHM system and made simple economical calculations to prove the cost efficiency of such a system. One obvious scenario is preventing catastrophic failures of wind turbine blades. However, since no statistics on catastrophic event is available, it was not possible to calculate benefits of such a system.

Blade inspection is another scenario where the effect of blade SHM system is evident. **Table 2** compares the current scenario (visual blade inspection by a team of highly skilled professionals working at height) with using the suggested SHM system. In this case, it was possible to evaluate the potential savings the system can bring.

It became also obvious that bringing the system into the commercial level is impossible without active participation of the potential customers, and a number of steps were taken in this direction. These steps are described in the next section.

Dissemination

The following steps ensuring awareness of potential customers about the blade SHM system were taken:

1. In order to simplify dissemination, a portable (80 cm long) setup was manufactured. Based on the setup, a video was filmed explaining the approach, instrumentation and the main damage detection and localization steps and demonstrating the results. The video is placed in YouTube, on B&K official channel.
2. Based on the data collected via interviews with wind turbine operators and maintenance company (Total Wind), we produced a generic business case showing the advantages of SHM system implementation.
3. Meeting with the Fleet Managers Group:
Leading operator companies working in Scandinavian energy market, including E.ON, Vattenfall, DONG and Statkraft organized an informal group of fleet/asset managers, whose everyday duty is to fulfil the Operation and Management program on wind turbines fleet.
We were invited to such a meeting in October 2014, where we demonstrated the system and the achieved results. The information was met with interest.
E.ON suggested equipping few of their offshore wind turbines with the prototype.
4. Meeting with Statkraft:
We demonstrated the project to the R&D of the fleet management department of Statkraft. Statkraft suggested equipping few their wind turbines with the prototypes, however under the condition that the wind turbine manufacturer is involved.
5. Meetings with a leading Danish wind turbine manufacture.
During January 2015, we presented the system to a leading Danish wind turbine manufacture. The information was met with the interest, and the manufacturer initiated internal business case to evaluate efficiency of the suggested solution.
6. Currently we are also invited to demonstrate the project to another leading Danish wind turbine manufacture; the meeting is scheduled to take place in April 2015.

7. The system was presented as a response to a call from NineSigma, a company representing the (unknown) energy company looking for a blade monitoring solution.
8. Together with DTU Wind, B&K presented the EUDP project at EWEA Offshore Conference and Exhibition, which took place in Copenhagen, 10-12 March 2015 (**Figure 12**). During the exhibition, we had a chance to show the results of the project to several potential customers, also including wind turbine blade manufactures.
9. The results of the project were published in commercial “Windpower Engineering & Development” journal, [16].
10. The developed SHM system prototype will be presented at VDI exhibition and conference “Schwingungen und Dynamik von Windenergieanlagen” in June 2015 in Bremen, Germany and in Husum Wind in Husum, Germany.
11. We also plan to present the prototype and the results in a number of scientific conferences during 2015 (DAMAS, IWSHM, IEEE EESMS).
12. During the project run, in order to evaluate the feasibility of the approach, a number of papers was presented in scientific conferences. The papers are listed in the dedicated section and in the Annex.
13. During WP3, the following dissemination activities took place:
 - Technical meeting series (2011-12)
 - Workshop on 18/19 June 2013
 - EWEA Offshore (10-12 March) 2015 presentations:
 - “Very large wind turbine rotor blades require damage tolerance and damage monitoring”
 - “Damage tolerant design and condition monitoring of composite material and bondlines in wind turbine blades: Failure and crack propagation”
 - DTU Wind E Report “Investigating Material Damage Propagation in Wind Turbine Blades” (May 2015)



Figure 12. DTU Wind booth at EWEA Offshore Exhibition in Copenhagen in March 2015. At the left, there is a poster inviting to attend a presentation of the EUDP project.

Utilization of project results

Results of dissemination

There is an obvious interest to the system from both types of potential customers: wind turbine manufactures and wind turbine operators. Two big energy operator companies, E.ON and Statkraft suggested equipping their wind turbines with the prototypes. However, they are not going to cover the expenses (except the downtime caused by installation). A big Danish wind turbine manufacturer makes a business case to decide if they want to start such a program, utilizing the project results.

Project result utilization

Now, B&K is considering a possibility of developing the SHM commercial system based on the developed prototype.

Patent

The key elements of the suggested SHM system were identified as patentable, and a patent application was filled (European Patent Application No. 14177876.1, "System and methodology for detecting structural damages of wind turbine rotor blades"). Authors: B&K and DTU Compute. Currently the patent is under prosecution.

Use for education

The project initiated a number of master student projects, listed in Table 4.

Table 4. Initiated master projects

Student name	University-department/co-supervisor	Project title	Comments
Mikkel Lagerbon	DTU Electro/B&K	Optimal sensor positioning for structural health monitoring	Investigation of the algorithm for finding optimal sensor location for SHM systems using topology optimization approach
Majse Granberg Hansen	DTU MEK/B&K	Structural Damage Detection using Multisensor Vibration Signals	Parametric study of the covariance method, used in the SHM prototype.
Morten Mengel Kaastrup	DTU MEK/B&K	Optimization of Sensor Positioning in Mechanical Structures	Algorithms for optimal sensor placement using topology optimization approach
Oscar Ramirez Requeson	DTU Wind/B&K	Identification of Modal Parameters Applying Operational Modal Analysis on a Full Scale Operating Vestas V27 Wind Turbine	Application of different modal analysis algorithms to operating data obtained from V27 measurement campaign
Rasmus Johan Johansen and Lasse Majaard Hansen	AAU Civil Eng./B&K	Damage localization in wind turbine blades by use of the damage location vector method	Application of different damage localization techniques to the data obtained from residential-size wind turbine blade and from V27

Commercial plan

We acknowledge that there is a long way from the current Technology Readiness Level (TRL), which we evaluate as a prototype level to a commercial product. During the final part of the project, we evaluated the necessary steps, which need to be done to get the TRL to the higher level. These steps include:

1. Thoughtful evaluation of the commercial side of the project:
 - a. How the end user will benefit from such a system
 - b. What shall be the overall system price level and the cost of the components
2. Identification of the missing parts:
 - a. Areas where more research is needed
 - b. Sensors and data acquisition system satisfying the requirements
 - c. Necessary certifications
3. More validation and testing on the modern wind turbines, with different blade designs

Our strategy is to continue working in this direction, developing a commercial version of the system. The strategy is to team up with system's potential customers in another dedicated project. The reasons for this are:

1. It is important to get the end customer from the beginning to ensure the project moves in a right direction;
2. Only such a partner/partners can provide necessary statistics to evaluate commercial feasibility of the system
3. Only such a customer can provide wind turbines for thoughtful testing and validation
4. During the project, the potential customer will become aware about the system and its capabilities

This dedicated project needs to be publicly funded since still high financial risk and a big amount of partners, which need to be involved into the project.

Project conclusion and perspective

Commercialization of the developed solution

It is clear that the SHM system developed during the project is of wind turbine owners' interest. If a commercial product was available and comfortably priced, there will be definitely a market for such a system. This clearly identifies the next goal: raise the Technology Readiness Level of the current prototype up to the level of commercial product while keeping the price affordable. We can identify the following steps to achieve the goal:

1. Make an economic model of a blade SHM solution. If such a system installed, how much will a wind turbine owner save on rotor O&M? This will define the price of the final product and serve as the selling point.
2. Improve the system durability: the sensors placed on the blades are subject to harsh environments, and they shall serve for 20+ years;
 - This calls for other types of vibration sensors, e.g. fiber-optic accelerometers or strain gauges.
 - The data acquisition unit placed in the rotor, remains one of the most fragile subsystems, and shall be made much more robust;
3. The system shall work together with other subsystems of the wind turbine, this integration is vital
 - The challenge is to design the system with modular architecture which is possible to build into wind turbines from different manufactures;
4. Make the system more attractive for potential customers: the sensors installed on the blade could be utilized for many other purposes, for example:
 - Lightning detection
 - Icing detection
 - Rotor unbalancing detection
 - Blade load assessment: assess to which degree the loading of a particular turbine complies with the design loads
5. Damage development prediction remains an important issue; more research shall be conducted in this field
 - Adaptive prediction of the remaining life time becomes possible but requires research activities
6. The information produced by the system shall be easily interpreted by non-experts, which calls for smart ways of information representation
 - Graphical user interface, including convenient tools for fleet overview
 - Predictive tools incorporated with economic model: estimating risks for different predicted scenarios.

Availability of such a system on the market will definitely improve the efficiency and reduce the cost of rotor O&M programs, contributing in reduction of cost and improving the attractiveness of wind energy.

Perspectives from modelling viewpoint (WP2)

- Damage detection as based on HAWC2 "super-element" damage formulation combined with an extended Kalman filter approach, and linked to this...
- Damage progression modeling ... using the "super-element" feature
- Damage detection as based on isotropy-independent non-parametric methods ... combined with a dedicated MAC-like damage "metric" (MAC: Modal Assurance Criteria)
- Fundamental understanding of the active pulse method ... to optimize sensor and actuator position.

Perspectives from material development viewpoint (WP3)

- A new damage tolerant design approach to reduce cost of energy for Offshore wind
- Strategic targets (2016-19) for DTU Wind materials research section
 - develop more damage resistant composites materials, combine with build-in sensors for damage detection, and increase the reliability of future wind turbine blades
 - Lifetime prediction, Extension, and Design upgrade for blades
- Employees (1 new senior scientist position in the area of SHM and NDE)
- Facility Integration and Hardware investment
 - Fiberlab expansion to include embedded sensors for damage detection and demonstration of structural health (SHM) technologies
 - Multi-channel Acoustic Emission systems, Fibre optic strain, etc.
- DTU Wind demo, V52 “Forskningsmølle” <http://tinyurl.com/mtaack3>
- Industry focused Project Partnerships within EU Horizon 2020
- Current Industry collaboration (LM, Siemens, SSP, Force, Fiberline, Tech. University Munich, Sandia Laboratories, etc.)

Perspectives from decision-making algorithms development (WP4)

- The current project has advanced our competences in the iterative process of setting up experimental design for wind turbines, evaluation of experimental outcomes, signal processing and statistical decision-making.
- The pipeline built in this project can form the basis even more robust statistical methods that may address the task of damage localization and the progression of damage over time.
- The unique data gathered with the operational turbine can be used for tests of more complex signal processing and statistical models
 - The data may also be used to investigate the feasibility of an actuator-free damage detection system.

Published papers

- [1] Tcherniak, D., Larsen G.C. (2013) Application of OMA to an Operating Wind Turbine: Now Including Vibration Data from the Blades. *Proc. Int. Operational Modal Analysis Conference (5th IOMAC)*, Guimarães, Spain.
- [2] Yang, S., Tcherniak, D., Allen, M. S. (2014) Modal Analysis of Rotating Wind Turbine using Multi-blade Coordinate Transformation and Harmonic Power Spectrum, *Proc. 32nd Int. Modal Analysis Conference (IMAC XXXII)*, Orlando, FL, USA.
- [3] Tcherniak, D. (2014) Loss of Rotor Isotropy as a Blade Damage Indicator for Wind Turbine Structural Health Monitoring Systems. *Proc. European Workshop on Structural Health Monitoring (EWSHM)*, Nantes, France.
- [4] Larsen, G.C., Berring, P., Tcherniak, D., Nielsen, P.H., Branner, K. (2014) Effect of a Damage to Modal Parameters of a Wind Turbine Blade. *Proc. European Workshop on Structural Health Monitoring (EWSHM)*, Nantes, France.
- [5] Ulriksen, M.D., Tcherniak, D., Kirkegaard, P.H., Damkilde, L. (2014) Operational Modal Analysis and Wavelet Transformation for Damage Identification in Wind Turbine Blades. *Proc. European Workshop on Structural Health Monitoring (EWSHM)*, Nantes, France.
- [6] Mevel, L., Gueguen, I., Tcherniak, D. (2014) LPTV Subspace Analysis of Wind Turbine Data. *Proc. European Workshop on Structural Health Monitoring (EWSHM)*, Nantes, France.
- [7] Tcherniak, D., Yang, S., Allen, M.S. (2014) Experimental characterization of operating bladed rotor using harmonic power spectra and stochastic subspace identification. *Proc. Int. Conference on Noise and Vibration Engineering (ISMA)*, Leuven, Belgium.
- [8] Tcherniak, D., Allen, M.S. (2015) Experimental Characterization of an Operating Vestas V27 Wind Turbine Using Harmonic Power Spectra and OMA SSI, *Proc. Int. Operational Modal Analysis Conference (5th IOMAC)*, Gijon, Spain.
- [9] Ramirez, O., Tcherniak, D., Larsen, G.C. (2015) Comparative Study of OMA Applied to Experimental and Simulated Data from an Operating Vestas V27 Wind Turbine, *Proc. Int. Operational Modal Analysis Conference (5th IOMAC)*, Gijon, Spain.
- [10] McGugan, M., Pereira, G., Sørensen, B.F., Toftegaard, H., Branner, K. (2015) Damage tolerance and structural monitoring for wind turbine blades. *Phil. Trans. R. Soc. A 373*: 20140077.
<http://dx.doi.org/10.1098/rsta.2014.0077>
- [11] Tcherniak, D., Mølgaard, L.L. (2015) Vibration-based SHM System: Application to Wind Turbine Blades. *Proc. 11th Int. Conference on Damage Assessment of Structures (DAMAS)*, Ghent, Belgium.
- [12] Hansen, L.M., Johansen, R.J., Ulriksen, M.D., Tcherniak D., Damkilde, L. (2015) Statistical evaluation of characteristic SDDL-induced stress resultants to discriminate between undamaged and damaged elements. *Proc. 11th Int. Conference on Damage Assessment of Structures (DAMAS)*, Ghent, Belgium.
- [13] Johansen, R.J., Hansen, L.M., Ulriksen, M.D., Tcherniak D., Damkilde, L. (2015) Damage localization in a residential-sized wind turbine blade by use of the SDDL method. *Proc. 11th Int. Conference on Damage Assessment of Structures (DAMAS)*, Ghent, Belgium.
- [14] Garcia, D., Tcherniak, D., Trendafilova, I. (2015) Damage assessment for wind turbine blades based on a multivariate statistical approach. *Proc. 11th Int. Conference on Damage Assessment of Structures (DAMAS)*, Ghent, Belgium.
- [15] Buliga, A., Jensen, F.M. (2014). Blade Failure Catalogue Ver. 2. *Bladena*
- [16] Tcherniak, D., Hansen, J.J. (2015) Algorithms Simplify and Predict Blade Maintenance, *Windpower Engineering & Development*. February 2015 issue.

- [17] Ulriksen, M.D., Damkilde, L., Tcherniak, D., (2015) Damage detection in an operating Vestas V27 wind turbine blade by use of outlier analysis, *Submitted to Environmental, Energy and Structural Monitoring System (EESMS) Conference*.

Annex

The Annex contains the copies of the papers listed in the previous section.



IOMAC'13

5th International Operational Modal Analysis Conference
2013 May 13-15 Guimarães - Portugal

APPLICATION OF OMA TO AN OPERATING WIND TURBINE: NOW INCLUDING VIBRATION DATA FROM THE BLADES

Dmitri Tcherniak¹, and Gunner Chr. Larsen²

ABSTRACT

The presented study continues the work on application of Output Only Modal Analysis (OMA) to operating wind turbines. It is known from previous studies that issues like the time-varying nature of the equations of motion of an operating wind turbine (in particular the significant harmonic components due to the rotor rotation) as well as the considerable aerodynamic damping make OMA of operating wind turbines a difficult task. While in the previous works OMA was based on data provided by sensors mounted on the wind turbine tower and nacelle, we here attempt to improve the results by instrumenting the blades as well. It is believed that the availability of vibration data from the blades will improve the observability of the main global vibration modes (especially the heavily damped out-of-plane modes), and thus will assure a better estimation of modal parameters, especially the damping.

The paper discusses the technical challenges regarding blade instrumentation and data acquisition, data processing applied to eliminate the time-varying nature of an operating wind turbine in the resulting eigenvalue problem and, finally, it presents and discusses the initial results.

Keywords: OMA, Operating Wind Turbine, Blade Acceleration Measurements, Multi-blade (Coleman) transformation

1. INTRODUCTION

An optimal, economically efficient design of wind turbines requires understanding of wind turbine dynamics. Dedicated aeroelastic simulation packages have been developed for aiding engineers in the wind turbine industry to design efficient wind turbines by simulating their dynamic response under different wind conditions, and thereby estimating their performance and durability during the life time. However, numerous uncertainties are inevitable in the numerical modeling (including numerical models and algorithms behind the scenes, properties of the materials used in the design, joints of substructures, their boundary conditions, etc.). This requires validation of the numerical model against reality and, if necessary, a corresponding model tuning.

¹ Research Engineer, Brüel & Kjær Sound & Vibration Measurement, dtcherniak@bksv.com

² Senior Scientist, DTU Wind Energy, Technical University of Denmark, gula@dtu.dk

Session 1, Dmitri Tcherniak, Gunner C. Larsen

A typical engineering approach to analyze structural dynamics of a wind turbine involves its representation as a linear time-invariant (LTI) system of equations followed by its modal decomposition. However, modeling an operating wind turbine, even by a simple analytical model [1, 2], one arrives at a time-variant system, whose equations of motion (EOM) can be written as a set of first order equations:

$$\dot{\mathbf{x}}(t) = \mathbf{A}(t)\mathbf{x}(t), \quad (1)$$

where \mathbf{x} is a state vector describing the state of the rotating rotor with N blades and its non-rotating supporting structure:

$$\mathbf{x} = \{\dot{q}_{1,1}, \dot{q}_{1,M}, \dots, \dot{q}_{N,1}, \dot{q}_{N,M}, \dot{s}_1, \dots, \dot{s}_L, q_{1,1}, q_{1,M}, \dots, q_{N,1}, q_{N,M}, s_1, \dots, s_L\}^T, \quad (2)$$

in which the state of each blade is described by M variables, q_{ij} , where the first index is the blade number, and the second index is the number of the variable on the blade. s_1, \dots, s_L describe the non-rotating part. Assuming the rotor speed, blade pitch and yaw angle not changing significantly during the observation period, one arrives at a periodic system. If we further assume moderate deflection perturbations on a mean deflection field, the system of equations may finally be approximated by a linear periodic time variant (LPTV) system with periodic system matrix

$$\mathbf{A}(t+T) = \mathbf{A}(t), \quad (3)$$

where T is the rotor revolution period.

There are two common approaches to LPTV systems: 1) Lyapunov-Floquet (L-F) transformation [3]; and 2) Coleman transformation (also known as multi-blade transformation, MBC) [4]. MBC is more straightforward but assumes, however, rotor isotropy, and is thus applicable only for wind turbines with at least 3 blades (uniformly azimuthally distributed). L-F transformation does not have these limitations. L-F transformation does not have these limitations. It can be shown that under MBC-specific assumptions, there is a similarity between these two transformations [5].

In the case of a three-bladed rotor, the MBC transformation transforms each set of variables $\{q_{1,k}, q_{2,k}, q_{3,k}\}^T$ into so-called multi-blade coordinates given by

$$a_{0,k} = \frac{1}{3} \sum_{i=1}^3 q_{i,k}, \quad a_{1,k} = \frac{2}{3} \sum_{i=1}^3 q_{i,k} \cos \psi_i, \quad b_{1,k} = \frac{2}{3} \sum_{i=1}^3 q_{i,k} \sin \psi_i, \quad (4)$$

where ψ_i is the azimuth angle of the i^{th} blade¹.

After substituting the multi-blade coordinates into the EOM, the original LPTV system will convert to an LTI system:

$$\dot{\tilde{\mathbf{x}}}(t) = \tilde{\mathbf{A}} \tilde{\mathbf{x}}(t), \quad (5)$$

with a new time invariant system matrix $\tilde{\mathbf{A}} = \text{const}(t)$, and the state vector

$$\tilde{\mathbf{x}} = \{\dot{a}_{0,1}, \dot{a}_{1,1}, \dot{b}_{1,1}, \dots, \dot{a}_{0,N}, \dot{a}_{1,N}, \dot{b}_{1,N}, \dot{s}_1, \dots, \dot{s}_L, a_{0,1}, a_{1,1}, b_{1,1}, \dots, a_{0,N}, a_{1,N}, b_{1,N}, s_1, \dots, s_L\}^T. \quad (6)$$

Applying the MBC transformation to analytically derived EOM for a simple but representative model of a wind turbine, followed by model decomposition, Hansen [1] arrives at modes in multi-blade (MB)

¹ For a three-bladed rotor, $\psi_2 = \psi_1 + 2\pi/3$ and $\psi_3 = \psi_1 + 4\pi/3$. Note, $\sum_{i=1}^3 \cos \psi_i = 0$ and $\sum_{i=1}^3 \sin \psi_i = 0$.

coordinates, which are subsequently translated into the original coordinates x by the inverse MBC transformation:

$$q_{i,k} = a_{0,k} + a_{1,k} \cos \psi_i + b_{1,k} \sin \psi_i \quad (7)$$

Here some interesting features of wind turbine dynamics become apparent. For example, the theory predicts that the blade dynamics can be described as a sum of collective, backward- and forward-whirling components which are evolving with the change of the rotor speed [1].

The approach described above presumes the EOM are known. Let us now focus on the experimental parameter identification when the EOM are not known. The use of L-F transformation was demonstrated by Allen and coworkers [6]. In the presented study, another approach is utilized: the time histories of acceleration signals measured on the blades are combined with the measured azimuth angle into the MB coordinates (4); and subsequently, a standard output only modal analysis algorithm (e.g., OMA SSI) is applied to the obtained MB time histories. This approach was first suggested in [7] and demonstrated on simulated time histories from the ALSTOM Eco-100 wind turbine. The presented paper applies the same approach to the measured full-scale data.

In 2010, Brüel & Kjær and ALSTOM Wind conducted a project aimed at modal identification of operating 3MW Eco-100 wind turbine [8, 9]. In that project the measurements were done on the tower and nacelle only. The project showed that most of the lower tower and rotor global modes could be successfully extracted from the tower/nacelle measurements only. By means of Campbell diagram, the evolution of the modal frequencies and damping coefficients with rotor speed was demonstrated. Applying the same approach to a large number of datasets recorded during 5 months of observation, it was possible to provide estimation of uncertainties of modal parameters. However, since the blades were not instrumented, it was not possible to visualize the mode shapes of the rotor. Also the identification of the rotor modes based on the tower and nacelle mode shapes was not a straightforward task. Finally, the uncertainties with damping estimation especially for out-of-plane modes were too high. It is anticipated that availability of the data from the blades will help to overcome the abovementioned problems.

To the authors' knowledge, there are very few published works which refer to vibration measurements on a wind turbine rotor while operating, for example [10]. Perhaps, the main limiting factor is technical difficulties in obtaining such data. Indeed, there are many technical challenges such as mounting accelerometers on the blades isotropically; wireless data transfer from the rotating part to the ground and synchronization of the data from the rotor with the data from the non-rotating parts (tower and nacelle). In order to collect enough data for different wind conditions, the sensors and data acquisition system should be able to survive under sometimes harsh weather conditions for a long time, not to mention that the acquisition system should be robust enough to operate unmanned. This defines the scope of the paper: the main focus is on the description of the measurement system and the setup. The feasibility of the setup is demonstrated by the results for the case when the turbine is on brake (i.e., not rotating). However, we have to limit the scope of the paper presenting only the preliminary results for an operating wind turbine that are available at the time of writing.

2. MEASUREMENT SYSTEM AND INSTRUMENTATION

The availability of a wind turbine often defines the scale of the measurement campaign. Vestas V27 which belongs to DTU Wind Energy, (former Risø Danish National Lab for Sustainable Energy) was chosen for the present campaign. On today's scale, this is a small wind turbine with 225kW rated power, 27 m rotor diameter and the hub about 30 m above the ground. However, despite its age, V27 has a design similar to many modern horizontal-axis wind turbines; most importantly,



Figure 1. Vestas V27

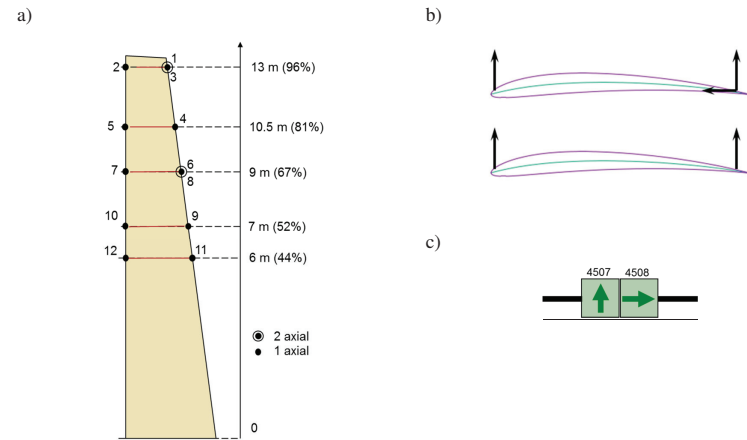


Figure 2 a) Accelerometers location on the blade; b) blade sections equipped with three and two accelerometers; c) placement of the accelerometers with the side mounted and top mounted connectors.

it is pitch-regulated and has three blades. The blades are relatively stiff, and their small size determines the high rotor speed: nominally 46 RPM.

2.1. Instrumentation of the blades

Selection of the number of accelerometers to be mounted on each blade is a result of a compromise between the spatial resolution of the obtained mode shapes (which is directly linked with the ability to identify higher modes) and the complexity and cost of the acquisition system. Knowing the approximate shapes of the lowest flapwise, edgewise and torsional modes, it was decided that 12 channels would be used per blade. The same approximated mode shapes aided with the choice of the accelerometer locations: 5 blade sections were chosen; 10 accelerometer positions were selected to monitor the flapwise vibrations (to resolve flapwise and torsional modes), and two positions were selected for edgewise vibration monitoring (Figure 2). Experience gained as results of numerical simulations using the HAWC-2 simulation software guided the selection of the accelerometers' sensitivity. Three types of accelerometers were chosen¹: the less sensitive to be located closer to the blades, tip, more sensitive – closer to the blades' root. The accelerometers with top-mounted connector were used in the edgewise monitoring, while those with side-mounted connector were used for the flapwise monitoring (Figure 2c).

For MBC transformation, it is important that accelerometers on all blades are mounted similarly, for example, that the position and orientation of the accelerometers mounted at point 1 (Figure 2) on all three blades are as similar as possible. This is quite difficult to implement in practice since it involves precise work at height. Due to a small size of V27, it was possible to dismount the entire rotor and place it on the ground, which significantly simplified the instrumentation task. In order to ensure similarity in accelerometers position and orientation, a special template was made (Figure 3a). A laser distance meter ensured the same distance from each blade section to the hub. The accelerometer cables run on the outer surface of the blade, along the trailing edge. Some free cable length was allowed to account for blades' operational deformation. The cables were fixed with silicon and covered by "helicopter tape" (Figure 3b).

¹ B&K Type 4507-B-006 (0.2-6000Hz, 500mV/g, $\pm 14g$), Type 4508-B-004, same specifications as the first one but with top mounted connector and more sensitive Type 4507-B-002 (0.4-6000Hz, 1000mV/g, $\pm 7g$).

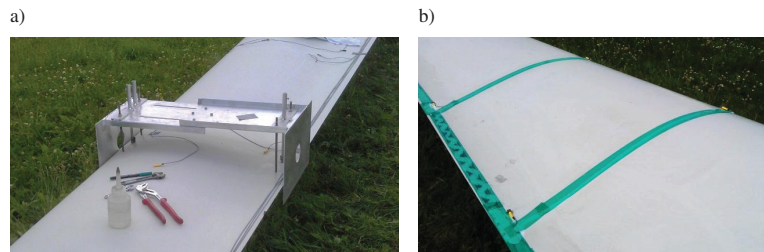


Figure 3 a) Template for accelerometer mounting; b) Cabling

2.2. Data acquisition system

The data acquisition system consists of two parts: a 42-channel front-end in the hub and one 12-channel module in the nacelle. Special requirements are set for the sub-system in the hub: since it shall be rotating with the rotor and is exposed to tough environmental conditions, it shall be extra robust and waterproof. It was decided to implement the system based on 5-Module Brüel & Kjaer (B&K) LAN-XI frame Type 3660-C fitted with three 12-channels modules Type 3053-B-120 with 50-pin Sub-D panel (one module per blade). This panel ensures the robust connection of accelerometer cables to the front-end. The fourth module is a 6-channel Type 3050-A-060 with a panel equipped with four LEMO and two BNC connectors. This module collects data from a synchronization IRIG-B signal as well as from two DC accelerometers for measuring azimuth and pitch angle signal. The purpose of this equipment will be explained later.

The frame was placed in a waterproof box (Figure 4a) together with a Cisco access point AP-1262 and an IRIG-B time code generator ES-292. The box was mounted inside the V27's spinner (Figure 4b). The equipment in the box is powered over a slip ring (24VDC).

The nacelle sub-system is a 12-channel B&K LAN-XI data acquisition module Type 3053-B-120. Three 3-axial accelerometers¹ placed on the nacelle structure are connected to the module. The tower is not instrumented in the current scenario. There is also a high-speed shaft tachoprobe and an IRIG-B signal generator connected to the same module.

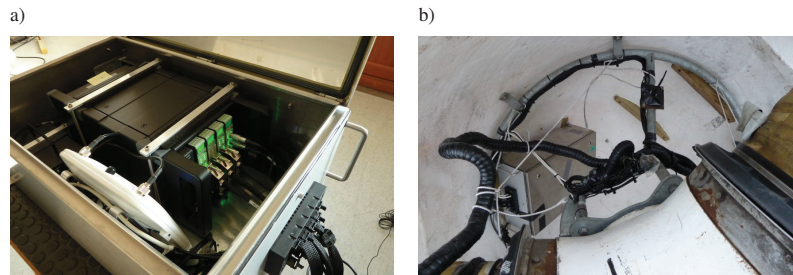


Figure 4 a) Waterproof box with 42-ch. data acquisition system; b) the box mounted inside V27's spinner.

¹ B&K Type 4506-B-3 (0.3-2000Hz, 500mV/g, ±14g)

2.3. Wireless data transmission

B&K LAN-XI data acquisition modules transmit data using Ethernet protocol. This makes it possible to employ a standard 3rd party wireless access point to replace a wired link by a wireless connection between the rotating and non-rotating sub-systems. In order to avoid drops in connection, advanced access points were employed. Cisco AP-1262 supports wireless protocol 802.11n ver.2 with multiple-input multiple-output with two spatial streams. This is important in the current scenario where transmitting and receiving parts move against each other, and the line of sight between antennas is often blocked by rotating elements.

The connection employs two AP-1262. One is inside the waterproof box and uses two omnidirectional 5GHz antennas for data transmission. The other is located in the nacelle and receives the data using two directional antennas.

2.4. Other equipment

MBC-transformation requires the instantaneous position of the rotor (azimuth angle) as well as orientation of the blades (pitch angle). In the previous project [8, 9], the pitch, yaw and azimuth angles were possible to obtain from the wind turbine control system. This is not the case with the current setup. V27 does not allow any access to its control system; thus the pitch and azimuth angles that are necessary for the modal analysis need to be measured.

The azimuth is measured indirectly by means of two DC accelerometers (B&K Type 4574-D, 0-500Hz, 200mV/g, ±10g). The accelerometers are mounted inside the waterproof box.

In-plane and out-of-plane stiffness of the rotor depends on pitch angle. The pitch on V27 is regulated mechanically using a hydraulically driven rod passing inside the main shaft. The position of the rod defines the pitch angle and a position sensor (ASM WS10-420T) is employed to measure the rod position. There is a geometrical non-linearity between pitch angle and rod position, and to resolve this, a multi-point sensor calibration was performed.

The two DC accelerometers and the pitch sensors are connected to the hub front-end.

A laser tachoprobe (B&K Type 2981) is mounted on the generator providing one pulse per revolution of the high speed shaft. The tacho signal is used to estimate the rotation speed of the rotor. The tachoprobe is connected to the nacelle front-end.

2.5. Synchronization

B&K LAN-XI technology uses Precision Time Protocol (PTP) for module synchronization over Ethernet. However, the wireless Ethernet protocols cannot guarantee that the transit time of a message going from the master module to a slave module is equal to the transit time of a message going from the slave to the master, which is one of the main PTP assumptions. This means that LAN-XI modules cannot be synchronized when a wireless connection is used.

In order to overcome this, external synchronization events can be utilized. A GPS signal holds information about precise time, and it can be used for module synchronization. An IRIG-B signal can be generated from the GPS signal by means of IRIG-B code generator (e.g., ES-292). IRIG-B signal (Figure 5) is an amplitude modulated signal with 1kHz carrier frequency which encodes precise time. By recording IRIG-B signals synchronously with other signals, on two non-synchronized front-ends, one can post-synchronize the two data streams.

Figure 5 shows two IRIG-B signals, the top one is recorded by the nacelle front-end, the bottom one by the hub front-end. There is about 0.5ms delay between the two signals. The delay constantly changes, and can become both positive and negative. The biggest delay observed in the recordings was about 2 ms, which may result in a 72^o phase error on 100Hz if post-synchronization is not performed.

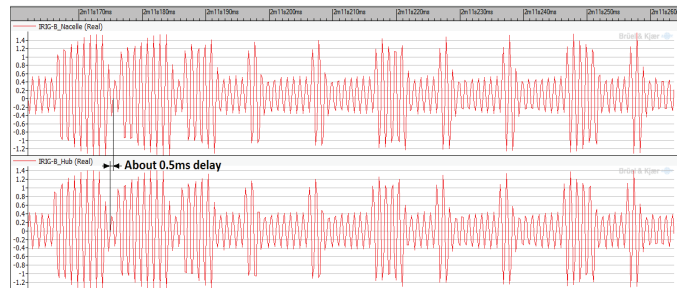


Figure 5. IRIG-B signals from the nacelle front-end (top) and hub front-end (bottom) and the delay between them.

3. MEASUREMENTS

The data collected by the hub and nacelle front-ends are transmitted via standard Ethernet cable to a computer located on the first platform in the tower (about 4m above ground). No analysis is performed; the data are simply recorded to an external hard disk using B&K PULSE Time Data Recorder Type 7708. A total of 51 channels are sampled at 4096Hz. Such a high sampling frequency is not necessary for modal analysis where the concerned modes have frequencies below 40Hz. The high sampling frequency was chosen as the data will be used for purposes that are out of scope of this paper. The data is saved in 5 minutes chunks with the possibility of appending the chunks if post-processing requires a longer time history.

The measurements were started on 31 October 2012, and are going on at the time of writing. Weather condition information during the observation period is available from one of the weather masts located nearby the V27. The weather mast provides full information including temperature, wind speed and wind direction at different heights, etc., stored as mean values and standard deviations for every 10-minute interval.

4. RESULTS

At the time of writing, only preliminary results are available. Three cases are considered below: the wind turbine with brake applied; idle case and normal operating case.

4.1. V27 with the brake engaged

This case is the simplest for analysis but it is quite a rare state of a wind turbine. Typically, when a wind turbine is not operating, it is set to *idle*. This means that the blades pitch set to maximum thus creating least aerodynamic loads from the wind. The rotor freely and slowly rotates due to wind loading. The idle case will be considered in the next section.

When the brake is engaged, the rotor is fixed. In the case of no pitch and yaw activity, the wind turbine becomes a time-invariant system. This greatly simplifies modal analysis since all OMA assumptions are fulfilled. This trivial case is briefly considered here to revisit the main modes of a typical horizontal axis wind turbine.

The V27 brake was engaged when one of the blades was pointing upwards and 15 minutes of data were recorded. OMA was performed using B&K PULSE OMA Type 7760, and the Stochastic Subspace Iterations with Un-weighted Principal Components (SSI UPC) method was employed.

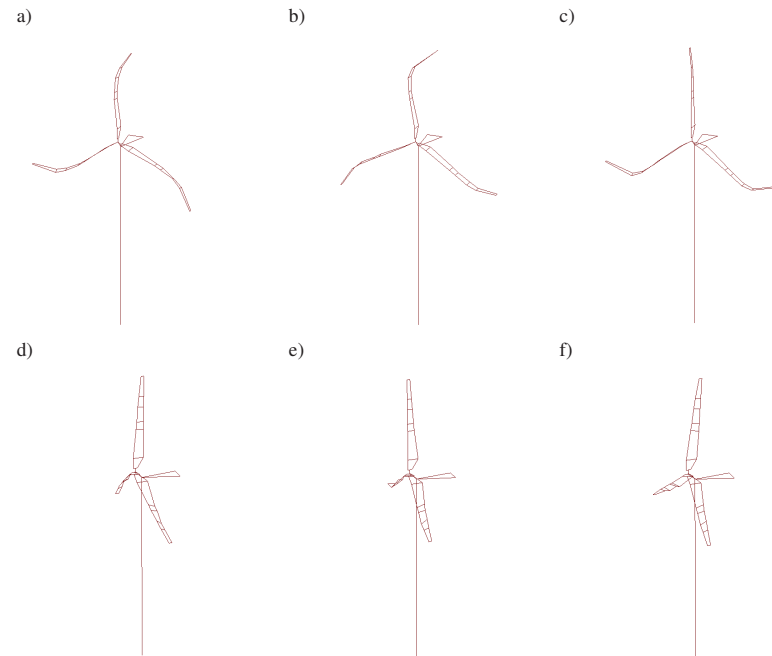


Figure 6. Typical families of modes for a horizontal axis wind turbine. Top: 2nd in-plane mode, a) collective, b) yaw, c) tilt; Bottom: 1st out-of-plane mode: d) collective, e) yaw, f) tilt.

Let us consider a *single* blade clamped at the root. The blade has a number of modes can be categorized into three categories: flapwise, edgewise and torsional. This subdivision is artificial since the modes often interact. Now let us consider a *rotor* with three almost identical blades joined together via the hub. Each mode of a *single* blade constitutes a *family* of three rotor modes. Depending on their phase and the reaction of the rest of the structure, the modes in the family are called collective, tilt- and yaw-mode [1]. Figure 6 demonstrates two such families. The second flapwise mode of the single blade becomes a family of *three* second in-plane modes (since the pitch is almost 90° when the brake is engaged), Figure 6 a,b,c. The first edgewise mode of the single blade becomes a family of three first out-of-plane modes, Figure 6 d,e,f. The rotor modes interact with the nacelle and tower, and can also involve torsional motion of the blades. The frequencies of the modes in the same family differ since the supporting structure (the tower and nacelle) is not symmetric. In-plane modes have generally higher damping compared to the out-of-plane modes due to the higher aerodynamic damping of a blade in flapwise direction.

4.2. Idle case

The idle and braked cases are very similar: the turbine is not operating and the pitch angle is set to maximum. However, from the dynamic perspective the cases are different. Allowing free rotation of the low-speed shaft adds an extra degree of freedom to the system. This should affect the modes involving rotor in-plane motion, mainly collective modes and drive-train modes.

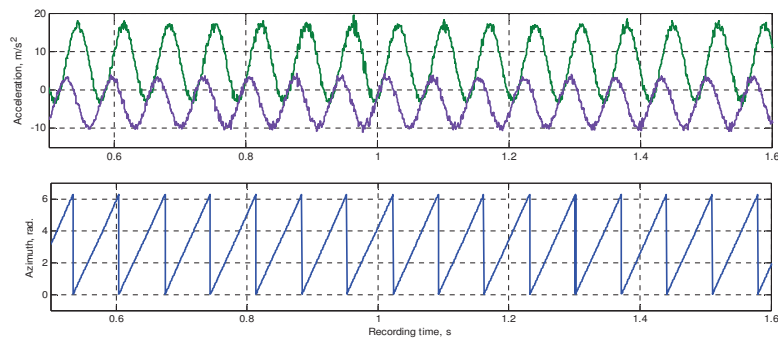


Figure 7. Top: row DC accelerometers signals; bottom: calculated azimuth angle.

As mentioned above, when the turbine is idle, the rotor is slowly rotating due to wind loading. This prevents the modelling of idling wind turbine as an LTI system. At the same time, the speed of rotation is not constant, which prevents using methods designed for LPTV systems.

To overcome this, one has the following options:

- 1) Use the datasets where the rotor is not rotating for a sufficiently long observation time. However, according to experience, this happens only when no wind is present. Unfortunately, in this case, there is also no wind excitation of the structure that can cause vibrations sufficient for application of OMA.
- 2) Ignore data from the blades. As was shown in [9], it is possible to identify the modal parameters based on the accelerations measured on the non-rotating parts only. In this case, however, the mode shapes of the rotor will not be observed.

4.3. Operating case

For the operating case, the datasets characterized by constant rotor speed and no pitch activity were selected. Signals from the DC accelerometers were LP-filtered to refine the sinusoidal component due to the rotor rotation in the field of gravity. Subsequently, the mean was subtracted from the obtained time histories to remove the DC-offset due to the centrifugal force due to eccentricity of the DC-accelerometer mounting point. Using zero-crossings of these conditioned time histories, the azimuth angle was estimated assuming constant rotor speed within each half revolution which, taking into account the huge moment of inertia of the rotor, is believed to be a valid assumption¹. The input and output of the algorithm outlined above are shown in Figure 7.

Since the azimuth angle can be determined up to a constant phase, it is also possible to use a high-speed shaft tachometer signal for this purpose. However, the exact gear ratio of the V27 gearbox was not known. Using the known approximate gear ratio could lead to a significant bias error in the azimuth estimation during a long observation period; thus this method was not used.

The estimated instantaneous rotor azimuth angle was used to convert the accelerations measured on the rotating parts into multi-blade coordinates according to (4). The acceleration signals measured on non-rotating parts were appended to the multi-blade coordinate time histories as they are. Subsequently, a standard OMA SSI was applied to the aggregated dataset. The results are the modal parameters of the underlying LTI system. The modal frequencies and damping coefficients can be used directly; the visualization of the physical mode shapes can be obtained from the inverse Coleman

¹ This assumption was verified against the RPM-profile calculated based on the HSS tachometer signal.

transformation (7), where ψ_1 could either be selected fixed or changing in time as $\psi_1(t) = \Omega t$, where Ω is the mean rotor angular velocity.

At the time of writing, analysis of the data is not complete; just a few datasets were processed to check the validity of the results (Figure 8). As expected, the harmonics are clearly seen in the spectra, which calls for some harmonic removal pre-processing, either by synchronous averaging or by the cepstral-based method suggested in [11]. Also, since the OMA assumptions are not completely fulfilled under operating loading [12], many sporadic computational modes are experienced. It has been shown [13], that a clustering approach can be successfully used for filtering these modes.

5. FURTHER RESEARCH

It is planned to develop a procedure that will be able to apply all above-mentioned pre-processing steps (post-synchronization, harmonic removal, multi-blade transformation) and perform SSI-based modal parameters estimation in an automatic manner. As for the post-processing, automatic clustering will filter out the computational modes. Having the modal parameters for known weather conditions will allow creation of a map of normal/reference states of the particular wind turbine, which can be used, for example, for structure health monitoring purpose.

Multi-blade coordinate transformation employed in this study assumes rotor isotropy as well as isotropy of the sensors. In reality these assumptions are never exactly fulfilled. Therefore it is also appealing to take advantage of the Lyapunov-Floquet analysis approach, which does not set any requirements regarding the isotropy.

6. CONCLUSIONS

The paper presents the main steps to convert a periodic time-variant dynamic system to a time-invariant analogy, which then can be analysed using conventional output-only modal analysis. The approach, which has been previously validated on simulated data, is now being applied to full scale measured data. For this reason, a data acquisition system was designed and mounted on a test Vestas V27 wind turbine. The system is capable of measuring accelerations on the blades when the turbine is operating, and synchronizing the data stream from the rotating part with the data measured on non-rotating part of the wind turbine. The details of the acquisition system are given. Some preliminary results of output-only modal analysis applied to a parked and operating wind turbine are presented and discussed.

ACKNOWLEDGEMENTS

The work is partly supported by EUDP (Danish Energy Technology Development and Demonstration Programme), grant number 64011-0084 "Predictive Structure Health monitoring of Wind Turbines". The authors greatly appreciated the help from DTU Wind Energy technicians who made the instrumentation of the test V27 wind turbine possible.

REFERENCES

- [1] Hansen M.H. (2003) Improved Modal Dynamics of Wind Turbines to Avoid Stall-induced Vibrations. *Wind Energy* 6:179-195

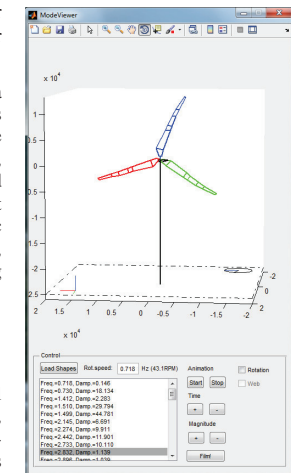


Figure 8. MATLAB® GUI for mode visualization on operating wind turbine. Presumably, the first in-plane forward whirling mode is shown.

- [2] Bir G. (2008) Multiblade Coordinate Transformation and Its Application to Wind Turbines. In: *Proc. ASME Wind Energy Symposium* Reno, Nevada
- [3] Johnson W. (1980) *Helicopter Theory*. Princeton University Press: Princeton, NJ.
- [4] Meirovitch L. (1970) *Methods of Analytical Dynamics*. McGraw-Hill, New-York.
- [5] Skjoldan P.F., Hansen M.H. (2009) On the similarity of the Coleman and Lyapunov-Floquet transformations for modal analysis of bladed rotor structures. *Journal of Sound and Vibration* 327: 424-439
- [6] Allen M.S., Sracic M.W., Chauhan S., Hansen M.H. (2011) Output-only modal analysis of linear time-periodic systems with application to wind turbine simulation data. *Mechanical Systems and Signal Processing* 25: 1174-1191
- [7] Tcherniak D., Chauhan S., Rossetti M., Font I., Basurko J., Salgado O. (2010). Output-only Modal Analysis on Operating Wind Turbines: Application to Simulated Data. In: *Proc. of European Wind Energy Conference*, Warsaw, Poland
- [8] Tcherniak D., Basurko J., Salgado O., Urresti I., Chauhan S., Carcangiu C.E., Rossetti, M. (2011) Application of OMA to operational wind turbine. In: *Proc. of Int. Operational Modal Analysis Conference*, Istanbul, Turkey
- [9] Chauhan S., Tcherniak D., Basurko J., Salgado O., Urresti I., Carcangiu C.E., Rossetti M. (2011) Operational Modal Analysis of Operating Wind Turbines: Application to Measured Data. In: *Proc. 29th Int. Modal Analysis Conference*
- [10] Adams D., White J., Rumsey M., Farrar C. (2011) Structural health monitoring of wind turbines: method and application to a HAWT. *Wind Energy* 14: 603-623.
- [11] Randal R.B., Peeters B., Antoni J., Manzano S. (2012) New cepstral methods of signal pre-processing for operational modal analysis. In: *Proc. Int. Conference on Noise and Vibration Engineering (ISMA)*, Leuven, Belgium.
- [12] Tcherniak D., Chauhan S., Hansen M.H. (2010) Applicability Limits of Operational Modal Analysis to Operational Wind Turbines. In: *Proc. 28th Int. Modal Analysis Conference*
- [13] Tcherniak D., Carcangiu C.E., Rossetti, M. (2012) Application of OMA to Operational Wind Turbine: Methods for Cleaning Up the Campbell Diagram. In: *Proc. Int. Conference on Noise and Vibration Engineering (ISMA)*, Leuven, Belgium.

Modal Analysis of Rotating Wind Turbine using Multiblade Coordinate Transformation and Harmonic Power Spectrum

Shifei Yang

Shifeiy@gmail.com

Department of Engineering Physics

University of Wisconsin-Madison

Dmitri Tcherniak

Research Engineer

dmitri.tcherniak@bksv.com

Briuel & Kjaer SVM

&

Matthew S. Allen

Associate Professor

msallen@engr.wisc.edu

Department of Engineering Physics

University of Wisconsin-Madison

Abstract

Understanding and characterization of wind turbine dynamics, especially when operating, is an important though challenging task. The main problem is that an operating wind turbine cannot be truly modeled as a time invariant system, which limits the applicability of conventional well-established modal analysis methods. This paper compares two experimental techniques that characterize the dynamic behavior of an operating horizontal axis wind turbine (Vestas V27, 225kW, rotor diameter 27m, 12 accelerometers on each blade). The first method uses a multiblade coordinate transformation to convert the time periodic system into a time invariant one, assuming that the system is perfectly isotropic. Conventional operational modal analysis then can be applied to identify the modal parameters of the time invariant model. The second method processes the periodic response directly based on an extension of modal analysis to linear time periodic systems. It utilizes the harmonic power spectrum, which is analogous to the power spectrum for a time invariant system, to identify a periodic model for the turbine. This work demonstrates both of these methods on measurements from the operating turbine and discusses the challenges that are encountered. The procedure is demonstrated by using it to extract the time-periodic mode shapes of the first edge-wise modes, revealing that this turbine apparently has non-negligible blade-to-blade variations and hence the dynamics of these modes are considerably different than one would expect for an anisotropic turbine.

1. Introduction

The design of modern wind turbines heavily relies on accurate numerical models, which are used extensively to simulate the dynamic behavior of the wind turbines under different operating conditions. As a consequence, good experimental tools are necessary to validate the numerical models. However, it is quite challenging to experimentally characterize the dynamics of a wind turbine, especially when it is operating. One significant challenge is that many real turbines cannot be adequately modeled as a Linear Time Invariant (LTI) because of blade-to-blade variations, stratification in the flow field, and rotation of the rotor. If the angular speed of the rotor is constant then a wind turbine might be modeled as a Linear Time Periodic (LTP) system in order to characterize its behavior. This requires other methods, different from the conventional well-established modal analysis methods that are normally used for LTI systems.

This paper compares two experimental techniques for identifying wind turbines; the multiblade coordinate (MBC) transformation and the harmonic power spectrum. The MBC transformation, also known as the Coleman transformation, was first introduced in [1]. The idea behind the MBC transformation is to substitute the deflections of the blades measured in the blade coordinate system by some special variables, which combine the deflections of all three blades. MBC transformation results in elimination of the periodic terms in the equations of motion, thus making the system time invariant so that conventional modal analysis techniques can be applied. A fundamental requirement for the MBC transformation is that the rotor is isotropic [2], namely that all blades are identical and symmetrically mounted on the hub. When focusing on experimental techniques, it is also necessary that measurement system is symmetric, i.e. the sensors are mounted identically on all three blades [3]. In a prior work, Tcherniak et al. used the MBC transformation on simulated wind turbine data in order to obtain a wind turbine Campbell diagram, i.e. a graph presenting the dependency of the modal parameters on the rotor speed [4].

The second method, the harmonic transfer function for linear time periodic systems, was developed to process the response of the linear time periodic system directly [5]. It is known that when a single frequency input is applied to an LTI structure, the response will be at the same frequency but with a different phase and amplitude. In contrast, the response of an LTP system will contain a component at the excitation frequency as well as an infinite number of its harmonics, separated by an integer multiple of rotation frequency. The harmonic transfer function is analogous to the transfer function of a time invariant system, but relates the exponentially modulated input (i.e., an input signal described by a central frequency and a series of equally spaced harmonics) to the exponentially modulated output at the same collection of frequencies. Allen et al. extended the harmonic transfer function to the case where the input cannot be directly measured by introducing the harmonic power spectrum [6], and the modal parameters of a 5MW turbine were identified from simulated data. Later, the harmonic power spectrum was combined with continuous-scan laser Doppler vibrometry, measuring the first few mode shapes along a single blade of a parked 20KW wind turbine under wind excitation [7].

In this work, both the MBC transformation and harmonic power spectrum were employed to process measurements from an operating turbine under wind excitation. First, the formulation of *modes* of an LTV system used in both methods is discussed and compared. Then, the methods are applied to a horizontal axis wind turbine (Vestas V27, 225kW, rotor diameter 27m), which was instrumented with accelerometers on three blades and in the

nacelle [3]. The identified modal parameters from both methods are discussed and compared to evaluate their validity. The rest of this paper is organized as follows: Section 2 introduces the theoretical basis for the MBC transformation and the harmonic power spectrum; Section 3 introduces the wind turbine and sensor arrangement. Sections 4-6 demonstrate the analysis applied to the data; Section 7 summarizes the paper.

2. Theory

2.1. Multiblade Coordinate Transformation

A multiblade coordinate transformation (MBC) is typically used to convert degrees of freedom (DOFs) measured on the blades, i.e. in the rotating frame, to a non-rotating frame [8], making it possible to combine the blade DOFs with those on the tower and the nacelle. In the case of a three-bladed rotor, the sets of three coordinates $\{q_{1,k}, q_{2,k}, q_{3,k}\}^T$ measured at the position k on blades 1, 2, 3 will be converted to the sets of three multiblade coordinates $\{a_{0,k}, a_{1,k}, b_{1,k}\}^T$ given by

$$a_{0,k} = \frac{1}{3} \sum_{i=1}^3 q_{i,k}, \quad a_{1,k} = \frac{2}{3} \sum_{i=1}^3 q_{i,k} \cos \phi_i, \quad b_{1,k} = \frac{2}{3} \sum_{i=1}^3 q_{i,k} \sin \phi_i, \quad (1)$$

Where ϕ_i is the instantaneous azimuth angle of the i^{th} blade, and $k = 1 \dots M$ is a DOF number. The transformation assumes the blades are evenly distributed, i.e., $\phi_i = \phi_1 + 2\pi(i-1)/3$, $i = 1, 2, 3$. The backward transformation, from the multiblade coordinates to the blade coordinates is given by

$$q_{i,k} = a_{0,k} + a_{1,k} \cos \phi_i + b_{1,k} \sin \phi_i. \quad (2)$$

Typically the equation of motion (EoM) is written for a mixture of blade and tower/nacelle DOFs,

$$\mathbf{M} \ddot{\mathbf{x}} + \mathbf{C} \dot{\mathbf{x}} + \mathbf{K} \mathbf{x} = \mathbf{0}, \quad (3)$$

with

$$\mathbf{x} = \{q_{1,1}, \dots, q_{1,M}, \dots, q_{3,1}, \dots, q_{3,M}, s_1, \dots, s_L\}^T, \quad \mathbf{x} \in R^{3M+L}, \quad (4)$$

where s_l , $l=1 \dots L$ are DOF measured in the non-rotating frame. For an operating wind turbine, the mass matrix \mathbf{M} , gyroscopic/damping matrix \mathbf{C} and stiffness matrix \mathbf{K} are periodic in time: $\mathbf{M}(t)=\mathbf{M}(t+T)$, $\mathbf{C}(t)=\mathbf{C}(t+T)$, $\mathbf{K}(t)=\mathbf{K}(t+T)$, where $T=2\pi/\Omega$ is a period of the rotor rotation and Ω is its circular frequency. Thus Eq. (3) describes a linear time periodic (LTP) system, and application of the classical modal approach is impossible since the basic assumption of the modal decomposition, that the system under test is linear and time invariant, is violated here.

Using Eq. (2) to substitute the coordinates $q_{i,k}$ into Eq. (4), and leaving coordinates s_l unchanged, one arrives at EoM in multiblade coordinates:

$$\mathbf{M}_B \ddot{\mathbf{z}} + \mathbf{C}_B \dot{\mathbf{z}} + \mathbf{K}_B \mathbf{z} = \mathbf{0}, \quad (5)$$

where

$$\mathbf{z} = \{a_{0,1}, a_{1,1}, b_{1,1}, \dots, a_{0,M}, a_{1,M}, b_{1,M}, s_1, \dots, s_L\}^T, \quad \mathbf{z} \in R^{3M+L}. \quad (6)$$

Hansen et al. [2, 9] state that, if the rotor is isotropic, the matrices \mathbf{M}_B , \mathbf{C}_B and \mathbf{K}_B are constant, and thus MBC transformation converts the LTP system into an LTI system. Bir [8] generally disagrees with this statement but admits that, under the rotor isotropy assumption, the MBC transformation filters out all periodic terms from the EoM, except those that are integer multiples of 3Ω . In the same paper, Bir also clarifies some typical misconceptions regarding MBC, one of them is the necessity of the stationarity of the rotor speed ($\Omega=const$).

In any event, converting the LTP system in Eq. (3) into the LTI system in Eq. (5) allows the application of the classical modal approach to the new system, i.e., presenting the system dynamics as a superposition of modes, and finding the corresponding modal parameters: modal frequencies, damping and mode shapes. This paper concerns output-only modal analysis, i.e., the operating wind turbine is loaded by pure wind and unmeasured forces due to the rotation of the turbine. Then the obtained mode shapes are transferred back to the blade coordinates using Eq. (2). In [4], this method was applied to simulated wind turbine data; this paper extends the analysis to the measured data and compares it with the results from another method, outlined in the next section.

When considering a time variant mechanical system, the term ‘‘mode’’ becomes somehow vague. If an operating wind turbine with isotropic rotor is described in multiblade coordinates, the system becomes LTI where the ‘‘modes’’ are well defined. Let us consider a mode of system (5), and assume it has the following modal parameters: the eigenvalue

$$\lambda_r = -\zeta_r \omega_r + j \omega_r \sqrt{1 - \zeta_r^2}, \quad (7)$$

where ζ_r represents the modal damping and ω_r is the undamped natural frequency. The corresponding mode shape is

$$\psi_r = \{a_{0,1}, a_{1,1}, b_{1,1}, \dots, a_{0,M}, a_{1,M}, b_{1,M}, s_1, \dots, s_L\}^T, \quad \psi_r \in C^{3M+L}. \quad (8)$$

The elements of the mode shape vector are complex numbers.

Employing a backward MBC transformation, it is possible to map this mode into the natural blade coordinates. For rotor angular speed Ω , the motion at the k^{th} DOF on the i^{th} blade corresponding to this mode will be:

$$q_{i,k}(t) = \gamma_{i,k}(t) + \alpha_{i,k}(t) + \beta_{i,k}(t), \quad (9)$$

where

$$\begin{aligned} \gamma_{i,k}(t) &= e^{j(\omega_r - \zeta_r \omega_r) t} a_{0,k}; \\ \alpha_{i,k}(t) &= \frac{1}{2} e^{j(\omega_r + \Omega) t - \zeta_r \omega_r t} (a_{1,k} - j b_{1,k}) e^{j \frac{2\pi}{3} (i-1) t}; \\ \beta_{i,k}(t) &= \frac{1}{2} e^{j(\omega_r - \Omega) t - \zeta_r \omega_r t} (a_{1,k} + j b_{1,k}) e^{-j \frac{2\pi}{3} (i-1) t}, \end{aligned} \quad (10)$$

As one can see, in the *blade coordinates* the modes of the LTI system in Eq. (5) occur in groups of three, with frequencies: $\omega_r - \Omega$, ω_r , and $\omega_r + \Omega$. In general each of these modes could have a different damping ratio, ζ_r , although in eq. (10). The γ component does not depend on blade's number i , meaning that all three blades oscillate

in phase; this is a so-called *collective* mode. The *backward whirling* (or *anti-symmetric*) mode α has a frequency $\omega_r + \Omega$; blade number $i+1$ lags behind blade number i by -120° . The *forward whirling* mode β has frequency $\omega_r - \Omega$; blade number $i+1$ lags behind blade number i by $+120^\circ$.

2.2. Harmonic Power Spectrum of LTP system

A single frequency input to an LTI system causes a response at the same frequency. In contrast, the same input to an LTP system, e.g., a wind turbine, causes a response that includes the excitation frequency and also an infinite number of its harmonics. An Exponentially Modulated Periodic (EMP) signal space [5] is defined to contain the frequency component at the single excitation frequency as well as its harmonics. Specifically, if the frequency of interest was ω then the EMP signal would consist of a collection of sinusoids at frequencies $\omega \pm n\Omega$, each having a different amplitude and phase. The harmonic transfer function is a matrix that relates an EMP input signal (expressed as a vector of harmonic amplitudes at $\omega \pm n\Omega$) to an EMP output signal. Details about how to derive the harmonic transfer function and then the harmonic power spectrum can be found in [10].

In practice, one would often like to express a measured signal as an EMP signal, for example in order to compute transfer functions. This is done by creating several frequency shifted copies of the signal. Specifically, suppose an output $y(t)$ is measured. An EMP output signal in the frequency domain would be expressed as,

$$\mathbf{Y}(\omega) = [\dots Y_{-1}(\omega) Y_0(\omega) Y_1(\omega) \dots]^T \quad (11)$$

where $Y_n(\omega)$ is the FFT of the n^{th} modulated output signal $y_n(t)$,

$$y_n(t) = y(t)e^{-jn\Omega t} \quad (12)$$

This paper primarily focuses on how to interpret the harmonic power spectrum in order to identify the natural frequencies and time periodic mode shapes of an operating wind turbine, which is modeled as an LTP system.

Previous works have shown that the harmonic power spectrum of an LTP system can be expressed in a modal summation form as,

$$S_{yy}(\omega) = E(\mathbf{Y}(\omega)\mathbf{Y}(\omega)^H) = \sum_{r=1}^N \sum_{l=-\infty}^{\infty} \frac{\bar{\mathbf{C}}_{r,l} \mathbf{W}(\omega) \bar{\mathbf{C}}_{r,l}^H}{[j\omega - (\lambda_r - j\Omega)][j\omega - (\lambda_r - j\Omega)]^H} \quad (13)$$

r^{th} mode

where $E()$ is the expectation and $()^H$ is the Hermitian. $\mathbf{Y}(\omega)$ is the exponentially modulated output signal defined in Eq. (11). Eq. (13) has a similar mathematical form as the power spectrum of an LTI system,

$$S_{yy}(\omega) = E(Y(\omega)Y(\omega)^H) = \sum_{r=1}^N \frac{\psi_r S_{UV}(\omega) \psi_r^H}{[j\omega - \lambda_r][j\omega - \lambda_r]^H} \quad (14)$$

where $Y(\omega)$ is the spectrum of measured output for the LTI system. The numerator in Eq. (13) contains $\mathbf{W}(\omega)_r$, which is the auto-spectrum of the net force exciting the r^{th} mode of the time periodic system. This is similar to the

input autospectrum, $S_{UV}(\omega)$ in Eq. (14), which reduces to an identity matrix when the structure is excited with uncorrelated white noise.

However, there are also two notable differences between the harmonic power spectrum in Eq. (13) and the conventional power spectrum in Eq. (14). First, the harmonic power spectrum not only contains a summation over the modes, whose eigenvalues are λ_r , but each mode also appears at several harmonics $\omega_r - l\Omega$. Hence, the harmonic power spectrum has peaks near each natural frequency ω_r , and also at the frequencies $\omega_r - l\Omega$ for any integer l . Second, the mode vector $\bar{\mathbf{C}}_{r,l}$ in the harmonic power spectrum is no longer a collection of vibration amplitudes at different measurement locations (note the definition of mode in Section 2.1), as ψ_r in Eq. (14). Instead, $\bar{\mathbf{C}}_{r,l}$ consists of the Fourier coefficients that describe the r^{th} time periodic mode shape collected into a vector as,

$$\bar{\mathbf{C}}_{r,l} = [\dots C_{r,-1-l} \quad C_{r,-l} \quad C_{r,l} \quad \dots]^T \quad (15)$$

$$C(t)\psi_r(t) = \sum_{l=-\infty}^{\infty} C_{r,l} e^{jl\Omega t}$$

$C(t)$ is the output vector in the state space model of the equation of the motion [11], indicating which DOF is being measured. For the wind turbine measurement using accelerometers, $C(t)$ is simply a one at each sensor location. Theoretically, a periodic mode shape $\psi_r(t)$ should be described with a Fourier series of infinite order, yet one would expect that most systems can be well approximated with a finite, perhaps even small number.

The harmonic power spectrum is estimated in a conventional manner. Assuming $n = -p \dots p$ is used to modulate the acquired output, the modulated signal forms a matrix of $2p+1$ copies of the signal at a certain number of frequency lines. The harmonic power spectrum then has a dimension of $(2p+1) \times (2p+1)$ by the number of frequency lines. Since each column (or row) in the harmonic power spectrum contains similar information about the LTP system, only the primary column (center column) is used in the identification. The procedure of identifying time periodic modes from the harmonic power spectrum can be summarized as,

1. Record the response $y(t)$ at any sensor on the wind turbine under random excitation.
2. Construct the exponentially modulated periodic output signals in the time domain using $y_n(t) = y(t)e^{jn\Omega t}$, with $n = -p \dots p$.
3. Split the modulated output signals into many sub-blocks with the desired level of overlap. Apply a Hanning window to each block and compute the spectra of modulated output signals, $Y_n(\omega)$.
4. Compute the primary column of the harmonic power spectrum with $S_{yy}(\omega)_{n,0} = E(\mathbf{Y}(\omega)Y_0(\omega)^H)$ where the expectation operator denotes the average over all of the sub-blocks.
5. Use peak-picking or curve-fitting routines to identify the r^{th} natural frequency ω_r and the mode vectors $\bar{\mathbf{C}}_{r,l}$ at different harmonics.
6. Align $\bar{\mathbf{C}}_{r,l}$ for various l to compare different estimates of the same mode vector using Eq. (15). Apply

singular value decomposition to find the best estimate from all Fourier coefficient vectors[7].

- Use Eq. (15) to reconstruct the time periodic mode shape $\psi_r(t)$.

3. Experimental Setup

This paper applies the two methods described in the previous section to operational measurements from a Vestas V27 wind turbine. The Vestas V27 is a 225kW medium size upwind pitch regulated wind turbine (Figure 1a). An extensive measurement campaign took place from October 2012 through May 2013. Each blade of the wind turbine was instrumented with 12 accelerometers (Bruel and Kjaer Type 4507 and 4508), including 10 accelerometers in the flapwise direction (five on the leading edge and five on the trailing edge) and two accelerometers in the edgewise direction (Figure 1b). Since the MBC-based method requires symmetry of the measurement system, special care was taken to mount the sensors on all three blades as similar to each other as possible, both location- and direction-wise. The nacelle was instrumented with three triaxial accelerometers (Figure 1c). In order to estimate the instantaneous rotor position (azimuth) and rotor angular speed, two DC accelerometers, attached to the rotor's hub, were employed. To improve the estimate of the azimuth angle, a tachoprobe was also installed on the wind turbine's High-Speed Shaft (the HSS, connects the gearbox to the electrical generator). A pitch sensor was installed inside the hub; its readings were used for selecting recordings with no or relatively small pitch activity. In addition, two IRIG-B signals were used to synchronize the signals from the rotor and nacelle sensors. In total, 40 channels were recorded using B&K LAN-Xi data acquisition modules located in the hub and wirelessly transferred to the nacelle, where another 11 channels were measured. All channels were recorded synchronously at a sampling frequency of 4096Hz. Additional details regarding the measurement setup can be found in [3].

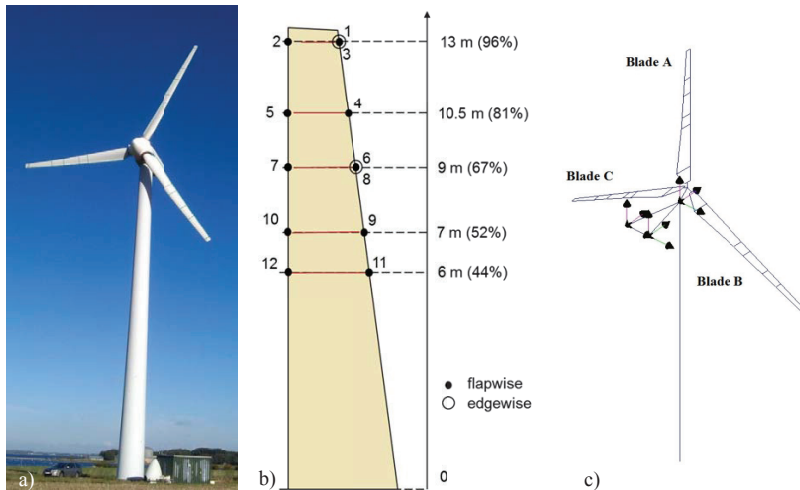


Figure 1. a) Vestas V27 with blades instrumented with accelerometers; b) Location and orientation of the accelerometers on the blades c) Location of triaxial accelerometers in the nacelle.

As described previously, the operating wind turbine is modeled as an LTP system. This modeling assumes constant rotor speed during the observation period. Unfortunately, the rotating speed is rarely constant in practice. Figure 2 shows a five minute portion of the time history of the rotating speed computed from one of the DC accelerometers. The rotating frequency varies from 0.527Hz to 0.543Hz over this time interval. Therefore, the first step was to select the datasets where the rotating speed is the steadiest. Furthermore, any pitch activity changes the in-plane and out-of-plane stiffness of the blade. Thus the second criterion was to select the datasets with minimum pitch activity. This was done using filtering and sorting options of the recording database. Eventually, the data taken at Dec.16, 2012 was selected (20 minutes long). The rotating speed, pitch angle and wind speed (30m above the ground) for this data set are listed in Table 1.

The correct azimuth angle is a key parameter for both MBC and harmonic power spectra based methods. A lot of attention was paid to derive the azimuth angle from the readings of three redundant sensors: two DC accelerometers located in the hub and the tachoprobe measuring HSS angular speed (the exact gear ratio is around 23.3333). It was found that the tachoprobe provided the most accurate measurement of the rotating frequency. The average rotating frequency over this 20 minute measurement was 0.5369Hz with a standard deviation of 0.0007Hz. This average rotating frequency was then used to compute the azimuth angle of each blade.

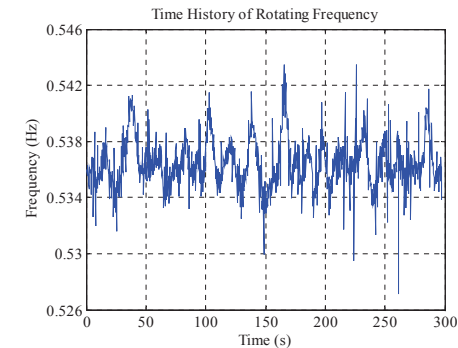


Figure 2 Time history of rotating frequency

Table 1 Test conditions for the selected dataset

	DC1 (Hz)	DC2 (Hz)	Tacho (Hz)	Pitch Angle (°)	Wind speed (m/s)
Mean	0.5370	0.5370	0.5369	-0.2150	4.7300
Maximum	0.5536	0.5548	0.5385	-0.0525	6.6850
Minimum	0.5228	0.5159	0.5352	-0.4925	2.6250
Standard deviation	0.0064	0.0074	0.0007	0.0850	0.6710

4. Preliminary Analysis

This section describes a preliminary analysis of the measured data, which can be conducted before stepping into the more complex modeling techniques. For the preliminary analysis, four sensors were selected, see Table 2. These sensors were located on the trailing edge at the tip, and at 9m from the root of the blade.

Table 2 Acceleration signals selected for analysis

Name (Figure 1b)	Description
1f	Tip, trailing edge, flapwise direction
3e	Tip, trailing edge, edgewise direction
6f	9m from the root, trailing edge, flapwise
8e	9m from the root, trailing edge, edgewise direction

First, the power density spectra (PSD) of the signals was calculated ($\Delta f=1.125 \cdot 10^{-2}$ Hz; block size 89 s; 67% overlap; Hanning window; 38 averages); the PSD of the tip acceleration signals averaged over 20 minutes of observation time, are shown in Figure 3.

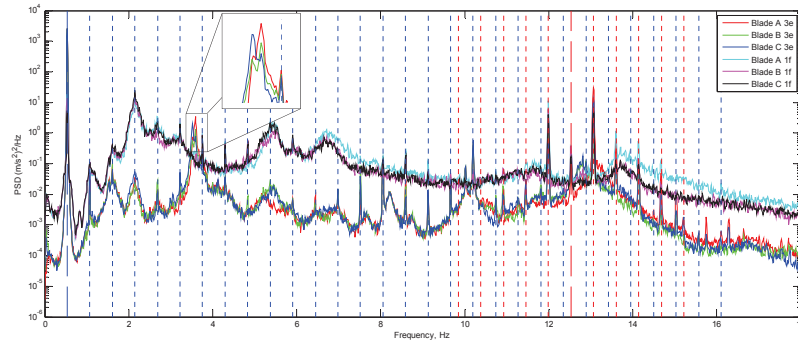


Figure 3 PSD of the tip acceleration signals. Blue dash line – rotor fundamental, blue dotted lines – rotor harmonics; red dashed line – high speed shaft fundamental, red dotted lines – its sidebands.

Analyzing Figure 3, one can observe:

1. The level of the flapwise vibrations is higher than the level of edgewise vibrations;
2. At low frequencies, the response in both flapwise and edgewise directions is heavily dominated by harmonics. Two families of the harmonics can be identified: the first are the harmonics of the rotor (shown by the blue vertical lines in Figure 3), the second family is due to the HSS fundamental frequency at 12.52 Hz modulated by the rotor frequency (the red vertical lines in Figure 3);

3. The effect of the “fat tails” mentioned in [12] can be clearly seen on the lowest rotor harmonics. The higher harmonic peaks (starting from the 5th rotor harmonic) become narrower, and eventually have the appearance of typical harmonic peaks.
4. Flapwise vibrations are less contaminated by the rotor and gearbox harmonics at higher frequencies;
5. The readings of the accelerometers located in the same positions on different blades are not identical, which is either due to imprecise mounting or different dynamic characteristics of the blades (which is possible since one of the blade of this particular wind turbine was replaced some years ago). Since the MBC transformation assumes rotor isotropy and symmetry of the observation system, this could be a serious obstacle for the application of the MBC-based method. In contrast, the harmonic power spectrum method does not require these assumptions.
6. Note the double peak at approximately 3.5 Hz on the edgewise signal spectra (see the inset): one may expect a double peak (since the frequencies of the two anti-symmetric modes may slightly differ) but it is not normal that the higher frequency peak and the lower frequency peak dominate at different blades. If the rotor was isotropic, the shape of the spectra averaged over many rotor revolutions is expected to be the same for all three blades. Therefore this observation rather speaks for the rotor anisotropy than for the imperfection of the sensors mounting.

Since the harmonics are undesirable in further analysis, the time-synchronous averaging (TSA) algorithm was employed to remove the harmonics. TSA was applied in two runs, first removing the rotor harmonics, and second – the sidebands of the HSS fundamental frequency. The tachometer events are generated from the instantaneous rotor azimuth $\phi_i(t)$, which is estimated as explained in Section 3. The detailed explanation of the TSA method can be found in [13]. Due to the “fat tails” phenomena, TSA does not significantly affect the lowest rotor harmonics but effectively removes the higher harmonics and HSS sidebands.

Along with the PSD, the singular value decomposition (SVD) can shed some light on how many independent vectors should be used to describe system behavior at different frequencies. The SVD was performed on the 3x3 cross-spectra matrix computed between the sensors located at the same point on all three blades. Figure 4 shows the three singular values computed for the signal 3e after the harmonics were removed by TSA.

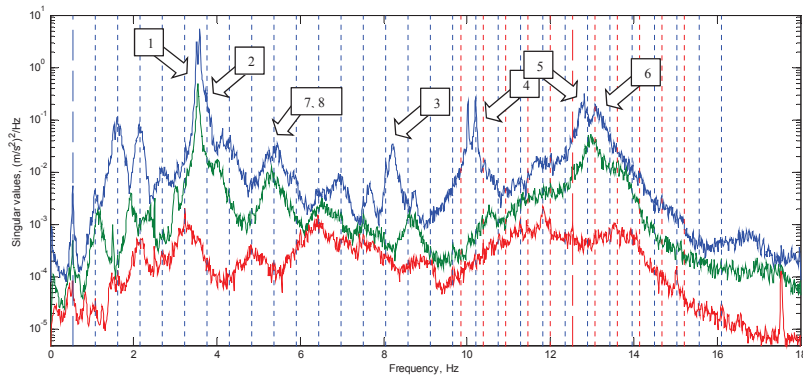


Figure 4 Singular values of the cross-spectra matrices calculated for sensors 3e on all three blades

If focusing on the edgewise vibrations, SVD reveals some expected modal behavior, for example, arrows #1,2 and #5,6 in Figure 4 denote the two edgewise anti-symmetric modes, #3,#4 are perhaps the edgewise collective modes, #7,8 are the traces of the two flapwise anti-symmetric modes, which also have an edgewise component. However, at this point this is just a guess-work; the modal analysis shall reveal the true dynamics of the wind turbine.

The next step will be to apply the MBC transformation to the data according to Eq. (1). The instantaneous rotor azimuth $\phi(t)$, which participates in Eq. (1) is estimated as explained in Section 3. The geometrical interpretation of multiblade coordinates can be found in [14]. The spectra of the multiblade coordinates a_0 , a_1 and b_1 are shown in Figure 5.

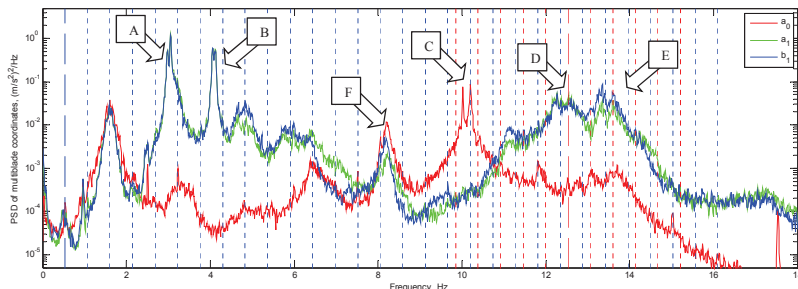


Figure 5 PSD of multiblade coordinates for 3e sensor location.

Analyzing Figure 5, one can observe the following:

1. The peak at 1Ω (rotor fundamental) has almost disappeared, while the peak at 3Ω (3^{rd} harmonic, the so-called *blade passing frequency*) has increased. This agrees with Bir's statement that MBC transformation can be considered as a filter stopping all harmonics except those that are integer multiples of 3Ω [8].
2. The anti-symmetric coordinates a_1 and b_1 (green and blue curves respectively) follow each other closely, in contrast the symmetric (collective) coordinate a_0 (red curve) is quite distinct. Thus MBC effectively separated collective blade behavior from the anti-symmetric.
3. There are two types of behavior of the peaks identified in the blade spectra (Figure 4): some peaks like peaks #1,2 become two well separated peaks #A,B while the other peaks like #4 keep their location (peak #C). The first type of peaks is typical for anti-symmetric (or whirling) modes, while the second type – for collective modes. In blade coordinates, the whirling modes are often very close in frequencies (e.g. peak pair #1, 2 and pair #5, 6 in Figure 4). In multi-blade coordinates, these peaks are typically separated: peak pair #1, 2 becomes #A,B and pair #5, 6 becomes #D,E). The distance between the new peaks in the pairs is about 2Ω .

It is also important to note that the peaks seen on the MBC coordinates (Figure 5) can also be traced in the nacelle acceleration spectra (Figure 6). This makes it possible to identify many rotor modes using only tower and nacelle data, was reported in [15].

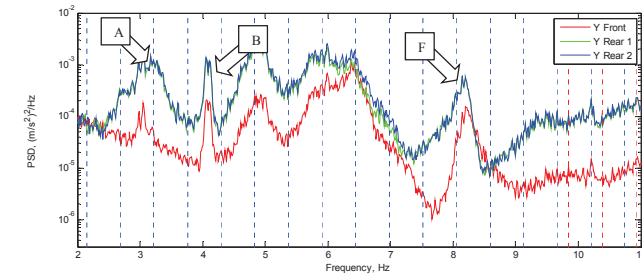


Figure 6 PSD of the nacelle acceleration signals, side-to-side direction: red – front, green – rear right, blue – rear left. The letters denoting the peaks are the same as in Figure 5.

5. Modal Analysis of Operational Turbine using Multiblade Coordinate Transformation

The analysis performed so far is purely signal processing, with no modeling introduced and no assumptions made. In the following sections, we assume that the structure under test is LTP, and will model its dynamics via modal decomposition.

In this section we perform operational modal analysis (OMA) on the experimentally obtained data pre-processed by harmonic removal and multiblade coordinate transformation, as detailed in section 4. The new time histories become the input to OMA. As will be explained later, the main focus is placed on the edgewise motion, since it has more interesting time-periodic behavior.

The OMA stochastic subspace identification (SSI) algorithm (Bruel and Kjaer Type 7760) was used for identification. Twelve channels (3 x (1f, 3e, 6f, 8e, Figure 1b)) were selected for the analysis. The data were decimated 10 times; thus the new sampling rate is 40.96Hz.

Typically, modal analysis software uses test object geometry in order to visualize measured DOFs and to animate the modes. In the case of multiblade coordinates such visualization is not physical; however it is found very useful in order to give mode nomenclature. Figure 8 shows the simple geometry used for the visualization. DOFs 10* denote multiblade coordinate a_0 , 20* are a_1 and 30* are b_1 . Points *03 correspond to the blade tip, and ones *08 – to the middle of the blade. Z-direction corresponds to flapwise DOFs, and Y – to edgewise direction. If, when animating the mode, a_0 dominates, this is a collective mode. Dominating a_1 and b_1 indicate anti-symmetric (whirling) modes. If the phase between a_1 and b_1 is -90° , this is a backward whirling mode; the phase of $+90^\circ$ indicates the forward whirling. If DOFs *03 and *08 move in-phase, this is a first bending mode, while anti-phase points to the second bending mode. Identification of higher modes is restricted by the low spatial resolution, especially in the edgewise direction.

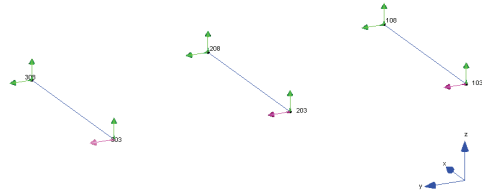


Figure 7 Simple geometry indicating 6 multiblade coordinates

Figure 8 shows the stabilization diagram in the range 2.8-4.4Hz corresponding to peaks #A,B in Figure 6; the corresponding mode table is shown below. SSI algorithm finds 4 edgewise modes, shown in bold in the table, the other modes are flapwise dominated or noise modes, which are not considered here. The modes IIBW-1 and IIFW-1 (abbreviations for in-plane 1st bending, back- or forward whirling respectively) are both originated from the peak at 3.51Hz on the edgewise signals spectra; the frequencies of these modes are $3.51 \mp \Omega$ respectively. The modes IIBW-2 and IIFW-2 are originated from the peak at 3.58Hz, and their frequencies are $3.58 \mp \Omega$. The presence of the four modes found by OMA-SSI in multiblade coordinate data is an indication of rotor anisotropy; these modes are not physical, this is an artifact due to the violation of the rotor isotropy assumption.

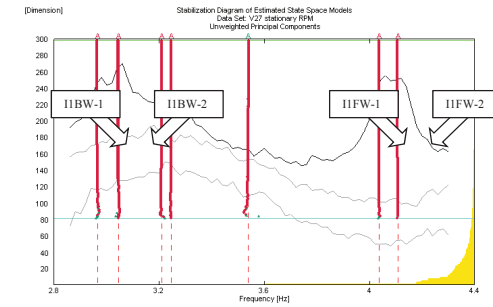


Figure 8 Stabilization diagram around first in-plane modes

Table 3 Modal parameters of the mode shown in Figure 8

Mode	Frequency [Hz]	Damping Ratio [%]	Notes	(Average) Phase difference between a_1 and b_1 (at the tip)
IIBW-1	2.97	2.8	$3.51 - \Omega$	-86.1°
IIBW-2	3.05	1.8	$3.58 - \Omega$	-87.4°
IIFW-1	4.04	1.1	$3.51 + \Omega$	85.2°
IIFW-2	4.11	0.8	$3.58 + \Omega$	90.2°

Indeed, if the rotor was isotropic, the (averaged) spectra of the accelerations measured on all three blades should have almost identical magnitude, and the phase between the signals measured on the neighboring blades should be equal and their sum should be $0 \pm 360^\circ$: $\phi_{AB} = \phi_{BC} = \phi_{CA} = \phi$ and $\phi_{AB} + \phi_{BC} + \phi_{CA} = 0 \pm 360^\circ$. This is only possible if the phase is either 0° (for collective behavior) or $\pm 120^\circ$ (“+” for forward whirling and “-” for backward whirling). Suppose the vibrations of the i^{th} blade have a peak at a certain frequency ω : $q_i = A \sin(\omega t - \phi(i-1))$. Depending on the phase ϕ , after the MBC transformation in Eq. (1), one obtains the multiblade coordinates according to Table 4.

Table 4 Multiblade coordinates dependence on phase ϕ

ϕ	a_0	a_1	b_1	Phase between a_1 and b_1	Mode name
0	$A \sin(\omega t)$	0	0	Not defined	collective
$+120^\circ$	0	$A \sin((\omega + \Omega)t)$	$-A \cos((\omega + \Omega)t)$	$+90^\circ$	forward whirling
-120°	0	$A \sin((\omega - \Omega)t)$	$A \cos((\omega - \Omega)t)$	-90°	backward whirling

This means that in the case of the isotropic rotor, a peak in the blade vibration spectra should become one peak in the multiblade coordinate spectra, not two, as we experienced here. Only one mode would then be found at that peak (in MBCs) but here two modes have erroneously been extracted. Here, we observe two closely spaced peaks in the blade spectra around 3.5Hz (Figure 3) which presumably correspond to backward and forward whirling modes; let’s denote the frequencies of the peaks by ω_{BW} and ω_{FW} respectively. If the rotor was isotropic, the

spectral magnitudes of all three blades would be approximately the same, and the phase would be -120° at ω_{BW} and $+120^\circ$ at ω_{FW} . After MBC transformation, we would discover two peaks in the MBC spectra: the backward whirling mode at $\omega_{BW,MBC} = \omega_{BW} - \Omega$ and forward whirling at $\omega_{FW,MBC} = \omega_{FW} + \Omega$, and these modes would then correspond to the backward and forward whirling modes of the MBC system.

Unfortunately, in the case of the anisotropic rotor, this analysis does not bring such clear results. Applying MBC transformation here, we found four modes at $\omega_{BW} - \Omega$, $\omega_{BW} + \Omega$, $\omega_{FW} + \Omega$ and $\omega_{FW} - \Omega$, as it is seen in Figure 8. Thus, one can conclude that use of the MBC transformation cannot be recommended in the case of anisotropic rotors. Instead, we will recommend the Harmonic Power Spectrum method demonstrated below.

6. Modal Analysis of Operational Turbine using the Harmonic Power Spectrum method

The turbine rotated at an average speed of 0.5369Hz. The measured response of the blades in the edgewise direction on all three blades (in-plane sensors 3e and 8e) as well as the response on the front of the nacelle in the lateral and vertical directions were collected into a response vector with 8 outputs. This response was then exponentially modulated with $n = -4 \dots 4$ according to step 2 in Sec. 2.2, using the response at the tips of the three blades as references. Then, the modulated signals were split into 73 sub-blocks with a block size of 119s (64 revolutions) and 88% overlap. A Hanning window was applied to reduce the leakage. The resulting harmonic power spectrum matrix had 72 outputs (8 points and 9 harmonics for each) by 3 references. The complex mode indicator function (CMIF) of this HPSD matrix was then found and is shown in 9. Similar to that in preliminary analysis, the rotor harmonics and a cluster of sideband harmonics around 12.52Hz due to the HSS dominate the response. Observing more closely, one can see another cluster of peaks centered around 3.59Hz with several strong sideband harmonics, each separated with the rotating frequency. Those peaks are evidence of linear time periodic behavior and will be the focus of the following analysis.

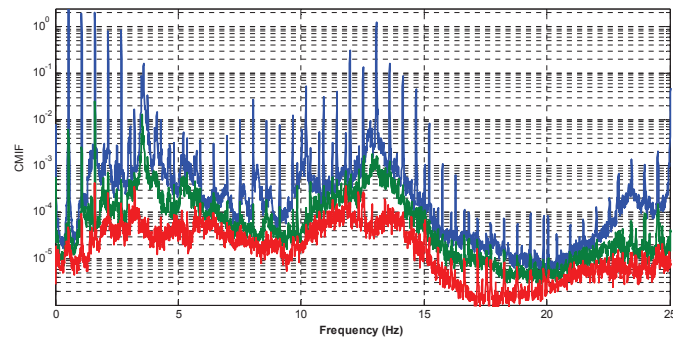


Figure 9 Complex Mode Indicator Function of the Harmonic Power Spectrum Matrix for the 8 edgewise sensors using the edgewise response at the blade tips as references.

Figure 10 shows an expanded view of the spectrum near 3.5 Hz, where the first edgewise modes of the blades are most active. The spectrum clearly shows two peaks near 3.5 Hz and the shape of the first (blue) and

second (green) singular value curves strongly suggests that two modes are present at that peak. Several modulations of the peak are also seen near 3.0, 4.0 and 4.5 Hz. The full harmonic power spectrum matrix was curve fit using a variant of the AMI algorithm [16, 17], focusing only on the peaks near 3.5 Hz. Two modes were identified with natural frequencies 3.5184 and 3.5867 Hz and damping ratios 0.00569 and 0.00355. The mode vectors for each mode are vectors of Fourier coefficients which describe the motion of the mode at the natural frequency, plus motion at nine harmonics of the natural frequency for $n = -4 \dots 4$. This is summarized in Figure 11, which shows the magnitude and phase of the response at several points on the turbine for each harmonic of each of these modes. As the motion is quite a bit more complicated than for an LTI system, some care will be taken to explain the meaning of this result.

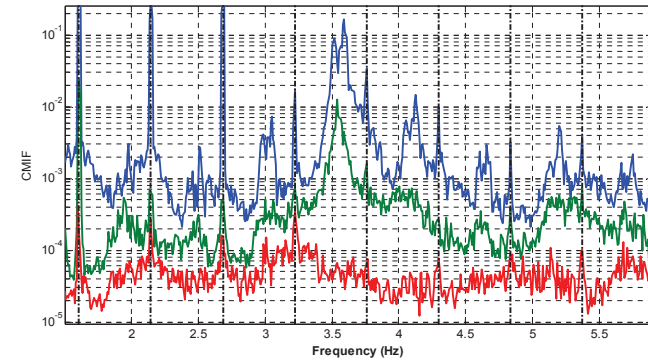


Figure 10 Zoom in on Harmonic power spectrum in Fig. 9.

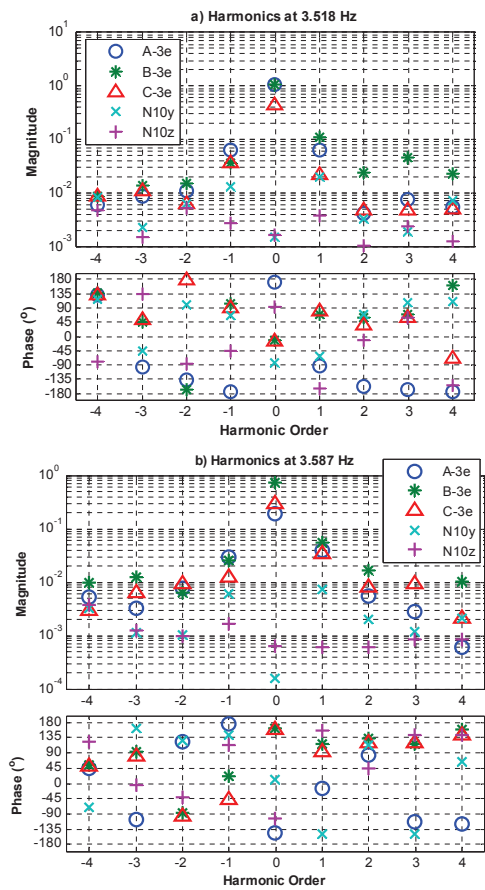


Figure 11 Identified Fourier coefficients on all the blades plotted against harmonic order a) Harmonic at 3.52Hz b) Harmonic at 3.59Hz

First consider the mode at 3.518 Hz. The mode shape in Figure 11 shows that the motion of the blades is dominated by motion at the 0th harmonic, or 3.518 Hz. Blade A moves about 180° out of phase with blades B and C. On the other hand, the tower motion is predominantly at the -1 and 1 harmonics, or 2.982 and 4.055 Hz. This was evident in Figure 6 which showed the spectrum of the motion of the nacelle. The blades also exhibit some vibration at these frequencies, although at 4.055 Hz it is about an order of magnitude smaller than the dominant motion and at 2.982 Hz it is smaller still. The higher harmonics ($|n|>1$) are quite small and so their validity is questionable.

The mode at 3.587 Hz behaves in a similar manner, with the dominant motion being at the 0th harmonic and with relatively weak higher harmonics. The motion of the tower is also considerably smaller in this mode. In this mode blade A is about 45° out of phase with the other two blades and blade B has significantly higher amplitude than the other blades. It is interesting to note that these two modes do follow the expected trends for the edgewise modes of an isotropic wind turbine. As illustrated in [6] and [9] and discussed in the previous section, a wind turbine typically exhibits backward and forward whirling modes, which in the tower reference frame (or in MBCs) occur at the tower vibration frequencies, or 2.982 and 4.055 Hz in this case. In the blade reference frame these modes would be closely spaced, and occur approximately equidistant between the two frequencies observed in the tower. While these modes are typically closely spaced (even repeated for an isotropic turbine, see e.g. [9]) they can be distinguished by the phase of the motion of the blades as discussed previously. The LTP modes identified for these two edgewise modes do not seem to follow the expected trends, but fortunately the motion observed is readily described by a linear time periodic model; the identified time-periodic shapes could be used to predict the motion of the structure or to validate a model that included the anisotropy of the turbine.

Figure 12 shows the deformation pattern that the structure would experience as a result of only the 0th harmonics at 3.518Hz and 3.587Hz. Since the motion of the blades is dominated by the 0th harmonic, one can imagine the blades deforming into this shape and while simultaneously oscillating with perturbations about 10% as large as these at the -1 and +1 harmonics. (These deformation shapes are also precisely what one would obtain if a conventional output-only modal analysis were performed.) The vibration amplitude at the hub (Position=0 m) is shown as zero to aid in visualizing the blade motion. The blades clearly have different amplitudes in each mode, yet the two sensors on each blade move precisely at the same phase and the deformation shapes are as one might expect for a first bending mode of a cantilever beam. Figure 13 shows the motion of the blades in the 1st harmonic in a similar format. It is interesting that these harmonics also show about the same phase across the sensors on each blade, yet these shapes are different than those at the 0th harmonic. The net effect of these harmonics would be to cause the total deformation of the blades to change somewhat from blade to blade over each 3.52 or 3.59 Hz cycle.

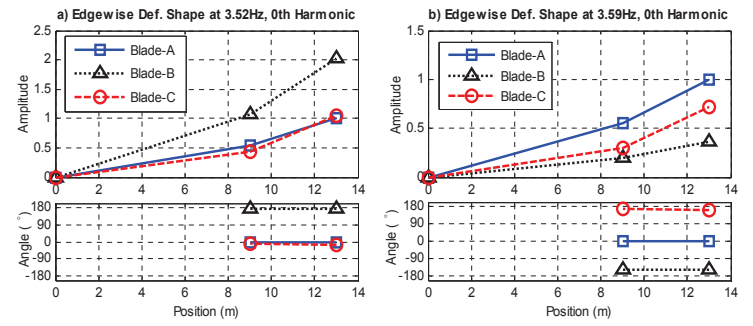


Figure 12 Deformation shape identified by AMI in 0th harmonic a) at 3.518Hz b) at 3.587Hz.

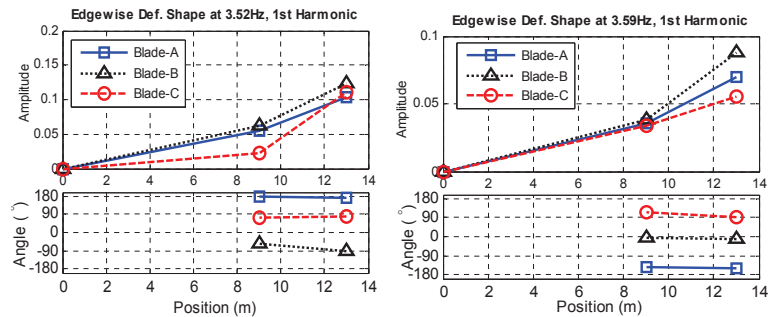


Figure 13 Deformation shape identified by AMI in 1st harmonic for modes centered at a) at 3.518Hz b) at 3.587Hz.

7. Conclusion

An operating wind turbine has to be modeled as an LTP system to correctly characterize its time periodic behavior. In this work, two methods suitable for LTP systems, namely, the multiblade coordinate transformation and the harmonic power spectrum, were employed to identify the modes of an operating wind turbine. The vibration data were obtained from an operating Vestas V27 wind turbine instrumented with accelerometers on the blades and the nacelle.

From the accelerometer readings, it was observed that the wind turbine rotor is anisotropic; therefore the MBC transformation will fail to convert the LTP system into an LTI system. It was shown that application of the MBC transformation lead to erroneous results. In contrast, the harmonic power spectrum does not require the rotor to be isotropic. The method was successfully applied; for demonstration purposes, and two edgewise (in-plane) bending modes were identified and analyzed in detail. In this particular case, the experimental data revealed that the magnitude of the sideband harmonics in the blade reference frame was an order of magnitude lower than the central frequency component. If these sidebands were negligible then one could use straightforward operational modal analysis on the data. However, then one is faced with a dilemma because the same modes appear at different frequencies in the tower measurements. In any event, the harmonic spectrum method allows one to easily identify the harmonic content in each mode and to robustly determine the number of modes present in the data.

Comparing the two methods in application to experimental modal analysis of operating wind turbine, the harmonic power spectrum method is strongly recommended for most cases. Firstly, since the rotor isotropy is not initially known, using of MBC transformation may result in an erroneous modal identification. Secondly, the MBC method requires instrumentation of all three blades and, besides this, a precise symmetric mounting of accelerometers on the blades. If the sensors on one blade should fail then the method cannot be used. The harmonic power spectrum method does not require this, which makes it much more practical in a real life situation. The harmonic power spectrum directly identifies the natural frequencies, damping ratios and the periodically time-varying modes that describe the motion of the blades in the rotating frame and the motion of the tower in the fixed frame. These modal parameters can be compared with the analytically derived modes of the turbine, obtained

through a Floquet analysis, to validate an anisotropic model for the turbine. The methods will be further compared and these ideas will be further developed in the next stage of the work.

References:

- [1] R.P.Coleman, "Theory of self-excited mechanical oscillations of hinged rotor blades," available from <ntrs.nasa.gov>, Langley Research Center1943.
- [2] M. H. Hansen, "Improved modal dynamics of wind turbines to avoid stall-induced vibrations," *Wind Energy*, vol. 6, pp. 179-195, 2003.
- [3] D. Tcherniak and G. C. Larsen, "Applications of OMA to an operating wind turbine: now including vibration data from the blades," presented at the 5th International Operational Modal Analysis Conference, Guimarães - Portugal, 2013.
- [4] D. Tcherniak, S. Chauhan, M. Rossetti, I. Font, J. Basurko, and O. Salgado, "Output-only Modal Analysis on Operating Wind Turbines: Application to Simulated Data," presented at the European Wind Energy Conference, Warsaw, Poland, 2010.
- [5] N. M. Wereley, "Analysis and Control of Linear Periodically Time Varying Systems," PhD, Department of Aeronautics and Astronautics, Massachusetts Institute of Technology, Cambridge, 1991.
- [6] M. S. Allen, M. W. Sracic, S. Chauhan, and M. H. Hansen, "Output-Only Modal Analysis of Linear Time Periodic Systems with Application to Wind Turbine Simulation Data," *Mechanical Systems and Signal Processing*, vol. 25, pp. 1174-1191, 2011.
- [7] S. Yang and M. S. Allen, "Output-Only Modal Analysis Using Continuous-Scan Laser Doppler Vibrometry and Application to a 20kW Wind Turbine," *Mechanical Systems and Signal Processing*, vol. 31, August 2012 2011.
- [8] G. Bir, "Multiblade Coordinate Transformation and Its Application to Wind Turbine Analysis," presented at the 2008 ASME Wind Energy Symposium, Reno, Nevada, 2008.
- [9] P. F. Skjoldan and M. H. Hansen, "On the similarity of the Coleman and Lyapunov-Floquet transformations for modal analysis of bladed rotor structures," *Journal of Sound and Vibration*, vol. 327, pp. 424-439, 2009.
- [10] S. Yang and M. S. Allen, "A Lifting Algorithm for Output-only Continuous Scan Laser Doppler Vibrometry," presented at the AIAA, Hawaii, 2012.
- [11] C.-T. Chen, *Linear system theory and design*, 3rd edition ed.: Oxford University Press, Inc, 1999.
- [12] D. Tcherniak, S. Chauhan, and M. H. Hansen, "Applicability limits of Operational Modal Analysis to Operational wind turbines," presented at the 28th International Modal Analysis Conference (IMAC XXVIII), Jacksonville, Florida, 2010.
- [13] T. Jacob, D. Tcherniak, and R. Castiglione, "Harmonic Removal as a Pre-processing Step for Operational Modal Analysis: Application to Operating Gearbox Data," presented at the VDI-Fachtagung Schwingungen von Windenergieanlagen 2014.
- [14] M. H. Hansen, "Aeroelastic stability analysis of wind turbines using an eigenvalue approach," *Wind Energy*, vol. 7, pp. 133-143, 2004.
- [15] D. Tcherniak, J. Basurko, O. Salgado, I. Urresti, S. Chauhan, C.E.Carcangui, and M. Rossetti, "Application of OMA to Operational Wind Turbine," presented at the International Operational Modal Analysis Conference, Istanbul, Turkey, 2011.
- [16] M. S. Allen, "Global and Multi-Input-Multi-Output (MIMO) Extensions of the Algorithm of Mode Isolation (AMI)," Doctorate, George W. Woodruff School of Mechanical Engineering, Georgia Institute of Technology, Atlanta, Georgia, 2005.
- [17] M. S. Allen and J. H. Ginsberg, "A Global, Single-Input-Multi-Output (SIMO) Implementation of the Algorithm of Mode Isolation and Applications to Analytical and Experimental Data," *Mechanical Systems and Signal Processing*, vol. 20, pp. 1090-1111, 2006.

EWSHM 2014: LOSS OF ROTOR ISOTROPY AS A BLADE DAMAGE INDICATOR FOR WIND TURBINE STRUCTURAL HEALTH MONITORING SYSTEMS

Dmitri Tcherniak

Brüel & Kjaer SVM, Skodsborgvej 307, Nærum 2850, Denmark
dmitri.tcherniak@bksv.com

ABSTRACT

Modal-based damage features utilizing asymmetry of the rotor whirling mode shapes arising from rotor anisotropy are examined by Floquet analysis, and output-only modal analysis is applied to simulated vibrations of a rotating rotor.

KEYWORDS : *wind turbine blade, rotor anisotropy, Floquet analysis, OMA*

INTRODUCTION

Blades of modern wind turbines are complex high-tech structures, and their cost constitutes a significant part of the entire wind turbine cost. While operating, the blades are heavily loaded and exposed to harsh weather conditions, especially for off-shore wind turbines. If damage to the blades develops to a critical level it may cause catastrophic consequences. If the damage leads to partial or complete loss of structural integrity, the repair is extremely costly, or may even be impossible. This calls for automatic blade health monitoring systems, which are able to automatically detect and report the damage, follow up on damage development and guide the blade Operational and Maintenance program in general.

The approach presented in this paper is not new: we apply operational modal analysis (OMA) to vibration data measured on an operating wind turbine [1]. The changes in the obtained modal parameters are used to detect and localise the damage. However, in this study, we use a pragmatic view: we are looking for the blade damage features sufficiently *sensitive*, and these features should be *observable* in a real-life situation. The following two examples demonstrate the opposite: It is known that damage changes natural frequencies of the structure. However, many conclude [2] that these changes are not sensitive to the damage, i.e., the damage must grow an extreme amount to change the natural frequencies significantly enough to be detectable. It is also known that the mode shapes of flapwise blade modes can be used to localise blade damage [3]. However, it was shown [4, 5] that for operating wind turbines, the flapwise modes are not observable with the accuracy level sufficient for damage localisation.

We also admit that OMA, though being a valuable tool for big structures, is not perfectly suited for operating wind turbines. The acting aerodynamic loads do not satisfy OMA assumptions [6] and, in general, an operating wind turbine cannot be modelled as a time-invariant system. A linear time-periodic (LTP) system is a better model for an operating wind turbine; for modal decomposition of such systems, a number of dedicated methods have been developed, e.g., [7, 8]. However, here we also use a pragmatic approach: the goal is not to perform a perfect modal identification, but rather define the dynamic features which can be used for confident damage detection.

This explains the selection of damage features for this study: From practical experience [5], it was noticed that the magnitude and phases between the blades for *whirling modes* demonstrate high level of sensitivity to blade damage. Also from experience [4, 5], it is known that the *edgewise whirling* modes can be identified with a high level of confidence. Based on these considerations, it was decided to examine how a slight rotor anisotropy due to damage influences the mode shape of the in-plane whirling modes, with the focus on phase and magnitude of the blade motion.

This paper suggests the following investigation strategy: Section 1 sets up a lumped-mass model of a three-bladed rotor, simple but sufficient for catching the first in-plane rotor modes. The equations of motion are derived, and modal decomposition based on Floquet analysis is performed. This analytical approach provides almost exact modal decomposition and helps understanding of the dynamics of the undamaged (isotropic) and damaged (anisotropic) rotor.

Section 2 is based on a simulated experiment of the lumped-mass model: it assumes the equations of motion are not known; the dynamic of the simplified system loaded by random forces is simulated, and the resulting time histories are input to OMA. The results will prove if OMA is capable of confidently providing the damage features, now from the experimental viewpoint.

1 SIMPLIFIED ROTOR MODEL

A simple six degree-of-freedom (DOF) system (Figure 1) models a rotating rotor and the supporting tower/nacelle structures. Each blade is modelled as two beams with lengths a and b , connected by a linear angular spring with stiffness k_j , $j=1...3$, where j is the blade index. The blades are evenly distributed over the rotor, the blades' azimuth angles are: $\psi_j(t) = \psi(t) + 2/3\pi(j-1)$. Lumped masses m_j are attached to the ends of the outer beams. The rotor rotates with the angular speed Ω about point C attached to the mass m_N , the latter models the nacelle. The mass is supported by two springs with stiffnesses k_H and k_V , which model the tower. The drivetrain has a moment of inertia I_D and stiffness k_D . A similar lumped parameter system is considered in [10], however, there the focus was on the out-of-plane rotor motion.

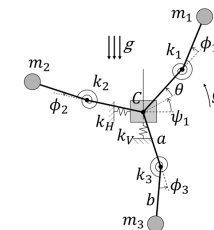


Figure 1: Simplified rotor system

The system is described by six coordinates: x_C and y_C are coordinates of point C , deflection of each blade from a straight line is described by angle ϕ_j , and θ is the drivetrain angular vibrations.

Equations of motion (EoM) are derived using the Lagrange method. The linearized EoM can be written as:

$$\mathbf{M}(t)\ddot{\mathbf{y}}(t) + \mathbf{G}(t)\dot{\mathbf{y}}(t) + \mathbf{K}(t)\mathbf{y}(t) = \mathbf{0}, \quad (1)$$

where: $\mathbf{M}(t)$, $\mathbf{G}(t)$ and $\mathbf{K}(t)$ are mass, gyroscopic and stiffness matrices. The matrices depend on the rotor azimuth $\psi(t)$; for constant rotor speed Ω , $\psi(t) = \Omega t + \psi_0$, the matrices are periodic with period $T = 2\pi/\Omega$: $\mathbf{M}(t) = \mathbf{M}(t + T)$, $\mathbf{G}(t) = \mathbf{G}(t + T)$, $\mathbf{K}(t) = \mathbf{K}(t + T)$. The vector $\mathbf{y}(t) = \{x_C(t), y_C(t), \phi_1(t), \phi_2(t), \phi_3(t), \theta(t)\}^T$ describes the physical DOFs of the system measured from the equilibrium position.

The Coleman (also known as *multiblade coordinate* or *MBC*) transformation converts the blade DOFs $\phi_j(t)$ to multiblade coordinates [9]:

$$a_0(t) = \frac{1}{3} \sum_{j=1}^3 \phi_j(t); \quad a_1(t) = \frac{2}{3} \sum_{j=1}^3 \phi_j(t) \cos(\psi_j(t)); \quad b_1(t) = \frac{2}{3} \sum_{j=1}^3 \phi_j(t) \sin(\psi_j(t)). \quad (2)$$

The Coleman transformation converts only blade DOFs, keeping the other DOFs unchanged. In matrix form the transformation can be written as:

$$\mathbf{y}(t) = \mathbf{D}(t) \mathbf{w}(t), \quad (3)$$

where: $\mathbf{w}(t) = \{x_c(t), y_c(t), a_0(t), a_1(t), b_1(t), \theta(t)\}^T$ is the vector of multiblade coordinates. The matrix \mathbf{D} can be easily derived from (2) or found in e.g., [9]. It has the following properties [9]: $\mathbf{D}(t)^{-1} = \mathbf{\Gamma D}(t)$, $\mathbf{D}(t) = \mathbf{D}(t)\mathbf{R}$ and $\dot{\mathbf{D}}(t) = \mathbf{D}(t)\mathbf{R}^2$ where $\mathbf{\Gamma}$ and \mathbf{R} are time invariant matrices. Applying the transformation to (1), using the above-mentioned properties and pre-multiplying by $\mathbf{D}(t)^{-1}$ yield the equation of motion in multiblade coordinates:

$$\mathbf{M}_D(t)\ddot{\mathbf{w}}(t) + (2\mathbf{M}_D(t)\mathbf{R} + \mathbf{G}_D(t))\dot{\mathbf{w}}(t) + (\mathbf{M}_D(t)\mathbf{R}^2 + \mathbf{G}_D(t)\mathbf{R} + \mathbf{K}_D(t))\mathbf{w}(t) = \mathbf{0}, \quad (4)$$

where: $\mathbf{M}_D(t) = \mathbf{\Gamma D}(t)^T \mathbf{M}(t) \mathbf{D}(t)$, $\mathbf{G}_D(t) = \mathbf{\Gamma D}(t)^T \mathbf{G}(t) \mathbf{D}(t)$ and $\mathbf{K}_D(t) = \mathbf{\Gamma D}(t)^T \mathbf{K}(t) \mathbf{D}(t)$. The important property of the Coleman transformation is that the matrices $\mathbf{M}_D(t)$ and $\mathbf{G}_D(t)$ are time-invariant for isotropic rotors: $m_1 = m_2 = m_3 = m$ and $k_1 = k_2 = k_3 = k$. For an isotropic rotor, $\mathbf{K}_D(t)$ is time-periodic with period $T/3$ due to the gravity.

For isotropic rotors, when the influence of gravity can be neglected, the Coleman transformation converts time-periodic EoM (1) into the time-invariant one. This allows application of conventional modal decomposition based on eigenvalue analysis of EoM (4). The results obtained by this approach lead to understanding of the collective and whirling components of the modes [9, 11].

In this study a deviation from the rotor isotropy is in focus, and the eigenvalue analysis cannot be applied. Still, since the considered deviations are assumed to be small, the results of the eigenvalue analysis of (4) might be useful as a starting point and the baseline for comparison.

Let's consider the rotor becoming slightly anisotropic, either due to damage, which causes some reduction of the stiffness of one of the blades, or by ice formation which causes a difference between the blade masses. In this situation, EoM (4) will have time-periodic coefficient matrices.

To obtain a solution to time-periodic EoM, several techniques could be employed. In his PhD thesis, Skjoldan describes and compares several methods (Table 3.1 in [12]), but in this study, classical Floquet analysis was chosen as the most appropriate¹.

The first order form of (1):

$$\dot{\mathbf{x}}(t) = \tilde{\mathbf{A}}(t)\mathbf{x}(t), \quad (5)$$

where: $\mathbf{x}(t) = \{\dot{\mathbf{y}}(t)^T, \mathbf{y}(t)^T\}^T$ is the state vector (in multiblade coordinates) and $\tilde{\mathbf{A}}(t) = \tilde{\mathbf{A}}(t + T)$ is the periodic system matrix, the size of which is 12×12 :

$$\tilde{\mathbf{A}}(t) = \begin{pmatrix} -\mathbf{M}(t)^{-1}\mathbf{G}(t) & -\mathbf{M}(t)^{-1}\mathbf{K}(t) \\ \mathbf{I}_{6 \times 6} & \mathbf{0}_{6 \times 6} \end{pmatrix}. \quad (6)$$

Extending Coleman transformation to the first order form:

$$\dot{\mathbf{x}}(t) = \mathbf{B}(t)\mathbf{z}(t), \quad (7)$$

one arrives at the first order equation in multiblade coordinates:

$$\dot{\mathbf{z}}(t) = \mathbf{A}(t)\mathbf{z}(t), \quad (8)$$

where $\mathbf{A}(t) = \tilde{\mathbf{A}}(t)\mathbf{B}(t)$.

Following [13], the analysis is performed in a number of steps:

1. The *fundamental matrix* of the system is built: Equation (8) is numerically integrated for 12 linearly independent initial conditions. Denoting the solution for the j^{th} initial condition at time t as $\boldsymbol{\varphi}_j(t)$, the fundamental matrix is written as:

$$\boldsymbol{\Phi}(t) = [\boldsymbol{\varphi}_1(t) \quad \dots \quad \boldsymbol{\varphi}_{12}(t)], \quad (9)$$

where: $\boldsymbol{\Phi}(0) = \mathbf{I}$.

2. Then the *monodromy matrix* is computed as:

$$\mathbf{C} = \boldsymbol{\Phi}(0)^{-1}\boldsymbol{\Phi}(T) = \boldsymbol{\Phi}(T); \quad (10)$$

3. As *Lyapunov-Floquet transformation* transforms the time-periodic system (8) into a time-invariant one, we can compute its system matrix \mathbf{R} as:

$$\mathbf{R} = \frac{1}{T} \ln(\mathbf{C}); \quad (11)$$

4. Eigenvalue decomposition of matrix \mathbf{R} is performed:

$$\mathbf{R} = \mathbf{V}\boldsymbol{\Lambda}\mathbf{V}^{-1}, \quad (12)$$

where the columns of \mathbf{V} are the eigenvectors \mathbf{v}_j , and the diagonal elements of $\boldsymbol{\Lambda}$ are the eigenvalues $\lambda_j = \sigma_j + i\omega_j$, the real part is the damping and the imaginary part is the frequency. Actually, the same eigenvalues can be obtained as:

$$\lambda_j = \ln(\rho_j)/T, \quad (13)$$

where ρ_j are the eigenvalues of the monodromy matrix \mathbf{C} .

5. The *periodic mode shape* of the system (8) in the multiblade coordinates, is:

$$\mathbf{r}_j(t) = \boldsymbol{\Phi}(t)\mathbf{v}_j e^{-\lambda_j t}, \quad (14)$$

6. and in the blade coordinates is:

$$\mathbf{u}_j(t) = \mathbf{B}(t)\mathbf{r}_j(t) = \mathbf{B}(t)\boldsymbol{\Phi}(t)\mathbf{v}_j e^{-\lambda_j t}. \quad (15)$$

7. Since the logarithm in (13) is complex, any $\lambda_j = \sigma_j + i(\omega_j \pm n\Omega)$, $n \in \mathbb{Z}$ are also eigenvalues of \mathbf{R} . Similar to the principal value of a complex logarithm, the principal frequency is defined as

$$\omega_{pj} = \omega_j - n_j\Omega, \quad n_j: \omega_{pj} \in]-\Omega/2; \Omega/2] \quad (16)$$

and the principal eigenvalue as $\lambda_{pj} = \sigma_j + i\omega_{pj}$.

8. The j^{th} periodic mode shape (14) computed for the principal eigenvalue λ_{pj} is expanded to the Fourier series, and the most dominant Fourier component is identified, and its frequency is $n_{0j}\Omega$. For isotropic rotor, in the absence of gravity, the frequencies $\omega_{pj} + n_{0j}\Omega$ coincide with the eigenfrequencies of the time-invariant system (4).
9. Finally, the periodic mode shape in blade coordinates (15) is also expanded to the Fourier series. The dominating Fourier components will be concentrated around the frequency $\omega_{pj} + n_{0j}\Omega$; the behaviour of these components for different degrees of anisotropy are examined in the next section.

2 EXAMINATION OF THE MODAL DYNAMIC

For examination of the rotor modal behaviour, the following parameters were chosen: $m_N = 446 \cdot 10^3 \text{ kg}$, $m_1 = m_2 = m_3 = 41.7 \cdot 10^3 \text{ kg}$, $k_1 = k_2 = k_3 = 2.006 \cdot 10^8 \text{ N} \cdot \text{m}$, $k_D = 10^8 \text{ N} \cdot \text{m}$, $k_H = 2.6 \cdot 10^6 \text{ N/m}$, $k_V = 5.2 \cdot 10^8 \text{ N/m}$, $I_D = 2.6 \cdot 10^7 \text{ kg} \cdot \text{m}^2$, $a = b = 13.1 \text{ m}$, $\alpha = 2\pi \cdot 0.16 \text{ rad/s}$. These parameters approximate to the parameters of a generic 10 MW wind turbine model. A proportional damping term was introduced to (1): $(\alpha \mathbf{M}(t) + \beta \mathbf{K}(t))\dot{\mathbf{y}}(t)$; $\alpha = 0.05$, $\beta = 0.003$ were chosen for the examination.

After Coleman transformation, in the absence of gravity, equation (4) is time-invariant, and can be readily analysed using conventional eigenvalue analysis. Six modes are obtained and identified as vertical and horizontal motion of the nacelle mass, drivetrain mode and three rotor modes: collective, backward (BW) and forward (FW) whirling. When using the Coleman approach, as it follows from [9, Equation (17)], each mode may contain up to three frequency components, the magnitude of all three blades are the same, and the phase lag of the *whirling components* will always be $\pm 120^\circ$.

In the presence of gravity, and/or when the rotor is anisotropic, the Floquet analysis needs to be applied. Figure 2 shows the Fourier components of the BW mode, its principal frequency is $\omega_{pBW} \approx 0.48 \text{ rad/s}$ and $n_{0BW} = 4$. When the rotor is isotropic, with no gravity (Figure 2a), the mode consists of three components, (i) horizontal motion of the nacelle (x_c coordinate) at frequency $\omega_{pBW} + 4\Omega \approx 4.50 \text{ rad/s} = 0.716 \text{ Hz}$, (ii) BW at $\omega_{pBW} + 5\Omega \approx 5.51 \text{ rad/s} = 0.876 \text{ Hz}$ and (iii) FW at $\omega_{pBW} + 3\Omega \approx 3.50 \text{ rad/s} = 0.556 \text{ Hz}$. The horizontal motion is superimposed by a much smaller vertical

¹ With insignificant changes, this paper uses the notations and follows derivation given in [13], where more details are provided.

motion (y_c). The mode is called *backward whirling* since the rotor dynamic is dominated by this component. The FW component vanishes completely if the rotor support is symmetric, i.e., $k_v = k_H$.

Figure 2 also shows the complexity plots of the BW component. The phase lag between all three blades is the same, -120° , and the amplitudes of the blades are also exactly equal.

As mentioned before, the same results could be obtained without Floquet analysis, by a much simpler Coleman transformation followed by eigenvalue decomposition of the system matrix \mathbf{A} in (8), which is time-invariant in this case.

Due to gravity this mode gets enriched by more components, but only two are significant: those at $\omega_{pBW} + 6\Omega \approx 6.51 \text{ rad/s} = 1.04 \text{ Hz}$ and $\omega_{pBW} + 7\Omega \approx 7.52 \text{ rad/s} = 1.20 \text{ Hz}$, Figure 2b. As observed from the complexity plot, the blade amplitude is the same, so is the lag, -120° .

Let's introduce a slight rotor anisotropy by reducing the stiffness of the third blade: $k_3 = 0.99k$. Due to this, a horizontal motion appears at $\omega_{pBW} + 6\Omega \approx 6.51 \text{ rad/s} = 1.04 \text{ Hz}$, but its magnitude is significantly smaller than the main horizontal motion. More interesting, one can see that the blades' phase lag deviates now from -120° . In addition, the amplitudes of different blades are not the same anymore, Figure 2c.

This behaviour becomes more pronounced when the stiffness k_3 decreases more, Figure 2d. This phenomena was also observed when the mass of one of the blades was changing.

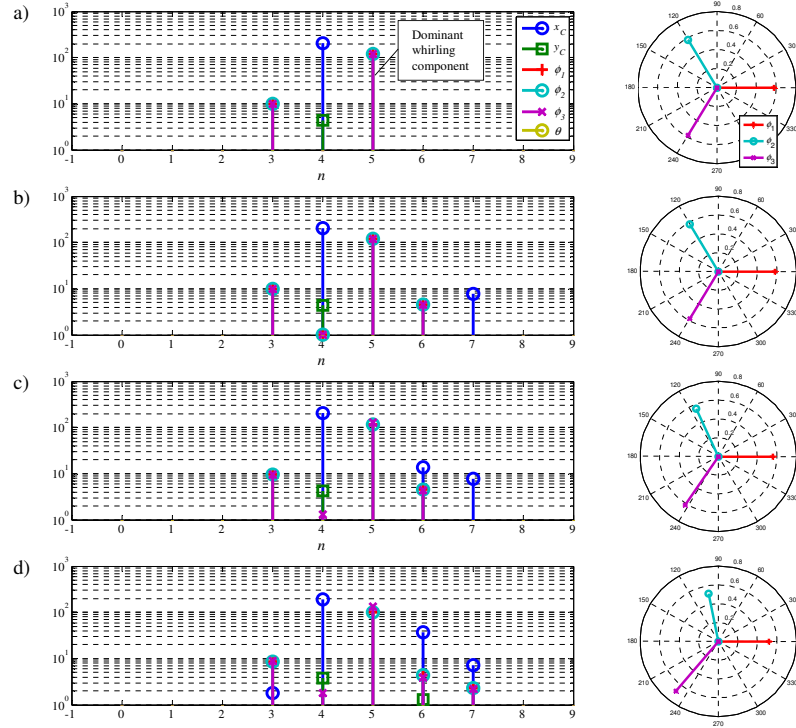


Figure 2: Backward whirling mode. Left: magnitude of Fourier components; right: complexity plot of the dominant whirling component $n=5$. a) Isotropic rotor, no gravity; b) isotropic rotor, with gravity; c) anisotropic rotor, $k_c=0.99k$; d) anisotropic rotor, $k_c=0.97k$.

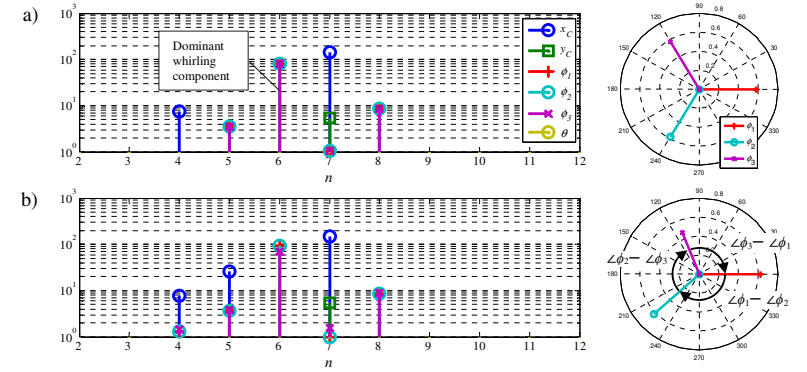


Figure 3: Forward whirling mode. Left: magnitude of Fourier components; right: complexity plot of the dominant whirling component $n=6$. a) Isotropic rotor, with gravity; b) anisotropic rotor, $k_3=0.97k$.

Figure 3 shows the Fourier components of the FW mode. For the isotropic rotor case, when no gravity is present, its principal frequency is $\omega_{pFW} \approx -0.383 \text{ rad/s}$ and $n_{0FW} = 7$. The mode is dominated by the horizontal motion of the nacelle at frequency $\omega_{pFW} + 7\Omega \approx 6.66 \text{ rad/s} = 1.06 \text{ Hz}$ and FW at $\omega_{pFW} + 6\Omega \approx 5.65 \text{ rad/s} = 0.899 \text{ Hz}$. The magnitude of the BW at $\omega_{pFW} + 8\Omega \approx 7.66 \text{ rad/s} = 1.22 \text{ Hz}$ and the other components is significantly smaller. The mode is called *forward whirling* since the FW component dominates the rotor dynamics; the BW component is small and vanishes completely for the symmetric rotor support.

One may notice that the frequency of the dominating whirling components of the two considered modes are very close: 0.876 Hz and 0.899 Hz . This is not just a coincidence. This phenomenon can be explained by the close natural frequencies of the vertical and horizontal rotor modes when the rotor does not rotate, see e.g., the Campbell diagram [11, Figure 2]. If the stiffness values of the supporting structure are equal, $k_v = k_H$, one should expect the frequencies of the dominating whirling components of the two previously described modes to be exactly the same.

3 DAMAGE FEATURES

Based on the observations above, several modal-related damage features are suggested: (i) phase between the blades for the whirling component; (ii) amplitudes of the whirling component; (iii) amplitude of the non-dominant horizontal component. The sensitivity of these damage features are examined below.

The first suggested damage feature is based on the shape of the dominant whirling component of the two whirling modes. These Fourier components are $n=5$ for BW and $n=6$ for FW modes (see Figures 2, 3). Figure 4a shows how the phase lag depends on k_3 . The calculation of the phase lag is visualized in Figure 3b, right. One per-cent reduction of k_3 causes the change of the phase lag between two undamaged blades by about 5-6% and 2-3% between damaged and undamaged blades.

All three blades have the same magnitude for isotropic rotors, but start to differ when the rotor becomes anisotropic, see Figure 4c,d for BW and FW modes respectively; the blades amplitude is normalized against the amplitude of the isotropic rotor. The damaged blade amplitude increases for the BW mode and decreases for the FW mode. The changes are about 4-6% for 1% reduction of k_3 .

It is important to note that both features give the indication of which blade is damaged.

Non-dominant horizontal component also changes with increase of rotor anisotropy. This is the Fourier component $n=6$ for the BW mode and $n=5$ for the FW mode (Figure 2,3); it increases about

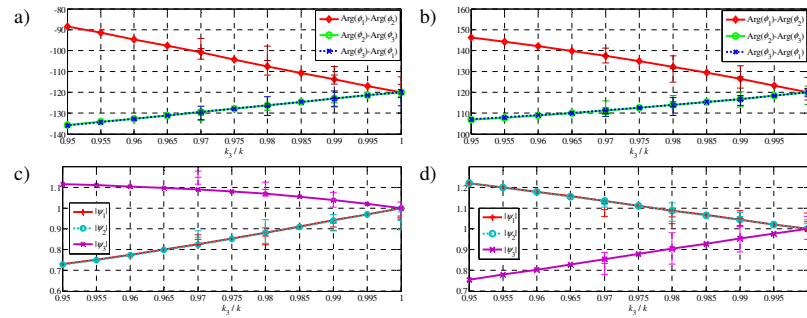


Figure 4: Damage features vs. stiffness k_3 . a) phase lag BW mode; b) same, FW mode; c) normalized blades amplitudes, BW mode; d) same, FW mode.

5-7% per 1% reduction of k_3 . This damage feature does not indicate damage location. However, it does not require getting measurements from the blades and can be extracted from the nacelle acceleration measurements.

For comparison, a one per-cent decrease of k_3 causes only 0.14-0.17% change of the natural frequencies. Therefore, these damage features used in typical SHM systems are more than 30 times less sensitive to damage than those described here.

4 OBSERVABILITY

The analytical study in the previous section was based on the known EoM. In this section, the same system is being studied from the experimental point of view, with the objective of finding out if the suggested damage features are derivable from experimental data.

In this section, we model a measurement system installed on the test object (Figure 1): accelerometers are attached to the tips of all blades, measuring in the tangential direction; two more accelerometers measure vertical and horizontal motion of the nacelle and an angular vibration accelerometer is installed on the drivetrain. All DOFs are excited by a random uncorrelated broadband noise. This excitation satisfies OMA assumptions but we acknowledge that the real aeroelastic forces are different [6]. Here the EoM is numerically integrated, and response time histories for the physical DOFs are obtained and converted to the signals that would be measured if the sensors were installed. From this point, we assume that the excitation forces and EoM are not known, so the damage features will be derived from the observed responses.

For the simulations, MATLAB's *ode45* routine was used, 7200 s long time histories corresponding to 1152 rotor revolutions were synthesized and sampled at 50 Hz. The time histories were used as an input to Brüel & Kjær Type 7760 OMA software. The modal analysis was performed by the Stochastic Subspace Iteration SSI algorithm. Four system states, one undamaged and three damaged ($k_3=0.99, 0.98$ and 0.97) were analysed. To collect statistics, five different load realisations were generated for each state, thus in total 20 analyses were performed.

Note the direct application of OMA to the data - neither Coleman transformation nor any other pre-processing were applied. Therefore, it was not expected to acquire the non-dominant components of the modes. In order to identify them, more sophisticated methods are required, e.g., the method based on Harmonic Power Spectra, either in frequency or time domain [5, 14].

The results of the simulated experiment are shown as error bars in Figure 4. The centre tick denotes the mean of the five OMA runs, the upper and lower ticks denote 95% confidence interval. The damage features derived from the OMA results are in agreement with analytical values - there is significant dispersion, especially for the magnitudes but the general tendency and the curves slope are correctly reflected, which is the most important for damage features of a SHM system.

5 CONCLUSION

Novel damage features for a potential SHM system of a wind turbine rotor are suggested and examined. The features are modal-based and utilise mode shape asymmetry due to rotor anisotropy caused by blade damage. It is demonstrated that these features are significantly more sensitive to the damage compared to the natural frequencies of the rotor. It was also shown that these features are observable in a real life scenario, i.e., they can be obtained by OMA performed on measured vibrations.

A simple 6 DOF analytical model of a rotating rotor was considered. Using Floquet analysis the exact modal decomposition was performed, and the sensitivities of the suggested damage features were numerically computed as a function of the damage size.

A simulated experiment confirmed that the damage features can be extracted from measured vibration responses using OMA.

ACKNOWLEDGEMENTS

The work is partly supported by EUDP (Danish Energy Technology Development and Demonstration Programme), grant number 64011-0084 "Predictive Structure Health monitoring of Wind Turbines".

REFERENCES

- [1] D. Montalvão, N.M.M. Maia, A.M.R. Ribeiro. A Review of Vibration-based Structural Health Monitoring with Special Emphasis on Composite Materials. *The Shock and Vibration Digest*, 38(4):295-324, July 2006.
- [2] W. Fan, P. Qiao. Vibration-based Damage Identification Methods: A Review and Comparative Study. *Structural Health Monitoring*, 10(1):83-111, April 2010
- [3] M.D. Ulriksen, D. Tcherniak, P.H. Kirkegaard, L. Damkilde. Operational Modal Analysis and Wavelet Transformation for Damage Identification in Wind Turbine Blades. *Proceedings of 7th European Workshop on Structural Health Monitoring*, Nantes, France, July 2014 (accepted for publication).
- [4] D. Tcherniak, J. Basurko, O. Salgado, I. Urresti, S. Chauhan, C.E. Carcangiu, M. Rossetti. Application of OMA to operational wind turbine. *Proceedings of Int. Operational Modal Analysis Conference*, Istanbul, Turkey, May 2011.
- [5] S. Yang, D. Tcherniak, M.S. Allen. Modal Analysis of Rotating Wind Turbine using Multiblade Coordinate Transformation and Harmonic Power Spectrum. *Proceedings of 32nd Int. Modal Analysis Conference*, Orlando, FL, USA, February 2014
- [6] D. Tcherniak, S. Chauhan, M. H. Hansen. Applicability limits of Operational Modal Analysis to Operational wind turbines. *Proceedings of the 28th Int. Modal Analysis Conference (IMAC XXVIII)*, Jacksonville, FL, USA, February 2010.
- [7] M.S. Allen, M.W. Sracic, S. Chauhan, M.H. Hansen. Output-Only Modal Analysis of Linear Time Periodic Systems with Application to Wind Turbine Simulation Data. *Mechanical Systems and Signal Processing*, 25:1174-1191, 2011.
- [8] P.F. Skjoldan, M. H. Hansen. On the similarity of the Coleman and Lyapunov-Floquet transformations for modal analysis of bladed rotor structures. *Journal of Sound and Vibration*, 327:424-439, 2009.
- [9] M.H. Hansen. Improved Modal Dynamics of Wind Turbines to Avoid Stall-induced Vibrations. *Wind Energy* 6:179-195, 2003.
- [10] P.F. Skjoldan, O.A. Bauchau. Determination of Modal Parameters in Complex Nonlinear Systems. *Journal of Computational and Nonlinear Dynamics*, 6(3) 2011.
- [11] M.H. Hansen. Aeroelastic Instability Problems for Wind Turbines, *Wind Energy*, 10: 551-577, 2007.
- [12] P.F. Skjoldan. Aeroelastic Modal Dynamics of Wind Turbines Including Anisotropic Effects. *PhD Dissertation*, 2011.
- [13] P.F. Skjoldan. Modal Dynamics of Wind Turbines with Anisotropic Effects. *47th AIAA Aerospace Sciences Meeting*, Orlando, FL, USA, January 2009.
- [14] D. Tcherniak, M. Allen, S. Yang. Experimental characterization of operating wind turbine using Harmonic Power Spectra and Stochastic Subspace Identification. *Conference on Noise and Vibration Engineering (ISMA)*, Leuven, Belgium, September 2014 (accepted for publication).

EFFECT OF A DAMAGE TO MODAL PARAMETERS OF A WIND TURBINE BLADE

Gunner Chr. Larsen¹, Peter Berring¹, Dmitri Tcherniak², Per Hørlyk Nielsen¹, Kim Branner¹

¹ DTU Wind Energy, Technical University of Denmark, P.O. Box 49, Roskilde 4000, Denmark

² Brüel & Kjær SVM, Skodsborgvej 307, Nærum 2850, Denmark

gula@dtu.dk

ABSTRACT

This study reports structural dynamic characteristics obtained experimentally from an extensive testing campaign on a 34m long wind turbine blade mounted on a test-rig under laboratory conditions. Further, these experimental results have been compared with analog numerical results obtained from a very detailed FE model of the same blade using 3D solid elements. Both an undamaged and a damaged blade are investigated, and it is observed that the natural frequencies of the first few modes of the blade change very little due to a significant artificial damage imposed in trailing edge, whereas the mode shapes - especially if decomposed into the flapwise, edgewise and torsional components - contain information which might be helpful for detecting and localizing wind turbine blade damages.

KEYWORDS : *Dynamic characteristics, FE modeling, OMA, structural damages, wind turbine blade.*

INTRODUCTION

Today, there are no doubts left that Structural Health Monitoring (SHM) becomes a trend in modern civil engineering. Indeed, in many cases it is economically advisable to replace traditional periodic visual checks of the structure with permanent automatic monitoring of its behavior based on sensor readings. This is especially valid for off-shore wind turbines, which in general are expensive and hard to access due to their remote location and associated challenges caused by weather conditions. One of the challenges a developer of SHM systems will face is the difficulty of testing and verifying the system. Indeed, if a SHM prototype is installed on an operating wind turbine, it may take years before the structure gets damaged, if it ever occurs. The solution to this problem could be simulation environments, where different damages can be modeled, and the *dynamics* of the damaged structure can be simulated. It is then important, that the damage modeling is realistic, in the sense that the dynamic properties of the real damaged structure and its numerical counterpart are the same. This is the topic of the present paper.

The paper describes the full-scale experimental setup, the data processing and the resulting dynamic characteristics for both an undamaged and a damaged blade configuration. The dynamic characteristics of the two blade configurations are subsequently compared with analog numerical results derived from detailed FEM simulations, and conclusions are drawn.

1 EXPERIMENTS

To study and compare the dynamic characteristics of a damaged wind turbine blade and the corresponding undamaged blade, a full-scale 34m blade, manufactured by SSP Technology A/S, was mounted to a test rig under laboratory conditions (cf. Figure 1). The blade was positioned horizontally with the suction side pointing towards the ground.



Figure 1: The 34m blade in the experimental Blade Test Facility at DTU Wind Energy. Left: Suction of blade. Right: Upper (pressure) side of blade. Accelerometers is marked with a red arrow

Several test campaigns were carried out throughout the experiment. The first test was carried out on the undamaged blade. This (reference) test was subsequently followed by tests, where artificial damages were introduced in the trailing edge 18,8m and onwards from the root. In the damaged part of the blade the adhesive between the upper and lower part of the shell was removed to mimic a crack in the trailing edge (cf. Figure 2). The first the damage had a length of 20cm along the blade, and this damage was progressively extended throughout the test campaigns, reaching a length of 120cm in the final test, and thus extending from 18,8m to 20,0m as measured from the blade root. The damaged part of the trailing edge was re-established after tests to enable the blade to be used for other experiments, and the first (reference) tests on the undamaged blade was repeated to investigate whether the re-established trailing edge had affected the dynamic properties of the blade.



Figure 2: The artificial trailing edge damage introduced in the 34m blade

1.1 Instrumentation

Figure 3 sketches the architecture of the measurement system. Twenty triaxial accelerometers B&K Type 4524B were mounted along the blade leading and trailing edges in ten measurement stations located 3.9m; 8m; 11.6m; 14.8m; 17.6m; 20.2m; 22.6m; 24.7m; 26.9m and 28.9m, respectively, from the root).

A substantial effort was made to ensure the position and alignment of the accelerometers in relation to the main axes of the blade, which is a key requirement for a good estimation of the mode shapes.

Since the size and flexibility of the blade prevent the use of conventional tools for measuring lengths and angles, a specially manufactured template was used. Using the template and knowing the geometry of the blade sections, the accelerometers were mounted with sufficiently high precision. Swivel bases B&K Type UA1473 were used to facilitate accelerometer mounting with required orientation.

In order to simplify the measurement setup and reduce the length of the accelerometer cables, a distributed data acquisition system was implemented: every four accelerometers were connected to a 12-ch. data acquisition module B&K Type 3053-B located nearby the accelerometers. The supporting structure was additionally instrumented by 6 triaxial accelerometers (B&K Type 4506). All data acquisition modules were connected to a Cisco Ethernet switch (SG300-10MP), which supports Precise Time Protocol (PTP) and Power over Ethernet (PoE) features. This solves modules' powering and synchronization issues, further reducing the number of cables and the set-up time.

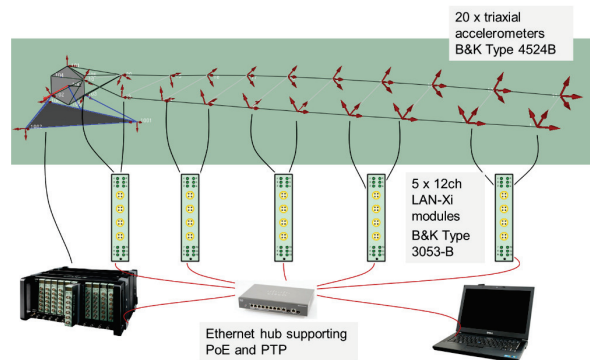


Figure 3: Measurement system architecture. The red arrows show location and orientation of the accelerometers

1.2 Excitation and data acquisition

Since OMA was chosen as dynamics characterization tool, a stochastic excitation needs to be applied. This excitation has to be distributed over the entire structure; be uncorrelated and to have a flat spectrum in the frequency range of interest. In practice, the excitation was performed by several persons hitting the blade at a number of positions using heavy wooden sticks wrapped with foam. An excitation time span of 20 minutes was chosen in order to have a sufficient number of oscillations at the lowest frequency of interest (evaluated to about 1.4Hz). B&K Pulse software was used for data acquisition.

1.3 Data analysis

The experimental data were analyzed using B&K Operational Modal Analysis software Type 7760 (OMA) [1], which, contrary to traditional Modal Analysis (MA), does not require the excitation forces to be recorded, but alternatively *assumes* these to be uncorrelated white noise sources distributed over the entire structure. OMA SSI UPC (Stochastic Subspace Identification, Un-weighted Principal Components) algorithm was utilized.

For each recorded 20 minutes time series, three additional analyses were conducted by splitting the 20 minute time series in three consecutive, partly overlapping, time series, each with a length of 7 minutes. This allowed us to analyze variability of the obtained modal parameters as well as to estimate confidence intervals for experimentally obtained modal parameters. Also, by comparing

the results emerging from each of these three 7 minute time series with the analog results emerging from the full 20 minute time series, the potential influence of recording span lengths was studied.

2 FEM MODELING

The blade dynamics as well as the effect of the damage (trailing edge opening) introduced in the full-scale blade were also investigated numerically using a detailed FE model. The blade was modeled using the commercial finite element pre and post-processor MSC/PATRAN [2]. The model was generated utilizing the DTU Wind Energy's in-house software Blade Modeling Tool (BMT), and MRC/MARC [3] was applied as the solver in all analyses.

2.1 Modeling details

As 20-noded layered continuum elements were used to model the blade structure, a volume representation of the geometry was required. This geometry was generated using BMT together with MSC/PATRAN. 25 cross-sections/aerodynamic profiles were applied in the modeling scheme, which describes the outer geometry of the blade. The curves defining these cross-sections were offset according to the layup definition in order to represent the thickness of the laminates. Finally, the individual cross-sections were connected by spline curves and interpolation surfaces to obtain a volume representation of the blade.

The process described in the previous paragraph was handled automatically by BMT, which in this model utilizes 48 regions/solids to assign the different properties. Variations in thickness between regions results in tapered solids. The model applied in these studies has approximately 40.000 elements. The composite layup was modeled with 15-44 plies though the thickness via BMT, and composite properties were assigned to layered 20-noded continuum elements.

The blade is mounted on a test rig, which is a welded steel construction. This rig was modeled including an estimated flexibility of rig. In these studies the rig is included as a spring/beam system, which is coupled to the blade via a MPC element. Investigations have shown that the flexibility of the rig has only marginal effect on the simulated eigenvalues and eigenvectors of the blade.

The same damage as applied in the experimental test campaign (trailing edge opening) was modeled in the FE model. The adhesive bound was deboned from the lower (pressure side) trailing edge, i.e. the elements were not joined in the interfaces on the area between the adhesive bound and the trailing edge laminate. Contact conditions were, however, not applied in these studies.

The modal analyses were performed by applying the Lanczos method in MSC/MARC. Earlier studies were performed to investigate the effect of including the preloading generated by gravity as a load step before performing the modal analyses. The influence of including gravity turned out to be so limited, that it was decided not to include this in the reported numerical results. An example of a mode shape associated with the damaged blade is shown in Figure 4.

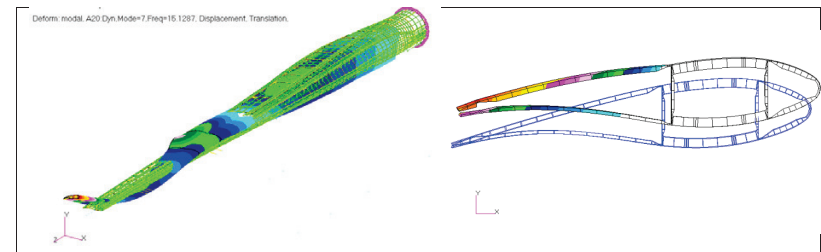


Figure 4: The numerical results of mode 7 of the damaged blade. This mode is primary a combination of flap and edge deflections.

3 RESULTS

The study compares the results from OMA analysis on the full-scale undamaged and damaged blade with the results from respective eigenvalue solutions of the FE models. The lowest 7 natural frequencies (eigen values) together with their associated mode shapes (eigen vectors) are investigated. In addition two higher order experimental modes, without an obvious numerical counterpart but with interesting identification properties, are reported.

As for the experimental analysis, flapwise deflection was defined by $y_c = (y_{LE} + y_{TE})/2$; edge wise deflection was defined by $x_c = (x_{LE} + x_{TE})/2$; and torsion deflection was defined by $\alpha_c = \arctan(y_{LE} - y_{TE})$, where x_{LE} , x_{TE} , y_{LE} , y_{TE} are respectively edge- and flapwise displacements of the leading and trailing edges measured at the same radial coordinate of the blade. Note, that the defined torsional deflection differ from a physical rotation, but can be considered as a rotation type parameter amplifying the blade outboard rotations, where the chord lengths are smaller compared to the chord lengths associated with the inner part of the blade.

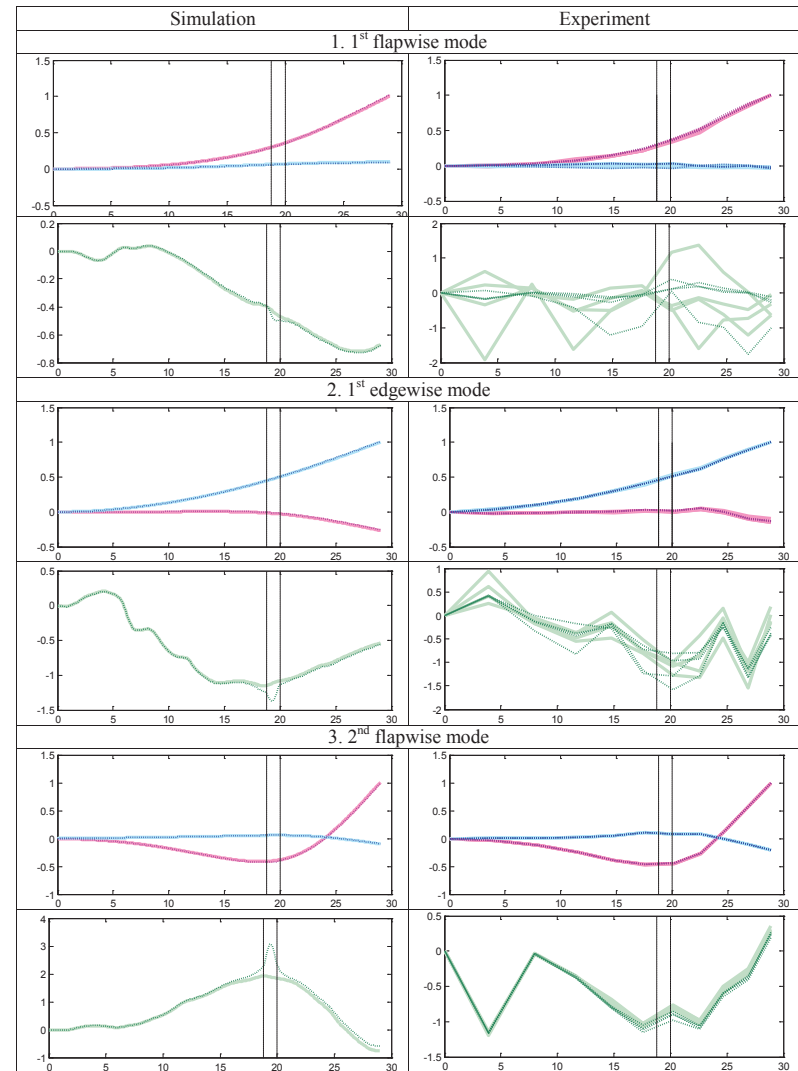
Figure 5 shows the components of the investigated mode shapes. The left column of the figure displays the FEM results, and the right column shows the corresponding experimental results. Mode shapes referring to the undamaged blade are identified by thick solid lines, whereas mode shapes associated with the damaged blade are plotted as thin dotted lines. Further, red lines refer to flapwise components, blue refers to edge wise components; and green refers to torsion components, respectively. The dashed vertical black lines indicate the boundary of the imposed damage. The experimentally based graphs additionally also show the variability among the experimental mode shapes obtained from the three 7 minute time series and the 20 minute time series, respectively. To ease the comparison between experimental and numerical results, the mode shapes were normalized by defining the tip displacement of the dominating bending modal component as equal to unity.

As for damage detection, two types of “identifier” characteristics can be observed for the *numerical results* corresponding to local and global blade modal type of behavior, respectively. These “identifiers” are predominantly visible in the torsion model component, which is in agreement with the type of damage imposed, where one of the cross sectional cells are opened, and therefore mainly affects the torsion stiffness properties. However, for higher order modes, moderate effects can also be seen in the flap and edge wise modal components. The local modes reflect a local deformation/opening of the blade shell at position of the damage, but with no effect on the blade global deflection pattern. From a practical perspective, such identifiers are not very useful for damage detection, because an unsuitable amount of sensors are required to resolve all possible relevant local modes. This is contrary to damage identifiers based on changes in a blade global mode (e.g. mode 5), where one heuristically can represent the damage as a stiffness “hinge” mainly affecting the blade mode in the regime extending from the damage and to the blade tip. Like for the local modes, information on the damage location is therefore also resulting.

Turning to the *experimental results* little scatter among the four analyzed data sets (i.e. 3x7 minute series and the 20 minute series, respectively) is observed for the bending components of the modal shapes. This is contrary to the torsion components, where large variability is observed, especially associated with torsion mode components with very modest amplitudes. This most likely relates to the fact that the torsion signal is derived as the difference between two flapwise signals of comparable size, thus implying relatively high sensitivity to measurement noise/errors. Other explanations could be differences in the damping properties. The main difference between applying 20 minute time series and 7 minute time series is more favorable stabilization diagrams.

Comparing experimentally determined modal shapes with the analog modal shapes resulting from the numerical analysis, a very convincing agreement is found between the *flapwise* and *edge wise* modal components for the investigated first 7 modes. The experimental results do not resolve the *local* damage effects on these modes, but this could not be expected since no accelerometers were positioned at the damage location. As for the *torsion* component, the comparison shows significant differences in shape as well as in magnitude. However, despite the observed shape differences, qualitative similarities are also observed, as global modal effects are seen for the torsion component

in both experiments and numeric’s for mode 3, mode 4 and mode 7, respectively. Consistent with this observation, absolutely no effect of the damage on the global torsion component is observed for mode 6 in the experimental as well as the numerical results.



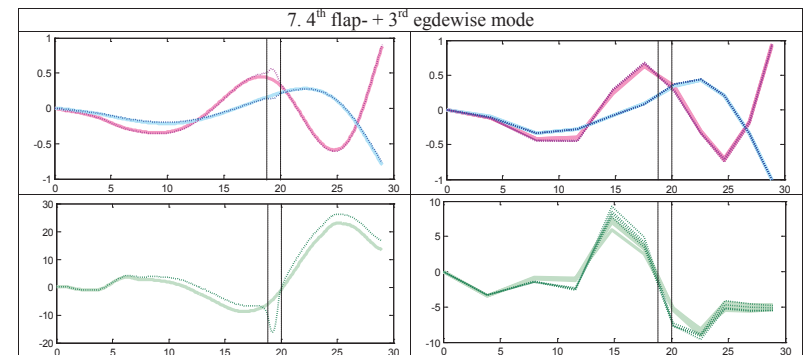
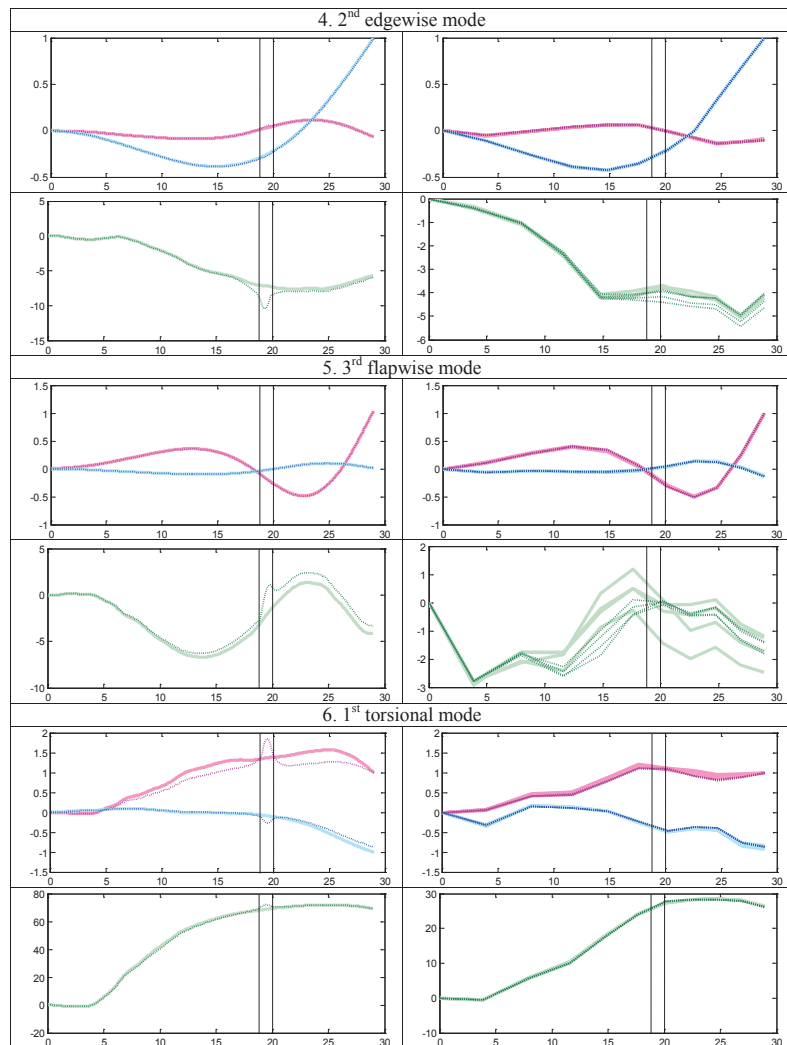


Figure 5: Blade mode shapes. Left column: numerical results; right column: experimental results.

Additionally two higher order modes are identified by OMA, which cannot directly be paired with analog modes from the numerical analysis. These modes show relative high sensitivity to the damage, and they are therefore included and shown in Figure 6.

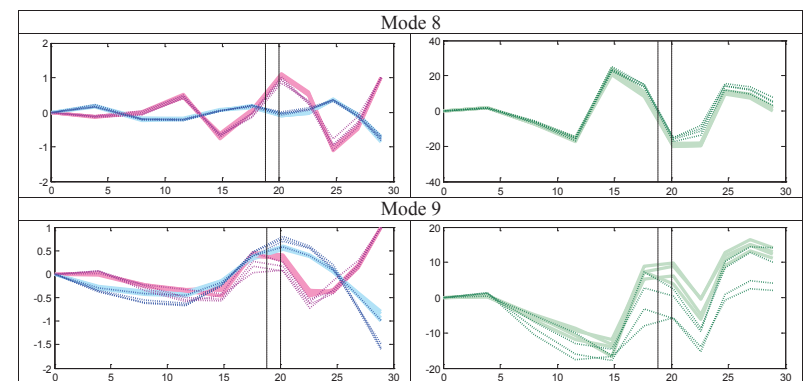


Figure 6: Higher order experimental mode shapes with high sensitivity to the imposed damage

Finally, the results for the corresponding natural frequencies are shown in Table 1 for the two blade configurations and including both the experiment and the numerical analysis.

Table 1: Simulated and measured natural frequencies for the damaged and the undamaged blade

Mode	Name	Damaged blade		Undamaged blade	
		OMA [Hz]	FEM [Hz]	OMA [Hz]	FEM [Hz]
Mode 1	1st flap	1.36	1.37	1.36	1.38
Mode 2	1st edge	1.86	1.81	1.86	1.80
Mode 3	2nd flap	4.21	4.20	4.21	4.22
Mode 4	2nd edge	7.12	7.09	7.12	7.10
Mode 5	3rd flap	9.17	9.39	9.19	9.41
Mode 6	1st torsion	12.4	11.8	12.4	11.9
Mode 7	4th flap + 3rd edge	15.0	15.1	15.0	15.2

As seen good agreement is observed between predicted and measured natural frequencies for both the undamaged and the damaged blade. It is furthermore seen, that the natural frequencies display no sensitivity to the investigated damage for all practical purposes.

CONCLUSION

A very convincing agreement between measured and simulated results has been demonstrated for the natural frequencies as well as for the bending components of the mode shapes. However, significant differences in shape and/or magnitude are observed for the torsion components of the mode shapes, especially when associated with torsion mode components with very modest amplitudes.

It was also observed that the natural frequencies of the investigated modes of the blade change very little due to the imposed trailing edge damage, with changes being significantly below the uncertainties of OMA. However, the mode shapes, when decomposed into the flapwise, edgewise and torsional components contain information, which might be helpful for detecting and localizing damages in the trailing edge of the blade.

ACKNOWLEDGEMENTS

The work is supported by EUDP (Danish Energy Technology Development and Demonstration Programme), grant number 64011-0084 "Predictive Structure Health monitoring of Wind Turbines".

REFERENCES

- [1] Zhang L, Brincker R, and Andersen P. 2005. An Overview of Operational Modal Analysis: Major Development and Issues, Proc. of 1st Int. Operational Modal Analysis Conference (IOMAC-2005).
- [2] MSC/PATRAN. MSC Software Corporation: Patran [cited May 2014]. Available from: <http://www.mscsoftware.com/product/patran>.
- [3] MSC/MARC. MSC Software Corporation: Marc [cited May 2014]. Available from: <http://www.mscsoftware.com/product/marc>.

OPERATIONAL MODAL ANALYSIS AND WAVELET TRANSFORMATION FOR DAMAGE IDENTIFICATION IN WIND TURBINE BLADES

Martin D. Ulriksen¹, Dmitri Tcherniak², Poul H. Kirkegaard¹, Lars Damkilde¹

¹ Dept. of Civil Engineering, Aalborg University, Sohngaardsholmsvej 57, Aalborg, Denmark

² Brüel & Kjær Sound & Vibration Measurement A/S, Skodsborgvej 307, Nærum, Denmark

mdu@civil.aau.dk

ABSTRACT

The presented study demonstrates an application of a previously proposed modal and wavelet analysis-based damage identification method to a wind turbine blade. A trailing edge debonding was introduced to a SSP 34 m blade mounted on a test rig. Operational modal analysis (OMA) was conducted to obtain mode shapes for undamaged and damaged states of the blade. Subsequently, the mode shapes were analyzed with one-dimensional continuous wavelet transformations (CWTs) for damage identification. The basic idea of the method is that structural damage will introduce local mode shape irregularities which are captured in the CWT by significantly magnified transform coefficients, thus providing combined damage detection, localization, and size assessment. It was found that due to the nature of the proposed method, the value of the identification results highly depends on the number of employed measurement points. Since only a limited number of measurement points were utilized in the experiments, valid damage identification can only be obtained when employing high-frequency modes.

KEYWORDS : Wind Turbine Blades, Debonding, Wavelet Transformation, Operational Modal Analysis.

INTRODUCTION

While failure can happen in any structural component of the wind turbine, one of the most common and critical components to fail is the blade [1]. Here, several damage types can occur [2], and in extreme situations, the entire blade can be destroyed. Since the blades account for 15-20 % of the total wind turbine costs [3], a great need in a dedicated blade structural health monitoring (SHM) system, facilitating 3-level damage identification, i.e. detection, localization, and assessment, c.f. [4], was identified. The different proposed blade SHM methods utilize a wide range of quantities like temperature, noise, and vibration. As described in [5], the applicability of each of these methods is primarily tested on the basis of controlled laboratory tests, or by finite element (FE) simulations. With both of these methods, significant simplifications and idealizations are made with regard to, i.a., environmental effects. Under these conditions, several simple methods comparing pre- and post-damage quantity values, e.g. modal parameters, have exhibited potential for damage detection. However, under conditions that are more realistic, these methods are inapplicable since environmental effects and noise contamination typically will conceal the direct changes of the previously mentioned quantities. As an example, it is stated in [6] how environmental effects can account for up to 5 % changes in eigenfrequencies, which, as is also demonstrated in the present study, cannot be expected to be exceeded by damage-induced eigenfrequency changes. Due to the general inadequacy of the simple methods, current research within the field of blade SHM is leveled mainly at developing more sophisticated and robust methods that, for example, include advanced signal processing or statistical analysis, see e.g. [7].

The present paper documents the application of the early-proposed vibration-based method, employing continuous wavelet transformation (CWT) of spatial mode shape signals for damage detec-

tion, localization, and assessment on a full-scale wind turbine blade. In [8, 9], similar studies were conducted as CWTs were used to identify different cracks in residential-sized wind turbine blades. In these studies, the mode shapes were derived through experimental modal analysis (EMA), where an impact hammer was used for excitation. In the present study, operational modal analysis (OMA) is used to obtain the mode shapes and this means we can examine the applicability of the proposed damage identification method for blades under conditions that resemble in-service conditions more closely. Additionally, this paper uses a simple damage indicator, inspired by modal assurance criterion (MAC), which expresses the similarity between pre- and post-damage wavelet transforms.

The paper is organized as follows: the first section describes the test object, the damage, the measurement system, and the conducted experiments; while the following section gives the basics of CWT and describe the application of the method to the mode shapes.

1. OMA OF SSP 34 M BLADE

1.1 Test object

A 34 m long wind turbine blade, designed and manufactured by SSP, was mounted on an indoor test rig as shown in Figure 1. The SSP 34 m blade is made from epoxy fiberglass and has a mass of 4,600 kg [10].



Figure 1 : SSP 34 m blade mounted on the test rig. (a) Root-to-tip view. (b) Tip-to-root view.

1.2 Measurement system

The measurement system consisted of 20 triaxial accelerometers (Brüel & Kjær Type 4524-B) mounted on leading and trailing edges at ten stations along the blade, see Figure 2(a). The distances between the neighboring stations differed along the blade, from 4,100 mm at the blade root to 2,000 mm at the tip.

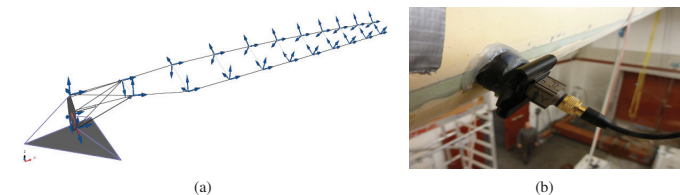


Figure 2 : Accelerometer mounting on SSP 34 m blade. (a) Accelerometer location and orientation. (b) Utilized accelerometers (Brüel & Kjær Type 4524-B) mounted on a swivel base (Brüel & Kjær UA-1473).

Location and orientation of the accelerometers have a key importance for getting correct mode shapes: their location and orientation in reality should be as close as possible to the coordinates and orientation of measurement DOFs documented in the modal analysis software. In this project, this was achieved by using a dedicated template that was aligned against the foil profile at the stations, and the accelerometers were fixed on swivel bases according to the template. In Figure 2(b), a picture of an accelerometer mounted on a swivel base is shown.

Due to large distances between measurement points, it was advantageous using a distributed data acquisition system based on five, 12-channel, Brüel & Kjær LAN-XI modules Type 3053-B-120. Each module served two stations, i.e. four triaxial accelerometers, and was placed near the sensors, therefore keeping the length of the accelerometer cables minimal. The modules were powered via an Ethernet cable, which was also used for data transfer and modules synchronization.

1.3 Data acquisition

According to OMA assumptions, the excitation is required to be distributed over the entire structure, it needs to be uncorrelated, and have a flat spectra in the frequency range of interest. The blade was excited by several people hitting the blade at a number of positions with heavy wooden sticks wrapped in foam.

Data from the accelerometers was recorded during approximately seven minutes, corresponding to at least 500 oscillations at the lowest frequency of interest, which was identified as approximately 1.3 Hz.

1.4 Damage

To ensure that the damage introduced to the blade model is realistic, a study of typical structural blade damages was conducted and some of the critical ones were chosen for further work.

In [2], 15 blades of 300 kW wind turbines and 81 blades of 100 kW wind turbines, all with a lifetime range of between 16 and 19 years, were inspected. As a result of these inspections, several different damage types were found and subsequently categorized into the three overall groups; cracks, edge damages, and debondings. Of these damage types, the most frequently occurring and severe were debondings plus longitudinal and transverse cracks near and at the blade edges. These all required structural repairs for the blades to operate properly, c.f. [2]. Consequently, in the present study we decided to treat one of these specific damage types, namely a trailing edge debonding, see Figure 3.



Figure 3 : Debonding introduced in the trailing edge of an SSP 34 m blade. (a) Original drilled debonding. (b) Extended debonding.

The debonding was first introduced by drilling a series of holes perpendicular to the trailing edge, such that the glue connecting the shells was removed to yield the damage depicted in Figure 3(a). Subsequently, the debonding was gradually extended using a hammer and a chisel, resulting in the 1,200 mm long debonding shown in Figure 3(b). The extended debonding was located between 18,800 mm and 20,000 mm from the blade root.

1.5 Experiment and analysis

First, a series of OMA tests was performed on the undamaged blade and then the blade with different lengths of debonding. The damage was repaired according to the blade guidelines, and one more OMA test was conducted.

Since some additional, no-visible, inner-damage could occur when operating with the heavy hammer and chisel, it was decided to focus on two states; the state just before the damage was repaired, and the state right after the repair. For each of these states, a 20 minute long data set was available. The data set was split into three equal segments, each about seven minutes long, and OMA was performed on each of the segments. OMA was also performed on the entire 20 minute data sets to see if more data would enhance the OMA algorithm performance. Therefore, in total, eight states were considered, with states 1-4 and 5-8 characterizing the 'damaged' state and 'undamaged' state, respectively.

Brüel & Kjær OMA software Type 7760 was employed, and the stochastic subspace identification (SSI) algorithm was applied to the data. The ten lowest modes were identified for all eight states. In Table 1, the mode names and their frequencies (the mean and 95 % confidence estimated from four averages) are presented. Additionally, the ten mode shapes are plotted in Figure 4 for all eight states.

Table 1 : First ten modes for damaged and undamaged states of SSP 34 m blade.

Mode number	Mode type	Frequencies [Hz]			
		Damaged		Undamaged	
		Mean	Confid.	Mean	Confid.
1	1st flap	1.35	0.01	1.36	0.01
2	1st edge	1.86	0.01	1.86	0.01
3	2nd flap	4.21	0.01	4.21	0.00
4	2nd edge	7.12	0.01	7.12	0.00
5	3rd flap	9.17	0.01	9.19	0.06
6	1st torsion	12.37	0.01	12.40	0.02
7	3rd edge + 4th flap	14.19	0.06	14.16	0.10
8	4th flap + 3rd edge	14.98	0.01	14.99	0.01
9	Complex shape	15.33	0.02	15.48	0.03
10	Complex shape	17.99	0.05	18.08	0.04

2. DAMAGE IDENTIFICATION IN SSP 34 M BLADE

Using the OMA method presented in Section 1., the modal parameters for the SSP 34 m blade were extracted. Even though the experiment was conducted in a well controlled test-rig environment, the changes in the natural frequencies due to the damage are comparable with the dispersion due to measurement noise, see Table 1. Further, direct visual comparison of the mode shapes plotted in Figure 4 could not provide valid information to facilitate damage identification. Consequently, a more sophisticated and robust method, in the form of CWT, was employed.

2.1 Basics of CWT

The idea of the proposed damage identification method is to apply CWT to the spatial mode shape signals and thereby identify damage-induced irregularities in these signals. In this section, focus

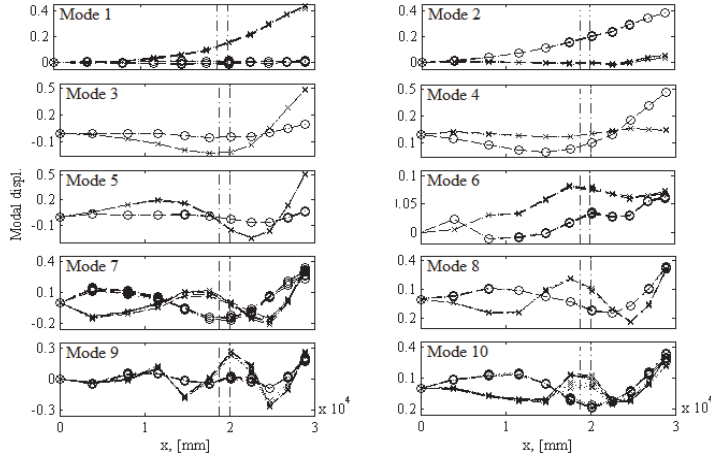


Figure 4 : Flapwise (×) and edgewise (○) components of the first ten mode shapes of damaged (···) and undamaged (---) SSP 34 m blade. The dashed vertical lines mark the debonding location.

will be on describing the basics of CWT and its applicability in damage identification. The latter includes employment of mode shape signal interpolation and extrapolation procedures for improving the wavelet transform as a damage indicator.

By comparing the spatial mode shape signal, $f(x) \in L^2(\mathbb{R})$, to the wavelet function, $\psi(x) \in L^2(\mathbb{R})$, at various wavelet scales, $a \in \mathbb{R}^+$, and positions, $b \in \mathbb{R}$, the CWT

$$Wf(a, b) = \frac{1}{\sqrt{a}} \int_{\mathbb{R}} f(x) \psi^* \left(\frac{x-b}{a} \right) dx \quad (1)$$

is obtained as the inner product of $f(x)$ and the complex conjugated, indicated with the superscript *, of the so-called wavelet family. The wavelet family consists of functions constructed from dilations and translations of ψ , that is

$$\psi_{a,b}(x) = \frac{1}{\sqrt{a}} \psi \left(\frac{x-b}{a} \right), \quad (2)$$

thus large values of a correspond to big wavelets and consequently coarse features of $f(x)$, while low values of a correspond to fine details of $f(x)$. In Equation (2), the factor $\frac{1}{\sqrt{a}}$ is applied as a normalization operator such $\|\psi_{a,b}(x)\| = \|\psi(x)\|$.

2.2 CWT for damage identification

Because of the effectively limited duration of the waveform, signals with abrupt changes can be better analyzed with a wavelet than with a smooth sinusoid. This is exploited in the proposed damage identification method, where the idea is that structural damage in the blade will induce local mode shape irregularities. These are then captured in the CWT by significantly magnified transform coefficients, thus providing level 3 damage identification. However, studies in [7], for example, suggest that the effectiveness of CWT for damage identification is typically increased when the derivatives of the mode

shapes are examined. This can easily be exploited since

$$\int_{\mathbb{R}} x^k \psi(x) dx = 0, \quad k = 0, 1, \dots, n-1, \quad (3)$$

in which it is stated how a wavelet has n vanishing moments when $k = n-1$. This means that a wavelet with n vanishing moments is orthogonal to polynomials up to degree $n-1$, thus resulting in zero-valued wavelet coefficients for these polynomials. By rewriting Equation (1) into a convolution, the following is obtained:

$$Wf(a, b) = \left(\frac{d^n}{dx^n} f * \psi'_a \right) (b) = \left(f * \frac{d^n}{dx^n} \psi'_a \right) (b) \quad \because \quad \psi'_a(x) = \frac{1}{\sqrt{a}} \psi^* \left(\frac{-x}{a} \right), \quad (4)$$

hence the CWT of the n th derivative of the mode shape is found directly as a convolution of the original mode shape and a wavelet with n vanishing moments.

In the present study, several wavelet types were tested, and it was found that a real-valued Gaussian wavelet with four vanishing moments, i.e.

$$\psi(x) = \frac{d^4}{dx^4} (C_4 e^{-x^2}) = 4C_4 e^{-x^2} (4x^4 - 12x^2 + 3), \quad (5)$$

yields the best results in the damage identification analyses of the SSP 34 m blade. Consequently, this particular wavelet was used. The constant in Equation (5) is found such the Euclidean norm $\|d^4 \theta(x)/dx^4\|^2 = 1$. By employing scaling and position variables, the wavelet is dilated and translated accordingly.

2.2.1 Mode shape interpolation

When conducting modal analysis to derive spatial mode shapes, a finite, and often reduced, number of measurement points are employed, resulting in introduction of discontinuities in the CWT due to low resolution. In order to overcome this issue, a smoothing scheme was applied in the form of cubic spline interpolation, where the original mode shape signals were oversampled with an increment of 10 mm.

2.2.2 Mode shape extrapolation

Since the CWT, cf. Equation (1), is an infinite integral transformation, adverse boundary effects will be introduced when employing the finite mode shape signal and wavelet function. These boundary effects will yield significant increases/decreases in the CWT coefficients at the boundaries which may conceal actual damage-induced CWT coefficient extrema. Therefore, an extrapolation scheme was included for removal of these boundary effects by shifting them to outside the interval in which the mode shapes are defined. Several studies, see e.g. [11], suggest using cubic spline extrapolation, but in the present study, it was found that linear extrapolation utilizing the two outermost points at each end of the smoothed signal yields the most effective removal of adverse boundary effects. It is important to notice that this approach of course depends on the spatial resolution in the smoothed signals.

2.3 CWT of SSP 34 m mode shapes

By convolving the SSP 34 m mode shapes with the chosen Gaussian wavelet, CWTs were derived for both damaged and undamaged states. By this means, it was found that valid damage identification can only be obtained when inspecting the CWTs of the flapwise components of mode shape 8, which

is a combination of the 4th flapwise and 3rd edgewise bending modes, see Table 1 and Figure 4. In Figure 5, this is depicted based on the full series measurements, that is, state 1 and 5. It was observed that similar results were obtained consistently for the other measurement states.

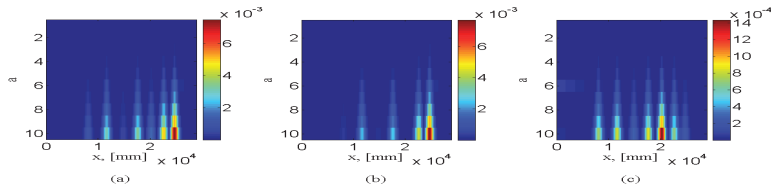


Figure 5 : CWTs of the 8th mode flapwise components, with damage location $x \in [18, 800 \text{ mm}; 20, 000 \text{ mm}]$. (a) Damaged (1st state). (b) Undamaged (5th state). (c) Difference between damaged and undamaged.

Evidently, the damage-induced irregularities are not sufficient for the post-damage CWT to work as an independent damage indicator. However, when the CWTs from the undamaged states are subtracted from the post-damage counterparts, the maximum CWT coefficients are obtained at $x \approx 20,000 \text{ mm}$, where the damage is located. Thus, the debonding can be validly detected and localized. Regarding size assessment, it was observed that multiple distinct CWT peaks occur at non-damaged areas, making it troublesome to point out the peaks induced by the actual damage. Several studies, see e.g. [11], have suggested employing a statistical threshold value below which all CWT coefficients are set to zero for eliminating the non-damage CWT peaks. A similar statistical approach was tested in the present study, but it was found that a very fine measurement density is needed to provide a sufficient threshold value and therefore the approach was discarded.

As an alternative to visually inspecting the CWT plots for damage identification, a simple damage indicator was introduced for level 1 damage identification, i.e. detection. The indicator is inspired by the MAC typically used in modal analysis (Cross-MAC), leading to the damage index

$$DI_{a,ij} = \frac{|\beta_{a,i}^T \gamma_{a,j}|^2}{\beta_{a,i}^T \beta_{a,i} \gamma_{a,j}^T \gamma_{a,j}} \in [0; 1], \quad (6)$$

where $\beta_{a,i}$ is the CWT coefficient vector of the undamaged reference mode shape i at scale a , while $\gamma_{a,j}$ is the CWT coefficient vector of either pre- or post-damage mode shape j at scale a , i.e. $\gamma \supseteq \beta$. By choosing state 5 as the undamaged reference and subsequently analyzing the flapwise components of mode shape $i = j = 8$ at scales $a \in [5; 10]$, the DI values presented in the box-and-whisker plot in

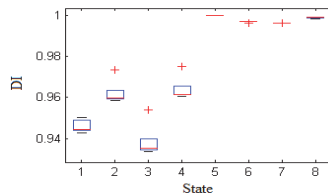


Figure 6 : Box-and-whisker plot of DI values for flapwise components of mode shape 8, with state 5 as reference. The central mark in each box is the median, the edges of the box are the 25th and 75th percentiles, the whiskers extend to the most extreme data points not considered outliers (± 2.7 times the spreading), and outliers are plotted individually.

Figure 6 were derived. It is noticed that the results for $a \in [1; 4]$ were discarded in the analyses, as the high-frequency nature of these low scales increase the sensitivity towards measurement noise.

Evidently, the DI values decrease in the post-damage states, i.e. 1-4. The significance of these reductions are quantified through the box-and-whisker plot. Here, it is clearly seen that the DI value changes in the post-damage states are significant and cannot be categorized as measurement uncertainties, therefore implying that the changes must arise from the introduction of debonding.

CONCLUSION

The paper deals with modal and wavelet analysis-based damage identification in wind turbine blades. The studied damage identification method is based on modal analysis for derivation of structural mode shapes, which are subsequently signal-processed in the spatial domain and analyzed by means of one-dimensional CWT. The method allows combined detection, localization, and assessment of structural damage. In the presented study, the abilities of the method were demonstrated by detection and localization of a 1.2 m trailing edge debonding of a 34 m blade. It was found that this type of damage could be validly detected and localized when comparing pre- and post-damage CWTs of the 8th blade mode. Regarding damage assessment in this mode, it was found that multiple distinct CWT peaks occur at non-damaged areas, thus it is troublesome to point out the peaks induced by the actual damage.

ACKNOWLEDGMENTS

The work was partly supported by EUDP (Danish Energy Technology Development and Demonstration Programme), grant number 64011-0084 "Predictive Structure Health monitoring of Wind Turbines".

The authors would like to thank DTU Wind Energy for giving access to the test object and research engineer Per Hørlyk Nielsen for his great assistance in setting up and conducting the experiment.

REFERENCES

- [1] M. M. Khan, M. T. Iqbal, and F. Khan. Reliability and condition monitoring of a wind turbine. *Proceedings of 18th Annual Canadian Conference on Electrical and Computer Engineering*, 2005.
- [2] S. Ataya and M. M. Z. Ahmed. Forms of discontinuities in 100 KW and 300 KW Wind Turbine Blades. *Proceedings of 10th World Wind Energy Conference & Renewable Energy Exhibition*, 2011.
- [3] F. M. Larsen and T. Sørensen. New Lightning Qualification Test Procedure for Large Wind Turbine Blades. *Proceedings of International Conference on Lightning and Static Electricity*, 2003.
- [4] A. Rytter. *Vibration Based Inspection of Civil Engineering Structures*. Ph.D. Thesis, Aalborg University, Denmark, 1993.
- [5] J. F. Skov, M. D. Ulriksen, K. A. Dickow, P. H. Kirkegaard, and L. Damkilde. On Structural Health Monitoring of Wind Turbine Blades. *Proceedings of 10th International Conference on Damage Assessment of Structures*, 2013.
- [6] O. S. Salawu. Detection of structural damage through changes in frequency: a review. *Journal of Engineering Structures*, 19:718–723, September 1997.
- [7] C. C. Ciang, J.-R. Lee, and H.-J. Bang. Structural health monitoring for a wind turbine system: a review of damage detection methods. *Measurement Science and Technology*, 19:122001, December 2008.
- [8] M. D. Ulriksen, J. F. Skov, K. A. Dickow, P. H. Kirkegaard, and L. Damkilde. Damage Identification in Wind Turbine Blades - A Modal and Wavelet Analysis-based Method. *To appear*.
- [9] L. Doliński and M. Krawczuk. Damage detection in turbine wind blades by vibration based methods. *Journal of Physics: Conference Series*, 181:012086, September 2009.
- [10] SSP Technology. SSP 34m. <http://www.sspstech.com/solutions/ssp-blade/ssp-34m.aspx>. Accessed 14.03.2014.
- [11] S. Loutridis, E. Douka, L. J. Hadjileontiadis, and A. Trochidis. A two-dimensional wavelet transform for detection of cracks in plates. *Engineering Structures*, 27:1327–1338, August 2005.

LPTV SUBSPACE ANALYSIS OF WIND TURBINES DATA

Laurent Mevel¹, Ivan Gueguen², Dmitri Tcherniak³

¹ Inria, Rennes, France

² IFSTTAR, Nantes, France

³ Bruel and Kjaer, SVM, Copenhagen, Denmark

laurent.mével@inria.fr

ABSTRACT

The modal analysis of a wind turbine has been generally handled with the assumption that this structure can be accurately modeled as linear time-invariant. Such assumption may be misleading for stability analysis, especially, with the current development of very large wind turbines with complex dynamic behavior (nonlinearity, aeroelastic coupling). Therefore in this paper, the inherent periodically time-varying dynamics of wind turbines (and for rotating systems, in general) is taken into account. Recently a subspace algorithm for modal analysis of rotating systems has been proposed. It is tested on a simulated and real data from a wind turbine.

KEYWORDS : *Modal Analysis, Wind Turbines, Stochastic Subspace Periodic Systems*

INTRODUCTION

The vibration analysis is a primary task for assessing the structural integrity of wind turbines. With the recent development of large and very large offshore wind turbines, this task is becoming increasingly complex and very costly in money and in technical logistics. Developing new techniques that allow an online vibration monitoring and that reduce the need to recurrent inspections and maintenance is, then, one of the most challenging goals of wind engineering for the next years. Vibration monitoring lies on modal analysis. When the wind turbine is assumed to be approximated by a linear time-invariant (LTI) model, this analysis is straightforward and now well known for engineers. Wind turbines are inherently periodically time-varying (LPTV) systems. Under isotropy assumption, these systems can be approximated by a LTI model where the equations of motion are written in the whirling coordinate frame. This transform is called the multi-blade coordinate transform or Coleman transform [1]. Wind turbines are very often subject to important internal (structural properties, asymmetries) and external (gravity load, aerodynamic effects) anisotropies. The periodic dynamics should, then, be taken into account for an accurate characterization. The class of periodic systems is considered to be a bridge between the time-invariant case and the time-varying one. Recently subspace algorithms for LPTV systems have been proposed. These algorithms are applied to both a numerical model of an operating wind turbine and some real data from a Vestas system.

1. FLOQUET THEORY

1.1 Dynamical model

A widely used mathematic representation of dynamical systems is the state space model. For a rotating system, this model writes in continuous-time (See [2]) as follows:

$$\dot{x}(t) = A(t)x(t) + v(t) \quad (1a)$$

$$y(t) = C(t)x(t) + w(t) \quad (1b)$$

where $u(t) \in \mathbb{R}^m$ is the input vector and $y(t) \in \mathbb{R}^r$ the output vector or the observation. The relationship between the input and the output takes place through an intermediate variable which is the state vector $x(t) \in \mathbb{R}^n$. Equation (1a) is named the *state equation* and (1b) is the so-called *output equation* or *observation equation*. The vectors $v(t)$ and $w(t)$ are noises assumed to be white Gaussian. The number n of components in $x(t)$ is the *system order*. Finally, the matrices A , C are respectively named the *dynamic matrix*, the *observation matrix*. The periodicity of the system originates from the periodicity of these matrices, $A(t+T) = A(t)$, $C(t+T) = C(t)$, where the smallest T for which this periodicity is verified is the period of the system. In general, this period is equal to $2\pi/\Omega$ where Ω is the constant rotation speed of the rotor.

1.2 Floquet modal analysis

According to the Floquet theory, if A is continuous in time, or at least piecewise continuous and if an initial condition $x(t_0) = x_0$ is fixed, then a solution of the homogeneous equation $\dot{x}(t) = A(t)x(t)$ is guaranteed to exist (See [3,4] for further details). The main achievement of the Floquet theory is to show that the solution matrix of $\dot{x}(t) = A(t)x(t)$ can be factorized as a purely periodic matrix $P(t)$ of period T and a time-dependent exponential term function, such that:

$$\Phi(t) = P(t)e^{Rt} \quad (2)$$

Lyapunov has used the result above to transform Equation (1) into an *equivalent autonomous system*, by introducing a new state variable:

$$x(t) = P(t) \cdot z(t) \quad (3)$$

Replacing the state variable x by the new variable z in Equation (1) gives:

$$\dot{z}(t) = Rz(t) + P^{-1}(t)v(t) \quad (4a)$$

$$y(t) = CP(t)z(t) + w(t) \quad (4b)$$

This main result makes the modal analysis straightforward and comprehensive for periodic systems: the modal frequencies are derived from the eigenvalues of R (called *Floquet exponents*) and the modeshapes are the product of the eigenvectors by the periodic matrix $\tilde{C}(t) = CP(t)$. Let $\mu_i = \mu_i^R + i\mu_i^I = \rho_i + i\omega_{p,i}$ be a Floquet exponent. Then, as in time-invariant case the damping ratio and the modal frequency are defined as:

$$\xi_i = \frac{-\rho_i}{|\omega_{p,i}|\sqrt{1+\rho_i^2/\omega_{p,i}^2}}, \quad f_i = \frac{|\omega_{p,i}|\sqrt{1+\rho_i^2/\omega_{p,i}^2}}{2\pi} \quad (5)$$

1.3 Stability analysis

The stability or the instability of the system is entirely defined by the characteristic exponents or the damping ratios ξ . In other words, in order to analyze the stability of the periodic system (1), we have just to compute the transition matrix over a period, namely the matrix R . We have thus:

- if all the Floquet exponents have negative real parts (resp., the damping ratios are positive), System (1) is *asymptotically stable* (all the solutions converge to the null solution)
- if there exist a Floquet exponent (resp., a damping ratio) with a positive real part (resp. negative), then System (1) is *unstable* (there is a solution that diverges indefinitely from the null solution)
- if some Floquet exponents (resp. damping ratios) have null real parts (resp. are null) where the other exponents have negative real parts, then the system is in critical state called *the limit of stability* or *neutral stability*. It can be stable or unstable.

1.4 Periodic Subspace Identification

Using the Lyapunov-Floquet transform, the fast discretization of System (1) at a sampling rate τ yields the following periodic system with period $T_d = \frac{T}{\tau}$ (See [5]):

$$z_{k+1} = Fz_k + \Gamma_k v_k \quad (6a)$$

$$y_k = \tilde{C}_k z_k + w_k \quad (6b)$$

where $\Gamma_k = \int_0^\tau e^{R\gamma} d\gamma \cdot P_k^{-1}$. The purpose of the identification algorithm below is to extract the discrete Floquet exponents, namely, the eigenvalues of F . From these eigenvalues, one can, then, compute the frequencies and the damping ratios defined in (5).

For periodic systems, one can not mix data arbitrarily. In fact, notions like covariance or correlation have just sense only when they are computed on some subsequences of data (See [6]). For instance, the j^{th} data subsequence is the subsequence of the outputs $(y_{j+iT_d})_i$.

The idea for such systems is to build Hankel matrices with correlations of same subsequences. Consider the Hankel matrix $\mathcal{H}_{p,q}^{(j)}$ defined as:

$$\mathcal{H}_{p,q}^{(j)} = \begin{bmatrix} R_1^{(j)} & R_2^{(j)} & \dots & R_q^{(j)} \\ R_2^{(j+1)} & R_3^{(j+1)} & \dots & R_{q+1}^{(j+1)} \\ \vdots & \vdots & \ddots & \vdots \\ R_{p+1}^{(j+p)} & R_{p+2}^{(j+p)} & \dots & R_{q+p}^{(j+p)} \end{bmatrix} \quad (7)$$

where $R_l^{(k)}$ is defined as follows:

$$R_l^{(k)} = \frac{1}{N} \sum_{i=0}^{N-1} y_{k+iT_d} y_{k-l+iT_d} \quad (8)$$

As shown in [7], when N goes to infinity, $R_l^{(k)}$ converge to a function of the correlation of the $(k-l)^{\text{th}}$ state subsequence and the $(k-l)^{\text{th}}$ data subsequence and of the system matrices. Replacing the $R_l^{(k)}$'s by their expressions, the Hankel matrix writes also:

$$\mathcal{H}_{p,q}^{(j)} = \frac{1}{N} \sum_{i=0}^{N-1} \mathcal{Y}_{j+iT_d}^+ \mathcal{Y}_{j+iT_d}^{-T} \quad (9)$$

When N goes to infinity, the Hankel matrix $\mathcal{H}_{p,q}^{(j)}$ can be factorized into the observability matrix and the controllability matrix as in the time-invariant case:

$$\mathcal{H}_{p,q}^{(j)} = \mathcal{O}_p^{(j)} \mathcal{C}_q^{(j)} \quad (10)$$

The observability and the controllability matrices are defined this time as in citeMeyer1975:

$$\mathcal{O}_p^{(j)} = \begin{bmatrix} \tilde{C}_j \\ \tilde{C}_{j+1} F \\ \vdots \\ \tilde{C}_{j+p} F^{j+p} \end{bmatrix} \quad (11)$$

$$\mathcal{C}_q^{(j)} = [F G^{(j-1)} \quad \dots \quad F^q G^{(j-q)}] \quad (12)$$

where $G^{(k)}$ is the state-output cross correlation of the k^{th} invariant subsequence, when N goes to infinity: $G^{(k)} = \frac{1}{N} \sum_{i=0}^{N-1} z_{k+iT_d} y_{k+iT_d}^T$.

1.5 Algorithm 1

Let build the Hankel Matrix, denoted $\mathcal{H}_{p,q}^{(j+)}$, such that the future data are shifted from the past data by a period T_d :

$$\mathcal{H}_{p,q}^{(j+)} = \frac{1}{N} \sum_{i=0}^{N-1} \mathcal{Y}_{j+(i+1)T_d}^+ \mathcal{Y}_{j+iT_d}^{-T} \quad (13)$$

Since \tilde{C}_k and $G^{(k)}$ are periodic for all k , we get the following factorization:

$$\mathcal{H}_{p,q}^{(j+)} = \mathcal{O}_p^{(j+T_d)} F^{T_d} \mathcal{C}_q^{(j+T_d)} = \mathcal{O}_p^{(j)} F^{T_d} \mathcal{C}_q^{(j)} \quad (14)$$

Consider the total Hankel matrix that stacks $\mathcal{H}_{p,q}^{(j)}$ and $\mathcal{H}_{p,q}^{(j+)}$:

$$\mathcal{H}_{p,q,tot} = \begin{bmatrix} \mathcal{H}_{p,q}^{(j)} \\ \mathcal{H}_{p,q}^{(j+)} \end{bmatrix} = \begin{bmatrix} \mathcal{O}_p^{(j)} \\ \mathcal{O}_p^{(j)} F^{T_d} \end{bmatrix} \mathcal{C}_q^{(j)} = \mathcal{O}_{p,tot} \mathcal{C}_q^{(j)} \quad (15)$$

An estimate $\tilde{\mathcal{O}}_{p,tot}$ of the total observability matrix $\mathcal{O}_{p,tot}$ can be obtained from a singular value decomposition of the total Hankel matrix (See [7]).

1.6 Algorithm 2

In [8,9], the authors proposed a subspace-based algorithm for the extraction of the Floquet multipliers from the computation of two successive Hankel matrices $\mathcal{H}_{p,q}^{(j)}$ and $\mathcal{H}_{p,q}^{(j+1)}$, then a resolution of a least squares equation. This algorithm estimates the matrix F up to two different time-varying transforms $\hat{T}^{(j)}$ and $\hat{T}^{(j+1)}$, such that the output of the algorithm is related to the desired estimate as $\hat{T}^{(j+1)-1} \hat{F} \hat{T}^{(j)}$. In order to solve this problem some approximation has been made as in [10]. This approximation may hold only for very low rotation speeds. For wind turbines, it makes sense. As a consequence, it will yield to the estimation of the instantaneous transition matrix instead of the Floquet matrix. This matrix is useless for stability analysis but can be useful for damage detection. In this paper, both algorithms will be considered.

2. APPLICATION TO A WIND TURBINE MODEL

This simulation is based on materials from [11]. The Three-blade wind turbine model considered herein is the same as in [12, 13]. This model allows to represent the coupled side-side tower and edgewise blade response of the wind turbine. For the side-side flexibility, we represent it by rendering it into an equivalent spring that connects the hub to the ground. The blades are represented by a rigid body connected to the hub by means of equivalent hinges, whose characteristics in terms of offset from the axis of rotation and stiffness are chosen so as to match the first edgewise natural frequency of the blade. The gravity effect is taken into account. The blade stiffness varies periodically under the effects of its own weight. These effects depend on the blade azimuthal position in its travel round the rotor disk. The mechanical model is sketched in Figure 1. For simplicity, only one blade is represented.

The structural characteristics are reported in Table I. Figure 1 (right) shows the variation of the real part of the system's Floquet exponents against the rotor speed. These parameters go positive for some speed values range; first, between 1.8 rad/s and 3.5 rad/s and second, between 6.8 rad/s and 9.7 rad/s. Since the nominal rotation speed for such large wind turbines is rather close to the first region, the vibration monitoring will focus on the region between 1 and 2 rad/s. Using Matlab, time series data are simulated from the mechanical model. The scenario consists in simulating a rotational speed's acceleration from 1,1 rad/s to 2 rad/s (close to instability) with a step of 0.1rad/s.

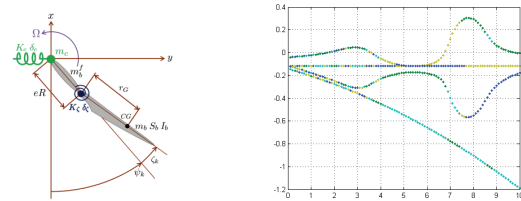


Figure 1 : Scheme of the wind turbine model and Campbell diagram - real parts vs. rotor speed

Table 1 : Rotor-tower model system and main parameters

Parameter	Value
Number of blades	3
Rated rotor speed	1.2 rad/s
Hinge offset	25.651
Mass of hub	7.5E+4 kg
Blade mass (movable part)	1.4482E+4 kg
Blade mass (fixed part)	1.0873E+4 kg
Blade static moment	2.7116E+5 kgm
Blade moment of inertia	7.4881E+6 kgm ²
Edgewise spring damper	1.7555E+6 Nms
Tower spring stiffness	7.3116E+5 Nm-1
Tower spring damper	1.3294E+4 NSm-1
Edgewise spring stiffness	2.1192E+8 Nm
Rotor radius	75 m

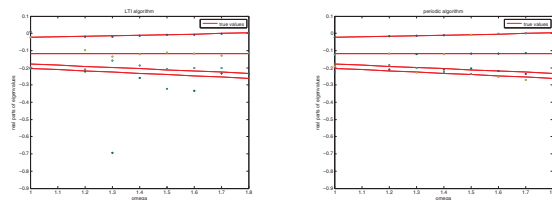


Figure 2 : Campbell diagram - real parts vs. rotor speed

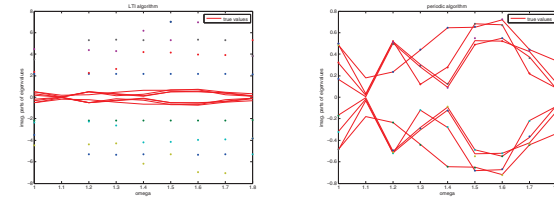


Figure 3 : Campbell diagram - imag parts vs. rotor speed

The goal will be to detect the trend to positive values: hence, to detect a change in the values of the Floquet exponents' real parts from their values at the reference. The number of Floquet exponents is equal to the degrees of freedom of the wind turbine: $n=4$.

It is clear that the Floquet estimated modes match the theoretical values whereas the modes obtained by classical SSI can be very far from the truth (See Figures 2 and 3).

3. MODAL ANALYSIS OF A IN OPERATIONAL WIND TURBINE

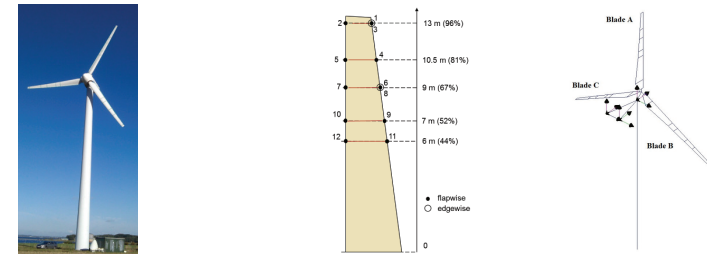


Figure 4 : a) Vestas V27 with blades instrumented with accelerometers; b) Location and orientation of the accelerometers on the blades c) Location of triaxial accelerometers in the nacelle.

We demonstrate the method described above using the data collected from an operating wind turbine during a measurement campaign, which took place from October 2012 until May 2013; the technical details can be found in [14]. A medium size upwind horizontal axis pitch regulated Vestas V27 wind turbine (Figure 4) was used as a test object. Each of the three blades were instrumented by 12 monoaxial accelerometers, 10 in blade's flapwise direction and two in the edgewise direction. In order to catch blade's torsion, the flapwise accelerometers were mounted on both leading and trailing edges of the blades. Thus, five measurement sections along the blade were established; the location of the section was selected using the lowest blade mode shapes generated by FE analysis. In addition, the rotor instrumentation included a pitch sensor and two DC accelerometers; the latter ensured the measurement of the rotor azimuth angle. The data was collected by a 42-channels Bruel and Kjaer LAN-Xi frontend mounted on the rotor hub, and wirelessly transferred to the nacelle. The nacelle instrumentation consisted of three triaxial accelerometers, two located at the rear of the nacelle, and one under the main bearing. In addition, a tachoprobe was used for measuring rotation speed of the high-speed shaft. The rotor and nacelle data streams were synchronized using IRIG-B time stamps extracted from GPS. Simultaneously, the weather parameters were recorded from a nearby weather mast; this included wind speed at different heights, temperature, precipitations and other parameters.

The weather parameters were recorded averaged for every ten minutes intervals. The weather data and the metadata extracted from the measured signals were stored in a database enabling quick search according to different criteria and their combinations. Compared to helicopter rotors, the rotational speed of wind turbine rotors is much lower. The rotor speed of modern wind turbines is regulated by the wind turbine control system and depends on its design. This particular wind turbine was mainly running in two modes: 32 and 43 RPM. For bigger multi-megawatt wind turbines the rotor speed is much lower and might be below 10 RPM. Such low speeds might be problematic for the presented method since it requires information from many rotor revolutions at approximately constant speed, which might be seldom available due to constantly changing wind speed and direction. Using the database, a longest period with almost constant rotor speed was identified: the period spans 8 hours 30 minutes, with the mean wind speed 4.6 m/s, the mean rotor speed 32.2 RPM and almost no pitch activity. During this period, the rotor performed 16417 revolutions. Using the database utility, the continuous time histories spanning the entire period were extracted, decimated down to 102.4Hz sampling frequency and used as an input for the analysis. Additional details regarding the measurement setup can be found in [14, 15].

It has already been shown in [7], that the classical SSI is theoretically wrong when applied to LPTV data. The objective of this experimentation is to qualitatively evaluate if the error is significant when the rotor blade speed is low.

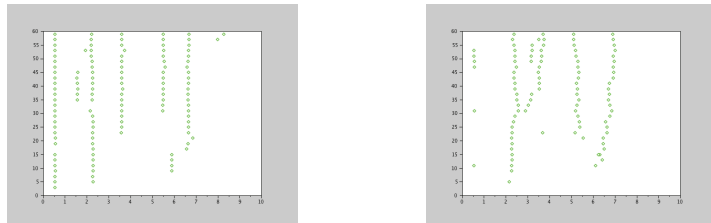


Figure 5 : SSI vs LPTV : short sequence of data

The short sequence data is as such, 12 sensors, a sampling frequency of 200HZ and a rotational frequency of 0.5369Hz for 240000 samples. This is long enough to process a classical SSI but notice that the quality of the LPTV algorithm is related to the number of periods which is very low, around 650. The performance to be expected for the LPTV algorithm on a LPTV system is the same as the classical SSI applied on a LTI system with 650 samples.

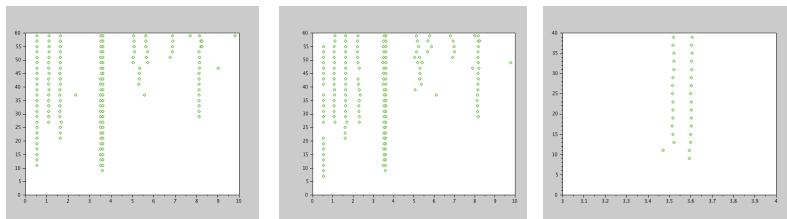


Figure 6 : SSI vs LPTV : long sequence of data

The long sequence is using only six sensors, at 102.4Hz and at a rotating speed of 0.536501Hz. Now, the number of periods for the periodic algorithm is 16K and the algorithm has enough data to

get stable results. As a matter of fact, both the classical and the periodic SSI achieve similar results stressing that the periodic behavior at that speed is not prevalent. Still the periodic SSI is the only one to be guaranteed to be correct. Both algorithms exhibit the correct modes at 3.51HZ and 358Hz as explained in [14, 15].

CONCLUSION

LPTV subspace identification has been investigated for both a simulated and real data from a wind blade systems. Two algorithms were considered. The first one yields Floquet modes of a rotating structure at any given speed. Floquet modes are important because they are symptoms of instability and are thus quantities to monitor in a SHM system. It has been shown that Floquet modes can be significantly different from the modes given by the classical SSI. Another LPTV algorithm is considered. It is shown that at low speed, this algorithm gives similar modes to the classical SSI for that given example. Structural modes can be interesting for assessing damage. There are nonetheless no guarantee that for another example, classical SSI will yield to exploitable results. Still, when the anisotropy of the system is low, a LTI approach can be considered as a rough approximation of the LPTV behavior. Further work will focus on Floquet modes monitoring and computation of uncertainty bounds.

REFERENCES

- [1] G. Bir. Multi-blade coordinate transformation and its applications to wind turbine analysis. In *ASME Wind Energy Symposium*, 2008.
- [2] G. Genta. *Dynamics of Rotating Systems*. Springer, 2005.
- [3] G. Floquet. Sur les équations différentielles linéaires à coefficients périodiques. *Annales scientifiques de l'ENS*, 12:47–88, 1883.
- [4] J. J. Dacunha and J. M. Davis. A unified floquet theory for discrete, continuous, and hybrid periodic linear systems. *Journal of Differential Equations*, 251, 2011.
- [5] L. Ma and P. A. Iglesias. Quantifying robustness of biomedical network models. *BMC Bioinform*, 3(38), 2002.
- [6] R. Meyer and C. Burrus. A unified analysis of multirate and periodically time-varying digital filters. In *Transactions on Circuits and Systems*, vol. 22, 1975.
- [7] Ahmed Jhinaoui, Laurent Mevel, and Joseph Morlier. A new ssi algorithm for lptv systems: application to a hinged-bladed helicopter. *Mechanical Systems and Signal Processing*, 42(1):152–166, January 2014.
- [8] A. Jhinaoui, L. Mevel, and J. Morlier. Subspace identification for linear periodically time-varying systems. In *Proceedings of the 16th IFAC Symposium on System Identification (SYSID)*, 2012.
- [9] A. Jhinaoui, L. Mevel, and J. Morlier. Extension of subspace identification to lptv systems: Application to helicopters. In *Proceedings of the 30th International Modal Analysis Conference (IMAC-XXX)*, 2012.
- [10] K. Liu. Identification of linear time-varying systems. *Journal of Sound and Vibration*, 206(4):487–505, 1997.
- [11] Ahmed Jhinaoui, Laurent Mevel, and Joseph Morlier. Vibration monitoring of operational wind turbine. In *Proc. 9th International Workshop on Structural Health Monitoring*, Stanford, CA, USA, 2013.
- [12] CL Bottasso and S Cacciola. Model-independent periodic stability analysis of wind turbines. *Wind Energy*, 2012.
- [13] CL Bottasso and S Cacciola. Periodic stability analysis of wind turbines. *EWEA 2012 Annual Event, Copenhagen, Denmark*, 2012.
- [14] Dmitri Tcherniak and GC Larsen. Applications of oma to an operating wind turbine: now including vibration data from the blades. In *5th international operational modal analysis conference (IOMAC), Guimarães*, 2013.
- [15] Shifei Yang, Dmitri Tcherniak, and Mathew Allen. Modal analysis of rotating wind turbine using multiblade coordinate transformation and harmonic power spectrum. In *32th international modal analysis conference (IMAC), Orlando*, 2013.

Experimental characterization of operating bladed rotor using harmonic power spectra and stochastic subspace identification

D.Tcherniak¹, S. Yang², M.S. Allen³

¹ Brüel and Kjær Sound and Vibration Measurement
Skodsborgvej 307, Nærum 2850, Denmark
e-mail: dtcherniak@bksv.com

² Turbomachinery Systems, Praxair Inc.
175 East Park Drive, Tonawanda, NY 14150

³ Department of Engineering Physics, University of Wisconsin-Madison
535 Engineering Research Building, 1500 Eng. Drive, Madison, WI 53706, USA

Abstract

The dynamic response of mechanical systems with rotating elements (for example, operating wind turbines) cannot be described using a classical linear time-invariant (LTI) formulation because the mass and stiffness matrices can be periodically varying while the rotor rotates. Such systems belong to the class of linear periodic time variant (LPTV) systems, which require special treatment for their experimental identification. For instance, the Harmonic Power Spectra (HPS) method, which is based on Floquet theory, can be applied. Following this method, the experimentally obtained responses are exponentially modulated using the rotational frequency, the HPS matrix is computed between the modulated responses and is used as the input to Operational Modal Analysis (OMA). The latter provides frequencies of the modes and the Fourier coefficients for reconstructing the time periodic mode shapes. In authors' prior works the HPS method has been applied in the frequency domain. The presented study extends the HPS method to the time domain, which makes it possible to use the powerful stochastic subspace identification (SSI) techniques for modal identification, which lead to more accurate parameter estimates and can treat modes with close frequencies. The advantage of the suggested approach is that it allows the use of existing implementations of SSI, thus providing a simple tool for modal identification of periodic systems.

1 Introduction

Operational modal analysis (OMA) [1], a method of extracting the modes and hence a linear dynamic model of a structure from operational measurements, has become a mainstream technology in the past few decades. Often the structures of interest involve rotating machinery (e.g., operating wind turbines), which makes the application of well-established OMA techniques invalid since the structure under test is not time invariant, and this violates the main assumption of modal analysis. If the structural properties change periodically, the structure can be modelled as a linear periodic time variant (LPTV) system. Currently the number of studies on identification of LPTV systems remains limited. Study [2] suggested using so-called Coleman (also known as multiblade coordinate, MBC) transformation as a preprocessing step to OMA. By changing variables to a rotational frame, Coleman transformation converts the LPTV system to LTI, which then allows application of wide range of classical modal identification techniques. However, this method can only be applied to isotropic rotors, i.e. when all blades have identical mass and structural properties. In addition, for rotors rotating in vertical plane, as in a case of horizontal axis wind turbines (HAWT), the gravity introduces forces that break symmetry and can cause the system to exhibit liner time periodic

behavior. This prevents using the transformation for in-plane modes. Jhinaoui [3] suggested a subspace identification method specially developed for rotating systems. The method identifies the underlying Floquet eigenstructure of the rotating system and uses the samples obtained at the same position of the rotor at consecutive revolutions. Allen suggested using harmonic power spectra (HPS) for structures identification and extended experimental modal analysis to LPTV systems [4] and later to OMA in [5]. This framework has been used quite extensively to extract the mode shapes from continuous-scan laser vibrometer measurements [6-9] and the authors recently applied it to measurements from an operating wind turbine in [10].

The first step when computing HPS is to modulate the measured time histories by multiplying them by $e^{-im\Omega t}$ where Ω is the rotation frequency of the turbine and m is some integer. Then, the theory shows that the augmented set of measurements can be processed using standard curve fitting techniques or peak picking to extract the natural frequencies and damping ratios. The theory also explains how to relate the amplitudes of the harmonics in the response to the time-varying mode shapes. The method described in [5] uses *frequency domain* modal algorithms to extract modal parameters; in this paper, we refer to this method as H-OMA-FD. The presented paper extends this technique to *time domain* OMA; the suggested approach is referred as H-OMA-TD.

The consequence of the harmonic modulation process is that it causes the modulated time series to be complex and hence not amenable to analysis by conventional OMA SSI routines. This work proposes an approach that circumvent this difficulty so that powerful and robust OMA subspace identification (SSI) algorithms can be used to extract the structure's modal parameters.

2 Theoretical background

The state space model of an N degrees of freedom linear time periodic system can be written as,

$$\begin{aligned}\dot{\mathbf{x}}(t) &= \mathbf{A}(t)\mathbf{x}(t) + \mathbf{B}(t)\mathbf{u}(t) \\ \mathbf{y}(t) &= \mathbf{C}(t)\mathbf{x}(t) + \mathbf{D}(t)\mathbf{u}(t)\end{aligned}\quad (1)$$

where $\mathbf{A}(t)$ is the system matrix, $\mathbf{B}(t)$ is the input matrix, $\mathbf{C}(t)$ is the output matrix, and $\mathbf{D}(t)$ is the direct input matrix. All these matrices are periodic with time. For example, the classical system with mass, damping and stiffness matrices \mathbf{M} , \mathbf{C}_d and \mathbf{K} with the following equation of motion,

$$\mathbf{M}(t)\ddot{\mathbf{z}}(t) + \mathbf{C}_d(t)\dot{\mathbf{z}}(t) + \mathbf{K}(t)\mathbf{z}(t) = \mathbf{f}(t)\quad (2)$$

can be written in this form using $\mathbf{x}(t) = [\mathbf{z}(t)^T \quad \dot{\mathbf{z}}(t)^T]^T$ see [6] for further details. For any initial state and input pair $(\mathbf{x}(t_0), \mathbf{u}(t_0))$, a unique solution $\mathbf{y}(t)$ exists and can be written in terms of the state transition matrix $\Phi(t, t_0)$ [12].

$$\mathbf{y}(t) = \mathbf{C}(t)\Phi(t, t_0)\mathbf{x}(t_0) + \mathbf{C}(t) \int_{t_0}^t \Phi(t, \tau)\mathbf{B}(\tau)\mathbf{u}(\tau)d\tau + \mathbf{D}(t)\mathbf{u}(t)\quad (3)$$

The general solution (with the direct input matrix $\mathbf{D}(t)$ equals zero) is the basis of the Floquet analysis and was used in [13] and [5] to derive the harmonic transfer function and HPS used in operational modal analysis.

2.1 Floquet Analysis

The state transition matrix $\Phi(t, t_0)$ is the key to obtain the general solution in Eq.(3). When the system is linear time invariant, i.e., $\mathbf{A}(t)=\mathbf{A}$ and other coefficient matrices are constant, the state transition matrix is $e^{\mathbf{A}\times(t, t_0)}$, which can be further decomposed as,

$$\Phi(t, t_0) = e^{\mathbf{A}\times(t, t_0)} = \mathbf{P}e^{\Lambda\times(t, t_0)}\mathbf{P}^{-1}\quad (4)$$

where \mathbf{P} is the matrix of eigenvectors of the system matrix \mathbf{A} and Λ is a diagonal matrix of eigenvalues.

On the other hand, when the system is periodic, i.e., $\mathbf{A}(t) = \mathbf{A}(t + T)$, where $T = 2\pi/\Omega$ is the fundamental period, the dynamics of the periodic system has to be studied using Floquet theory [12,14-16] because $\Phi(t, t_0) \neq e^{\mathbf{A}(t) \times (t-t_0)}$. The Floquet theory introduces a coordinate change to the system matrix $\mathbf{A}(t)$ and transforms the LPTV system to an LTI system. As a result, the state transition matrix becomes,

$$\Phi(t, t_0) = \bar{\mathbf{P}}(t) e^{\mathbf{L} \times (t-t_0)} \bar{\mathbf{P}}(t_0)^{-1} \quad (5)$$

Here $\bar{\mathbf{P}}(t)$ is a periodic matrix. The eigenvalues of \mathbf{L} are called the *Floquet exponents* [15,16] and it is important to note that they are still constant even though $\mathbf{A}(t)$ is time periodic. If all Floquet exponents are non-zero and non-repeated, i.e., \mathbf{L} is nonsingular, then there exists a nonsingular matrix \mathbf{R} that diagonalizes \mathbf{L} with $\mathbf{L} = \mathbf{R}\mathbf{A}\mathbf{R}^{-1}$. Then, the state transition matrix in Eq.(5) becomes,

$$\Phi(t, t_0) = \mathbf{P}(t) e^{\mathbf{A} \times (t-t_0)} \mathbf{P}(t_0)^{-1} \quad (6)$$

where $\mathbf{P}(t) = \bar{\mathbf{P}}(t)\mathbf{R}$ is a matrix of time periodic eigenvectors for the LPTV system [17]. The state transition matrix can be further decomposed into the following modal summation form,

$$\Phi(t, t_0) = \sum_{r=1}^{2N} \Psi_r(t) \mathbf{L}_r(t_0) e^{\lambda_r(t-t_0)}, \quad (7)$$

where $\Psi_r(t)$ is the r^{th} column of $\mathbf{P}(t)$, and $\mathbf{L}_r(t)$ is the r^{th} row of $\mathbf{P}(t)^{-1}$. λ_r is the r^{th} Floquet exponent that is analogous to the r^{th} eigenvalue of an LTI system. The r^{th} Floquet exponent can be written in terms of the damping ratio ζ_r and natural frequency ω_r as $\lambda_r = -\zeta_r \omega_r + i\omega_r \sqrt{1 - \zeta_r^2}$ for an underdamped mode. Thus the steady state response $\mathbf{y}(t)$ in Eq.(3) becomes,

$$\mathbf{y}(t) = \sum_{r=1}^n \mathbf{R}_{y,r}(t) e^{\lambda_r(t-t_0)} \quad (8)$$

$$\mathbf{R}_{y,r}(t) = \mathbf{C}(t) \Psi_r(t) \mathbf{L}_r(t_0) \mathbf{x}(t_0)$$

The residue matrix $\mathbf{R}_{y,r}(t)$ is periodic and can be expanded in a Fourier series. Here we shall presume that the residue matrix can be adequately represented using a fixed number $2N_B+1$ of terms,

$$\mathbf{R}_{y,r}(t) = \sum_{n=-N_B}^{N_B} \mathbf{B}_{n,r} e^{in\Omega(t-t_0)}, \quad (9)$$

where $\mathbf{B}_{n,r}$ is the n^{th} Fourier coefficient matrix of the r^{th} mode. So, the output $\mathbf{y}(t)$ becomes,

$$\mathbf{y}(t) = \sum_{r=1}^{2N} \sum_{n=-N_B}^{N_B} \mathbf{B}_{n,r} e^{(\lambda_r + in\Omega)(t-t_0)}. \quad (10)$$

This equation reveals that the response of each mode of the system is a sum of damped sinusoids, with several sideband harmonics around each natural frequency.

2.2 Harmonic Transfer Function

Similar to what was shown above for the transient response, when an LPTV system is excited by a sinusoidal force at some frequency, the response will be at the same frequency and at an infinite number of its harmonics, each separated by the fundamental frequency Ω . At first glance it seems that it would be impossible to use a linear transfer function for a system such as this. However, Woreley overcame this difficulty by augmenting the input and output signals with frequency shifted copies of each and then the couplings between the frequencies can be accounted for in the augmented version [18]. Specifically, the m^{th} modulated signal is given by

$$\mathbf{y}_m(t) = \mathbf{y}(t) e^{-im\Omega t} \quad (11)$$

for $m \in \mathbb{N}, m = -M \dots M$. The Fourier transform of each signal is denoted $\mathbf{y}_m(\omega)$. The frequency shifted copies are then collected as $\mathbf{Y}(\omega) = [\dots \mathbf{y}_{-1}^T(\omega) \mathbf{y}_0^T(\omega) \mathbf{y}_1^T(\omega) \dots]^T$, then the harmonic transfer function (HTF) can be established for the LPTV system. The HTF is completely analogous to the commonly known transfer function for LTI systems.

The harmonic transfer function is derived by inserting this modulated signal into the general solution in Eq. (3), and using the modal solution from in Eq. (7). The harmonic balance approach is taken to match the terms with the same frequency in the exponent $e^{(i\omega + im\Omega)t}$. After much algebra and organization, a harmonic transfer function is obtained in terms of the modal parameters of the state transition matrix,

$$\mathbf{Y}(\omega) = \mathbf{G}(\omega) \mathbf{U}(\omega), \quad (12)$$

where $\mathbf{U}(\omega) = [\dots \mathbf{u}_{-1}^T(\omega) \mathbf{u}_0^T(\omega) \mathbf{u}_1^T(\omega) \dots]^T$ is the exponentially modulated input in the frequency domain. And,

$$\mathbf{G}(\omega) = \sum_{r=1}^{2N} \sum_{l=-\infty}^{\infty} \frac{\bar{\mathbf{c}}_{r,l} \bar{\mathbf{b}}_{r,l}}{i\omega - (\lambda_r - il\Omega)} \quad (13)$$

$$\bar{\mathbf{c}}_{r,l} = [\dots \bar{c}_{r,-l-1} \quad \bar{c}_{r,-l} \quad \bar{c}_{r,-l+1} \quad \dots]^T$$

$$\bar{\mathbf{b}}_{r,l} = [\dots \bar{b}_{r,l+1} \quad \bar{b}_{r,l} \quad \bar{b}_{r,l-1} \quad \dots]$$

The m^{th} term in the vector $\bar{\mathbf{c}}_{r,l}$ is $\bar{c}_{r,l}$, which is the $(m-l)^{\text{th}}$ Fourier coefficient (or vector of Fourier coefficients) of $\mathbf{C}(t)\Psi_r(t)$. Note that the mode vectors $\bar{\mathbf{c}}_{r,l}$ acquired at different peaks describe the same shape but the elements are shifted in position in each vector. For example, supposing the mode vector at frequency λ_r is $\bar{\mathbf{c}}_{r,0} = [0 \ a \ b \ c \ 0]^T$, the mode vector at $\lambda_r + \Omega$ should be $\bar{\mathbf{c}}_{r,-1} = [a \ b \ c \ 0 \ 0]^T$ multiplied with an unknown constant, and the mode vector at $\lambda_r - \Omega$ should be proportional to $\bar{\mathbf{c}}_{r,1} = [0 \ 0 \ a \ b \ c]^T$. A least squares approach can be used to extract the best estimate of the mode vector $\bar{\mathbf{c}}_{r,l}$ from the multiple estimations. Similarly, $\bar{\mathbf{b}}_{r,l-m}$ is the $(l-m)^{\text{th}}$ Fourier coefficient of $\mathbf{L}_r(t)^T \mathbf{B}(t)$.

2.3 Harmonic Power Spectrum

In practice one has presumably measured the response of an LPTV system to an excitation that satisfies OMA assumptions, and the measured responses are a collection of time histories recorded at N_o DOFs: $\mathbf{y}(t) \in \mathbb{R}^{N_o}$, sampled with sampling frequency F_s . These time histories are then exponentially modulated by multiplying by $e^{-im\Omega t}$, $m = -M \dots M$ to obtain a collection of responses $\mathbf{y}_m(t) \in \mathbb{C}^{N_o(2M+1)}$ and hence the harmonic power spectrum (HPS) matrix found in the conventional manner as in the LTI case:

$$\mathbf{S}_{yy}(\omega) = \mathbb{E}(\mathbf{y}_m(\omega) \mathbf{y}_m(\omega)^H), \quad (14)$$

where $\mathbb{E}()$ is the expectation, and $()^H$ denotes the Hermitian transpose. Retaining only the dominant terms, the HPS can be written in the following form in terms of the modes of the LPTV system,

$$\mathbf{S}_{yy}(\omega) \approx \sum_{r=1}^{2N} \sum_{l=-\infty}^{\infty} \frac{\bar{\mathbf{c}}_{r,l} \mathbf{W}(\omega) \mathbf{c}_{r,l}^H}{[i\omega - (\lambda_r - il\Omega)][i\omega - (\lambda_r - il\Omega)]^H} \quad (15)$$

The terms $(\lambda_r - il\Omega)$ cause the HPS to have a peak near the system's eigenvalues or Floquet exponents, λ_r , and also at the eigenvalue plus some integer multiple of the fundamental frequency l . Here $\mathbf{W}(\omega)_r$ is related to the auto-spectrum of modulated input signal. In output-only modal analysis of LTI systems, the input is assumed to be uncorrelated random white noise and the auto spectrum of input signal becomes constant. The same assumption is used for LPTV systems.

The HPS has the same modal summation form as the power spectrum of an LTI system,

$$\mathbf{S}_{YY}^{\text{LTI}}(\omega) = \sum_{r=1}^N \frac{\varphi_r S_{UU}^{\text{LTI}}(\omega) \varphi_r^H}{[i\omega - \lambda_r][i\omega - \lambda_r^*]^H}. \quad (16)$$

This function produces a peak in the spectrum when the excitation frequency ω is near the natural frequency $\text{Im}(\lambda_r)$, and the peak can be curve-fitted to identify the natural frequencies, damping ratios and mode shapes of the system. Hence, the same algorithms for LTI systems can be used to identify modal parameters of an LPTV system, and the same intuition that is used to interpret frequency response functions can also be used to interpret the harmonic transfer function. However, there are a few differences that must be noted in signal processing:

- An LPTV system theoretically has an infinite number of peaks for each mode. The peaks occur at the frequencies $\omega = \text{Im}(\lambda_r - i l \Omega)$. If the observed mode shapes $\mathbf{C}(t)\Psi_r(t)$ are constant in time, $\bar{\mathbf{c}}_{r,l}$ and $\bar{\mathbf{b}}_{r,l}$ contain only one nonzero term, i.e., $\bar{\mathbf{c}}_{r,0}$ and $\bar{\mathbf{b}}_{r,0}$. Then, Eq. (13) and Eq. (15) reduce to the familiar relationship for an LTI system.
- The mode vectors of an LTI system describe the spatial pattern of deformation of a mode. For an LPTV system, the vectors $\bar{\mathbf{c}}_{r,l}$ consist of the Fourier coefficients that describe the time periodic spatial deformation pattern.

2.4 Complex Time Series: Rigorous Approach

In the approach outlined above the measured signal $\mathbf{y}(t)$ is multiplied by $e^{-im\Omega t}$, which could also be written as $e^{-im\Omega t} = \cos(m\Omega t) - i \sin(m\Omega t)$. Hence, one could obtain the same result by multiplying the signals by a sine and cosine to form the real and imaginary parts separately. Eq. (15) shows that the HPS is simply a sum of damped exponential terms. One can show that each term leads to an exponential term in the time domain of the form $\mathbf{A}_{r,l} e^{(\lambda_r - i l \Omega)t}$.

The residue matrix at the l^{th} harmonic of the r^{th} mode is defined as follows:

$$\mathbf{A}_{r,l} = \frac{\bar{\mathbf{c}}_{r,l} \mathbf{W}(\omega) \bar{\mathbf{c}}_{r,l}^H}{\zeta_r \omega_r}. \quad (17)$$

Hence, if the signal is modulated with a real sine and cosine rather than with $e^{-im\Omega t}$, and the residues obtained are $\mathbf{A}_{r,l}^S$ and $\mathbf{A}_{r,l}^C$ for the sine and cosine cases respectively, then the desired residues should simply be

$$\mathbf{A}_{r,l} = \mathbf{A}_{r,l}^C - i \mathbf{A}_{r,l}^S. \quad (18)$$

The disadvantage of this approach, is that the signals become twice as large (twice as many outputs) compared to the case where complex time series are allowed. Also note that the sine and cosine terms should be treated simultaneously in a global curve fitting algorithm, to assure that the residues obtained correspond to precisely the same poles.

2.5 Simplified approach

This algorithm takes a different approach, seeking to produce a time series that is real and yet has the same spectrum for all positive frequencies. To explain it, it is helpful to first recall that when using the conventional approach, one forms the HPS matrix $\mathbf{S}_{YY}(\omega)$ as (14), $\mathbf{S}_{YY}(\omega) \in \mathbb{C}^{N_o(2M+1) \times N_o(2M+1)}$. Then several rows of the matrix are selected, and peak-picking is used to determine modal parameters. It is important to note that for peak-picking one uses only the frequencies $0 < \omega < \pi F_S - M\Omega$, i.e. those lying in the positive part of the frequency axis.

The presented study suggests replacing the frequency domain peak-picking method by more robust OMA-SSI algorithms, which are available in some commercial software packages (for example, Bruel and Kjaer

Type 7780). Thus, its combination with the exponential modulation will allow the traditional OMA-SSI to be readily applied to LPTV systems.

The problem, however, is that the commercial OMA-SSI does not accept complex time histories. In order to circumvent this limitation, the following is suggested: Assume there is a procedure that converts the exponentially modulated time histories $\mathbf{y}_m(t) \in \mathbb{C}$ to new time histories $\tilde{\mathbf{y}}_m(t)$ with the following properties:

$$\tilde{\mathbf{y}}_m^{(n)}(t) \in \mathbb{R} \quad (19)$$

$$\mathcal{F}(\tilde{\mathbf{y}}_m(t)) = \mathcal{F}(\mathbf{y}_m(t)) \text{ for } \omega \in [0, \pi F_S], \quad (20)$$

where $\mathcal{F}(\cdot)$ denotes the Fourier transform. The first property ensures the new signals are usable in the available implementations of the SSI-OMA algorithms, while the second means that

$$\tilde{\mathbf{S}}_{YY}(\omega) = \mathbf{S}_{YY}(\omega) \text{ for } \omega \in [0, \pi F_S], \quad (21)$$

i.e. the new time histories $\tilde{\mathbf{y}}_m(t)$ have the same frequency content and phase relations as the positive half of the harmonic power spectra which is being utilized in the HPS method.

From properties (19) and (20), one can readily derive the algorithm converting $\mathbf{y}_m(t)$ to $\tilde{\mathbf{y}}_m(t)$:

1. For given exponentially modulated signals $\mathbf{y}_m(t)$ compute their periodogram $\mathcal{F}(\mathbf{y}_m(t))$ using a fast Fourier transform. The periodogram of complex $\mathbf{y}_m(t)$ is not a Hermitian function, i.e. its negative frequencies part is not a complex conjugate of the positive frequencies part;
2. Replace the negative frequencies part of the periodogram by the complex conjugate of the positive part;
3. Using inverse FFT, generate the new time signals $\tilde{\mathbf{y}}_m(t)$, which satisfy (19) and (20).

3 Results

To demonstrate the algorithm, let us consider a simple three-bladed rotor system, which is a rough model of a horizontal axis wind turbine (Figure 1). Each blade is modelled as a two-beams assembly; the beams are connected by a hinge with a linear angular spring with stiffness $k_j, j=1,2,3$, (here and below j is the blade index). A lumped mass m_j is attached to the end of the outer beam. The azimuth angles of the blades are: $\psi_j(t) = \Omega t + 2\pi(j-1)/3$, where the rotor angular speed Ω is assumed constant. The rotor is attached to the "nacelle" C with mass m_N supported by the "tower" modelled by two springs with stiffnesses k_H and k_V . The rotor is linked to the "drivetrain" with moment of inertia I_D and stiffness k_D .

For examination of the rotor modal behaviour, the following parameters were chosen, same as in [18]: $m_N = 446 \cdot 10^3 \text{ kg}$, $m_1 = m_2 = m_3 = 41.7 \cdot 10^3 \text{ kg}$, $k_1 = k_2 = k_3 = 2.006 \cdot 10^8 \text{ N} \cdot \text{m}$, $k_D = 10^8 \text{ N} \cdot \text{m}$, $k_H = 2.6 \cdot 10^6 \text{ N/m}$, $k_V = 5.2 \cdot 10^8 \text{ N/m}$, $I_D = 2.6 \cdot 10^7 \text{ kg} \cdot \text{m}^2$, $a = b = 13.1 \text{ m}$, $\Omega = 2\pi \cdot 0.16 \text{ rad/s}$. These parameters approximate a generic 10 MW wind turbine model.

The identical system was considered in [18], where the equations of motion were set up and the Floquet analysis was applied to investigate the influence of rotor's anisotropy to whirling components of the mode shapes.

Since this is a six degree-of-freedom system, one shall expect six modes, which are named as follows:

- the *vertical* and *horizontal* modes, dominated by vertical and horizontal motion of the mass C ;
- three rotor modes: one symmetric (also called *collective*), where all blades deflect in-phase, and two anti-symmetric, also called *whirling*;
- a "*drivetrain*" mode, where the most of potential energy is being stored in the stiffness k_D .

One must not expect pure modes, there is always some degree of interaction; the names are only given to reflect the dominating motion of the mode. The presented study focuses on the rotor modes since they have the most pronounced periodic behavior.

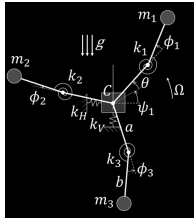


Figure 1. Considered system.

The presented study applies three methods to the system. First, we assume the equations of motion are known. This allows application of Floquet analysis and generates an (almost) exact solution; this solution serves as a baseline for comparison with two other methods. Next, we simulate an experimental scenario: we assume the equations of motion are unknown but we can observe the response of the system to excitation, which satisfies OMA assumptions: all DOFs are excited by uncorrelated broadband noise with a flat spectrum. Then both the conventional frequency domain HPS method and the suggested time-domain method are applied to the observed response, and the results are compared.

3.1 Floquet analysis

An overview and a detailed description of Floquet analysis can be found e.g. in [19]. Floquet analysis was applied to the system in Figure 1; the details are given in [18] and omitted here. As was mentioned in the theoretical section, Floquet analysis provides a modal decomposition, but for an LPTV system, the modes are periodic. Following the conventional approach, each periodic mode is Fourier expanded to harmonic (Fourier) components. The LTI system can then be thought as a special case of LPTV, where each mode has only one non-zero Fourier component. It can be shown that for an isotropic three-bladed rotor in the absence of gravity, each mode has three non-zero Fourier components. The Coleman transformation [20] utilizes this phenomena and allows conversion of the LPTV system to LTI system. A stronger periodicity of the system matrix in Eq. (1) requires more Fourier components to be included into consideration. For almost isotropic rotors, only few Fourier components have significant magnitude, and the smaller components can be neglected.

Figure 6a,c shows the magnitudes of the harmonic components obtained via Floquet analysis for isotropic rotor in the absence of gravity. Two modes are shown: forward whirling (FW) mode (which is dominated by x_C but named after its significant whirling component), and collective mode. The backward whirling (BW) is explained in details in Figure 7. As it was mentioned before, the modes of a (three-bladed) isotropic rotor in the absence of gravity can be fully described by only three Fourier components.

Figure 7 focuses on the BW mode. Figure 7c shows the magnitude of its three non-zero Fourier components: FW component (A), motion of the center mass (B) and BW component (C). The latter is about one order of magnitude higher than the FW component, it dominates the rotor dynamics, and the mode is named after this component. Figure 7a is a complexity plot showing the phase relation between the three blades. The left plot is for the FW component (A), where the phase between the consecutive blades is $+120^\circ$. The right plot is for the dominating BW component (C) with -120° phase.

Figure 8a,c,f shows the BW, FW and collective modes for anisotropic rotor in the presence of gravity. Compared to the isotropic rotor, the system matrix of the anisotropic rotor demonstrates higher and more complex variation with time, and, as a result, it requires more Fourier components to describe the periodic mode shapes (cf. Figure 6a,c and Figure 7b).

Table 2 provides the values of the Floquet exponents for both isotropic and anisotropic rotors.

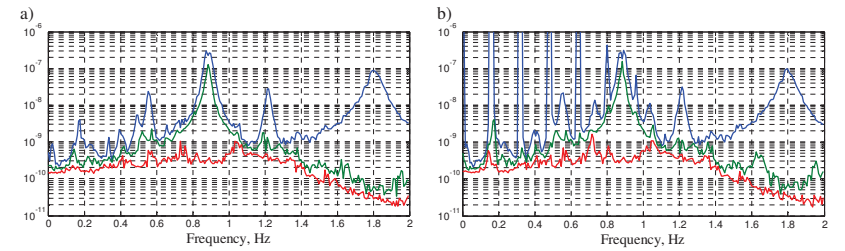


Figure 2. Complex Mode Indicator Function of the HPS Matrix for the 5 outputs using ϕ_1, ϕ_2, ϕ_3 as references. a) Isotropic rotor without gravity; b) Anisotropic rotor with gravity and $k_C = 0.97$.

3.2 Numerical experiment

As an input to the numerical experiment, we simulated the response of the rotor to uncorrelated broadband excitation. This excitation satisfies OMA assumptions, but we acknowledge that the aeroelastic forces acting on the wind turbine rotor in reality are different [21]. The equations of motion were numerically integrated using 4th order Runge-Kutta method, for 7200s (which correspond to 1152 rotor revolutions).

3.2.1 Results from H-OMA-FD

The simulated turbine rotates at 0.16Hz. The responses in the edgewise direction on all three blades (ϕ_1, ϕ_2, ϕ_3) and the responses of the nacelle in the lateral (X_C) and vertical (Y_C) directions were collected into a response vector of 5 outputs. The responses were then exponentially modulated with $m = -3 \dots 3$ according to Eq. (11). Then, the modulated signals were split into 575 sub-blocks with a block size of 119s (19 revolutions) with 85% overlap. A Hanning window was applied to each block to reduce the leakage. The cross power spectra between the modulated signals and the original signals ϕ_1, ϕ_2, ϕ_3 were computed respectively in each sub-block and averaged over the whole time history. The resulting harmonic power spectrum matrix had 35 outputs (5 outputs with 7 harmonics for each output) by 3 references. The complex mode indicator function (CMIF) of this HPS matrix is shown in Figure 2 for two cases, (a) isotropic rotor with no gravity, and (b) anisotropic rotor with $k_C = 0.97$ and with gravity. There are two dominant singular values peaks in the CMIF, with very close natural frequencies centered around 0.88Hz. All of the other peaks except for the peak at 1.8 Hz were spaced by $n \times 0.16$ Hz from the peaks at 0.88 Hz, indicating that the system has three modes dominating this frequency range, and two of which have noticeable periodic behavior.

Initially, a simple output-only extension of the Algorithm of Mode Isolation (AMI) algorithm that was used to curve fit the measurements. This gave a reasonable fit at all of the peaks, but this algorithm does not

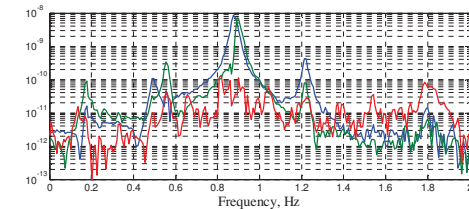


Figure 3. Spatially condensed MIMO measurements.

include the MIMO, hybrid approach described in [22, 23] which is necessary to separate modes with close natural frequencies. Hence, the only mode retained from AMI was the mode at 1.801 Hz, which was found to be the first collective mode of the rotor. The two close modes were estimated using frequency domain decomposition (FDD) [24]. Specifically, the spectra near the peak were collected and an SVD used to extract the first three dominant singular vectors. These were then used to condense the measurements to a set of three spectra, shown in Figure 3. This spatial condensation of the measurements effectively separated the two close modes, so that a simple single-mode fit could be applied to each curve to estimate the modal parameters. The natural frequencies and damping for the three rotor modes are given in Table 2. The magnitude of the Fourier components are shown in Figure 10a,c.

The next case considered is the case with gravity and with 3% anisotropy in one of the blades. Again, AMI identified the collective mode at 1.79 Hz, while the FDD was used to identify the other two modes. The modal parameters obtained are given in Table 2, and the mode shapes are in Figure 10e,g.

These results illustrate what can be done with a basic system identification method based on the HPS, and focus on the time-periodic blade modes. More sophisticated frequency-domain methods would be advisable to use, such as the AFPoly algorithm [25] or pLSCF [26].

3.2.2 Results from H-OMA-TD

The obtained response time histories became an input to the H-OMA-TD algorithm. Figure 4 sketches how the method is applied using B&K OMA software Type 7760. First, the dataset of time histories for all six DOFs obtained from the simulation (or from measurements) is harmonically modulated (using $m = -3..+3$ in the present study), thus generating six new datasets. The new (complex) time histories are converted to real time using the algorithm described in section 2.2. In OMA software, we construct 6 copies of the rotor geometry and assign the modulated datasets to the copies (Figure 4). The not modulated signals ($m=0$) are selected as projection channels (shown in pink). Then a standard OMA procedure is run (in the presented study, we used data driven OMA-SSI with un-weighted principal components, UPC), which extracts the modes.

A CMIF and the fragment of the stabilization diagram for the isotropic rotor in the absence of gravity are shown in Figure 5. In the range 0-1.5 Hz, OMA finds nine modes, however they are $\pm\Omega$ shifted realizations of the three structural periodic modes: Horizontal, BW and FW. This can be clearly seen when examining the mode shapes: those corresponding to the BW mode are shown in the insets.

Table 1 explains the interpretation of the mode shapes using the BW mode as an example. The rows in the table corresponds to the modes found by OMA-SSI (see Figure 5). Examining the middle row BW $n=0$, one can realize that the periodic mode consists of three Fourier components *oscillating at different frequencies*: the horizontal component at 0.72Hz, backward whirling component at 0.88Hz and very weak forward

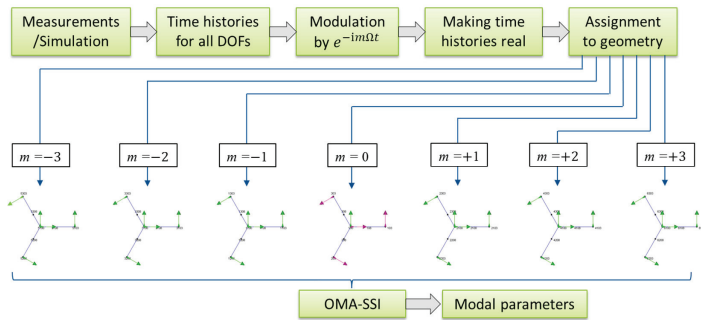


Figure 4. Flow of the suggested method

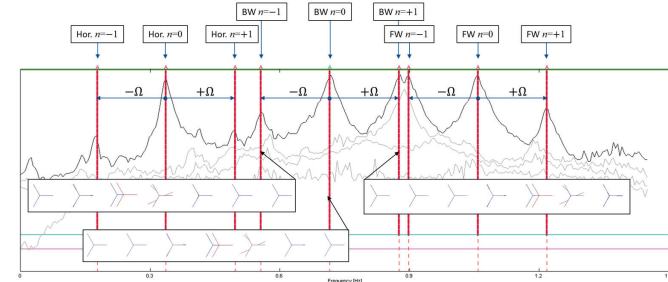


Figure 5. Fragment of the stabilization diagram (B&K Type 7760 OMA software) showing horizontal, BW and FW modes of the isotropic rotor with no gravity.

whirling component at 0.56Hz. While inspecting the top and bottom rows, one finds the same components at the same frequencies.

Note that the phase relations between DOFs are only valid inside each Fourier component and do not make sense between the components.

The values of the Fourier exponents are given in Table 2 and the magnitude of the Fourier components are shown in Figure 6bd and Figure 7d,e,f and compared with the results of analytical Floquet analysis. Both frequencies, damping and mode shapes are in a quite good agreement with the analytical values.

Figure 7 explains the results of H-OMA-TD in details using the BW mode as an example. The simulation was conducted for five different realizations of the excitation input, and the system identification was performed for each realization. Figures 7b,d,f show the mean magnitudes of the obtained Fourier components; the confidence bounds on the results based on the five observations are also shown. Though the H-OMA-TD algorithm produces many Fourier components, it can be seen that the confidence of the noise components is significantly lower (the confidence band is wider), and the false ones can be readily identified and filtered out. The true ones are shown inside the dotted region (Figure 7b,d,f), and coincide

Name	Frequency, Hz	Mode shape						
		$m=-3$	$m=-2$	$m=-1$	$m=0$	$m=+1$	$m=+2$	$m=+3$
BW $n=-1$	0.56							
		$0.56-3\Omega=0.08\text{Hz}$	$0.56-2\Omega=0.24\text{Hz}$	$0.56-\Omega=0.40\text{Hz}$	0.56Hz	$0.56+\Omega=0.72\text{Hz}$	$0.56+2\Omega=0.88\text{Hz}$	$0.56+3\Omega=1.04\text{Hz}$
BW $n=0$	0.72							
		$0.72-3\Omega=0.24\text{Hz}$	$0.72-2\Omega=0.40\text{Hz}$	$0.72-\Omega=0.56\text{Hz}$	0.72Hz	$0.72+\Omega=0.88\text{Hz}$	$0.72+2\Omega=1.04\text{Hz}$	$0.72+3\Omega=1.20\text{Hz}$
BW $n=+1$	0.88							
		$0.88-3\Omega=0.40\text{Hz}$	$0.88-2\Omega=0.56\text{Hz}$	$0.88-\Omega=0.72\text{Hz}$	0.88Hz	$0.88+\Omega=1.04\text{Hz}$	$0.88+2\Omega=1.20\text{Hz}$	$0.88+3\Omega=1.36\text{Hz}$

Table 1. Isotropic rotor with no gravity. Shapes of the Fourier components for BW mode for different n .

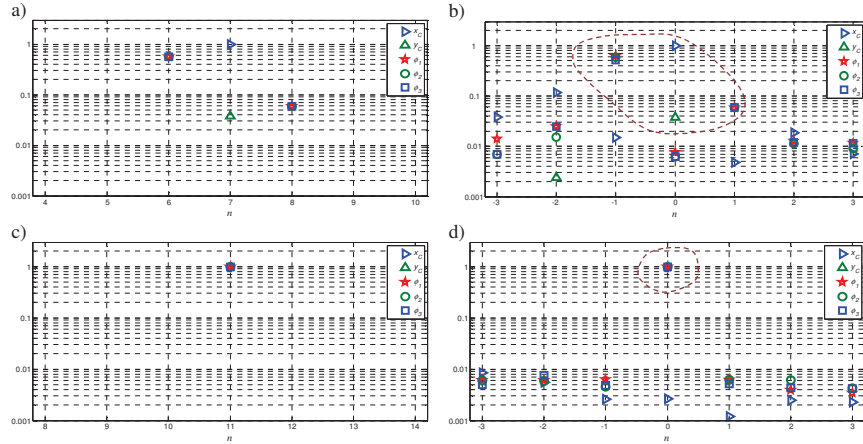


Figure 6. Isotropic rotor with no gravity. (a,b): FW mode; (c,d): collective mode. (a,c): Results of the Floquet analysis; (b,d): Results of H-OMA-TD for the simulated experiment.

with the analytical results obtained via Floquet analysis. Figure 7e shows the scatter of the shape of the BW and FW Fourier components (*cf.* analytical plots in Figure 7a).

Figure 8 compares the results of Floquet analysis with the results of H-OMA-TD for anisotropic rotor in the presence of gravity. The dashed lines surround the regions where the H-OMA-TD methods catches the Fourier components pretty well. These components dominate the dynamics of the mode, while the others are significantly lower in magnitude. The dotted line in Figure 8b shows the erroneous components which do not present in the analytical solution (Figure 8a). These components can be explained by the strong influence of the rotor harmonics present nearby the component frequencies (see the strong peaks in Figure 2b). Table 2 provides the Floquet exponents and compares them with the analytically ones; both agree quite well.

The complexity plots in Figure 9 compare the dominating Fourier components for the two whirling modes. The rotor anisotropy causes the asymmetry of the shapes. Despite the scatter, this observed asymmetry can be used as an indicator of a damage (here, the stiffness of blade #3 is reduced by 3%). This may also be used to localize the damage [18].

3.2.3 Result comparison

Table 2 provides Floquet exponents obtained analytically and compares them with the frequencies found by time- and frequency domain H-OMA methods. Regarding damping, one can notice that, if it is defined with a damping ratio, then it depends on chosen the natural frequency. The latter is not invariant since a shift by an integer multiplier of Ω is also a natural frequency (e.g. Table 1). However, the real part of the Floquet multipliers is invariant, and can be used to characterize the damping and system stability.

Figure 10 compares the magnitudes of modal components of BW and FW modes obtained by frequency and time domain methods for the isotropic rotor in the absence of gravity (Figure 10a-d) and anisotropic rotor when the gravity is present (Figure 10e-h). The dominant components of the modes are outlined by a dashed line. As one can observe, the two methods provide similar results, though the frequency domain method gets slightly wrong results reporting the different magnitudes of ϕ_1, ϕ_2, ϕ_3 for the isotropic case (outlined by the dotted lines). This might be possibly improved by using a multi-reference technique. The same can be

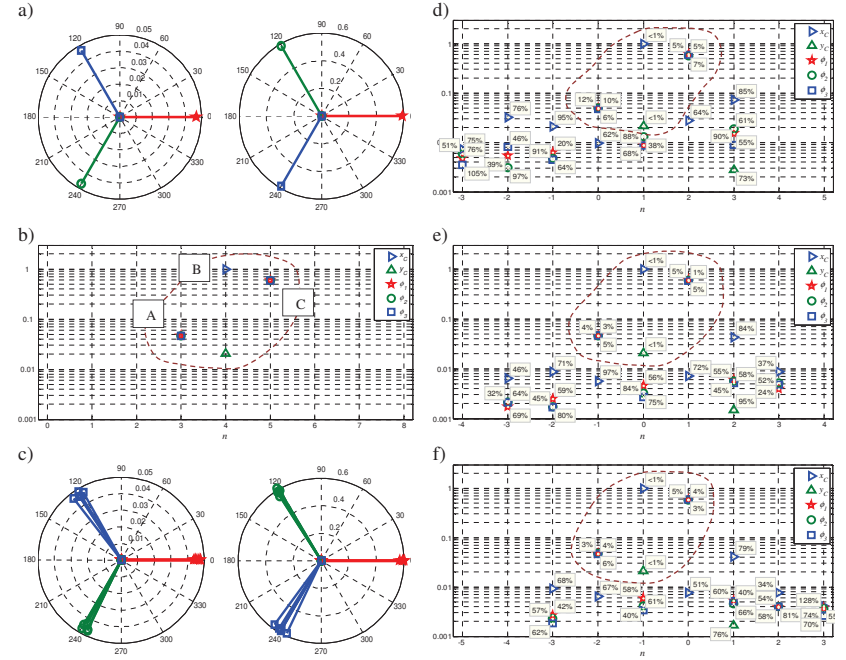


Figure 7. The BW mode of isotropic rotor with no gravity. a) Shapes of the FW (left) and BW (right) components (via Floquet analysis); b) Magnitude of Fourier components (via Floquet analysis); c) Same as (a) via H-OMA-TD; d-f) Magnitudes of Fourier components for: d) $n = -1$, e) $n = 0$, f) $n = +1$, as in Table 1. The per-cent values in the boxes are a half-width of the pointwise 95% confidence bands computed based on five analysis, using Student's t -distribution.

said regarding the phase. The natural frequencies reported by the two methods differ by Ω , which is natural for periodic systems. Actually, the mode shown in Figure 10a is fully comparable with the representation “BW $n=+1$ ” found in Table 1.

It is also interesting to compare the results of H-OMA-TD with the results of *direct* application of OMA to the measured data, thus ignoring the fact that the system is LPTV. This approach was used for example, in [18]. In the framework of the H-OMA-TD method, it means narrowing the range of m in (11) to 0. As it follows from Table 1, it will still be possible to extract the Fourier components (each found mode will be a Fourier component). If the LPTV nature of the system is recognized, one has to manually assemble the mode from the found Fourier components, knowing that they are separated by integer multipliers of Ω . It is also important to note that the mutual scaling of the Fourier components will be lost in this case.

4 Conclusion and future research

The study suggests a simple method of extending existing implementations of time domain OMA SSI algorithms to time periodic systems. The method consists of two steps: (i) harmonic modulation of the experimentally obtained time histories (by multiplication by $e^{-im\Omega t}$); (ii) making the obtained complex

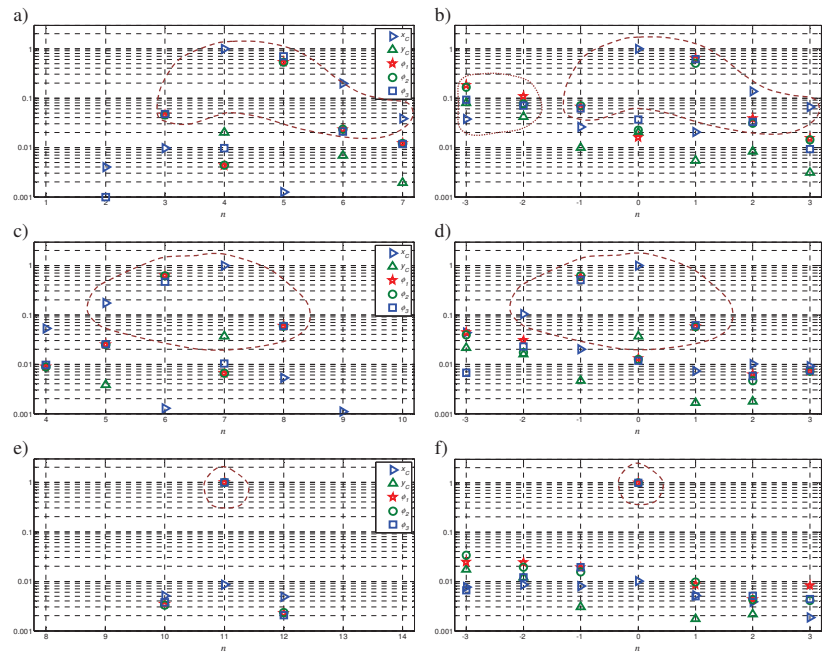


Figure 8. Magnitudes of the Fourier components for anisotropic rotor: BW (top row), FW (middle row) and collective (bottom). Left column: results of the Floquet analysis; right column: H-OMA-TD for simulated experiment. Dashed lines show the significant components, dotted line shows the erroneous results due to vicinity to strong rotor harmonics.

time histories real. The preprocessed data becomes an input to standard OMA algorithm. In addition, the authors give some advice on how to prepare the data for OMA, to more easily interpret the results.

The method is demonstrated on synthesized data obtained via simulation of a simple 3-bladed rotor subjected to random noise excitation. The results of this simulated experiment are validated against the analytical results from Floquet analysis and the results provided by the conventional HPS method implemented in the frequency domain. The suggested algorithm avoids the manual peak picking and allows automation, which could be useful, for example, in structure health monitoring systems.

The suggested method is originated from engineering practice, and requires a better mathematical foundation. Mode shape normalization and scaling when using acceleration measurements and estimation of damping ratio need to be addressed. Application of the method to real measurements from a wind turbine would be a natural next step.

Acknowledgements

The work is partly supported by EUDP (Danish Energy Technology Development and Demonstration Programme), grant number 64011-0084 "Predictive Structure Health monitoring of Wind Turbines".

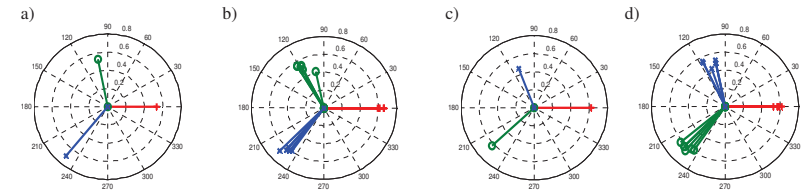
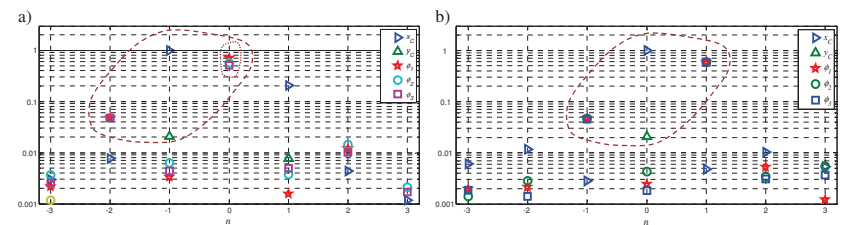


Figure 9. Complexity plots: anisotropic rotor. Blade #3 has a 3% reduction in stiffness. a) BW mode, the BW (dominating) component, exact solution; b) same, the H-OMA-TD results for five simulated experiments; c) FW mode, the FW (dominating) component, exact solution, d) same, the H-OMA-TD results for five experiments.

Mode Name	Floquet exponent $\lambda/(2\pi)$	n	Un-aliased Floquet exponent $(\lambda + n\Omega)/(2\pi)$	H-OMA-TD ($n=0$) (in Hz)	H-OMA-FD (in Hz)
<i>Isotropic rotor, no gravity</i>					
BW	$-0.0112 + 0.0764i$	4	$-0.0112 + 0.7164i$	$-0.0116(\pm 0.0013) + 0.7162(\pm 0.0008)i$	$-0.0140 + 0.7159i$
FW	$-0.0117 - 0.0610i$	7	$-0.0117 - 1.0590i$	$-0.0113(\pm 0.0007) + 1.0587(\pm 0.0025)i$	$-0.0102 + 1.0540i$
Collective	$-0.0348 + 0.0464i$	11	$-0.0348 + 1.8064i$	$-0.0353(\pm 0.0014) + 1.8064(\pm 0.0032)i$	$-0.0360 + 1.8006i$
<i>Anisotropic rotor, with gravity</i>					
BW	$-0.0111 + 0.0716i$	4	$-0.0111 + 0.7116i$	$-0.0122(\pm 0.0018) + 0.7121(\pm 0.0006)i$	$-0.0118 + 0.7129i$
FW	$-0.0116 - 0.0648i$	7	$-0.0116 - 1.0552i$	$-0.0113(\pm 0.0008) + 1.0547(\pm 0.0011)i$	$-0.0105 + 1.0549i$
Collective	$-0.0345 + 0.0378i$	11	$-0.0345 + 1.7985i$	$-0.0353(\pm 0.0019) + 1.7985(\pm 0.0032)i$	$-0.0286 + 1.7858i$

Table 2. Floquet exponents obtained analytically, by H-OMA-TD and H-OMA-FD.



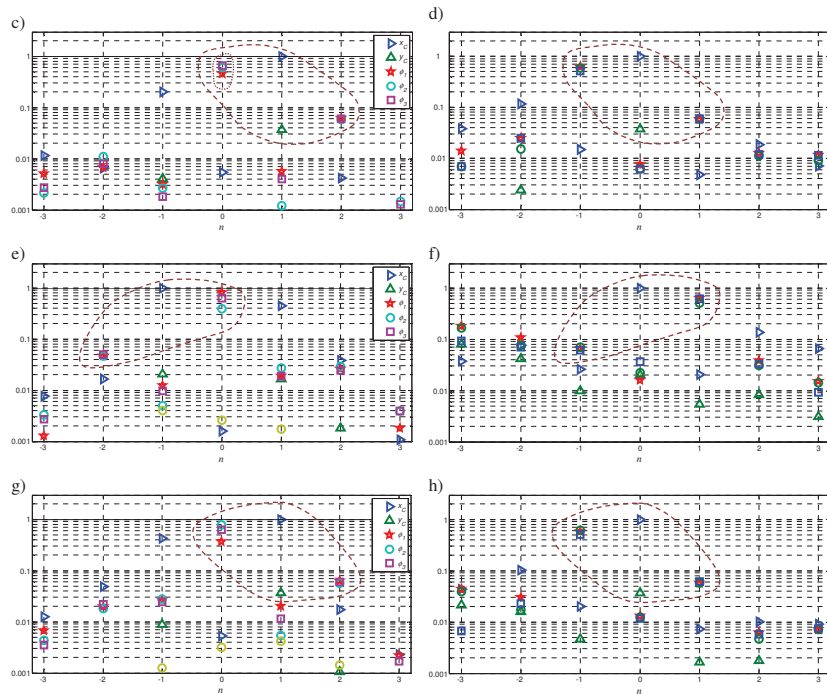


Figure 10. Magnitudes of modal components obtained by H-OMA-FD (left column) and H-OMA-TD (right column). a,b) Isotropic rotor in the absence of gravity, BW mode; c,d) same, FW mode; e,f) anisotropic rotor in the presence of gravity, BW mode; g,h) same, FW mode.

References

- [1] G. H. James, T. G. Carne, *Damping measurements on operating wind turbines using the natural excitation technique (NEXT)*. In *Proceedings of 11th ASME Wind Energy Symposium presented at the Energy Sources Technology Conference and Exhibition*. Houston, USA (1992). Vol. 12, pp. 75-81.
- [2] D. Tcherniak, S. Chauhan, M. Rossetti, I. Font, J. Basurko, O. Salgado. *Output-only Modal Analysis on Operating Wind Turbines: Application to Simulated Data*. In: *Proceedings of European Wind Energy Conference*, Warsaw, Poland (2010).
- [3] A. Jhinaoui, *Subspace-based identification and vibration monitoring algorithms for rotating systems*, PhD Thesis, Rennes, France (2014).
- [4] M.S. Allen, *Frequency-Domain Identification of Linear Time-Periodic Systems using LTI Techniques*, Journal of Computational and Nonlinear Dynamics, Vol. 4, No. 4 (2009).
- [5] M.S. Allen, M. W. Sracic, et al. *Output-Only Modal Analysis of Linear Time Periodic Systems with Application to Wind Turbine Simulation Data*, Mechanical Systems and Signal Processing Vol. 25 (2011), pp. 1174-1191.

- [6] S. Yang, M. S. Allen, *A Lifting Algorithm for Output-only Continuous Scan Laser Doppler Vibrometry*, In *Proceedings of 53rd AIAA Structures, Structural Dynamics, and Materials Conference*. Honolulu, Hawaii (2012).
- [7] S. Yang, M. S. Allen, *Output-Only Modal Analysis Using Continuous-Scan Laser Doppler Vibrometry and Application to a 20kW Wind Turbine*, Mechanical Systems and Signal Processing Vol.31 (2012), pp. 228-245.
- [8] S. Yang, M. S. Allen, *Transfer Functions to Measure Translational and Rotational Velocities with Continuous-Scan Laser Doppler Vibrometry*, In *Proceeding of 31st International Modal Analysis Conference (IMAC XXXI)*, Garden Grove, CA, USA (2013).
- [9] S. Yang, M. S. Allen, *Harmonic Transfer Function to Measure Translational and Rotational Velocities With Continuous-Scan Laser Doppler Vibrometry*, Journal of Vibration and Acoustics, Vol. 136, No. 2, (2014).
- [10] S. Yang, S., D. Tcherniak, M. S. Allen, *Modal Analysis of Rotating Wind Turbine using Multi-blade Coordinate Transformation and Harmonic power spectrum*, In *Proceedings of 32nd International Modal Analysis Conference (IMAC XXXII)*, Orlando, FL, USA (2014).
- [11] J. H. Ginsberg, *Mechanical and Structural Vibrations*. New York, John Wiley and Sons (2001).
- [12] C. Chen, *Linear Systems Theory and Design*. New York, Oxford University Press, Inc. (1999).
- [13] N. M. Wereley, *Analysis and Control of Linear Periodically Time Varying Systems*, PhD Thesis, Massachusetts Institute of Technology, (1991).
- [14] G. Floquet, *Sur Les Equations Lineaires a Coefficients Periodiques*, Ann. Sci. Ecole Norm. Sup., Vol. 12, (1883) pp. 47-88.
- [15] P. Hartman, *Ordinary Differential Equations*, New York, John Wiley & Sons, Inc. (1964).
- [16] J. Guckenheimer, P. Holmes, *Nonlinear Oscillations, Dynamical Systems, and Bifurcations of Vector Fields*. New York, Springer-Verlag New York Inc. (1983).
- [17] H. Hochstadt, *Differential Equations*. New York, Dover (1964).
- [18] D. Tcherniak, *Loss of Rotor Isotropy as a Blade Damage Indicator for Wind Turbine Structure Health Monitoring Systems*, In *Proceedings of European Workshop on Structure Health Monitoring (EWSHM)*, Nantes, France (2014).
- [19] P. F. Skjoldan, *Aeroelastic modal dynamics of wind turbines including anisotropic effects*, PhD Thesis, Roskilde, Denmark (2011).
- [20] M. H. Hansen, *Improved Modal Dynamics of Wind Turbines to Avoid Stall-induced Vibrations*. Wind Energy Vol. 6 (2003), pp.179-195
- [21] D. Tcherniak, S. Chauhan, M. N. Hansen, *Applicability Limits of Operational Modal Analysis to Operational Wind Turbines*. In *Proceedings of 28th Int. Modal Analysis Conference (IMAC)*, Orlando, FL, USA (2010).
- [22] M.S. Allen, *Global and Multi-Input-Multi-Output (MIMO) Extensions of the Algorithm of Mode Isolation (AMI)*, Doctorate, Georgia Institute of Technology (2005).
- [23] M. S. Allen, J. H. Ginsberg, *Global, Hybrid, MIMO Implementation of the Algorithm of Mode Isolation*. In *Proceedings of 23rd International Modal Analysis Conference (IMAC XXIII)*. Orlando, FL, USA (2005).
- [24] R. J. Allemang, D. L. Brown, *A Unified Matrix Polynomial Approach to Modal Identification*, Journal of Sound and Vibration Vol. 211, No. 3 (1998), pp. 301-322.
- [25] H. Vold, K. Napolitano, et al. *Aliasing in modal parameter estimation: An historical look and new innovations*. In *Proceedings of 25th International Modal Analysis Conference*. Orlando, FL, USA (2007).
- [26] P. P. Guillaume, P. Verboven, et al., *A Poly-Reference Implementation of the Least-Squares Complex Frequency-Domain Estimator*. In *Proceedings of International Modal Analysis Conference (IMAC XXI)*, Kissimmee, FL, USA (2003).



IOMAC'15

6th International Operational Modal Analysis Conference
2015 May12-14 Gijón - Spain

EXPERIMENTAL CHARACTERIZATION OF AN OPERATING VESTAS V27 WIND TURBINE USING HARMONIC POWER SPECTRA AND OMA SSI

Dmitri Tcherniak¹, and Matthew S. Allen²

¹ Brüel & Kjær Sound and Vibration Measurement A/S, dmitri.tcherniak@bksv.com

² Department of Engineering Physics, University of Wisconsin-Madison, msallen@engr.wisc.edu

ABSTRACT

The study addresses experimental identification of linear periodic time variant systems. The recently introduced Harmonic-OMA-Time Domain (H-OMA-TD) method is in focus. It is shown how this method can aid engineers and what additional information it can bring, compared to other methods. The method is demonstrated in application to experimental data obtained on operating wind turbine.

Keywords: Operating Wind Turbine, Periodic Time Variant Systems, LPTV, LTP, Floquet analysis, Fourier exponents.

1. INTRODUCTION

Modern wind turbines are designed to generate energy for a period of 20 to 25 years. Exposed to enormous loads and manufactured from light materials, the wind turbine structure is subjected to strong vibrations. To ensure the turbine produces energy and stays undamaged during the intended lifespan, the design engineers need to fully understand the dynamics of operating wind turbines. This is not a trivial task. The well-accepted modal analysis approach is only applicable under a very limited set of conditions, since its main assumption is that the system of interest is linear time invariant (LTI). Wind turbines are not linear time invariant if one considers the most natural reference frame, where the vibration of the blades is measured relative to the moving rotor reference frame and the tower is measured in the fixed reference frame. In that reference frame, the system contains stiffness terms that vary periodically with time so it is termed linear time periodic (LTP) or linear periodically time varying (LPTV). However, for several decades wind turbines have been modeled as LTI by using the multi-blade coordinate (MBC, or also known as Coleman) transformation, which replaces the motion of the individual blades with rotor coordinates that describe the motion of the rotor as a whole.

The MBC transformation provides a simple and intuitive approach for treating LPTV systems. It is a special coordinate transformation, which converts the equations of motion (EoM) of a bladed, rotating structure into a time invariant system [1]. After such a transformation, the obtained LTI system can be analysed by conventional modal analysis methods. This transformation only succeeds in producing a

LTI system if the rotor is perfectly isotropic and the blades are equally spaced, i.e., all blades are structurally identical and evenly and identically attached to the hub. Effects such as blade-to-blade variations, wind shear, active-pitch control, incomplete instrumentation (in an experiment) and gravitational stiffening cannot be captured with an LTI model. This work employs a more versatile approach where the turbine is modeled as an LPTV system, which requires application of other analysis techniques. Fortunately, modal analysis extends very naturally to LPTV systems (see, e.g., [2]), so this does not complicate experiments or analysis too dramatically.

Analysis methods for time periodic systems have existed for several decades, for example the MBC, transformation, Floquet analysis and Hill's method, and they are implemented in some of the simulation software that is used for designing wind turbines and helicopters [3]. While these works often present Floquet theory in a way that seems disconnected from LTI modal analysis, one key outcome of Floquet theory is that modal decomposition is still applicable to LPTV systems but the mode shapes are periodic (the eigenvalues or poles are constant). Expanded into Fourier series, each mode will consist of infinitely many components, each oscillating at frequency equal to the modal frequency plus an integer multiple of the rotational frequency. Hence, each time-varying shape is manifested by sidebands in the spectrum. Each sideband component will also have its own shape. In this regard, when performing frequency domain analysis the primary difference between LTI and LPTV systems is that the latter has multiple deformation shapes for each eigenvalue and these must be added to obtain each mode's complete, time-periodic mode shape.

Naturally, LPTV analysis produces the same result as the MBC transformation if the rotor is isotropic. Skjoldan et al. [4] demonstrated the similarity between MBC transformation and Floquet analysis, and showed that only three harmonic components are necessary to describe each mode shape of a three-bladed isotropic rotor. If the rotor is not isotropic, then MBC breaks down and more than three harmonics will be present for some or all of the modes. Using Floquet analysis, one can show that slightly anisotropic rotors require more than three components. However, numerical simulations demonstrated that sometimes only a few components are significant and the rest can be neglected without loss of the accuracy, see for example [5].

1.1. Experimental techniques for LPTV systems analysis

Engineering practice often requires design validation after the wind turbine prototype is constructed; this calls for *experimental* system identification. The tools allowing experimental dynamic characterization of LPTV systems are very limited: one can name MBC transformation adapted to experimental identification [6], the extension of SSI to LPTV systems based on angular resampling [7] and harmonic power spectra (HPS) method [2]. All these methods are output-only, i.e., they do not require measurement of the input to the system. Instead, they assume that the input forces excite all system modes, have broadband spectra and are uncorrelated.

1.1.1. Multiblade Coordinate Transformation (MBC)

The adaptation of the MBC transformation method to experimental modal analysis starts with pre-processing of the experimental data, namely, the conversion of the coordinates q measured in the rotating frame to the ground-fixed multi-blade coordinates a_0, a_1, b_1 :

$$a_{0,k} = \frac{1}{3} \sum_{i=1}^3 q_{i,k}, \quad a_{1,k} = \frac{2}{3} \sum_{i=1}^3 q_{i,k} \cos(\phi_i), \quad b_{1,k} = \frac{2}{3} \sum_{i=1}^3 q_{i,k} \sin(\phi_i), \quad (1)$$

where $i = 1, 2, 3$ is the blade index, k is the index of the DOF and ϕ_i is the azimuth of the i^{th} blade. After that, conventional OMA (for example, the SSI technique) is applied. The obtained modal parameters are then transferred back into the rotating system using the backward MBC transformation:

$$q_{i,k} = a_{0,k} + a_{1,k} \cos(\phi_i) + b_{1,k} \sin(\phi_i). \quad (2)$$

The overall process is shown schematically in Figure 1. The examples of this technique in application to operating wind turbine data can be found in [6], **Error! Reference source not found.**[10].

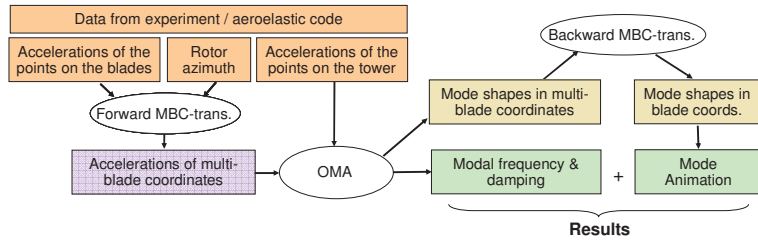


Figure 1. Adaptation of the MBC transformation method to experimental modal analysis (from [6]).

Assuming constant rotor speed Ω [thus the azimuth $\phi_i = \Omega t + \frac{2\pi}{3}(i-1)$], it can be easily shown that the mode shape of the r^{th} mode in the rotating frame is [1], [9]:

$$q_{i,k}(t) = A_{0,k} \sin(\omega_r t + \varphi_0) + A_{BW,k} \sin\left((\omega_r + \Omega)t + \frac{2\pi}{3}(i-1) + \varphi_{BW}\right) + A_{FW,k} \sin\left((\omega_r - \Omega)t - \frac{2\pi}{3}(i-1) + \varphi_{FW}\right), \quad (3)$$

where ω_r is the natural frequency of the r^{th} mode. The modal amplitudes and phases in (3) can be readily calculated from the corresponding eigenvector of the system in multi-blade coordinates. Analyzing (3), one can note that:

1. The mode shape is time-periodic.
2. It consists of three components.
3. The three components oscillate at frequencies ω_r , $\omega_r + \Omega$ and $\omega_r - \Omega$, respectively.
4. All three blades have the same oscillation magnitudes.
5. The phase between the blades is 0 for the first component (thus it is called *collective* component), -120° for the second (*backward whirling* component) and $+120^\circ$ for the third (*forward whirling* component).

As mentioned before, the MBC transformation assumes rotor isotropy. In reality, all rotors have some degree of anisotropy, which manifests itself in richer dynamics: one observes more components (sidebands) and the component shapes loose the regularity (equal blades' magnitude and $0/\pm 120^\circ$ phase) [11], [12]. As demonstrated above, MBC transformation is not capable of catching these phenomena, and consequently, application of MBC to anisotropic rotors may lead to erroneous results. This was observed, for example, in [10]. Furthermore, when dealing with measurements, the MBC requires the "isotropy" of the sensor setup: the sensors should be located at identical points on all blades and have the same orientation of measurement axis. Furthermore, if one sensor fails, then all sensors at that radial position must be discarded.

1.1.2. Lifting method

Jhinaoui et al. [7] suggested a subspace identification method specially developed for rotating systems. The method identifies the underlying Floquet eigenstructure of the rotating system and uses the special resampling procedure known as lifting ([13], [14], [15]), where the samples are obtained at the same position of the rotor at the consecutive revolutions. The drawback of the method is that it may crowd the frequency spectrum since the resampling procedure essentially aliases the signal, and it may require data from many rotor revolutions. The method showed good results for helicopter rotors, where the rotation speed is relatively high and allows thousands of rotor revolutions when the other parameters do not change. In the case of wind turbines, with their low rotation speeds, it is difficult to collect the data from several thousand rotor revolutions under the same environmental conditions (e.g., wind speed and direction) [16].

1.1.3. HPS method in frequency domain: H-OMA-FD

The rigorous proof and description of the HPS method can be found in [17]. The method is based on the concept of harmonic transfer functions [17], which were written in terms of a modal decomposition and used to develop a framework for operational modal analysis in [18]. The core of the method is the modulation of the response signals using the phasors rotating with the fundamental circular frequency Ω and its integer multipliers:

$$\mathbf{y}_m(t) = \mathbf{y}(t)e^{-jm\Omega t}, \quad (4)$$

where $\mathbf{y}(t)$ is a vector of N measured responses and m is an integer varying from $-M$ to M . The resulting vector consists of $N(2M+1)$ complex time histories.

The next step of the method is the calculation of the harmonic power spectra (HPS) matrix between the modulated signals; this is done in the same manner as in the LTI case:

$$\mathbf{S}_{YY}(\omega) = E(\mathbf{y}_m(\omega)\mathbf{y}_m(\omega)^H), \quad (5)$$

where $E(\dots)$ is mathematical expectation, $(\dots)^H$ is Hermetian transpose. Note that the resulting matrix is defined in the frequency domain. The theory in [18] shows that the HPS matrix can be presented in terms of modes of the LPTV system. Preserving only dominant terms, one can prove that the following is valid:

$$\mathbf{S}_{YY}(\omega) \approx \sum_{r=1}^{2K} \sum_{l=-\infty}^{\infty} \frac{\mathbf{c}_{r,l} \mathbf{W}(\omega) \mathbf{c}_{r,l}^H}{(j\omega - (\lambda_r - jl\Omega))(j\omega - (\lambda_r - jl\Omega))^H} \quad (6)$$

where λ_r are the Floquet exponents, $\mathbf{c}_{r,l}$ are the Fourier coefficients that describe the temporal and spatial deformation pattern of the periodic mode shape, and K is the number of modes. $\mathbf{W}(\omega)$ describes the input spectrum. Under the standard OMA assumptions regarding the excitation, namely that the input is uncorrelated random white noise, $\mathbf{W}(\omega)$ becomes constant.

The last task is to extract the Floquet exponents and Fourier coefficients from the HPS matrix. This can readily be done by employing one of the conventional frequency domain methods, for example, AMI [19] or more sophisticated AFPoly algorithm [20] or pLSCF [21].

1.1.4. H-OMA-TD: combination of HPS and OMA SSI

In operational modal analysis, the time domain techniques are sometimes more advantageous than the frequency domain ones, especially in the case of heavily damped structures, which is typical for operating wind turbines. The extension of HPS to the time domain was suggested and explained in [12]. We referred this extension as Harmonic OMA Time Domain (H-OMA-TD), to distinguish it from the frequency domain HPS method (H-OMA-FD). In that study, the method was applied to an analytical system: a six-degrees-of-freedom system representing a three-bladed rotor with blades that were flexible only in in-plane direction. The availability of the EoM allowed the application of Floquet analysis to obtain the analytical periodic modes. The analytical solution served as a reference for validation of the experimental identification. The response of the rotor to random loads was simulated and the resulting response time histories were used as an input to H-OMA-TD. The comparison with the analytical solution showed quite good agreement. The method was capable of catching the features of the anisotropic rotor dynamics, both qualitatively and quantitatively.

The presented study demonstrates the application of the method to data measured on a real object: an operating Vestas V27 wind turbine.

2. INTRODUCTION TO H-OMA-TD

The flow of H-OMA-TD is schematically shown in Figure 2. The measured responses (on the rotating and non-rotating parts of the structure) form vector $y(t)$. The rotational speed or, preferably, the rotor azimuth should be measured as well. The first step is the same as in H-OMA-FD, namely the modulation (4). The resulting time histories are complex (except the original time histories, which correspond to $m = 0$). Since the standard implementation of the OMA SSI algorithm can only accept real-valued time histories, a conversion is required. The conversion shall, however, retain the magnitude and phase relations between the original signals and their modulated copies. The method suggested in [12] takes the following steps:

1. For the exponentially modulated signals $y_m(t)$, compute their periodogram $\mathcal{F}(y_m(t))$ using a fast Fourier transform. The periodogram of complex $y_m(t)$ is not a Hermitian function, i.e., its negative frequency part is not a complex conjugate of the positive frequency part.
2. Replace the negative frequency part of the periodogram by the complex conjugate of the positive part.
3. Using inverse FFT, generate the new time signals $\tilde{y}_m(t)$, which are real.

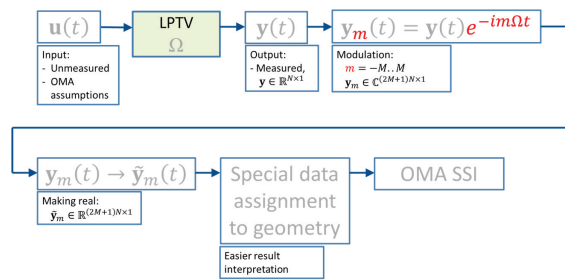


Figure 2. H-OMA-TD flow chart.

The next step, the *special data assignment to geometry*, is mainly to facilitate the mode visualization: indeed, the periodic mode shape is not easy to interpret; instead, we propose to visualize the component shapes.

Following the proposed approach, one has to create $2M$ “clones” of the geometry, for example, right and left from the original geometry, Figure 3. The m^{th} “clone” will visualize the m^{th} component. The data assignment shall be conducted accordingly: the time histories modulated with the given m shall be assigned to the m^{th} clone.

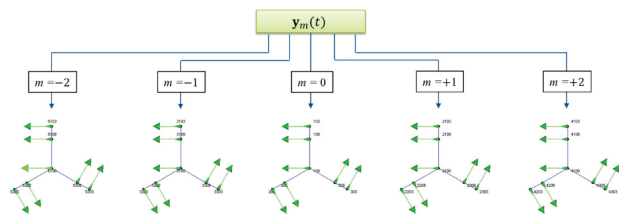


Figure 3. Assignment of the modulated signals to geometry.

3. VIBRATION MEASUREMENTS ON OPERATING VESTAS V27

A detailed description of the instrumentation and data acquisition was presented in [22]; this section provides a brief overview.

Vestas V27 is a 225kW pitch-controlled horizontal-axis wind turbine with 27 m rotor diameter (blade length is 13 m). The wind turbine is not new but has many features similar to those of modern wind turbines (Figure 4).

Each of the three blades of the wind turbine was instrumented by 12 monoaxial accelerometers, ten measuring in the flap- and two in the edgewise direction. Since the MBC transformation was considered as the main analysis tool, special care was taken to instrument all three blades as identically as possible in regard to both the accelerometers’ location and orientation. Also, the pitch angle and rotor azimuth were measured using dedicated sensors. The data was collected by a data acquisition front end located in the spinner and wirelessly transmitted the data to the nacelle. The front end was powered via a slip ring.



Figure 4. Vestas V27 wind turbine. The green strips on the blades are the tape protecting the accelerometer cables.

The nacelle vibrations were measured by three triaxial accelerometers, one located under the main bearing and the other two at the rear of the nacelle; a laser tachometer was used to measure the rotational speed of the high-speed shaft. To sample-synchronize the rotor and nacelle data streams, the IRIG-B GPS-based protocol was employed.

The measurement campaign started in October 2012 and ended in May 2013, thus covering a wide range of weather conditions and wind speeds. We recorded data during the entire campaign, except for short periods when the system was down. During the campaign, a few accelerometers were lost (it was discovered later that this was due to improper cabling). Using a data management system, it was straightforward to find recordings where the wind speed, RPM and pitch angle were not changing significantly, and these recordings were selected for the following analysis.

The data from this measurement campaign was already analysed and presented: In [9], the MBC and H-OMA-FD approaches were used for edgewise rotor modes. In [10], the MBC transformation was employed for both flap- and edgewise modes. In [16], the edgewise rotor modes were analysed using the lifting approach.

4. PROCEDURE AND RESULTS

The blade vibrations are caused by various loads. The wind-induced aerodynamic forces are the main contributor. Though intuitively these forces should satisfy OMA assumptions, the aerodynamic analysis shows that this is not true. The aerodynamic forces do not have flat frequency spectra; they are rather characterized by peaks at the rotation frequency and its harmonics with thick tails around each peak. More details can be found in [23]. Slight rotor unbalancing and aerodynamic interaction with the tower also cause some periodicity in the measured signals. In addition to this, the high-speed-shaft-related vibrations propagate through the low-speed shaft and, being sampled by the rotor frequency, appear as a series of sharp peaks at the higher frequencies separated by the rotor frequency (Figure 5).

An OMA algorithm may confuse the sharp peaks with the system modes. Therefore, it is advantageous to remove the deterministic component from the measured responses by dedicated methods (see. e.g., [24] for an overview). Since both rotor azimuth angle and the high-speed-shaft RPM measurements were available, we selected the Time Synchronous Averaging (TSA) method to remove the deterministic part from the response signals. The spectra from the edgewise tip accelerometer before and after TSA are shown in Figure 5 as an example.

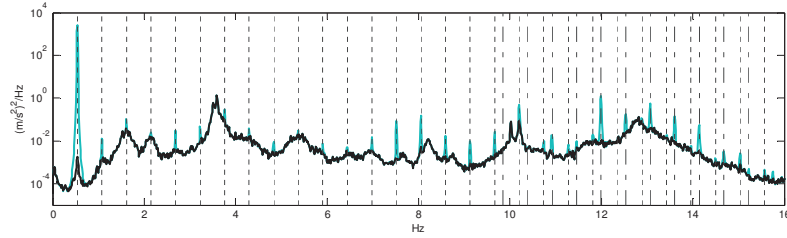


Figure 5. Power spectral density of the edgewise tip accelerometer of blade #2, before (green) and after (black) TSA. The dashed lines are rotor harmonics, dash-dot lines – high-speed-shaft-related harmonics.

An operating wind turbine has rich dynamics and variety of modes. However, the objective of the paper is not to describe V27's dynamics. It is rather to demonstrate the H-OMA-TD method and show how it can aid engineers, and what additional information it can bring, compared to other methods.

To demonstrate the method, we selected the in-plane rotor modes (which correspond to the edgewise blade motion). In total, seven signals were used: the edgewise accelerometer signals from each blade's tip and at 2/3 of the blade length, denoted $q_{1,tip}$ and $q_{1,mid}$, respectively, and the front nacelle acceleration in the side-to-side direction, x_N . Thus the vector $y(t)$ in (4) is:

$$y(t) = \{x_N(t), q_{1,tip}(t), q_{1,mid}(t), q_{2,tip}(t), q_{2,mid}(t), q_{3,tip}(t), q_{3,mid}(t)\}^T. \quad (7)$$

Twenty-minute-long recordings corresponding to 32 RPM and 43 RPM regimes were analyzed. The results presented below are for 32 RPM. The signals were pre-processed by TSA and then modulated with $M = 2$. Since the RPM was not exactly constant during the recordings, we used the measured azimuth $\phi_1(t)$ instead of Ωt in (4).

4.1. Whirling modes

The two first edgewise rotor modes are dominated by the whirling components, Figure 6; the magnitude of their closest sidebands is at least a decade less. The dominant components occur at 3.52Hz (forward whirling mode) and 3.59Hz (backward whirling mode), – the modes are named after their dominant component. The damping of these two modes is 0.5% and 0.8%, respectively. The shapes of the obtained components are similar to those obtained using the H-OMA-FD method; see Figure 11 in [9].

The magnitudes of the three blades are different and the phase lag between them is not $\pm 120^\circ$, as one would expect for the isotropic rotor. As we mentioned before, the MBC transformation cannot capture these features of the rotor dynamics. The idea of employing the magnitude and phase irregularity as an indicator of rotor anisotropy due to damage or ice formation was examined in [25].

The above-mentioned shape irregularity leads to erroneous and confusing results, which can be observed when applying the MBC transformation to anisotropic rotors: for example, the method finds four modes instead of two, see Figure 7a in [10].

Observing such a low magnitude of the sidebands, one may suggest that using dedicated LPTV methods for three-bladed rotors is not necessary and it only results in over complication of the analysis. Indeed, by setting $M = 0$, meaning that we simply applying OMA to the raw measured data, one will end up with almost the same results. This, however, is only relevant for these two particular modes, and the following examples will demonstrate much more complex dynamics of other modes, where the H-OMA-TD method has obvious advantages. Furthermore, a sideband with an amplitude that is an order of magnitude smaller than expected can still produce a significant error for certain harmonic *inputs*. The variation of the mode shapes in time might also lead to instability at other rotor speeds even though the sidebands are small at this speed.

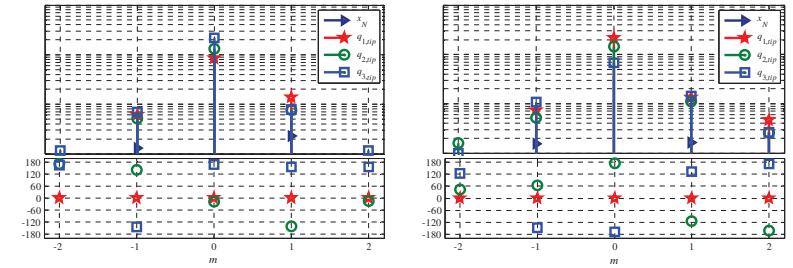


Figure 6. Shapes of the components of the forward whirling mode (left) and backward whirling mode (right): magnitudes and phases.

4.2. Collective mode

The dynamics of the first rotor collective mode are more interesting: though the collective component at 8.22Hz is dominant, the magnitude of the right and left sideband components is only about five times smaller (Figure 7). The damping of this mode is 1%. The component corresponding to the left sideband ($m = -1$) at 7.69Hz constitutes the forward whirling, and the right sideband ($m = 1$) at 8.76Hz is backward whirling; this can be seen from the phase lag between the blades. The central ($m = 0$) collective component has a significant tower part. Interesting to note, the collective mode is seemingly unaffected by the rotor anisotropy, whose effect was clearly seen in the whirling modes: here the blade magnitudes are almost equal and the phase lag between the blades is 0 for the collective component and $\pm 120^\circ$ for the whirling components. The magnitudes of the components corresponding to $m = \pm 2$ are 10 to 20 times smaller than the dominant one.

Since the rotor anisotropy does not play a significant role in the dynamics of this mode, the MBC transformation can be employed and will lead to the similar results: all three dominant components will be well identified. However, the proposed H-OMA-TD approach readily allows the visualization of the components, without involving any backward coordinate transformation.

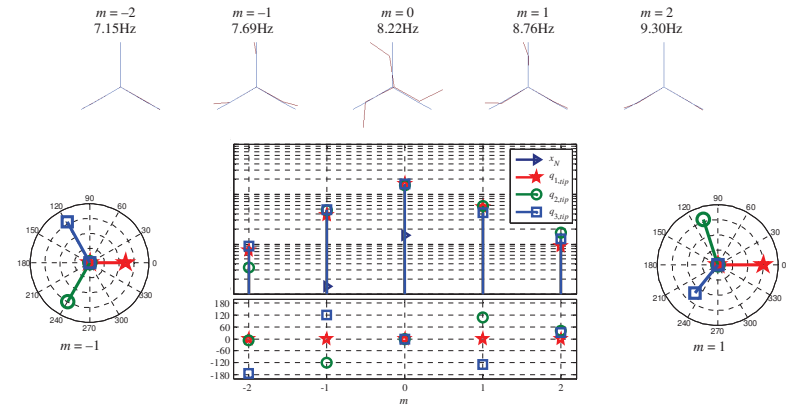


Figure 7. Shapes of the components of the collective mode. Top: visualization; bottom: magnitudes and phases. Sides: complexity plots of the whirling components.

4.3. Tower mode

The first side-to-side tower mode is observed at approximately 1Hz with damping 1.8%. This agrees well with the simulations and modal analysis performed on the nacelle data only [10]. However, utilizing the accelerometers mounted on the blades one can see that the expected side-to-side tower bending has a strong effect on the rotor. This declares itself as a strong collective rotor component at 1.54Hz ($m = 1$) and whirling component at 2.08Hz ($m = 2$), as shown in Figure 8. Actually, the dominant tower motion at 1.00Hz ($m = 0$) is also accompanied by the whirling rotor motion. It is important to note how easy it was to consider the tower and blade motions together using time-periodic H-OMA theory; these measurements would be more difficult to interpret without it.

Unfortunately, we cannot say anything certain for the components at $m = -1, -2$: the triaxial accelerometers used for the nacelle instrumentation had a high background noise level at frequencies below 0.7Hz, making the observations at these frequencies unreliable.

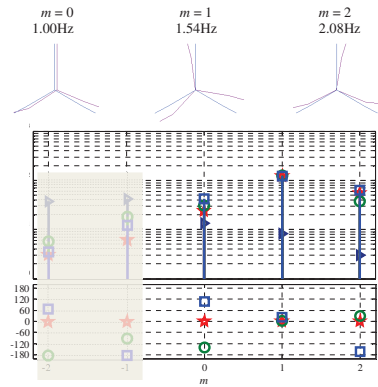


Figure 8. Shapes of the components of the first side-to-side tower mode. Top: visualization; bottom: magnitudes and phases. The components at $m = -1, -2$ are not reliable due to accelerometer noise, thus they are dimmed.

4.4. General observations

Examining the four modes, one cannot come to a clear guidance on how many modal components should be taken into consideration, i.e., which M to choose in Eq. (4). Both whirling modes are dominated by a single component, thus $M = 0$ might be sufficient; the collective mode has three significant components, thus M should be chosen greater than one. The tower mode perhaps require even more components. According to the theory behind MBC transformation, three components (i.e. $M = 1$) are sufficient to describe the dynamics of isotropic rotor in the absence of gravity. However, the gravity and slight rotor anisotropy may require more components. Increasing M , one automatically increases the number of signals y_m and hence, the complexity of the analysis. From authors' opinion, for three-bladed rotors with possible slight anisotropy, $M = 2$ is a reasonable choice. However, one needs to be careful applying this to, e.g., two-bladed rotors, where the periodic behaviour is much stronger. Also, if one is interested in behaviour that occurs over a small fraction of the cycle, say due to the blades passing the tower, then one might need many more harmonics.

5. CONCLUSION

The paper compares the recently suggested H-OMA-TD method with other methods intended to deal with time-periodic dynamic systems and demonstrates the method by application to experimentally obtained data from an operating wind turbine. It is shown that the method has a number of advantages:

1. It does not require rotor isotropy.
2. It allows using robust time domain OMA algorithms, such as OMA SSI:
 - It does not require any modification of OMA algorithms: a standard commercial implementations can be used
3. It correctly scales the magnitudes of the components with respect to each other, though the entire mode shape is normalized, as it is typical for OMA.
4. It does not require the data from many rotor revolutions for robust system identification.
5. It proposes the visualization scheme, which enables an easy interpretation of the periodic modes.

The method still misses a rigorous mathematical proof; so far, it is very much built on the analogy with H-OMA-FD method.

ACKNOWLEDGEMENTS

The work was partly supported by EU DP (Danish Energy Technology Development and Demonstration Programme), grant number 64011-0084 "Predictive Structure Health monitoring of Wind Turbines".

REFERENCES

- [1] Hansen, M.H. (2003) Improved Modal Dynamics of Wind Turbines to Avoid Stall-induced Vibrations. *Wind Energy*, 6, 179-195.
- [2] Allen, M. S. (2009) Frequency-Domain Identification of Linear Time-Periodic Systems using LTI Techniques, *Journal of Computational and Nonlinear Dynamics*, 4(24).
- [3] Peters, D. A. (1994) Fast Floquet theory and trim for multi-bladed rotorcraft, *Journal of the American Helicopter Society*, 39, 82-89.
- [4] Skjoldan, P. F., Hansen, M. H. (2009) On the similarity of the Coleman and Lyapunov-Floquet Transformations for Modal Analysis of Bladed Rotor Structures, *Journal of Sound and Vibration*, 327, 424-439.
- [5] Skjoldan, P.F. (2011) Aeroelastic Modal Dynamics of Wind Turbines Including Anisotropic Effects. *PhD Dissertation*. Risø, Technical University of Denmark, Denmark.
- [6] Tcherniak, D., Chauhan, S., Rossetti, M., Font, I., Basurko, J., Salgado, O. (2010) Output-only Modal Analysis on Operating Wind Turbines: Application to Simulated Data. *Proc. of European Wind Energy Conference*, Warsaw, Poland.
- [7] Jhinaoui, A., Mevel, L., Morlier, J. (2014) A new SSI algorithm for LPTV systems: application to a hinged-bladed helicopter. *Mechanical Systems and Signal Processing*, 42(1), 152-166.
- [8] Di Lorenzo, E., Manzato, S., Peeters, B., Marulo F. (2014) Structural health monitoring techniques applied to operating wind turbines, *Proc. of the 9th Int. Conference on Structural Dynamics, (EURODYN 2014)*, Porto, Portugal.
- [9] Yang, S., Tcherniak, D., Allen, M. S. (2014) Modal Analysis of Rotating Wind Turbine using Multi-blade Coordinate Transformation and Harmonic Power Spectrum, *Proc. 32nd Int. Modal Analysis Conference (IMAC XXXII)*, Orlando, FL, USA.
- [10] Requesón, O.R., Tcherniak, D., Larsen, G.C. (2015) Comparative Study of OMA Applied to Experimental and Simulated Data from an Operating Vestas V27 Wind Turbine, *Proc. Int. Operational Modal Analysis Conference (6th IOMAC)*, Gijón, Spain.
- [11] Skjoldan, P.F. (2009) Modal Dynamics of Wind Turbines with Anisotropic Effects. *Proc. of 47th AIAA Aerospace Sciences Meeting*. Orlando, FL, USA.
- [12] Tcherniak, D., Yang, S., Allen, M.S. (2014) Experimental characterization of operating bladed rotor using harmonic power spectra and stochastic subspace identification. *Proc. International Conference on Noise and Vibration Engineering (ISMA)*, Leuven, Belgium.

- [13] Luxemburg, L. A. (1990) Frequency analysis of time-varying periodic linear systems by using modulo p transforms and its applications to the computer-aided analysis of switched networks, *Circuits, Systems, and Signal Processing*, 9, 3-29.
- [14] Yang, S., Allen, M. S. (2014) Lifting to Simplify Output-only Continuous Scan Laser Vibrometry, *Mechanical Systems and Signal Processing*, 45, 267–282.
- [15] Allen, M. S., Sracic, M. W. (2010) A New Method for Processing Impact Excited Continuous-Scan Laser Doppler Vibrometer Measurements, *Mechanical Systems and Signal Processing*, 24, 721–735.
- [16] Mevel, L., Gueguen, I., Tcherniak, D. (2014) LPTV Subspace Analysis of Wind Turbine Data, *Proc. European Workshop on Structural Health Monitoring (EWSHM)*, Nantes, France.
- [17] Wereley, N. M. (1991) Analysis and Control of Linear Periodically Time Varying Systems. *PhD Thesis*, Department of Aeronautics and Astronautics, Massachusetts Institute of Technology, Cambridge.
- [18] Allen, M. S., Sracic, M. W., Chauhan, S., Hansen, M. H. (2011) Output-Only Modal Analysis of Linear Time Periodic Systems with Application to Wind Turbine Simulation Data, *Mechanical Systems and Signal Processing*, 25, 1174-1191.
- [19] Allen, M.S. (2005) Global and Multi-Input-Multi-Output (MIMO) Extensions of the Algorithm of Mode Isolation (AMI), *Doctorate thesis*, George W. Woodruff School of Mechanical Engineering, Georgia Institute of Technology, Atlanta, Georgia.
- [20] Vold, H., Napolitano, K. (2007) Aliasing in modal parameter estimation: An historical look and new innovations. *Proc. of International Modal Analysis Conference (IMAC XXV)*. Orlando, FL, USA.
- [21] Guillaume, P. P., Verboven, P. (2003) A Poly-Reference Implementation of the Least-Squares Complex Frequency-Domain Estimator. *Proc. of International Modal Analysis Conference (IMAC XXI)*, Kissimmee, FL, USA.
- [22] Tcherniak, D., Larsen G.C. (2013) Application of OMA to an Operating Wind Turbine: Now Including Vibration Data from the Blades. *Proc. Int. Operational Modal Analysis Conference (5th IOMAC)*, Guimarães, Spain.
- [23] Tcherniak, D., Chauhan, S., Hansen, M. N. (2010) Applicability Limits of Operational Modal Analysis to Operational Wind Turbines. *Proc. of Int. Modal Analysis Conference (IMAC XXVIII)*, Orlando, FL, USA.
- [24] Jacob, T., Tcherniak, D., Castiglione, R. (2014) Harmonic Removal as a Pre-processing Step for Operational Modal Analysis: Application to Operating Gearbox Data. *Proc. of VDI-Fachtagung Schwingungen von Windenergieanlagen*, Bremen, Germany.
- [25] Tcherniak, D. (2014) Loss of Rotor Isotropy as a Blade Damage Indicator for Wind Turbine Structural Health Monitoring Systems. *Proc. European Workshop on Structural Health Monitoring (EWSHM)*, Nantes, France.



IOMAC'15

6th International Operational Modal Analysis Conference
2015 May 12-14 Gijón - Spain

COMPARATIVE STUDY OF OMA APPLIED TO EXPERIMENTAL AND SIMULATED DATA FROM AN OPERATING VESTAS V27 WIND TURBINE

Oscar Ramírez¹, Dmitri Tcherniak², and Gunner Chr. Larsen³

¹ Research Assistant, DTU Wind Energy, Technical University of Denmark, orre@dtu.dk

² Research Engineer, Brüel & Kjær Sound and Vibration Measurement, dmitri.tcherniak@bksv.com

³ Senior Scientist, DTU Wind Energy, Technical University of Denmark, gula@dtu.dk

ABSTRACT

Today, design of wind turbines is extensively done by the implementation of numerical models. These models simulate the dynamic behaviour of full-scale wind turbines which helps to ensure the structural integrity of prototypes. However, these numerical models need validation from experimental results, and in turn, numerical and analytical modelling help improve and validate new experimental techniques. Wind turbines are complex dynamic systems that consist of mutually moving substructures under high dynamic loads. At a standstill, the system can be modelled as linear time-invariant (LTI), and modal analysis requirements are thus fulfilled for the dynamic characterization. Under operation, the system cannot be considered as LTI and must be modelled as a linear periodic time-variant (LPTV) system, which allows for the application of the related theory for such systems. One of these methods is the Coleman transformation, which transforms the vibrations expressed in the blade rotating coordinates to the fixed-ground frame of reference. The application of this transformation, originally from helicopter theory, allows for the conversion of a LPTV system to a LTI system under certain assumptions, among which is the assumption of isotropic rotors. Since rotors are never completely isotropic in real life, this paper presents the application of operational modal analysis together with the Coleman transformation on both experimental data from a full-scale Vestas wind turbine with instrumented blades and nacelle, and its representative numerical model with a fully isotropic rotor. The results show that the first tower and rotor edgewise modes are well identified, and that the rotor edgewise modes can be identified from the nacelle signals. The results also uncover the challenge the excitation forces imply for the identification of flapwise modes.

Keywords: wind turbines, structural dynamics, operational modal analysis, modal parameters, system identification, anisotropic rotors

1. INTRODUCTION

Cost of Energy (CoE) reduction is the main driver for the increase of wind turbine size. As the size grows, higher dynamic loads and response magnitudes may occur, which can decrease the lifetime of the wind turbine. Therefore, designers are required to understand wind turbine dynamics to succeed in obtaining a better balance between materials, performance and cost. The dynamic characterization is generally done in terms of modal parameters - modal frequencies, damping and mode shapes - where a proper estimation is essential, for instance, to avoid inconvenient cases such as coupling of modal frequencies with multiples of the rotational speed, or to predict the fatigue loads from which the structure suffers. This paper presents the findings obtained in [1], where the identification of modal parameters was performed on measurements from a full-scale Vestas V27 (hereafter, V27) wind turbine. Despite the fact that the V27 is an old wind turbine, its design is similar to modern wind turbines, as it features pitch- and yaw-control. The focus is on the frequency range 0-5 Hz, which includes the lowest global modes.

1.1. OMA on Wind Turbines

Wind turbines are huge structures, subjected to stochastic loading distributed over a substantial part of the structure, and therefore, Operational Modal Analysis (OMA) techniques sparked the interest of industry and academia because of the advantages of identifying modal properties based on response-only while operating. However, an operating wind turbine may violate some OMA assumptions, and some approximations must be made to apply OMA with a certain level of confidence. From the different algorithms OMA embraces, the Stochastic Subspace Identification (SSI) technique, described by Overschee and De Moor [2], seems the most applicable based on the success of previous research studies. In the present work, a commercial software package from Brüel & Kjær is used in which this method is already implemented.

1.2. State of the Art

The theoretical basis of this work was mainly laid by Hansen [3, 4], whose work describes the Coleman transformation and its main assumptions in depth; Bir [5], who developed a new Coleman transformation scheme, extending its applicability limit; and Skjoldan [6], who compared the Floquet and Hill methods for anisotropic rotors with the Coleman transformation for isotropic rotors. Recently, Mevel et al. developed a new subspace algorithm for the modal analysis of rotating systems and applied it to helicopter rotors [7]. Yang et al. [8] applied another method based on the extension of modal analysis to LPTV systems, the harmonic power spectrum (HPS), and made a comparison with the Coleman transformation followed by SSI using the blade accelerations of an operating Vestas V27. The latter concluded the Coleman transformation could lead to erroneous results due to rotor anisotropy.

To the authors' knowledge, there are only few research studies involving modal analysis of operating wind turbines. Tcherniak and Larsen [9] presented a full-scale study including blade instrumentation and data acquisition, the processing of data to convert the system to LTI and assessed preliminary results using parked, idling and normal operation cases of a Vestas V27. Di Lorenzo et al. [10] also used the Coleman transformation for modal identification of a Micon 65/13M. Further, Hansen et al. [11] estimated the aeroelastic damping of a NM80 2.75 MW operating prototype using strain gauges. They concluded that the SSI method can handle deterministic excitation from wind, and the first tower and rotor edgewise whirling modes could be identified. Tcherniak et al. applied SSI to an operating ECO 100 Alstom using accelerometers on the nacelle and tower, identified some rotor modes using only these signals, and produced experimental Campbell diagrams based on 4 months of measurements [12]. Van Der Valk and Ognó [13] identified the first four global eigenfrequencies in an idling Siemens offshore SWT-3.6 MW turbine using several strain gauges and one accelerometer, with the best results coming from the accelerometer.

1.3. Motivation

The main motivation of this work was to investigate how reliable the application of the Coleman transformation [14] is when comparing anisotropic and isotropic rotors. Other ideas to explore were: if modes could be identified using only the nacelle sensors and if flapwise modes could be identified successfully, since there is a lack of research regarding these modes. This research was performed on experimental data, as well as on its equivalent numerical model, implemented in the nonlinear aeroelastic code HAWC2. Both identification results were assessed against theoretical predictions from the linear aeroelastic stability tool HAWCstab2.

2. WIND TURBINE MODAL DYNAMICS

The dynamics of wind turbines are composed of three main substructures: tower, drivetrain and rotor. The tower deflects longitudinally and laterally with respect to the wind direction, where these two bending modes interact due to the gyroscopic coupling of the tower top and rotor. Also, the tower torsion couples to the yaw motion of the nacelle and rotor. The drivetrain facilitates the blades to rotate around its axis: taking one blade as reference, the azimuth angle is the angular position of that blade. The drivetrain consists of a main shaft, a gearbox and a generator, and introduces a torsional mode between the rotor hub and generator coupled with the blade's simultaneous edgewise bending (or flapwise bending, depending on the pitch angle). A single blade cantilevered at the hub has three mode families: flapwise, edgewise and torsion. It is difficult to find pure representatives of these families because the modes are typically a mixture of them.

2.1. Rotor Dynamics

The term rotor is understood as the assembly of blades attached to a hub. For each mode of a single blade, one can find three modes of the rotor: one symmetric - all blades deflect symmetrically - and two asymmetric - two blades deflect contrary to the remaining blade, as illustrated in Figure 1.



Figure 1: Components of the first flapwise mode

When the rotor starts rotating, the natural frequencies of the rotor modes change. The centrifugal stiffening can only partly explain this phenomenon. The qualitative change from LTI (when the rotor is not rotating) to LPTV system (when rotating) is the main reason of the major changes in dynamics. The modes of the LPTV system consist of components (known from the Floquet analysis as the Fourier components); the frequencies of these components are separated by the multiples of the rotational frequency Ω . This explains the separation of the backward (BW) and forward (FW) whirling components of the modes, which is typically illustrated by the Campbell diagram (e.g. Figure 2). Further details about the rotor dynamics are described in [3].

2.2. The Coleman Transformation

At a standstill, the system can be considered as LTI and all OMA assumptions are fulfilled. But when the wind turbine is under operation, the system is not LTI any more, and traditional modal analysis cannot be directly applied. The Coleman transformation, also known as multiblade coordinate transformation (MBC), converts the rotating blade coordinates to the non-rotating frame, transforming the system from LPTV to LTI. For a 3-bladed rotor, with the blades equally spaced, MBC is defined as

$$a_0 = \frac{1}{3} \sum_{k=1}^3 q_k \quad a_1 = \frac{2}{3} \sum_{k=1}^3 q_k \cos \psi_k \quad b_1 = \frac{2}{3} \sum_{k=1}^3 q_k \sin \psi_k \quad (1)$$

where $\psi_k = \Omega t + \frac{2\pi}{3}(k-1)$ is the azimuth angle of blade $k = 1, 2, 3$. The three multiblade coordinates a_0 , a_1 and b_1 replace the blade coordinates q_1 , q_2 and q_3 , measuring the same degree of freedom (DOF) on blade k , respectively. The inverse transformation back to the blade coordinates is

$$q_k = a_0 + a_1 \cos \psi_k + b_1 \sin \psi_k \quad (2)$$

The transformed blade coordinates in the non-rotating frame can be categorized in one symmetric a_0 (collective) and two asymmetric components a_1 and b_1 . For instance, if one assumes a flapwise deflection (aligned with the wind direction) of the blade coordinates q_k , a_0 will describe all blades deflecting symmetrically, while a_1 and b_1 will describe the FW and BW whirling motions, respectively (cf. Figure 1). This transformation results in a linear eigenvalue problem for which a solution defines a mode of the wind turbine. The mathematical derivation is detailed in [3].

3. EXPERIMENTAL DATA

The complete description of the conducted measurement setup to collect the experimental data can be found in [9], including details regarding equipment and challenges involving the instrumentation of the turbine. For the sake of simplicity, the information here just relates to the signals involved in the analysis.

3.1. Selection of Signals

Though each blade was instrumented with 12 accelerometers (10 in the flap- and 2 in the edgewise direction) only 4 signals per blade were selected for the present analysis. The corresponding sensors were located at 96% and 67% of the blade span, respectively. The reasoning behind this choice was firstly that these sensors are assumed sufficient to represent with confidence the lowest modes in the 0-5 Hz range and secondly to reduce the risk of misalignment by using sensors forming a 90° angle between them. The nacelle was instrumented with triaxial accelerometers targeted to identify not only the tower modes, but also the rotor modes, as Tcherniak et al. showed in [12].

3.2. Selection of Data Sets

A wind turbine may be modelled as an LPTV system, if the fluctuation of variables such as rotor speed, blade pitch and nacelle yaw is minimal. For this reason, the data set selection was based on a low standard deviation of these parameters. OMA requires a long time series for better performance of the algorithm, and here 20 minutes were believed to represent a good trade-off between computational time and the OMA data amount requirement. In addition, the V27 control system can only run the turbine at low and

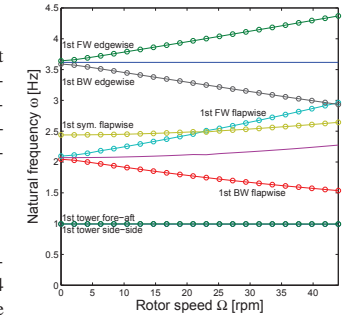


Figure 2: Campbell diagram for the V27

high rotor speed (Ω_{low} , Ω_{high}), approximately at 33 rpm and 43 rpm. Providing these considerations, two data sets are selected for detailed analysis. The wind excitation in the HAWC2 model was based on meteorological data from the selected time spans. Table 1 shows details from the selected data sets, including the relevant standard deviations on which their selection was based, and descriptive mean variables. The latter are compared to those obtained from the HAWC2 simulations in Table 2, and to the operational data used in HAWCStab2 in Table 3. It can be noticed that the HAWCStab2 operational data does not match perfectly for neither the high rotor speeds - leading to issues in the identification of modal frequencies - nor the mean pitch angle - leading to issues in the extracted damping ratios.

Parameter	Ω_{low}	Ω_{high}
Date	16/12/12	15/12/12
Time	11:10-11:30	05:10-05:30
Std. Dev. tacho	0.54 rpm	1.28 rpm
Std. Dev. pitch	0.09°	0.59°
Std. Dev. yaw	0.17°	0.02°
Std. Dev. wind speed	0.56 m/s	1.37 m/s
Max./min. power	0/0 kW	265/56.3 kW
Mean rotor speed	32.20 rpm	43.10 rpm
Mean wind speed	5 m/s	11 m/s
Mean pitch angle	0°	0.67°

Table 1: Details of data sets

Parameter	Ω_{low}	Ω_{high}
Mean rotor speed	32.24 rpm	43.22 rpm
Mean wind speed	5 m/s	11 m/s
Mean pitch angle	0°	0.74°

Table 2: HAWC2 modelling details

Parameter	Ω_{low}	Ω_{high}
Mean rotor speed	32.14 rpm	35.02 rpm
Mean wind speed	5 m/s	11 m/s
Mean pitch angle	0.41°	1.57°

Table 3: HAWCStab2 modelling details

4. SIMULATION VS. EXPERIMENT

The dynamic behaviour of the V27 was simulated using the aeroelastic code HAWC2 [15], intended for calculating wind turbine response in the time domain. HAWC2 can provide output channels to simulate the biaxial blade and triaxial nacelle acceleration sensors on the V27. The theoretical modal analysis is performed in HAWCStab2 [16], which predicts structural and aeroelastic modal frequencies, damping ratios and mode shapes, through open- and closed-loop aero-servo-elastic eigenvalue and frequency-domain analysis. Although the structural part of the two codes use the same beam element (Timoshenko), the kinematics of the codes are different. HAWC2 is based on a multi-body formulation, while HAWCStab2 is based on a co-rotational formulation. Figure 3 shows the predicted structural and aeroelastic modal frequencies and damping ratios during the entire operational range, from which results at 5 m/s and 11 m/s wind speed, respectively, corresponding to the selected data sets, were analysed for comparison.

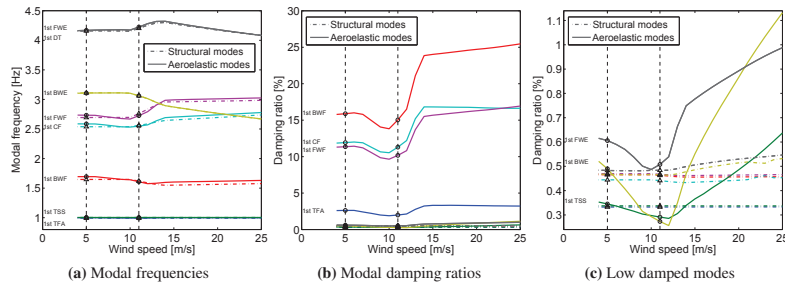


Figure 3: Predicted frequencies and damping ratios at Ω_{low} and Ω_{high} (5 m/s and 11 m/s)

Figure 4 shows the Power Spectral Density (PSD) from the nacelle and blade signals used to validate

the simulations against the experiment. A fairly good agreement is observed in Figure 4 (b,c), where besides the rotor harmonics, a peak is present between 6P and 7P. This could refer to an edgewise mode based on the previous theoretical predictions. However, the experimental data features a double-peak phenomenon that is inconsistent with the isotropic case and might refer to the effect of rotor anisotropy.

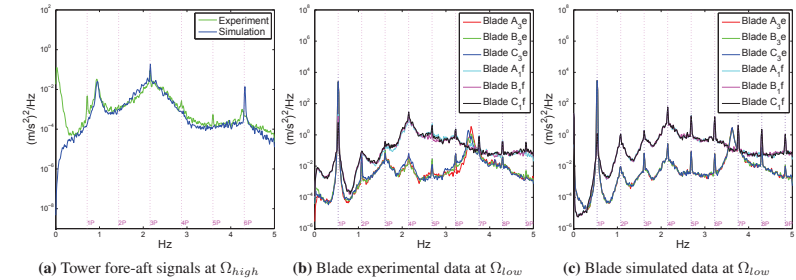


Figure 4: PSD of nacelle and outer section blades signals. Subscripts 1 and 3 denote flapwise and edgewise

5. SIGNAL ANALYSIS

Prior to the application of OMA, a natural step is to apply signal analysis, since this is not based on any assumptions and thus not prone to violate OMA assumptions. A singular value decomposition (SVD) is performed on the blade signals to get more information about the peak between 6P and 7P, according to Figure 5 (a,b).

Apparently, two singular vectors are required to describe that peak, and therefore, very likely unveil two modes at this frequency rather than one. Figure 5 (c,d) illustrates the application of the MBC to the blade signals, which gives indeed two peaks separated by 2Ω , thus suggesting the edgewise whirling components. The characteristic double peak in the experimental data is still present, but also the 3P and multiple harmonics are not removed in the isotropic case. This is contrary to the experimental data, where the rotor is anisotropic. The flapwise analysis does not give any useful information - reinforcing the statement formulated in [17], where the operational forces (aerodynamic loads) pose a challenge, resulting in non-flat spectra at lower frequencies interfered by the rotor harmonics.

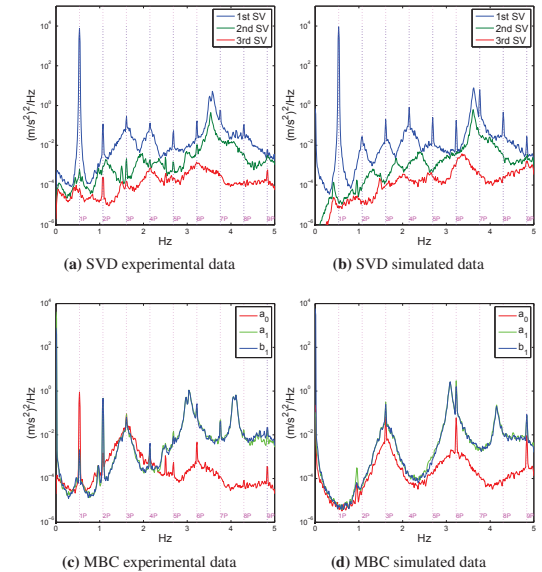


Figure 5: SVD and MBC applied on edgewise signals at Ω_{low}

6. MODAL IDENTIFICATION

The modal identification was performed on the experimental and simulated data using OMA software Type 7760 from Brüel & Kjær. The signals were first decimated to cover the frequency range of interest, 0-5 Hz. From the 4 selected signals per blade, only those 2 at the outer section were enabled as projected channels, since they provide more relevant information. The SSI unweighted principal component (UPC) technique was then performed on the data to identify the global tower and rotor modes (edge- and flapwise). The modal parameter identification was limited to a 1.5% damping ratio for in-plane modes (tower side-side, rotor edgewise) and to 20% for out-of-plane modes (tower fore-aft, rotor flapwise), according to the HAWCStab2 results (cf. Figure 3). Hence, all modes identified with damping ratios above these thresholds are ignored. The identification was supported with animations of the modes. These animations were, in the case of tower modes, a visual representation of the entire wind turbine, whereas in the case of the rotor modes they referred to the animation of the symmetric a_0 and asymmetric components, a_1 and b_1 . A collective component denotes the excited symmetric component, and an asymmetric component has two excited asymmetric components, where the phase difference indicates if it is a BW or FW component.

With the mentioned setup, the tower modes were well identified for both experimental and numerical HAWC2 cases, displaying a fine agreement among them, as can be seen in Figure 6 (a,b). The edgewise components were also identified successfully, using only the nacelle sensors. This agrees with [12], where the flapwise components could not be identified from the nacelle signals, and it was mentioned that their identification is more challenging, requiring the blades to be fitted with instruments. Actually, the flapwise components seemed to be identified around 3P, according to Figure 6 (a,b), but they could not be traced in either the PSD or the SVD analyses.

In parallel, Figure 7 shows the identified edgewise modes from the blade signals. This not only confirms the identification based on the nacelle signals, but also makes the identification much more straightforward, as compared to using nacelle sensors only.

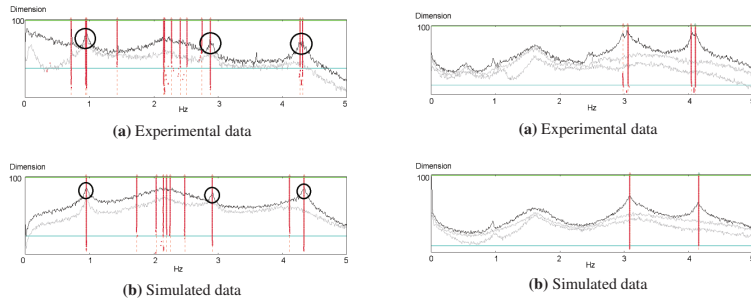


Figure 6: Tower modes at Ω_{high}

6.1. Induced Rotor Anisotropy in Simulated Data

In the edgewise components, one can notice a double-peak phenomenon that might be associated with rotor anisotropy (dissimilarities in blades or difference among sensor positions/orientations). From the blade signals, Figure 7 shows that the two peaks at each component requires the algorithm to identify double modes instead of a single one. To confirm the rotor anisotropy hypothesis, a test case was implemented in the numerical model, where the stiffness of one blade was different from the other two. The results are shown in Figure 8, where the double peak is found in a similar manner as in the experimental data. Apparently, the more different the blades are, the larger the frequency difference between the two

peaks.

6.2. Identification of Flapwise Components

In contrast, the identification of flapwise components required special treatment. First, both the experimental and numerical data were analysed following the same procedure as for the edgewise modes. However, no peaks were clearly visible. Next, a band-pass filter was applied between 1.4 and 3 Hz to improve the flapwise identification results without notable success. Therefore, as an attempt to understand what makes the identification of flapwise modes so difficult, a new strategy was attempted. An artificial impulse excitation in the numerical model was introduced that was expected to better meet OMA assumptions with respect to the operational forces. The drawback of this strategy is that the excitation is not ambient any more, and that the best identification results for the flapwise components in the experimental data are linked to the aforementioned band-pass filtering. This new approach was implemented in three different versions: impulse-only excitation; wind (no turbulence) added to the impulse excitation; and wind and turbulence added to the impulse excitation. Figure 9 illustrates the three different cases tested and highlights the three flapwise components identified independently of the excitation case. It can be observed in Figure 9 (a) that the flapwise mode components are clearly visible with only the impulse excitation acting as operational forces. When the wind is introduced in Figure 9 (b), the emerging excited peaks are overlapped which complicates the identification. Despite this, the algorithm was still capable of identifying all the components.

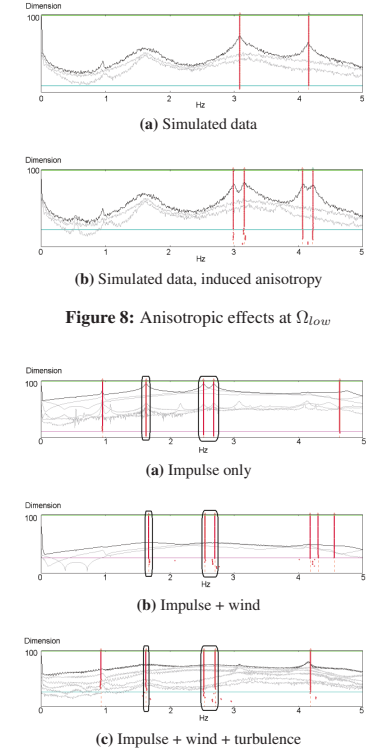


Figure 9: Flapwise components at Ω_{low}

	Frequencies [Hz]			Damping [%]			
	Mode (1st)	Experiment	Simulation	HAWCStab2	Experiment	Simulation	HAWCStab2
Ω_{low}	Tower fore-aft	0.95	0.95	0.99	1.90	2.15	2.62
	Tower side-side	0.96	0.96	1.00	1.35	1.68	0.35
	BW flapwise	1.84	1.63	1.69	10.15	11.34	15.88
	Sym. flapwise	2.63	2.54	2.59	7.00	11.05	11.92
	FW flapwise	2.79	2.71	2.73	9.30	10.91	11.36
	BW edgewise	3.04*/3.05	3.09*/3.09	3.11	1.2*/1.12	0.84*/0.61	0.49
FW edgewise	4.11*/4.11	4.16*/4.14	4.17	1.17*/0.62	0.75*/0.91	0.61	
Ω_{high}	Tower fore-aft	0.94	0.95	0.99	2.51	2.11	1.99
	Tower side-side	0.95	0.95	1.00	1.23	1.05	0.29
	BW flapwise	1.70	1.69	1.61	19.24	18.84	15.03
	Sym. flapwise	-	-	2.55	-	-	11.31
	FW flapwise	-	-	2.72	-	-	10.18
	BW edgewise	2.88*/2.87	2.91*/2.91	3.06	0.42*/0.35	0.59*/0.62	0.27
FW edgewise	4.31*/4.33	4.34*/4.34	4.23	0.69*/0.70	0.45*/0.50	0.51	

Table 4: Modal parameters comparison (*identification from nacelle sensors only)

However, an even higher impulse excitation was needed to properly identify these modes when adding the turbulence in Figure 9 (c), thus pinning down the turbulence as the major hurdle. This unexpectedly hinders the identification proportionally to the turbulence intensity, though the broad banded stochastic nature of turbulence is considered as a perfect excitation for OMA. Table 4 shows that, overall, the experimental and simulated results match well. It also displays discrepancies due to the flapwise problem mentioned above, as well as deviations in tower and edgewise modal parameters attributed to the HAWCStab2 model structural properties.

7. CONCLUSIONS

The paper presents modal identification of the lowest tower and rotor modes (except the torsional modes) of an operating V27 turbine. It was demonstrated that it is possible to extract modal parameters from experimental data by applying the MBC in conjunction with OMA SSL. The tower and rotor edgewise modes could even be extracted from the nacelle signals. However, a double peak phenomenon in the experimental data, caused by rotor anisotropy, complicated the identification of the edgewise mode components. The problem was circumvented using both the nacelle and blade signals. Using band-pass filtering, the flapwise components were also identified but with higher uncertainty. The reason of this high uncertainty is associated with the turbulence loading, resulting from a three-step numerically-based input parameter study.

ACKNOWLEDGEMENTS

EUDP (Danish Energy Technology Development and Demonstration Programme) is gratefully acknowledged for embracing the measurement campaign conducted between October 2012 and May 2013, under the project, "Predictive Structure Health monitoring of Wind Turbines", with grant number 64011-0084.

REFERENCES

- [1] Ramírez, O. (2014) Identification of Modal Parameters Applying Operational Modal Analysis on a Full Scale Operating Vestas V27 Wind Turbine. *Master's thesis*, Technical University of Denmark.
- [2] Van Overschee, P. and De Moor, B. (1996) *Subspace identification for linear systems: theory, implementation, applications*. Kluwer Academic Publishers.
- [3] Hansen, M. H (2007) Aeroelastic instability problems for wind turbines. *Wind Energy* Vol. 10, p. 551-577.
- [4] Hansen, M. H (2003) Improved modal dynamics of wind turbines to avoid stall-induced vibrations. *Wind Energy* Vol. 6, p. 179-195.
- [5] Bir, G. (2008) Multiblade coordinate transformation and its application to wind turbine analysis. *ASME Wind Energy Symposium*, Reno, Nevada.
- [6] Skjoldan, P. F. (2008) Modal Dynamics of Wind Turbines with Anisotropic Rotors. *Proceedings of 47th AIAA Aerospace Sciences Meeting*.
- [7] Mevel, L. and Gueguen, I. and Tcherniak, D. (2014) LPTV Subspace Analysis of Wind Turbines Data. *EWSHM - 7th European Workshop on Structural Health Monitoring*.
- [8] Yang S. and Tcherniak D. and Allen M. S. (2014) Modal Analysis of Rotating Wind Turbine Using Multiblade Coordinate Transformation and Harmonic Power Spectrum. *Topics in Modal Analysis I*, Vol. 7, p. 77-92, A Conference and Exposition on Structural Dynamics (Proceedings of the 32nd IMAC).
- [9] Tcherniak, D. and Larsen, G. C. (2013) Application of OMA to an Operating Wind Turbine: now including Vibration Data from the Blades. *Proceedings - 5th International Operational Modal Analysis Conference (IOMAC'13)*.
- [10] Di Lorenzo, E. and Manzato, S. and Peeters, B. and Marulo, F. (2014) Structural health monitoring techniques applied to operating wind turbines. *Proceedings of the 9th International Conference on Structural Dynamics*, EUROSDYN 2014.
- [11] Hansen, M. H. and Thomsen, K. and Fuglsang, P. and Knudsen, T. (2006) Two Methods for Estimating Aeroelastic Damping of Operational Wind Turbine Modes from Experiments. *Wind Energy*, Vol. 9, p. 179-191
- [12] Tcherniak, D. and Chauhan, S. and Basurko, J. and Salgado, O. and Carcangiu, C. E. and Rossetti, M. (2011) Application of OMA to Operational Wind Turbine. *Proceedings - 4th International Operational Modal Analysis Conference (IOMAC'11)*.
- [13] Van Der Valk P. L. C. and Ogno M. G. L. (2014) Identifying Structural Parameters of an Idling Offshore Wind Turbine Using Operational Modal Analysis. *Dynamics of Civil Structures*, Vol. 4, p. 271-281, A Conference and Exposition on Structural Dynamics, (Proceedings of the 32nd IMAC).
- [14] Coleman, R. P. and Feingold, A. M (1957) Theory of self-excited mechanical oscillations of helicopter rotors with hinged blades. *NACA Report 1351*, Langley Aeronautical Laboratory.
- [15] Larsen, T. J. and Hansen, A. M. -(2013) How 2 HAWC2, the user's manual. *Ris-R-1597 (ver. 4-4)(EN)*, Technical University of Denmark.
- [16] Hansen, M. H (2004) Aeroelastic stability analysis of wind turbines using an eigenvalue approach. *Wind Energy* Vol. 7, p. 133-143.
- [17] Tcherniak, D. and Chauhan, S. and Hansen, M. H. (2011) Applicability Limits of Operational Modal Analysis to Operational Wind Turbines. *Structural Dynamics and Renewable Energy*, Vol. 1, Society for Experimental Mechanics, p. 317-327 (Conference Proceedings of the Society for Experimental Mechanics Series; No. 10).

CrossMark
click for updates

Research

Cite this article: McGugan M, Pereira G, Sørensen BF, Toftegaard H, Branner K. 2015 Damage tolerance and structural monitoring for wind turbine blades. *Phil. Trans. R. Soc. A* **373**: 20140077.
<http://dx.doi.org/10.1098/rsta.2014.0077>

One contribution of 17 to a theme issue 'New perspectives in offshore wind energy'.

Subject Areas:

energy, materials science, structural engineering

Keywords:

damage tolerance, smart structure, offshore wind

Author for correspondence:

M. McGugan
e-mail: mamc@dtu.dk

Damage tolerance and
structural monitoring for
wind turbine blades

M. McGugan, G. Pereira, B. F. Sørensen, H. Toftegaard
and K. Branner

Technical University of Denmark, Frederiksborgvej 399,
4000 Roskilde, Denmark

BFS, 0000-0002-6435-6482

The paper proposes a methodology for reliable design and maintenance of wind turbine rotor blades using a condition monitoring approach and a damage tolerance index coupling the material and structure. By improving the understanding of material properties that control damage propagation it will be possible to combine damage tolerant structural design, monitoring systems, inspection techniques and modelling to manage the life cycle of the structures. This will allow an efficient operation of the wind turbine in terms of load alleviation, limited maintenance and repair leading to a more effective exploitation of offshore wind.

1. Introduction

(a) Offshore wind energy

The potential for offshore energy production in Europe is enormous. Industry projection from the European Wind Energy Association (EWEA, www.ewea.org) is for an increase from 5 GW in 2012 to 150 GW in 2030, and achieving that potential is an important objective of the European Communities. In 2008, the executive body of the European Union issued a communication detailing the Roadmap for Maritime Spatial Planning [1]. This roadmap was intended to balance the requirements of various sectorial interests using marine resources, and offshore energy (particularly wind) was anticipated to make very significant increases in the near to medium term.

However, in order to support this growth it is vital to make significant reductions in the cost of energy (CoE) of offshore wind, as was discussed at the most

important wind energy conference EWEA 2014 [2]. A radically different approach is needed to design and operate offshore wind turbines. This is what we propose in this paper.

The most eye-catching trend for wind energy structural components is the up-scaling history where new turbine designs have consistently provided larger turbines with higher power ratings. The most cost-effective way of increasing the power produced (PP) by a wind turbine is to increase the rotor diameter [3], currently prototype rotor blades exceed 70 m in length (SSP-technology: 7 MW-83.5 m. blade project, <http://tinyurl.com/ngutwhn>). The industry relies on advances in materials technology to deliver cost-effective light-weight structures.

Although larger turbines cost more to manufacture per unit (cost of turbine, CoT), this small relative increase is more than compensated for by the absolute saving possible when factoring cost of installation (CoI) and the cost of maintenance (CoM) with larger turbine units. These costs are factored against the PP:

$$\text{CoE} = \frac{(\text{CoT} + \text{CoI} + \text{CoM})}{\text{PP}} \quad (1.1)$$

The manual inspection of wind turbines (inconveniently placed on high towers in remote places) involves a certain amount of travel time as equipment and personnel are moved between them; higher MW turbines help to reduce this cost relative to the power output of the wind farm. However, economies of up-scaling for the operation of an offshore, multi-MW wind farm can be challenged as the consequence of a single turbine downtime is more significant, and all personnel operation offshore is more expensive. Therefore, cost reduction by using remote monitoring becomes increasingly attractive as a means to suppress unexpected downtime, and focus limited maintenance and repair operations.

(b) Multi-physics global model

Some research groups are working on a multi-physics global model [4–8], as represented by the scheme in figure 1. A multi-physics global model is defined as a fluid-structural interaction model that aims to capture and integrate several phenomena: meteorology, aerodynamics, hydrodynamics, aero-elasticity, structural vibration, energy output, control, etc. (For example, the integrated response of the tower pillar to the aerodynamic load on the blades and waves on the foundations.) However, this approach will not be achieved until all physical phenomena are sufficiently well understood. Wind turbines are a multi-physics problem, and the complexity of the structure and loading, and the variability and turbulence of the wind create challenges for the application of such a method. At this time, significant research effort is being made in order to fully research the most complex phenomena at each of the scales presented in figure 1. Obviously, it is not possible to predict the aerodynamical load history on a wind turbine rotor blade in detail for a 20-year period of time. There are two approaches to address this. One is to make lifetime predictions based on statistics. Another approach, as will be pursued here, involves the use of sensors to detect the conditions of the blades to obtain an updated lifetime prediction.

(c) Wind turbine rotor blade structures

A wind turbine rotor blade structure is defined in terms of its outer geometry and inner structural layout. It can be made from different materials and will be subjected to varying loads from wind and varying direction of gravity due to the rotation of the rotor. A typical turbine blade design is based on a load-carrying laminate in a rectangular hollow beam (spar). In another common blade design, there is no spar; instead there is a combination of a load-carrying laminate incorporated in the aero shell together with two shear webs [9]. The beam spar and the sandwich face sheets of the aero shell are made from fibre reinforced polymer composite materials (figure 2); the sandwich cores are made from polymeric foam or balsa wood and the blade is assembled with adhesives between the aero shells at the leading edge, between the spar and the aero shell and between the aero shells at the trailing edge.

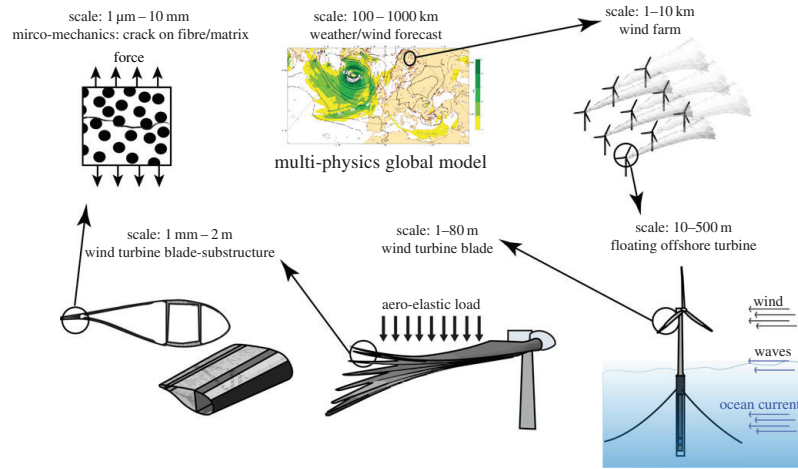


Figure 1. Multi-physics global model scheme. (Online version in colour.)

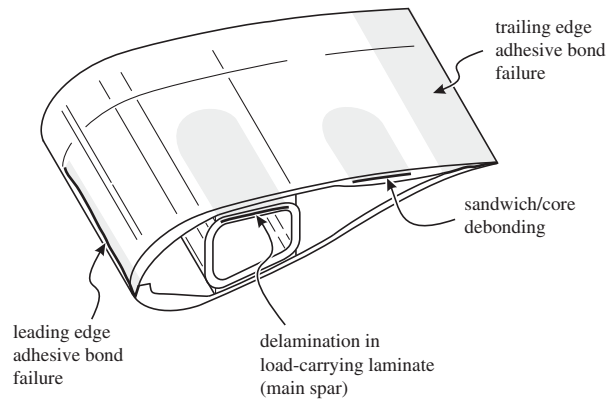


Figure 2. Schematics of major failure modes in a part of a wind turbine rotor blade. The shaded areas indicate cracked internal regions.

At the structural scale, a wind turbine rotor blade can develop various types of damage, such as cracks along adhesive joints (e.g. leading and trailing edges as well as internal bondlines at beam/laminate assemblies). Laminates can fail by cracks parallel to the fibre direction (e.g. splitting cracks and transverse cracks), fibre failure in tension (distributed damage) or compression (localized damage) and by delamination (cracking along the plane between plies). Of these, delamination of laminates and adhesive bonded joints are usually the most critical [9,10].

(d) Fibre reinforced polymer composite materials

Fibre reinforced polymer composite materials consist of two macroscopic phases, a stiff fibre phase (usually glass or carbon) and a polymer matrix (usually polyester or epoxy). One of the

advantages of fibre reinforced polymer composites is that the alignment of the fibres can be arranged to suit the required properties of the intended structure. Thus, the requirement for a stiff (but lightweight) structure means fibre orientations primarily along the length of the blade and an inherently anisotropic set of material characteristics. A key feature of structures designed using composite material is that the manufacturing process itself will determine certain characteristics of the material, and hence the behaviour of the final structure. All this is to say that when looking to optimize the properties of a wind turbine blade, it is necessary to consider material choice, design approach and the manufacturing process as an integrated issue.

For example, a common processing procedure is to stack layers of the dry reinforcement fibres before infusing with a thermosetting resin to create the finished composite material. This results in a laminated structure with significant stiffening mainly along the length direction of the blade. But the effect on out-of-plane properties and the weak interfaces between layers of the composite material needs to be understood at the material level, if the final structure is to be sound and resistant to any out-of-plane loading.

(e) Structural design philosophies

The design philosophy for fibre reinforced polymer structures was initially based on conservative analysis methods with large safety factors, underestimating the actual material properties and considering primarily the linear elastic material behaviour. As knowledge about materials and structures increased, it has now become possible to safely adopt more advanced design philosophies. This general trend to more advanced structural design is described elsewhere [11]. In wind turbine blade design, it is important to take into account different nonlinear effects as described in [12]. Failure of a wind turbine blade has small to minor consequence as the risk for human lives is small, especially offshore since persons are not close to the wind turbines. The optimal target reliability level can therefore be determined by cost-benefit analysis, where all the cost during the wind turbines design life is taken into account [13]. Partial safety factors can be calibrated to obtain the desired target reliability level for the structure [14]. And the uncertainties for the material properties for composite materials can be modelled [15]. Probabilistic design methods give a prediction for the risk of failure in average, but give, in principle, no information for the condition and risk of failure for a particular blade. However, this information is available within a structural design philosophy based on damage monitoring.

The approach is to use damage tolerant materials and a structural health and prognostic management system as part of a *condition-based maintenance* programme. It is an axiom of structural health monitoring (SHM) [16] that detectable changes in response must occur between undamaged and damaged states, thus implying damage tolerance. Damage tolerance (see §3b for details) is a property emerging from the particular combination of structure design, loading environment and material characteristics. Accepting that a distribution of damage types and locations can exist within the blades of an operating offshore wind farm, it follows that each wind turbine blade structure must be characterized individually with a unique 'damage map' for that structure. Evaluating the severity of the particular combination of damage types requires models that describe the progression parameters for each type under the full range of operating conditions. Only in this way can condition-based maintenance be effectively implemented.

2. Vision

Our vision consists of a damage tolerance approach that can be made using conditional inspections and models that describe progression for all known failure types [17,18]. The future design philosophy will be based on an SHM approach where sensors integrated during manufacture provide feedback that is used to optimize the entire life cycle. And this again requires an advance in materials knowledge to implement effectively.

The already established concept of composite materials structural design based on an integrated material/structure/manufacturing iteration should be extended to include

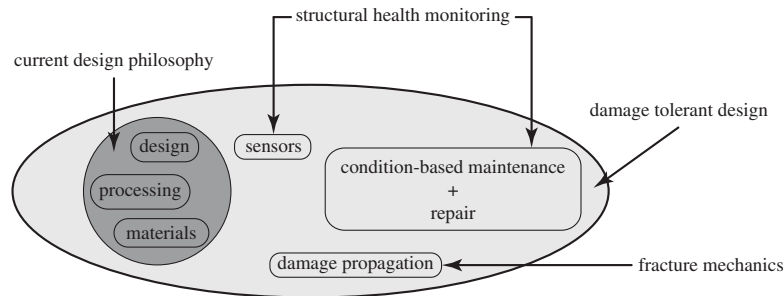


Figure 3. Expanded design and manufacturing process including SHM.

an application of the deeper material level (microscopic level) understanding of damage propagation. So in much the same way as structural load and stiffness requirements are already 'tailored' at the material level, optimization of the material properties can be used to match design objectives related to damage tolerance and reliability for the final structure. All this needs to be achieved in a framework of condition-based maintenance, remote monitoring and prognosis, as presented in figure 3.

It is important to appreciate that in comparison with aerospace structures, wind turbine rotor blades are unique in the sense that they are made of very large parts, using relative 'low-cost' composite materials and manufacturing methods. Requiring very strict quality control and allowing only parts with small manufacturing defect size may lead to a high rate of discarded blade parts. Obviously, this would lead to a higher blade price. An alternative approach, proposed here, is to allow more blades with manufacturing defects to be used in service by ensuring that the defects lead to stable damage, i.e. avoiding unstable blade failure.

For a given wind turbine design, the damage evolution will depend on structural details and materials properties that cannot be accurately controlled during manufacturing. Furthermore, each blade on a wind turbine in an offshore wind farm will experience its own, unique combination of load history. Consequently, blades will not undergo identical damage evolution. One blade may undergo a loading history that leads to more damage in one area, while another blade, having a different set of manufacturing defects and experiencing another load history, may develop damage in other areas of the blade.

The key features in the proposed condition-based maintenance approach can be summarized as follows. First, in the design phase, the designer will choose materials and structural layout that give a high damage tolerance. The designer also will decide on the type of sensors for damage detection and determines (from structural analysis) which areas are the most critical and where the sensor should be placed.

Next, in the manufacturing phase, sensors will be placed inside the rotor blade, either as sensors embedded in laminates and/or adhesive bond lines or mounted inside the blade after manufacturing. Sensor surveillance can cover transportation, installation and in-service operation, and be part of the post-manufacturing control by contributing to non-destructive inspection (NDI) procedures.

For the few blades that will develop serious damage, sensor alarms will be sent from the offshore wind turbine to the on-shore surveillance centre, which can then send out a maintenance team to inspect the blade at the position where the damage is detected. The team will use non-destructive techniques such as ultrasound scanning, radiography (X-ray), etc., to identify the damage type, its size and depth. This information will be used in detailed structural models (e.g. finite-element models) of the blade with the characterized damage to assess the residual fatigue life and residual strength, using information about fracture data (stress-strain, traction-separation, fatigue data) of the materials and the anticipated future load history. It will

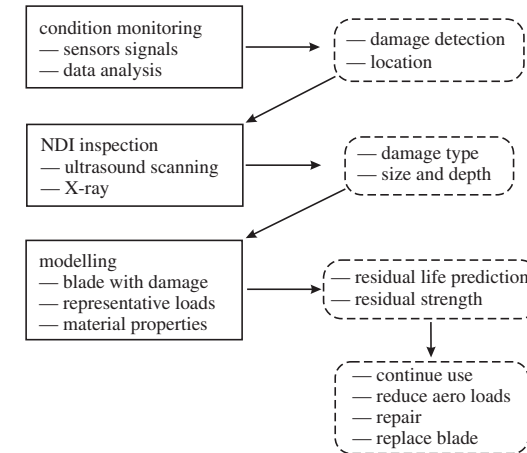


Figure 4. Condition monitoring modelling approach.

then be possible to assess the criticality of the damage and decide whether the blade can be used under normal operation, or whether the aero-loads should be reduced, or the blade repaired on site, or taken down (replaced with a new blade or repaired on shore).

Such an approach will allow the service life of blades to be decided by their damage state. There is thus potential for life extension beyond the original planned service life (typically now 20 years) for healthy blades that do not possess significant damage.

A condition-based approach also has the advantage that it is not critical to be able to calculate the aero-loads with high accuracy on all individual rotor blades in an offshore wind turbine park, since the damage evolution can be assessed on the basis of the sensor signal. The proposed approach, figure 4, consists of condition monitoring to detect damage, NDI methods to characterize the damage, and damage and fracture mechanical modelling to predict future damage evolution [19–21], creating the science-based knowledge required to make a decision about what to do.

The proposed new approach has some similarities with the 'retirement for cause' approach used in military aircrafts, where the lifetime of gas turbine engines is determined on the basis of the detection of flaws of a certain detectable size rather than being retired prematurely by the traditional predetermined life approach [22]. In the following section of the paper, the material properties contributing to structural damage tolerance are presented. These properties are the 'levers' that future designs will consciously use when engineering reliability from the material level to the structural level. The expanded design and manufacture process showed in figure 3 will include consideration of the approach for maintenance and repair that is to be adopted for the entire group of structures, and the integrated sensorization necessary to achieve remote characterization of the material and structural condition. Finally, the vision is presented of offshore wind farms designed using smart structure technology made possible by this deeper understanding of material behaviour.

3. Increasing reliability of offshore wind turbine blades by damage tolerance

(a) The concepts of distributed and localized damage

The loads on each material point within a rotor blade structure can be characterized mechanically by considering a small volume of the material. On the materials level, the load is characterized

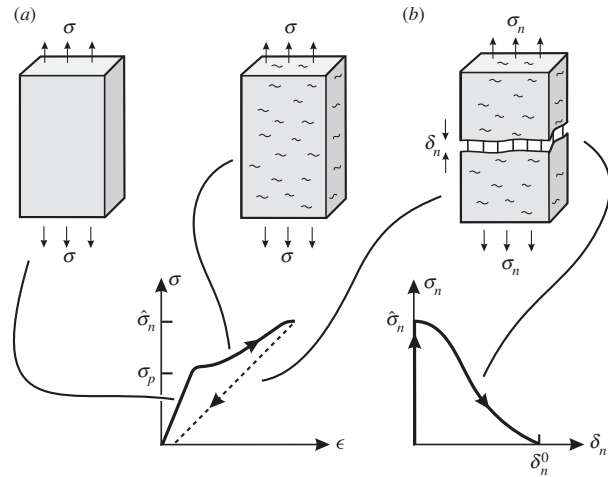


Figure 5. The relationship (a) between stress, σ , and strain, ϵ , is used to characterize deformation of undamaged material (linear stress–strain response) and material with distributed damage (nonlinear stress–strain response), while the relationship (b) between stress (traction), σ_n , and separation, δ_n , is appropriate for describing localized damage (fracture). Away from the localized damage, the material is unloaded along the dotted part of the stress–strain curve (a).

in terms of stress σ (defined as load per cross-sectional area), and deformation is characterized in terms of strain ϵ (elongation divided by original length). The stress–strain relationship ($\sigma - \epsilon$) of an undamaged material is in most cases linear (figure 5a). In a loaded wind turbine rotor blade, distributed damage (e.g. small cracks in the matrix and breakage of fibres in a composite material) can develop in some regions of the blade. The distributed damage may be characterized by the crack area per volume or the number of broken fibres per volume. Damage induces nonlinearity in the stress–strain relationship. Therefore, nonlinear stress–strain laws must be used to describe the mechanical response of materials experiencing distributed damage (figure 5a). Distributed damage may over time lead to localized damage. During localization, the material undergoes weakening in a so-called fracture process zone, so that its ability to transfer stress decreases, with increasing local deformation δ (separation). It is then appropriate to describe the material behaviour in terms of a traction–separation law ($\sigma_n - \delta_n$) (figure 5b). With increasing separation (corresponding to more localized damage), the traction that the fracture process zone can transmit decreases. When the end-opening of the fracture process zone δ_n^* exceeds a critical value δ_n^0 , the traction vanishes completely so that a crack surface forms. The traction–separation law is taken to be a material property, being the same law along the entire fracture process zone. The area under the traction–separation curve is the work of the traction, i.e. the fracture resistance.

Owing to the difference in stress levels for different parts of the blade and uneven distribution of the manufacturing defects, the damage state may vary from part to part between undamaged material, distributed damage and localized damage. Depending on the conditions, the localized damage may either exhibit stable or unstable crack growth. The damage state can be described by a ‘damage map’ in terms of the location, damage type and size, as well as a parameter indicating how close the damage state is to the critical condition (unstable crack growth).

Offshore wind turbine rotor blades will be subjected to high extreme wind loads (heavy storms) and lower, varying loads from wind changes and rotor rotation. Cyclic loads may induce fatigue damage evolution, i.e. stable crack growth occurring as a very small increase in the crack length during each load cycle. The crack can then become so long that it leads to unstable, fast

crack propagation at the maximum cyclic load, potentially leading to structural failure of the rotor blade. The condition for unstable crack growth is thus a key issue. The transition from stable to unstable crack growth can be analysed as crack growth under constant load (the maximum value of the cyclic load). The stability of crack growth will be the focus of the remainder of the section.

(b) Damage tolerant materials and structures

In the following, we will discuss how materials properties and structural design can be used to achieve enhanced damage tolerance, being the ability to sustain damage without unstable catastrophic failure. In particular, we wish to argue a design philosophy where materials and the structural design are chosen so that each structural detail can be designed to possess a high damage tolerance.

For distributed damage, damage tolerant behaviour is obtained as follows. For undamaged composite materials, the stress–strain behaviour is linear. Damage induces nonlinear stress–strain behaviour—the material decreases in stiffness with increasing damage. An undamaged material loaded beyond the linear-elastic limit σ_p will start to develop damage and thus exhibit nonlinear stress–strain behaviour up to the failure stress $\hat{\sigma}_n$ (strength). Damage tolerance requires that the materials strength should be significantly higher than its linear-elastic limit and that the damage can be detected by sensors. It then becomes possible to detect whether the material has been overloaded and to repair or replace the structure while the material still retains a strength above its design stress.

Material design can create composite laminates having nonlinear stress–strain behaviour even though most fibre types used in composite materials are linear elastic. A nonlinear stress–strain behaviour can be obtained by the use of laminates with multiple fibre orientations (enabling some layers to crack at lower strains, denoted ‘first-ply-failure’) or by the use of fibres having different failure strain (hybrid composites).

Localized fracture, such as delamination, can be analysed by fracture mechanics, e.g. by the use of traction–separation laws. With respect to the propagation of a crack, damage tolerance implies that the crack growth should be stable, requiring that the load level for unstable crack growth should be significantly higher than the load level that initiates crack growth. Classic fracture mechanics considers an energy balance between the energy supplied (or released) by the structure and the energy absorbed by the fracture processes at the crack tip. Crack growth will not occur when the energy released by the structure per unit crack advancements is less than the energy consumed by the crack tip fracture processes per unit crack advancement.

The energy released per unit cracked area depends on the magnitude of the applied load, the elastic properties and the shape of the structure. If the fracture resistance is constant, the crack growth can be stable (i.e. causing cracking to stop, denoted crack arrest) or unstable depending on how the energy released depends on the load and geometry, i.e. structure properties. The structure should be designed so that it can take the additional load when a crack has formed and the local region carries less load (figure 5b).

It is possible, however, to increase the amount of stable crack growth by designing interfaces that possess increasing fracture resistance with increasing crack extension. Rising fracture resistance, denoted R-curve behaviour, implies that the energy absorbed per unit area of the fracture process zone increases with the crack extension. Typically, the crack growth resistance increases from an initial value to a steady-state value. It follows that the stability of crack growth now depends on the load, geometry (including the initial crack length), and the fracture resistance of the material. Often in composites, delamination is accompanied by the formation of a crack bridging zone, where intact fibres connect the crack faces behind the crack tip. This can lead to a large-scale crack bridging zone, resulting in R-curve behaviour [23]. The bridging load, i.e. the normal traction σ_n as a function of the normal opening δ_n , $\sigma_n(\delta_n)$, plays a central role in the stability of crack growth, since the R-curve behaviour is related to the traction–separation law.

Two conditions for stable crack growth, expressed in terms of the bridging law parameters, are

$$J_{\text{ext}} = J_0 + \int_0^{\delta_n^*} \sigma_n(\delta_n) d\delta_n \quad \text{and} \quad \frac{\partial J_{\text{ext}}/\partial a}{\partial \delta_n^*/\partial a} \leq \sigma_n(\delta_n^*). \quad (3.1)$$

In (3.1), J_{ext} is the energy released per unit cracked area, J_0 is the energy at which cracking initiates, σ_n and δ_n are traction and separation (figure 5b), δ_n^* is the separation at the end of the crack and a is the crack length.

To obtain stable cracking during an increasing load, these two equations should be fulfilled at all times. The cracking will be unstable when the right-hand side inequality is violated.

Equation (3.1) makes it possible to think intelligently about the damage tolerance of almost any large-scale bridging cracking problem in a structural part of a wind turbine rotor blade. The left-hand sides of both equations include all the structural parameters (loads and structural geometry), whereas the right-hand sides depend only on the fracture properties. Thus, the initial structure design can be specified to achieve a minimum damage tolerance level throughout the blade. Once the load and geometry of the blades have been fixed, options to modify local stiffening, manufacturing specifications or material options allow an assessment of which traction–separation law (the right-hand side) gives the highest damage tolerance/longest stable crack extension. In this way, these relations are very helpful for both the structural designer and the material scientist.

(i) Optimizing materials damage tolerance with traction–separation laws

Micromechanical models of crack bridging show that the bridging traction depends on microscale parameters such as the fibre stiffness, the fibre diameter and the fibre/matrix debond energy [23,24]. It is thus possible to change the traction–separation laws by changing the properties of microscale parameters (this is sometimes called ‘microstructural optimization’). For instance, the surface of the fibres can be subjected to chemical or physical treatments before the processing of the composite material.

Crack bridging is only an effective toughening mechanism as long as fibres remain intact. If the fibre/matrix bond is too strong, the fibres break instead of peeling off and create crack bridging. Experimental work has shown that weakening the fibre/matrix interface can lead to more ‘surviving’ fibres, resulting in more fibre bridging [25]. By contrast, for layered structures, e.g. adhesive bonded joints, it has been shown that plasma treatment can increase the fracture resistance of the joint, causing the formation of a parallel crack within the laminate just outside the adhesive layer [26]. Yet another study has shown that simply changing the ply layup, the cracking mechanism changes from the propagation of a single crack to the development of two or three parallel cracks (with two or three bridging zones), resulting in a doubling or tripling of the fracture resistance [27]. These examples show that materials design can change the damage tolerance of materials significantly.

These observations suggest that fracture mechanics properties of fibre/matrix interfaces as well as the fracture mechanics properties of interfaces between layers in laminates play a central role in the fracture resistance of laminates. Mastering the interface design is thus the key to optimize fracture resistance. There are many interfaces across the laminate at which delamination cracks can potentially propagate. It is challenging and difficult to design and control the fracture properties of all interfaces. However, the concept of cohesive laws enables us to propose an idea to design/tailor laminates so that cracks will propagate along high-energy absorbing interfaces. The idea is that the normal stresses¹ σ_{22} are continuous and do not vary much across a thin layer, so that the normal tractions σ_n is almost the same for two neighbouring interfaces (figure 6). Therefore, we postulate that cracking will occur along the interface that possesses the lowest peak traction, $\hat{\sigma}_n$. Thus, it should be possible to design an interface such that it combines a low peak traction and a large work of the cohesive traction (e.g. by having a large critical opening; figure 6). Such an interface will then trap the cracking along a high energy-absorbing path and thus impart

¹For real applications where cracking is mixed mode, the shear stress σ_{12} and the shear traction σ_t should also be considered.

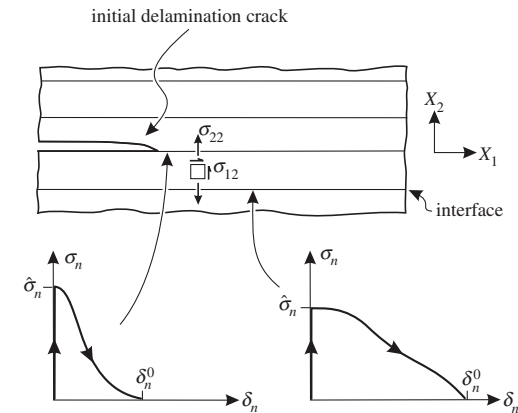


Figure 6. Cracking of a laminate having thin plies may shift to the neighbour interface if it has a lowest peak traction value.

high damage tolerance. Only a few low-strength, high-toughness interfaces may be needed. The design of interfaces is then reduced to designing and controlling fewer interfaces.

(ii) Possible definition of a structural damage tolerance index

It would be useful to have an index that would give a number for the safety margin of offshore wind turbine rotor blades.

A practical approach would be to consider various critical parts of the blade individually. Each structural part can then be modelled by numerical modelling, using typical defect or damage sizes (e.g. corresponding to the detection limit of NDI methods) and the relevant cohesive laws. Such progressive damage analysis should simulate the damage evolution from initiation to unstable growth. Onset of unstable damage growth gives a fracture load (that should exceed the expected service loads) and a change in the compliance of the structural part.

A damage tolerance index would enable the comparison of two designs made of the same material/interface or the same structural design made of two different materials and quantify which combination offers the most damage tolerant behaviour. Such an index D could for instance be a non-dimensional number with the characteristics that $D = 0$ indicates no damage tolerance (always unstable damage evolution or crack growth) while $D \rightarrow \infty$ indicates that damage or crack growth is always stable. A damage tolerance index could be defined by the structural compliance at which the cracking becomes unstable, C_c ,

$$D = \frac{C_c - C_0}{C_0}, \quad (3.2)$$

where C_0 is the compliance of the undamaged structural part of the blade. The compliance of a structural part is defined as the deflection of the structural part per unit applied load. A change in compliance due to damage may not be seen for the whole structure but only locally.

Furthermore, each structural part may contain one or more competing damage modes for which a damage tolerance index could be calculated.

Different damage modes are likely to have different damage tolerant index values. The structural designer should ensure that all damage types of all structural parts have sufficiently high D values, so that damage evolution can be detected by compliance changes. He can modify the structural design to raise the value of D of the damage mode that has the lowest D values, in order to ease the damage detection by compliance changes. In case the damage type and traction–separation laws are such that a sufficiently high compliance change cannot be obtained,

the damage detection must rely on sensors that are not based on compliance, e.g. acoustic emission sensors.

Then, the damage tolerance of the entire rotor blade could be assessed in a way similar to the 'damage map' mentioned in the Introduction, by a set of damage tolerance indices. It should be assessed whether unstable damage evolution of a structural part would lead to failure of the entire blade. The damage tolerance of specific material selections and alternative structural designs could then be compared in the design phase.

4. Structural health monitoring

An SHM system's main purpose is to give information about the presence of damage in an accurate way, its location with a good resolution for possible repair/maintenance, the type of damage (that in a complex structure like a wind turbine can be very diverse), the severity of the damage and finally prognostic information about the remaining operating life [28].

In fact, a great deal of sensor information is already available from offshore wind farms concerning the wind conditions, power output, temperatures, gearbox/drive-train vibrations and so on; but little or no sensor data specifically for the blades. As modern wind farms have a data handling and transfer framework already in place, an eventual monitoring suite for the blade condition can be designed to be a 'module' inside the already existing system. Furthermore, many of these other sources will provide valuable parametric data to the blade sensor outputs.

The current maturity level for state-of-the-art blade damage sensing is very broad, with a great deal of research at the material level on integration/embedding of promising sensors into the composites. This includes fibre-optic sensors using fibre Bragg gratings [29] or continuous optical fibre measurement [30], electrically conducting sensors based on conductive polymers and carbon fibres [31], acoustic emission methods using piezoelectric transducer materials for transmission and receiving of stress waves, spatial mapping of filament-matrix interface defects-reflectometry. Closer to application there are various sensor system approaches (including strain gauges [32], structural vibrations [33] and local stress wave [34]) that have been demonstrated as suitable to monitor damage initiation and growth within blades during structural blade testing in commercial or research facilities where support (including hardware control and NDI) is available and the loading conditions are known. In operation, particularly for long-term remote monitoring, commercial systems exist that can detect ice formation and report changes in vibration response (Blade Control-Bosch Rexroth, <http://tinyurl.com/nl48585>) or return strain readings measured around the root section (WindMeter-Fibersensing, <http://www.fibersensing.com/>). Although not fulfilling the definition of SHM given above, these systems indicate that issues of robustness, reliability, price competitiveness and functional operation can be overcome. In order to implement the methodology described in §2 (Vision), a suite of sensor approaches must be available within the designer 'toolbox' that can be combined and specified to meet the damage tolerance criteria. The resolution for detection of specific types of damage is given by the damage propagation modelling (figure 3), which in turn calibrates the sensor distribution. However, it is clear that a significant maturation of applied blade sensor technology is required.

Monitoring methods are needed from the manufacture process stage to ensure a certain level of quality, controlled cure of matrix material during processing and improve certification, to produce composite parts in a repeatable and consistent manner with defects such as dry-spots, cracks, delamination and moisture held within acceptable tolerances.

(a) Traditional design and operation methodology

The traditional design and operation methodology as shown in figure 7 is no longer optimal for this type of requirements; in particular, as blades become larger and more expensive to manufacture, the need for information feedback to maximize their lifetime utilization increases.

11

rsta.royalsocietypublishing.org Phil. Trans. R. Soc. A 373: 20140077

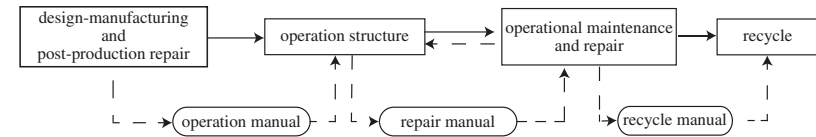


Figure 7. Life stages of a turbine: traditional design methodology.

A post-manufacture quality assessment using advanced NDI technology can identify defects in the blade. In most cases, these are minor, 'surface effect' problems that can be corrected easily. In some cases, however, a major structural repair will be necessary that involves removing material and laying new laminate in place. This operation is best done immediately after production with all manufacturing resources available and results in repairs giving close to the maximum theoretically possible structural strength recovery. The quality of the cured repair should also be inspected before the finished blade leaves the production facility. Once in operation, wind turbine blade damage can only be detected by visual inspections (since no sensors are built-in), either by blade maintenance crews or possibly from examining high-definition images obtained from the ground (Aether visual inspection for blades-Braendler <http://www.braendler.com/>). Such focused blade inspections are most usually done near the end of product warranty periods. The repair of damage on-site is clearly more challenging than those done in a manufacturing facility. Again the majority of problems identified on operating blades are characterized as 'maintenance' and involve correcting hairline surface cracks or pitting/erosion at the leading (or trailing) edge of the blade. In these cases, the recovery of a good surface finish is the success criterion for the maintenance effort. But occasionally a major structural repair will be necessary where working conditions are far from optimal: low temperatures, wet conditions and challenging access issues. The quality of the work will depend heavily on the training level of the technicians, the quality of the materials used, the resources (tools, platforms, tenting, heating, etc.) and the time available to do the repair. Ensuring the effectiveness of repair is also difficult as afterwards the blade surface is again returned to a good finish.

(b) Smart structure design

In either a post-production repair or an *in situ* structural repair the feedback from embedded sensors can improve confidence in the quality and effectiveness of the work undertaken. Furthermore, such feedback will help 'single-out' blades that return exceptional sensor responses, thus providing an early warning of structural damage in operation, which currently relies on purely visual observations of surface cracking.

The presence of sensors will provide feedback at each stage of the structure life cycle. For example, the design and manufacture process will become iterative with data from embedded sensors helping to make subtle improvements to the infusion and cure processes as well as making blade manufacture reactive to external effects and thus minimizing product variability. In operation, data returned from the structure will allow an analysis of the structural performance and a concurrent engineering approach with modified designs for the latest versions of the structure. The main function of the embedded sensors during operation is early detection of changes in response that could indicate damage present in the material or at interfaces/bondlines. The damage tolerance and structural monitoring methodology described in this paper requires a 'damage map' for each structure with an assessment of the blade condition using local and global damage indices. This permits a damage management approach with tools for avoiding (or alleviating) the structural loadings (high wind conditions) that will propagate damage in a particular blade.

All offshore turbines require on-site maintenance, but with detailed structure-specific response history available it becomes possible to make a more efficient application of maintenance tailored

12

rsta.royalsocietypublishing.org Phil. Trans. R. Soc. A 373: 20140077

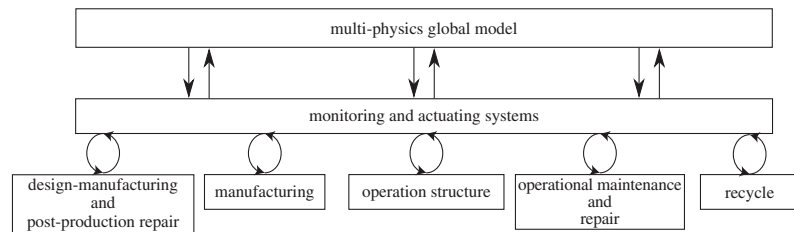


Figure 8. Life stages of a turbine: smart structure design.

to the need of each particular turbine. This is in contrast to the traditional methodology where generic manuals specify the amount of proactive maintenance required.

Normally, an expensive life assessment programme would be required in order to justify any decision to extend the service life of an entire group of structures. But with the approach shown in figure 8, all the relevant data are already available and near the design end-of-life this database of structure-specific histories allows a more informed management decision regarding reinsurance/recommissioning or decommissioning, resale and/or recycle.

5. Discussion

(a) The path towards condition monitoring-based approach

It is not realistic to jump from the conventional turbine to the proposed design and maintenance approach based on condition monitoring since at present not all tools required are fully demonstrated and mature. For sensors, for instance, a number of sensor types have been tested with satisfactory results in the laboratory or at prototype blade test. However, the durability over many years in a harsh offshore environment needs to be demonstrated. Concerning NDI methods, many of these have been successfully demonstrated in inspection of blades, both in the laboratory, full-scale prototype testing and in the field. Thus, these methods are demonstrated. Within progressively damage modelling, a lot of progress has been made over the past two decades. However, specific models of blade damage are not yet demonstrated. We think it is possible to bring in the tools for condition monitoring gradually, by applying them to dedicated problems, where information of damage evolution provide high value. For instance, testing sensors on wind turbine rotor blade during full-scale prototype testing is likely to be worth the cost, since more data on damage evolution during the test could lead to the detection of damage originating from a design weakness or poor manufacturing procedures, which could lead to the necessity of many blade repairs if the blade had gone into mass production. Likewise sensors should be used on blades where primary structural parts have been repaired, since the repaired area is likely to act as a site for damage initiation. Installation of a few sensors at a critical repair may thus provide very valuable information about the quality of repair, and may allow blades that would otherwise be discarded to be repaired and used.

The condition monitoring modelling approach in figure 4 requires developing the science-based knowledge available within sensor application (for detection), NDI (for characterization) and modelling (for prediction). A plausible order of steps of this gradual implementation of the proposed approach is given below.

Sensors:

- demonstrate sensors in the laboratory,
- sensor calibration of output against known damage (location, type, size, depth),
- sensor durability on subcomponent tests in the laboratory (long-term, cyclic loading),

- demonstrate sensors during full-scale blade tests,
- demonstrate sensors on repaired blades in operation, and
- demonstrate sensors on new blades in operation.

Modelling approach (prediction of progressive damage evolution):

- characterization of blade materials in terms of traction–separation laws (mixed mode),
- demonstration of predictability of static and cyclic crack growth on medium-sized specimens in the laboratory,
- development of models for major structural failure modes in rotor blades, and
- formulate guidelines for industrial use of model approach.

Based on the condition monitoring approach, a number of decisions can be made (figure 4), including the decision to repair a blade. If the blade is repaired, the repair techniques used should be documented scientifically and the repaired areas should be checked by NDI methods following the repair to document the quality of the repair. Steps to improve repair techniques are

- optimization of repair techniques in the laboratory (maximize residual strength and fatigue life),
- demonstration of repair methods on blade parts in the laboratory,
- development and demonstration of NDI methods for quality control, and
- formulation of guidelines for repair approach.

(b) Towards integration in the global model

Sensing and monitoring systems will undoubtedly continue to become cheaper, more robust and effective. This will increase the amount of monitoring systems in all the blade stages (manufacturing, testing, operation, maintenance, repair, etc.), leading to a better understanding and control of key parameters on the structure performance of the blade. For instance, dedicated sensors will regulate the manufacturing, improving the product quality and dedicated operation sensors will give information about the response of that structure, helping to identify exceptions and improving the limited inspection and maintenance functions.

Better structural models and improved multi-physics global integration will allow for damage management by automatically shutting down a turbine in local conditions likely to progress damage within that particular turbine, and will enable the modification of the operational limits for individual turbines based on their known damage condition. In other words, the ability of the smart turbine to analyse and adapt to environmental and structural conditions will lead to a more efficient operation of the wind turbine.

6. Summary

In this paper, we have outlined a future approach for the the design and maintenance of wind turbine rotor blades for offshore wind farms. This approach is based on the premise that it is not possible to manufacture large ‘perfect’ blades, and that large blades with manufacturing defects or damage are too costly to discard. Furthermore, since manual inspection is very costly for offshore wind turbines, we propose an approach that can handle blades with manufacturing defects, handling damage and in-service damage. The approach is based on the use of damage tolerant structural design and damage tolerant materials combined with built-in sensors that can detect damage evolution. The concept, which can be termed ‘condition monitoring and maintenance’, consists of detection of damages by sensors, characterization of damage (type and size) by NDI methods, model predictions of residual life, giving information that enables decision-making with respect to whether a damaged blade should be repaired or replaced. The majority of blades that do not develop significant damage will not require any manual inspection. Examples are given

on how materials can be tailor-made to provide higher damage tolerance. The development of more damage tolerant structures and damage tolerant materials could provide the technological opportunity that enables very large wind turbine rotor blades, approaching 100 m in length, in the future.

Funding statement. G.P. acknowledges the Seventh Framework Programme (FP7) for funding the project MareWint (Project reference: 309395) as Marie-Curie Initial Training Network. B.F.S. was partially supported by the Danish Centre for Composite Structures and Materials for Wind Turbines (DCCSM), grant no. 09-067212 from the Danish Strategic Research Council.

References

- Offshore Wind Energy: Action needed to deliver on the Energy Policy Objectives for 2020 and beyond, COM(2008) 768 final (Not published in the Official Journal). See http://europa.eu/legislation_summaries/energy/renewable_energy/en0001_en.htm.
- EWEA. 2014 Day Three, Recharge, Wednesday 12 March, 2014. See <http://www.ewea.org/annual2014/media-and-press/recharge-daily>.
- Jacobsen TK. 2011 Materials technology for large wind turbine rotor blades—limits and challenges. In *32nd Risø International Symposium on Material Science, Composite materials for structural performance: towards higher limits, Roskilde, Denmark, 5–9 September 2011* (eds S Fæster, D Juul Jensen, B Ralph, BF Sørensen), pp. 35–43. Holbæk, Denmark: Centertryk A/S.
- Qian C. 2013 Multi-scale modelling of fatigue of wind turbine rotor blade composites. PhD dissertation, Delft University of Technology.
- Bauchau OA. 2001 Modeling rotorcraft dynamics with finite element multibody procedures. *Math. Comp. Model.* **33**, 1113–1137. (doi:10.1016/S0895-7177(00)00303-4)
- Bottasso CL, Campagnolo F, Petrovic V. 2014 Wind tunnel testing of scaled wind turbine models: beyond aerodynamics. *J. Wind Eng. Ind. Aerodyn.* **127**, 11–28. (doi:10.1016/j.jweia.2014.01.009)
- EERA-DTOC Seventh Framework Programme (FP7)—European Energy Research Alliance—design tool for offshore wind farm cluster. See <http://www.eera-dtoc.eu/>.
- MAREWINT Seventh Framework Programme (FP7)—new MAterials and RELiability in offshore WIND Turbines technolog. See <http://www.marewint.eu/>.
- Sørensen BF, Holmes JW, Brøndsted P, Branner K. 2010 Blade materials, testing methods and structural design. In *Wind power generation and wind turbine design* (ed. Wei Tong), pp. 417–466. Southampton, UK: WIT Press.
- Toft HS, Branner K, Berring P, Sørensen JD. 2011 Defect distribution and reliability assessment of wind turbine blades. *Eng. Struct.* **33**, 171–180. (doi:10.1016/j.engstruct.2010.10.002)
- Braga DFO, Tavares SMO, da Silva LFM, Moreira PMGP, de Castro PMST. 2014 Advanced design for light weight structures: review and prospects. *Progr. Aerospace Sci.* **69**, 29–39. (doi:10.1016/j.paerosci.2014.03.003)
- Jensen FM, Puri AS, Dear JP, Branner K, Morris A. 2011 Investigating the impact of non-linear geometrical effects on wind turbine blade - Part I. Current issues and future challenges in design optimisation. *Wind Energy* **14**, 239–254. (doi:10.1002/we.415)
- Sørensen JD. 2009 Framework for risk-based planning of operation and maintenance for offshore wind turbines. *Wind Energy* **12**, 493–506. (doi:10.1002/we.344)
- Sørensen JD, Kroon JB, Faber MH. 1994 Optimal reliability-based code calibration. *Struct. Safety* **15**, 197–208. (doi:10.1016/0167-4730(94)90040-X)
- Toft HS, Branner K, Mishnaevsky Jr. L, Sørensen JD. 2013 Uncertainty modeling and code calibration for composite materials. *J. Compos. Mater.* **47**, 1729–1747. (doi:10.1177/0021998312451296)
- Worden K, Farrar CR. 2007 An introduction to structural health monitoring. *Phil. Trans. R. Soc. A* **365**, 303–315. (doi:10.1098/rsta.2006.1938)
- Sørensen BF et al. 2002 *Fundamentals for remote structural health monitoring of wind turbine blades—a preproject*, 36 p. (Denmark research center Risø. Risø-R; 1336(EN).)
- McGugan M, Larsen G, Sørensen BF, Borum KK, Engelhardt J. 2008 *Fundamentals for remote condition monitoring of offshore wind turbines*. Denmark Technical University, Risø National Laboratory for Sustainable Energy. 48 p. (Denmark research center Risø. Risø-R; 1639(EN).)
- Ataya S, Ahmed MMZ. 2013 Damages of wind turbine blade trailing edge: forms, location, and root causes. *Eng. Fail. Anal.* **20**, 480–488. (doi:10.1016/j.engfailanal.2013.05.011)
- Takoutsing P, Wamkeue R, Ouhrouche M, Slaoui-Hasnaoui F, Tameghe T, Ekemb G. 2014 Wind turbine condition monitoring: state-of-the-art review, new trends, and future challenges. *Energies* **7**, 2595–2630. (doi:10.3390/en7042595)
- Yang B, Sun D. 2013 Testing, inspecting and monitoring technologies for wind turbine blades: a survey. *Renew. Sustain. Energy Rev.* **22**, 515–526. (doi:10.1016/j.rser.2012.12.056)
- Suresh S. 1991 *Fatigue of materials*, pp. 501–502. Cambridge, UK: Cambridge University Press.
- Spearing SM, Evans AG. 1992 The role of fiber bridging in the delamination resistance of fiber-reinforced composites. *Acta Metall. Mater.* **40**, 2191–2199. (doi:10.1016/0956-7151(92)90137-4)
- Sørensen BF, Gamstedt EK, Østergaard RC, Goutianos S. 2008 Micromechanical model of cross-over fibre bridging—prediction of mixed mode bridging laws. *Mech. Mater.* **40**, 220–224. (doi:10.1016/j.mechmat.2007.07.007)
- Feih S, Wei J, Kingshott P, Sørensen BF. 2005 The influence of fibre sizing on the strength and fracture toughness of glass fibre composites. *Compos. part A* **36**, 245–255. (doi:10.1016/j.compositesa.2004.06.019)
- Kusano Y, Sørensen BF, Andersen TL, Toftegaard HL, Leipold F, Salewski M, Sun Z, Zhu J, Li Z, Alden M. 2013 Water-cooled non-thermal gliding arc for adhesion improvement of glass-fibre-reinforced polyester. *J. Phys. D Appl. Phys.* **46**, 135203. (doi:10.1088/0022-3727/46/13/135203)
- Rask M, Sørensen BF. 2012 Determination of the J integral for laminated double cantilever beam specimens: the curvature approach. *Eng. Fracture Mech.* **96**, 37–48. (doi:10.1016/j.engfracmech.2012.06.017)
- Rytter A. 1993 Vibrational based inspection of civil engineering structures. PhD thesis, Aalborg University, Denmark.
- Bernasconi A, Carboni M, Comolli L. 2011 Monitoring of fatigue crack growth in composite adhesively bonded joints using Fiber Bragg Gratings. *Procedia Eng.* **10**, 207–212. (doi:10.1016/j.proeng.2011.04.037)
- Zhou G, Sim LM. 2002 Damage detection and assessment in fiber-reinforced composite structures with embedded fiber optic sensors. *Smart Mater. Struct.* **11**, 925–939. (doi:10.1088/0964-1726/11/6/314)
- Cho JW, Choi JS. 2000 Relationship between electrical resistance and strain of carbon fibers upon loading. *J. Appl. Polym. Sci.* **77**, 2082–2087. (doi:10.1002/1097-4628(20000829)77:9<2082::AID-APP26>3.0.CO;2-W)
- Morfiadakis E, Papadopoulos K, Philippidis TP. 2000 Assessment of the strain gauge technique for measurement of wind turbine blade loads. *Wind Energy* **3**, 35–65. (doi:10.1002/1099-1824(200001/03)3:1<35::AID-WE30>3.0.CO;2-D)
- McGugan M, Larsen G, Sørensen BF, Borum KK, Engelhardt J. 2008 *Fundamentals for remote condition monitoring of offshore wind turbines*. Risø-R-1639(EN).
- Jørgensen ER, Borum KK, McGugan M, Thomsen CL, Jensen FM, Debel CP, Sørensen BF. 2004 *Full scale testing of wind turbine blade to failure—flapwise loading*. Risø-R-1392(EN).

Vibration-based SHM System: Application to Wind Turbine Blades

D Tcherniak¹, L L Mølgaard²

¹ Research Engineer, Brüel & Kjær Sound & Vibration Measurement A/S, Nærum, Denmark

² Senior Researcher, Department of Applied Mathematics and Computer Science, Technical University of Denmark, Lyngby, Denmark

E-mail: dmitri.tcherniak@bksv.com

Abstract. This study presents an vibration-based system designed for structural health monitoring of wind turbine blades. Mechanical energy is introduced by means of an electromechanical actuator mounted inside the blade. The actuator's plunger periodically hits the blade structure; the induced vibrations propagate along the blade and are measured by an array of accelerometers. Unsupervised learning is applied to the data: the vibration patterns corresponding to the undamaged blade are used to create a statistical model of the reference state. During the detection stage, the current vibration pattern is compared with the reference state, and the novelties can be associated with damage. The vibration pattern is described by the covariance matrix between the accelerometer signals. The mid-range frequencies are used: this range is above the frequencies excited by blade-wind interaction, thus ensuring a good signal-to-noise ratio. Simultaneously, the frequencies are low enough to be able to propagate the entire blade length, so good results can be obtained even using only one actuator. The system is demonstrated on a real 34m blade mounted on a test rig. Using the suggested approach, the system enables detection of, e.g., a 20cm long trailing edge opening under realistic noise conditions. It is also demonstrated that the system provides rough information about damage location. Progression of damage, if any, can also be detected.

1. Introduction

Wind turbine blades today are extremely complex and expensive structures; from the cost perspective, they constitute a significant asset for wind turbine owners. Therefore, monitoring of their structural health becomes economically rational, especially for big, remote (offshore) turbines.

There are many different approaches to SHM of wind turbine blades, varying by utilizing different physical phenomena, sensor types and signal processing; a detailed review can be found, for example, in [1]. The present study introduces a vibration-based, active system. *Vibration-based* means that changes in mechanical vibrations of the blade serve as a feature indicating blade damage. Active means that the vibrations are introduced artificially, by using a dedicated *actuator* mounted inside the blade; this contrasts with other vibration-based approaches which rely on ambient vibration of the blades due to wind. In authors knowledge, so far there is no evidence that the latter can provide damage detection resolution satisfying industry's demand. The suggested technique differs from another well-known active approach, *guided waves*, in the

¹ To whom any correspondence should be addressed.

frequency range used. If, in the guided waves case, the tens of kHz range is typical, the vibration frequencies excited by the suggested electromechanical actuator are normally below 1 kHz.

The vibrations induced by the actuator are picked by a number of accelerometers distributed over the monitored structure. The recorded signals are processed by the set of algorithms that determine whether or not the blade is damaged and find the location of the damage. A video demonstrating the SHM in action can be found in [2].

The *medium* frequency range which utilizes the proposed SHM is a compromise between the propagation range and detection resolution. Low-frequency vibrations can propagate long distances but are very insensitive to small areas of damage. It is well documented, see, for example, [3], that the modal parameters of the lowest blade modes are quite insensitive to blade damage, thus SHM systems utilizing changes in the modal parameters can only detect very significant damages. Ultrasonic range frequencies employed in the guided waves approach have good damage-detection resolution but the vibrations at such high frequencies quickly decay and cannot propagate long distances. This means the monitored blade has to be equipped with a large number of actuators and sensors, making such a system economically infeasible. The proposed approach utilizes the medium frequency range. Being well above the very low frequencies, where the blade is mainly excited by the wind, ensures satisfactory signal-to-noise ratio of the acceleration signals picked up by the accelerometers. At the same time, the frequency range is low enough for the vibrations to propagate long distances, and the experiments showed that a single actuator is sufficient to excite even a long modern blade. This also provides a good signal-to-noise ratio of the measured acceleration signals. On the other hand, the utilized frequency is high enough to ensure that the level of detection resolution is satisfactory for wind turbine owners; as it will be shown later, e.g., the system can detect a 20cm long trailing edge opening of a 34m blade.

Data-driven models for damage detection have been employed in numerous studies, for example, [4], with positive results. The experiments presented are often performed in laboratory conditions with models trained in a supervised setting where measurements from undamaged and damaged structures were available for the fitting. In contrast, the approach presented here is based on unsupervised anomaly detection, and thus does not require the learning of the damaged states. The SHM system is to be installed on an operational wind turbine continually monitoring the state so the algorithm must be robust to changing conditions such as wind, precipitation, and the operational modes such as changing rotational speeds and blade orientation. These phenomena may result in false alarms and the influence must therefore be investigated to implement a practical SHM system.

2. SHM system implementation on an SSP34m blade

Instead of making a general description of the proposed SHM system, this section uses one example of its implementation (namely, in application to an SSP34m blade). It is thought, however, that it should be easy to get a general idea about the concept of the proposed system and its usage. Before installing the SHM system on an operating wind turbine, its concept was



Figure 1. SSP34m blade mounted on the test rig

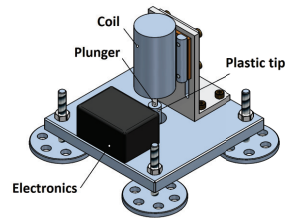


Figure 2. Design of electro-mechanical actuator.



Figure 3. Mounting inside an SSP34m blade

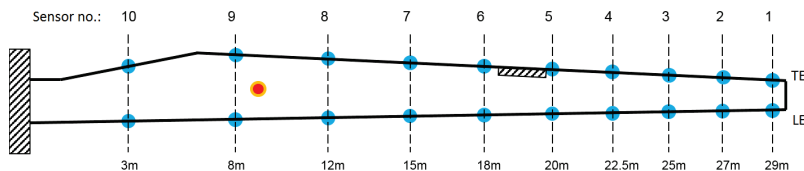


Figure 4. Test setup. Location of the actuator (●), accelerometers (●) and the damage (▨).

validated in laboratory conditions. An SSP34m blade, mounted on a test rig at DTU Wind Energy facilities in Roskilde, Denmark (figure 1), was instrumented, and a series of experiments were conducted on the blade in undamaged and damaged states.

2.1. SHM system hardware

The hardware of the SHM system consists of an electromechanical actuator and array of accelerometers.

The actuator is an electromechanical device consisting of two main parts (figure 2): a steel plunger and a coil. Driven by an electrical pulse, the coil ‘shoots’ the plunger towards the structure; after the hit, the plunger returns to its initial position by spring. Though, there is an advantage of measuring the injected force, the practical implementation of such sensors would be quite difficult and thus omitted in this study.

The actuator is meant to be mounted inside the blade, on the shear web or the spar cap (figure 3), in the root section of the blade, i.e., at the first third of the blade length. This area is typically easily accessible in most modern blades. From a few pretests, it became obvious that even one actuator can excite the entire blade. The chosen location of the actuator is shown in figure 4.

The blade was also instrumented with 20 Brüel & Kjær accelerometers Type 4524-B, ten on the leading edge (LE) and ten on the trailing edge (TE) (figure 4). The same accelerometer setup was used for modal analysis, therefore triaxial accelerometers were used [3]. However, in the experiment described, only the data from one axis, perpendicular to the blade surface, was used. We acknowledge that mounting sensors on wind turbine blades is a difficult task, especially in a retrofitting scenario. However, the last years advances in sensing technology, e.g. the fiber optic sensing, can make blade instrumentation feasible in the nearest future.

It should be mentioned that we did not use any systematic approach for selecting the number of accelerometers, their placement and the placement of the actuator. As mentioned before,

the accelerometers were reused from another modal analysis experiment, and the placement of the actuator was mainly driven by ease of access and a few pretests. A systematic approach to sensor/actuator placement may significantly improve the effectiveness of the SHM system and contribute to its cost reduction by reducing the number of sensors (and hence, data acquisition channels) by placing them at most optimal points. The first steps in this direction were taken by Parker, who used a genetic algorithm [5], and Lagerbon, who utilized a topology optimization approach [6].

A Brüel & Kjær data acquisition unit (see [3] for more details) was used for collecting the acceleration data. The unit also contains a signal generator, which was set to generate a rectangular pulse, which, after amplification, was fed to the actuator, resulting in an actuator hit. The data acquisition was triggered by this pulse, set to collect vibration data for a few milliseconds before and a few seconds after the pulse. Using the trigger significantly reduces the amount of data collected for the analysis.

The damage-detection algorithms are based on statistics to make detection more robust. In order to collect the necessary statistics, the blade in undamaged and damaged states was subjected to about fifty hits at each state. To speed up the experiment, the time between the successive hits were selected quite small, varying from one to five minutes. In real life application, the time between hits could be, for example, an hour or more.

2.2. Artificial damage

Only one type of damage was tested in the presented study: a trailing edge opening (figure 5). This damage is typical for many types of wind turbine blades, caused by de-bonding of the shells forming the pressure and suction sides of the blade. The damage was introduced into the blade gradually; we started with a 20cm trailing edge opening, drilling a series of holes through the glue between the pressure and suction sections of the blade. Then, using a saw, the holes were merged into one opening. After that, using a chisel and saw, the crack was gradually extended to 120cm; thus we had four damaged states: 20cm, 60cm, 90cm and 120cm. The data acquisition were conducted for each state, including the initial undamaged state, using about fifty actuator hits for each state.



Figure 5. Blade damage in the trailing edge, with the chisel used to introduce the damage



Figure 6. Bolts and metal plates used to change damage size in the second experiment.

When the damage was introduced, it was realized that operating with a heavy hammer and chisel can introduce some other unwanted changes into the blade, which can be erroneously associated with the effect of the damage. To avoid this, the experiment was repeated: the de-bonded parts of the blades were connected by bolts, placed 10cm from each other. The glue

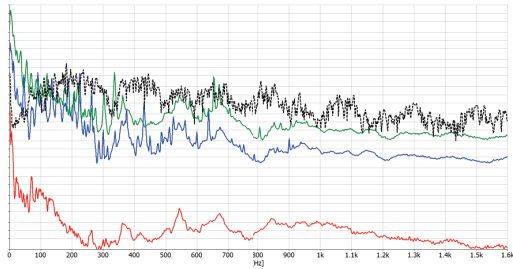


Figure 7. Power Spectral Densities (PSD) of the acceleration measured at the blade tip. V27 wind turbine:
— idle condition, moderate wind;
— operating at 32RPM, moderate wind;
— operating at 43RPM, strong wind,
⋯⋯ response from actuator measured on SSP34m.

removed between the pressure and suction parts was replaced by thin metal plates (figure 6). By tightening and loosening the bolts, it was easy to control the size and location of the opening without using the chisel.

2.3. Modelling of noise

Noise in the data is known to be a factor that can significantly reduce the robustness of damage-detection algorithms. In the case of operating wind turbines, the acceleration responses due to the actuator hits will overlap with the vibrations due to blade-wind interaction, and the vibrations due to the numerous mechanisms of the wind turbine, such as gearbox, generator, yaw and pitch mechanisms, cooling system, etc. To mimic such noise, vibration data measured on the blades of an operating Vestas V27 was used. This data was obtained during another measurement campaign, which is described in detail in [7]. Though the V27 and SSP34m blades are quite different (for example, the first one is 13m long, while the second is 34m), using this noise data was considered the best among other alternatives. Figure 7 shows the PSD of the acceleration measured at the tip of an operating V27 wind turbine under the different operating conditions. It should be mentioned that the presented study did not model the possible effects of varying weather conditions, such as temperature, wind speed and direction, etc. We also did not model the effects of different rotor speed and blade orientation (azimuth and pitch angles), which may strongly affect the robustness of the damage-detection algorithms.

3. Damage-detection method

The proposed damage-detection algorithm is based on an unsupervised anomaly detection method [8]. The method is based solely on modelling data obtained from the blade in a healthy state. This is in contrast to many earlier data-driven approaches that use supervised methods to detect a limited number of areas of damages introduced in experiments [4]. The supervised approach is consequently too restrictive for an operational system such as a wind turbine where it is impossible to perform experiments for all imaginable damage scenarios.

The damage-detection method is therefore based on a *training phase*, where we establish a model of the normal state exclusively from healthy state data, and subsequently a *detection phase* where a new sample is compared to the normal-state model.

The modelling of the normal state takes as input the multivariate accelerometer signal recorded from the sensors. The processing for the model can be split into three parts: preprocessing, feature extraction and statistical modelling.

The set of accelerometer signals for each hit requires some preprocessing steps to enhance the damage detection. The first step is *windowing*, in which the signal is truncated to start at the actuator trigger signal and end when the impulse from the strike has died out, i.e., after 1s.

Figure 7 compares the spectra of the blade tip response due to wind and due to the actuator hit. As mentioned before, the wind mainly excites low-frequency vibrations, while the actuator excites a wider range. If at low frequencies, the signal due to the actuator is buried in the noise due to wind, at higher frequencies the situation is the opposite, and one can expect a good signal-to-noise ratio if the low frequencies are filtered out. This observation helps select the cut-off frequencies of the applied high-pass or bandpass filter that is applied in the filtering step of the preprocessing.

3.1. Damage indicator

The data-driven modelling approach employed in this study requires the definition of a compressed representation of the state of the structure. A damage metric based on the covariance matrix between the time histories, similar to the one introduced in [5], is employed. Structural damage will change the energy propagation paths from the actuator to the accelerometers, and the vibration pattern due to actuator hit. Since the cross-covariance function is a measure of the similarity between two signals, the change in vibration pattern can be very well characterized by the change of the covariance matrix. The cross-covariance between signals x_1 and x_2 of length N is calculated as:

$$c_{x_1 x_2}(m) = \begin{cases} \sum_n^{N-m-1} \left(x_1(n+m) - \frac{1}{N} \sum_{i=0}^{N-1} x_1(i) \right) \left(x_2(n) - \frac{1}{N} \sum_{i=0}^{N-1} x_2(i) \right) & , m \geq 0 \\ c(-m) & , m < 0 \end{cases} \quad (1)$$

In this application, only the cross-covariance for lag 0, $m = 0$, is used for the damage indicator. Calculating the covariance for a set of M sensors, produces $M(M-1)/2$ distinct values for each hit that constitutes the damage indicator. Figure 8a and 8b show the covariance features for the SSP34m blade in an undamaged state and with an opening at 120cm. It is seen that the feature values change for the covariance between sensor $c_{x_2 x_{10}}$, $c_{x_4 x_{10}}$, and $c_{x_5 x_{10}}$, depicted in the lower left corner of the plots. Inspection of the covariance-feature vectors reveal that

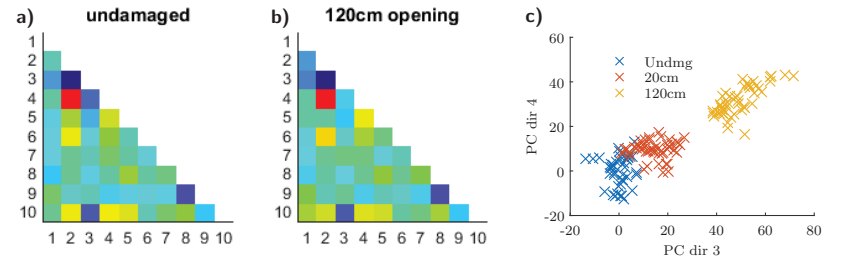


Figure 8. Covariance-based damage indicator using the 10 trailing edge accelerometers for the undamaged blade and the blade with 1.2m opening in trailing edge. The third panel shows the 3rd and 4th principal component dimensions for undamaged and two damage sizes

many of the dimensions are correlated, and in addition the dimensionality of the feature vectors grows quadratically with the number of sensors which could impede a statistical model of the samples. The dimensionality of the covariance-feature vectors is reduced using principal component analysis (PCA) [9]. The PCA is estimated using the samples from the undamaged case which produces a principal component space, that all samples are projected into. This projection is seen to separate damaged and undamaged samples quite well as illustrated in figure 8c. The dimensionality, i.e., the number of principal components, used for the PCA was chosen using a heuristic method. The method chooses the minimal number of principal components such that 99% of the variance in the data is accounted for.

3.2. Damage-detection metric

To evaluate whether a sample vector in the PCA-space, \mathbf{y} , is normal or damaged we use the Mahalanobis distance. The Mahalanobis distance is calculated as the distance between the normal-state samples \mathbf{X}_n , summarised by the mean $\mu_{\mathbf{X}_n}$ and the covariance matrix Σ , and the new sample:

$$d(\mathbf{y}, \mathbf{X}_n) = \sqrt{(\mathbf{y} - \mu_{\mathbf{X}_n})^\top \Sigma^{-1} (\mathbf{y} - \mu_{\mathbf{X}_n})}. \quad (2)$$

To make the decision whether a new sample \mathbf{y} is anomalous/damaged, a threshold must be chosen. This choice of threshold must either be based on observations of data from normal and from damaged blades, or chosen based on the normal-state data only. The former approach of supervised tuning of the threshold will have superior performance but requires that the system is trained on all damages seen. The current system uses the latter approach by calculating the distance for each normal-state sample $\mathbf{x}_{n,i}$ and then choosing the threshold as the maximum among the $d(\mathbf{x}_{n,i}, \mathbf{X}_n)$. This choice of threshold will thus classify all data in the training as normal.

3.3. Damage localization

The proposed SHM system also provides a rough damage localization. The localization is based on evaluation which elements of the covariance matrix are most affected. The damage is likely to be located between the sensors whose signals cross-covariance significantly changed (cf. figure 8a and 8b). Typically, several most affected elements of the covariance matrix indicate the damage position with precision, sufficient for damage severity evaluation and facilitation of its particular location for the repair.

4. Results

The damage-detection method was tested using data for the undamaged state and six different damage sizes of 20, 40, 60, 80, 100, and 120cm. The performance was evaluated using tenfold cross-validation to get unbiased estimates of the error rates shown in table 1. The results show a very low error rate already with the use of the 5 sensors at the trailing edge (TE) and has approximately similar performance for all damage sizes and as we add more sensors. A realistic instrumentation that uses both leading-edge (LE) and trailing-edge (TE) sensors also reaches the lowest observed error rates. As mentioned earlier, the algorithm was also tested with added

Table 1. Results of damaged vs. undamaged classification with different sensor configurations. The table shows the mean error rate (in %) from the tenfold cross-validation followed by the 95% confidence interval of the mean in brackets.

State	20cm	40cm	60cm	80cm	100cm	120cm
No. samples	53	52	52	48	49	53
TE1-5	2.0 [0.2;7.2]	2.1 [0.3;7.3]	2.1 [0.3;7.3]	2.2 [0.3;7.6]	2.1 [0.3;7.5]	2.0 [0.2;7.2]
TE1-6	3.1 [0.6;8.7]	3.1 [0.6;8.8]	3.1 [0.6;8.8]	3.2 [0.7;9.1]	3.2 [0.7;9.0]	3.1 [0.6;8.7]
TE1-7	5.1 [1.7;11.5]	5.2 [1.7;11.6]	5.2 [1.7;11.6]	5.4 [1.8;12.1]	5.3 [1.7;12.0]	5.1 [1.7;11.5]
TE1-10	2.0 [0.2;7.2]	2.1 [0.3;7.3]	2.1 [0.3;7.3]	2.2 [0.3;7.6]	2.1 [0.3;7.5]	2.0 [0.2;7.2]
TE1-5,LE1-5	2.0 [0.2;7.2]	2.1 [0.3;7.3]	2.1 [0.3;7.3]	2.2 [0.3;7.6]	2.1 [0.3;7.5]	2.0 [0.2;7.2]

artificial wind noise from an operational turbine to test the robustness of the damage-detection method in real operation. The results of these experiments are shown in figure 9. The wind noise is measured in terms of signal-to-noise ratio (SNR) between the clean signal in trailing edge sensor 1 from the arrival of the strike and 0.25s forward and the generated wind noise signal. The performance is measured using the well-established Area Under the (ROC) Curve (AUC) [10] that scores a binary classifier from perfect classification with a score of 1 to random guessing at a score of 0.5 independently of the chosen detection threshold. It is clear that all damage can be detected down to an SNR level of 0dB while larger areas of damage are detectable at even lower SNR levels.

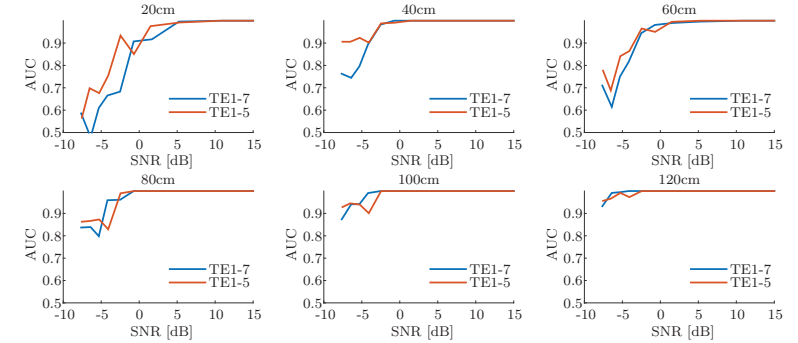


Figure 9. AUC for experiments with added wind noise. The legend in the figure shows the numbers of the trailing edge sensors used.

5. Conclusion

The paper presented a prototype of a vibration-based SHM system for wind turbine blades. The proposed approach is based on active excitation of the blade by an electro-mechanical actuator and measurements of the excited vibration by an array of accelerometers. The unsupervised abnormality detection method is employed for the analysis of the response signals for damage detection and localization. The method is demonstrated on a 34m wind turbine blade mounted on a test rig. It is shown that the proposed system is able to detect a 20cm length of trailing edge damage in presence of realistic (though artificial) noise.

Acknowledgments

The work was partly supported by EUDP (Danish Energy Technology Development and Demonstration Programme), grant number 64011-0084 Predictive Structure Health monitoring of Wind Turbines. The authors would like to thank DTU Wind Energy for giving access to the test object and research engineer Per Hørlyk Nielsen for his great assistance in setting up and conducting the experiment.

References

- [1] Hameed Z, Hong Y S, Cho Y M, Ahn S H and Song C K 2009 Condition monitoring and fault detection of wind turbines and related algorithms: A review *Renewable and Sustainable Energy Reviews* **13** 1–39 ISSN 13640321
- [2] 2014 Predictive structural health monitoring - Brüel & Kjær URL <https://www.youtube.com/watch?v=A7UyV-bc2w&feature=youtu.be>
- [3] Larsen G C, Berring P, Tcherniak D, Nielsen P H r and Branner K 2014 Effect of a Damage to Modal Parameters of a Wind Turbine Blade *EWSHM - 7th European Workshop on Structural Health Monitoring* (Nantes, France: IFFSTTAR, Inria, Université de Nantes) URL <https://hal.inria.fr/hal-01020347>
- [4] Fassio S D and Sakellariou J S 2007 Time-series methods for fault detection and identification in vibrating structures. *Phil Trans R S A* **365** 411–448 ISSN 1364-503X
- [5] Parker D L 2011 *Multi-objective design optimization framework for structural health monitoring* Ph.D. thesis Mississippi State University
- [6] Lagerbon M 2014 Optimal Sensor Positioning for Structural Health Monitoring Tech. rep. Technical University of Denmark
- [7] Tcherniak D and Larsen G C 2013 Application of OMA To an Operating Wind Turbine: Now Including Vibration Data *5th International Operational Modal Analysis Conference*
- [8] Tarassenko L, Clifton D, Bannister P, King S and King D 2009 Novelty detection *Encyclopaedia of Structural Health Monitoring* (John Wiley & Sons, Ltd) pp 653–675
- [9] Jolliffe I T 2002 *Principal Component Analysis* vol 98 (Springer) ISBN 0-387-95442-2
- [10] Fawcett T 2006 An introduction to ROC analysis *Pattern Recognition Letters* **27** 861–874 ISSN 01678655

Statistical evaluation of characteristic SDDLIV-induced stress resultants to discriminate between undamaged and damaged elements

L.M. Hansen¹, R.J. Johansen¹, M.D. Ulriksen¹, D. Tcherniak² and L. Damkilde¹

¹Dept. of Civil Engineering, Aalborg University, Niels Bohrs Vej 8, Esbjerg, Denmark

²Brüel & Kjær Sound & Vibration Measurement A/S, Skodsborgvej 307, Nærum, Denmark

E-mail: lhanse10@student.aau.dk, rjohan10@student.aau.dk, mdu@civil.aau.dk, dmitri.tcherniak@bksv.com, lda@civil.aau.dk

Abstract. The stochastic dynamic damage location vector (SDDLIV) method utilizes the vectors from the kernel of a damaged-induced transfer function matrix change to localize damages in a structure. The kernel vectors associated with the lowest singular values are converted into static pseudo-loads and applied alternately to an undamaged reference model with known stiffness matrix, hereby, theoretically, yielding characteristic stress resultants approaching zero in the damaged elements. At present, the discrimination between potentially damaged elements and undamaged ones is typically conducted on the basis of modified characteristic stress resultants, which are compared to a pre-defined tolerance value, without any thorough statistical evaluation. In the present paper, it is tested whether three widely-used statistical pattern-recognition-based damage-detection methods can provide an effective statistical evaluation of the characteristic stress resultants, hence facilitating general discrimination between damaged and undamaged elements. The three detection methods in question enable outlier analysis on the basis of, respectively, Euclidian distance, Hotelling's T^2 statistics, and Mahalanobis distance. The study of the applicability of these methods is based on experimentally obtained accelerations of a cantilevered residential-sized wind turbine blade subjected to an unmeasured multi-impulse load. The characteristic stress resultants are derived by applying the static pseudo-loads to a representative finite element (FE) model of the actual blade.

1. Introduction

Structural health monitoring (SHM) is widely employed within many systems, and the importance of its application for wind turbine blades is growing due to the increasing size and number of operating wind turbines, see, e.g., [1]. Vibration-based approaches are commonly applied in such a way that the dynamic response from the current state is compared to the representative response from the healthy reference state. In principle, the structure is potentially damaged if the current state differs significantly from the reference state namely due to changes in physical properties, typically a stiffness reduction.

The present paper concentrates on damage localization for which stochastic dynamic damage location vectors (SDDLIVs) are employed. The basis of the SDDLIV method is the damage location vector (DLV) method [4], in which the null space of the changes in the flexibility matrix from a pre- and post-damaged structure is utilized to locate the damage. The vectors that form the basis of the null

space are designated as DLVs, since that particular null vector associated with the lowest singular value is applied to an undamaged reference model as static-pseudo loads. The stresses in the model will, theoretically, approach zero in the damaged area(s).

The SDDLIV method is an extension of the DLV method that treats output-only measurements and includes the dynamics of the system by applying the null space of the changes in the transfer function matrix instead of the changes in the flexibility matrix. In [2], D. Bernal has proved that the method is applicable for localizing structural damages in numerical models of truss systems. Additionally, the applicability of the SDDLIV method has, by the authors of the present paper, been demonstrated in an experimental context with the residential-sized wind turbine blade shown in figure 1 [3]. Here, it was suggested that the implementation of a statistical procedure for discrimination between actual damage-induced irregularities and noise-induced ones may significantly improve the method. This is explored in the present paper where different statistical approaches to discriminate between damage and other irregularities in the aforementioned residential-sized wind turbine blade are tested. Thus, the study is based on the same experimental setup as the one presented in [3].

2. Experimental setup

The approximately 800 mm polymer blade is reinforced with carbon fibre and composed of two separable shells by means of 25 bolts along the leading and trailing edges. Different damage conditions can be examined by untightening one or more bolts. In the present study, the damage indicated in figure 2 is analysed.

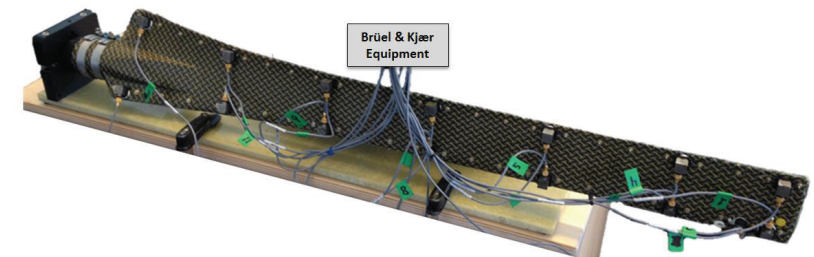


Figure 1. Experimental setup for OMA of the residential-sized wind turbine blade.

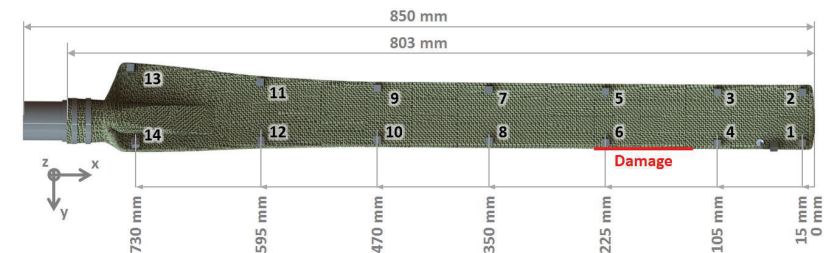


Figure 2. Dimensions of the blade, and location of the simulated damage.

The blade was subjected to unmeasured multi-impulse loads that were applied by hitting the structure randomly over the surface with a pencil. The response was captured by use of 14 equally spaced Brüel & Kjær uniaxial accelerometers, as illustrated in figure 2, which were measuring

perpendicularly to the surface. A sufficiently high sampling frequency of 8192 Hz was utilized throughout the experiments. The recordings were uninterrupted time series that were divided into smaller partitions in order to obtain more than one experiment from the different states.

3. Damage localization using the SDDL V method

The recordings from the reference state and the current state are mathematically described by means of system identification techniques. Here, the dynamic properties of the system are defined in a state matrix, A_c , and the output measurements are defined in an output matrix, C_c .

Generally, the state matrix and the output matrix contribute to establish the kernel of the transfer function which, as previously declared, is utilized for locating potential damages from changes between the two states. The basic form of the transfer function matrix is

$$G(s) = C_c(sI - A_c)^{-1}B_c + D_c, \quad (1)$$

where the input matrix, B_c , and the direct transmission matrix, D_c , are unknown since the system is purely stochastic with output-only measurements. An approach for estimating a fictive input is implemented from [2], hereby yielding

$$G(s) = R(s)D_c \quad (2)$$

where

$$R(s) = C_c A_c^{-2}(sI - A_c)^{-1} \begin{bmatrix} C_c A_c \\ C_c I \end{bmatrix}^\dagger \begin{bmatrix} I \\ 0 \end{bmatrix}, \quad (3)$$

with the dagger sign designating the Moore-Penrose pseudo-inverse. The direct transmission term, D_c , is assumed to be constant, because it is unaffected by the introduction of damage. The change in the transfer function matrix is then proportional to the change in $R(s)$, i.e.

$$\Delta G(s) \propto \Delta R(s) = R_d(s) - R_u(s). \quad (4)$$

The SDDL Vs, used as pseudo-loads, are estimated from the quasi-null space of $\Delta R(s)^T$ by singular value decomposition (SVD). In particular, the right singular vector associated with the smallest singular value is chosen to constitute the SDDL V.

The pseudo-loads are applied to a finite element (FE) model of the blade, which is based on an approximated 3D CAD geometry, discretized by equally sized first order shell elements. The model is calibrated against four experimentally-obtained natural eigenfrequencies and modes shapes of the undamaged blade. The pseudo-loads are applied at the same position and direction as the accelerometers.

4. Selection of s -values

The damage localization is not efficient for all s -values of the transfer function matrix. The guidance in [2] is to evaluate close, but not too close, to the poles of the system. Previous research by the authors of the present paper, see [3], reveals that a slight increase of an s -value corresponding to an identified system pole is applicable for damage localization, see figure 3.

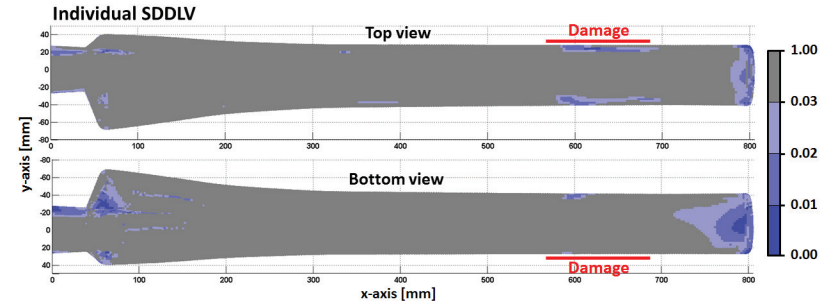


Figure 3. Stress field illustrating the normalized elemental mean von Mises stress for one SDDL V showing the appearance of the damage.

As shown in figure 3 and concluded in [3], the results of applying individual SDDL Vs imply that statistical evaluation can be included in the methodology to improve the damage localization. Such evaluation can be based on several experiments and/or several s -values. The s -value selection process is still a quite unexplored area of the SDDL V method, hence no strictly generalized guidance exists. The s -values can be chosen from infinite combinations of increments/decrements of the real and imaginary parts of an identified pole. In the present study, the two selection approaches depicted in figure 4 are tested, i.e. 10 s -values arranged in intervals of 2 to 20 % increment of the imaginary part and 28 s -values arranged in four branches of seven equally-spaced points from combinations of increments /decrements of the real and imaginary parts. It is noticed that the third flapwise bending mode is chosen, since it was most consistently excited during the experiments.

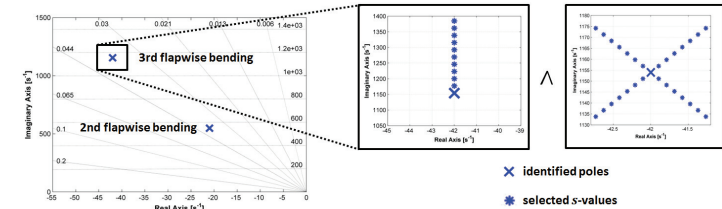


Figure 4. Selection of s -values based on the identified poles.

All the examined s -values are applicable for damage localization. However, the disturbance in the individual SDDL Vs is larger close to the pole.

The stresses evaluated along the four branches are not found to vary in any specific manner with regards to direction. Consequently, all experiments are evaluated for the 10 s -values to establish the basis of the statistical evaluation.

5. Methodology of statistical evaluation

Statistical evaluation using pattern recognition works by training a statistical baseline model from several healthy states followed by testing the current state against the baseline in order to capture any significant changes. For multivariate data, several outlier analysis methods based on, e.g., T^2 statistics, Q statistics and the Mahalanobis distance have been successfully applied for damage detection, see

e.g., [6] and [7]. The methods have the following of steps in common with the process of declaring the health of the structure:

- Train a baseline from the data measured in the healthy state.
- Determine a threshold defined by an appropriate quantile of the baseline.
- Test the current data using a pattern recognition technique for estimation of outliers.

In the present paper, it is tested whether some of these damage detection methods can be implemented in the SDDL V method to provide an effective statistical evaluation of the characteristic stress resultants obtained by applying the SDDL Vs to the FE model of the undamaged blade. The elements of the FE model are evaluated one by one, and the results are gathered in a three-dimensional matrix, with the structure depicted in figure 5.

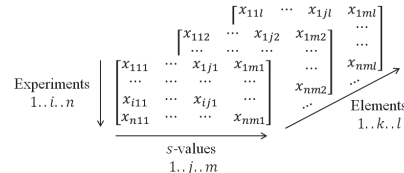


Figure 5. Suggestion for organizing the three-dimensional SDDL V data.

The outlier analysis methods used are based on Euclidean distance, T^2 statistics, and the Mahalanobis distance. The Euclidean distance is the distance between the current data from the experiment and the mean data from the experiments used for training, i.e.

$$d(x_{ik}) = \sqrt{\sum_{j=1}^m (x_{ijk} - \mu_{jk})^2}, \quad (5)$$

where $x_{ijk} \in \mathbb{R}$ is the stress resultant from the current experiment and $\mu_{jk} \in \mathbb{R}$ is the mean of the training data.

In the T^2 statistics-based method, the dimensionality is reduced to dimension r by use of principal component analysis (PCA). Hereby, the similarity between m characteristic stress resultants from the current experiment and the training data is derived through

$$T^2(x_{ik}) = (x_{ik} - \mu_{jk})P\Lambda^{-1}P^T(x_{ik} - \mu_{jk})^T \quad (6)$$

in which $P \in \mathbb{R}^{m \times r}$ and $\Lambda \in \mathbb{R}^{r \times r}$ contain, respectively, the eigenvectors and eigenvalues of the covariance matrix computed from the trained data. In this context, it is found that the dimensionality can be reduced to one-tenth of original size without losing any significant information.

The Mahalanobis-squared distance employs the inverse covariance matrix of the data, i.e.

$$D^2(x_{ik}) = (x_{ik} - \mu_{jk})\Sigma^{-1}(x_{ik} - \mu_{jk})^T, \quad (7)$$

where $\Sigma \in \mathbb{R}^{m \times m}$ is the covariance matrix of the training data.

The similarity measures calculated from any of the three above-mentioned methods need to be compared to a threshold calculated from data from the healthy structure. It has been chosen to calculate the threshold for each element matrix l based on the following steps:

- Test the first row of the undamaged data matrix and calculate the similarity using one of the three methods while applying the rest of the undamaged data matrix as the base.
- Repeat this for all vectors in the training matrix and sort the distances in descending order.
- The threshold is then equal to the value exceeded by 5 % of the similarity measures.

6. Results

The following results are based on 280 undamaged and 200 damaged experiments that are based on evaluation of 10 SDDL Vs in different points along the imaginary axis, as illustrated in figure 4. The variances of the experiments are reduced by taking the mean of 10 experiments and using these new vectors for the statistical evaluation. In this way, 28 undamaged and 20 damaged experiments are obtained, where the first 20 undamaged experiments are utilized for training the baseline. The previous research in [3] states that noise often appears in the area around the tip and root of the blade. Consequently, it is chosen to demonstrate the proposed statistical evaluation procedures for the locations shown in figure 6.

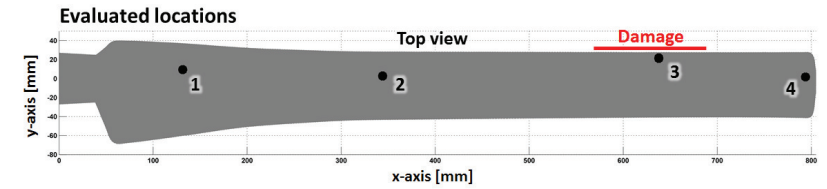


Figure 6. Location of elements utilized for inspection of the statistical evaluation.

Location 3 should, theoretically, be the only one to have distances higher than the calculated threshold in the damaged experiment, while distances at the other locations should be below the threshold. The results of the locations are presented in figure 7.

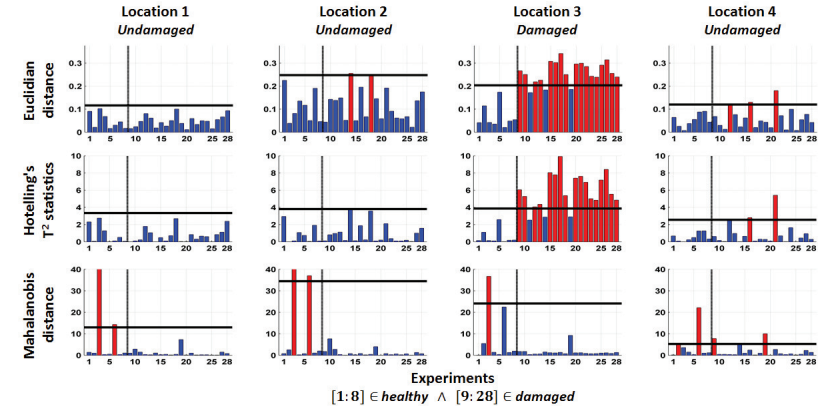


Figure 7. Statistical results from four locations by use of Euclidean distance, T^2 statistics, and Mahalanobis distance. The horizontal lines indicate the threshold and the vertical lines discriminate between the healthy experiments to the left and the damaged experiments to the right.

It appears that the two methods employing Euclidean distance and T^2 statistics detect the damage in location 3, without too many false alarms at any of the other locations. It is also noticed that the T^2 statistics-based method is slightly better than the Euclidean distance-based method. On the contrary, the Mahalanobis distance does not appear to be applicable to the measured data. This has been shown to improve if the data is taken as the mean of many more experiments, but that is a problem due to the limited amount of available data.

The Euclidean distance has been calculated for all elements using all of the damaged experiments, and in figure 8, the amount of experiments that yield a distance exceeding the threshold is presented as a percentage of all experiments. Evidently, the damage is clearly located and the amount of noise present in the plot is reduced significantly compared to the results from individual SDDLVs, see figure 3. The same procedure has been applied for the results of T^2 statistics. The results, which can be seen in figure 9, show how the damage is located practically perfect without any disturbances. It is noticed how the exact size of the damage is assessed, which is important information with respect to commercial applications.

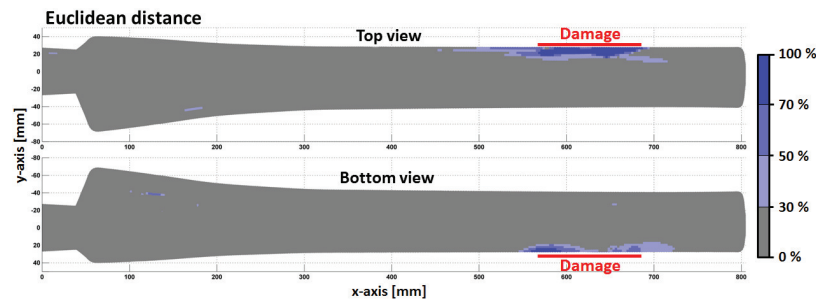


Figure 8. Statistical evaluation for SDDL-induced stress resultants using the Euclidean distance.

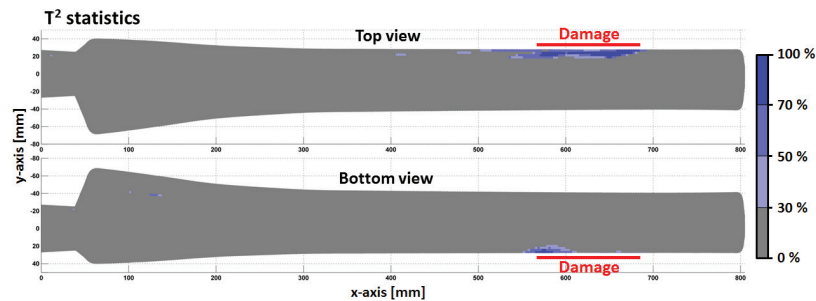


Figure 9. Statistical evaluation for SDDL-induced stress resultants using T^2 statistics.

7. Conclusion

The presented paper deals with the localization of damage in a residential-sized wind turbine blade by use of the SDDL method. The SDDL method has previously been demonstrated, by the authors, as capable of locating different damages in the aforementioned blade, although noise disturbances made it difficult to obtain unambiguous localization when using individual SDDLs. This is handled in the

present study by extending the SDDL method to contain a statistical evaluation yielding the final discrimination between damaged and undamaged areas.

The statistical evaluation is based on outlier analysis of the characteristic stress resultants, for a total of 10 s -values, in each element. The statistical patterns, i.e. mean vector and covariance matrix, are established on the basis of several experiments from the healthy state. Subsequently, data from the current state are tested against this pattern by alternate use of three different similarity measures, namely the Euclidean distance, T^2 statistics, and the Mahalanobis distance. While the Mahalanobis distance proves completely inapplicable, it is found that by employing either Euclidean distance or T^2 statistics, the damage is located unambiguously. Of the latter two approaches, T^2 statistics is preferable as it not only provides unambiguous localization but also assesses the size of the damage practically perfect.

Future research activities will deal with further improvement of the s -value selection process in order to establish a particular guidance. Moreover, a sensitivity study, in which the influence of damage size and location is examined, will be conducted.

8. Acknowledgement

The experimental part of the project was supported by the EUDP (Danish Energy Technology Development and Demonstration Programme) grant 64011-0084 "Predictive Structure Health monitoring of Wind Turbines". The authors also acknowledge Robert Flemming Mikkelsen who provided the blade for the experiments.

9. References

- [1] Ciang C C *et al* 2008 Structural health monitoring for a wind turbine system a review of damage detection methods *Meas. Sci. Technol.* **19** 122001
- [2] Bernal D 2010 Load vectors for damage location in systems identified from operational loads *J. Eng. Mech.* **136** 31-39
- [3] Johansen R J *et al* 2015 Damage localization in residential-sized wind turbine blade by use of SDDL method *Submitted to 11th International Conference on Damage Assessment of Structures*
- [4] Bernal D 2002 Load vectors for damage localization *J. Eng. Mech.* **128** 7-14
- [5] Van Overschee P and Moor B L R 1996 Subspace identification for linear systems theory implementation applications Kluwer academic publishers
- [6] Mujica LE *et al* 2010 Q-statistic and T^2 -statistic PCA-based measures for damage assessment in structures *Structural Health Monitoring* **10** 539-553
- [7] Balsamo L *et al* 2014 Damage Detection Using Large-Scale Covariance Matrix *Structural Health Monitoring Volume 5 Proceedings of the 32nd IMAC* **10** 89-97

Damage localization in a residential-sized wind turbine blade by use of the SDDLTV method

R.J. Johansen¹, L.M. Hansen¹, M.D. Ulriksen¹, D. Tcherniak² and L. Damkilde¹

¹Dept. of Civil Engineering, Aalborg University, Niels Bohrs Vej 8, Esbjerg, Denmark

²Brüel & Kjær Sound & Vibration Measurement A/S, Skodsborgvej 307, Nærum, Denmark

E-mail: rjohan10@student.aau.dk, lhansel0@student.aau.dk, mdu@civil.aau.dk, dmitri.tcherniak@bksv.com, lda@civil.aau.dk

Abstract. The stochastic dynamic damage location vector (SDDLTV) method has previously proved to facilitate effective damage localization in truss- and plate-like structures. The method is based on interrogating damage-induced changes in transfer function matrices in cases where these matrices cannot be derived explicitly due to unknown input. Instead, vectors from the kernel of the transfer function matrix change are utilized; vectors which are derived on the basis of the system and state-to-output mapping matrices from output-only state-space realizations. The idea is then to convert the kernel vectors associated with the lowest singular values into static pseudo-loads and apply these alternately to an undamaged reference model with known stiffness matrix. By doing so, the stresses in the potentially damaged elements will, theoretically, approach zero. The present paper demonstrates an application of the SDDLTV method for localization of structural damages in a cantilevered residential-sized wind turbine blade. The blade was excited by an unmeasured multi-impulse load and the resulting dynamic response was captured through accelerometers mounted along the blade. The static pseudo-loads were applied to a finite element (FE) blade model, which was tuned against the modal parameters of the actual blade. In the experiments, an undamaged blade configuration was analysed along with different damage scenarios, hereby testing the applicability of the SDDLTV method.

1. Introduction

Research activities on vibration-based structural health monitoring (SHM) systems for wind turbine blades have been growing rapidly over the last two decades, see, e.g., [1]. The most common approach is to compare collected data from a reference state, which is typically a healthy one, and the current state. The current state is potentially damaged if it differs significantly from the reference state. A typical partition of the damage identification process was suggested in [2] and contains the following four steps: 1) detection, 2) localization, 3) assessment and 4) consequence. There are plenty of well-documented methods for damage detection, see, e.g., [3], thus the present paper concentrates only on the damage localization process.

In [4], Bernal presented the damage location vector (DLV) method, which utilizes the null space of the changes in the flexibility matrix from a pre- and post-damaged structure to locate the damage. The method assumes that the system behaves linearly in both the pre- and post-damaged states. The vectors that form the basis of the null space are designated as DLVs, and they contain usable information about the location of the damage. It is proved in [4] that by applying a DLV as loads to the undamaged structure, the stresses in the damaged elements approach zero.

The DLV method only includes static properties of the system. However, it was lately extended to include the dynamics of the system, namely the dynamic damage location vector (DDLTV) method [5]. Here, the dynamics of the system is included by applying the changes in transfer function matrix, instead of changes in flexibility matrix, to obtain the static pseudo-loads [4].

The dynamic version is further extended to an output-only measurements scenario, which is designated as the stochastic dynamic damage location vector (SDDLTV) method [6]. Thus far, the SDDLTV method has primarily been tested in the context of numerical models of simple truss and frame structures, see, e.g., [6].

In the present paper, the SDDLTV method is applied to locate damages in a residential-sized wind turbine blade tested experimentally.

2. Test setup

To demonstrate the applicability of the SDDLTV method, experiments are performed on a cantilevered residential-sized wind turbine blade, see figure 1. Specifically, the structural vibration responses are measured for an undamaged and two damaged cases subjected to unmeasured multi-impulse loading conducted by tapping the blade with a pencil. For each case, a state space model, which forms the basis for determination of the pseudo-loads, i.e., SDDLTVs, is estimated from the collected acceleration data.

The blade depicted in figure 1 is about 800 mm long and constructed from a composite material, namely carbon-fibre-reinforced polymer. The blade was originally constructed for another project [7], and later modified for the purpose of testing different SHM methods. The blade is separable into two shells, which are assembled by means of 25 bolts along the leading and the trailing edges. Different damage conditions can be examined by untightening one or more bolt(s).

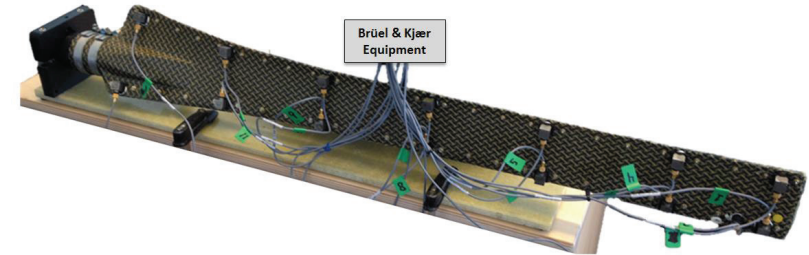


Figure 1. Experimental setup for test on the residential-sized wind turbine blade.

The blade is excited by hitting the structure randomly over the surface in order to simulate operational conditions, i.e., only the output vibrations are collected. The vibrations are captured by use of 14 equally spaced Brüel & Kjær Type 4507-B-004 uniaxial accelerometers along each edge of the blade, as illustrated in figure 1 and figure 2. The accelerometers are mounted, such that they measure perpendicularly to the surface; thus they do not measure in exactly the same direction.

For each experiment, the sampling frequency was set to 8192 Hz, since a sufficiently high sampling frequency is required to ensure that the dynamics of the system is captured properly. The recordings have duration of 200 seconds and are later divided into smaller partitions in order to obtain more than one experiment.

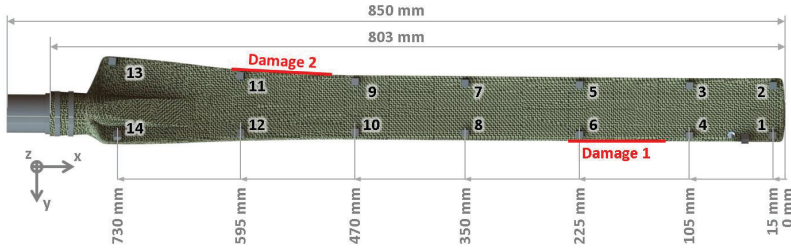


Figure 2. Dimensions of the blade and the locations of the two simulated damages.

The location and size of the two separately simulated areas of damages are shown in figure 2. Both of the damage areas are simulated with three bolts untightened, but kept in the blade to avoid mass changes between the experiments.

3. System identification

System identification techniques are used to mathematically describe the captured acceleration data. In this context, subspace identification is found to be applicable and the fundamental principle of this method is a state-space representation based on the output-only continuous time state-space model, see, e.g., [8].

$$\dot{x}(t) = A_c x(t) + w_k, \quad (1)$$

$$y(t) = C_c x(t) + v_k, \quad (2)$$

where $A_c \in \mathbb{R}^{n \times n}$ is the state/system matrix for the system containing the dynamic properties, $C_c \in \mathbb{R}^{m \times n}$ is the output matrix, while $x(t) \in \mathbb{R}^n$ and $y(t) \in \mathbb{R}^m$ are the state vector and the output vector. The two last vectors, $w_k \in \mathbb{R}^n$ and $v_k \in \mathbb{R}^m$, are unmeasured stationary noise/disturbances related to the process and the output, respectively. The sizes of the matrices and vectors depends on the order, n , of the state-space model and the number of outputs, m . The system identification is performed using MATLAB System Identification Toolbox, namely using N4SID. For each of the three system states, several state-space models are derived on the basis of different segments of the data. A total of 25 models are derived for each of the two areas of damage and used for estimating a corresponding SDDL. V.

4. SDDL method

The SDDL method is, as previously declared, based on the change in transfer function matrix for systems where the input is unknown and, as such, the transfer function matrix is inaccessible. Instead, the estimated state matrix and the output matrix are applied to estimate vectors from the kernel of the change in transfer function matrix. The transfer function is basically the relation between the output, $Y(s)$, and input, $F(s)$, in the Laplace domain, i.e.,

$$Y(s) = G(s)F(s) \quad (3)$$

where

$$G(s) = C_c(sI - A_c)^{-1}B_c + D_c. \quad (4)$$

The input matrix, B_c , and the direct transmission matrix, D_c , are not directly used for the estimation of the SDDL. V.s, as clarified in the following.

This basic form of the transfer function (4) is not applicable for stochastic systems with output only. In [5], an approach to estimate a fictive input from the state matrix and the output matrix is

documented. The idea is to use the fact that there should always be a correlation between the input and the output. The approach ends up in the following:

$$G(s) = R(s)D_c \quad (5)$$

where

$$R(s) = C_c A_c^{-p} (sI - A_c)^{-1} H_p^\dagger L, \quad (6)$$

with the value of the exponent $p = 0, 1, 2$, depending on whether the measurements are displacements, velocities or accelerations. The terms estimating a fictive input to the system are defined by

$$H_p = \begin{bmatrix} C_c A_c^{(1-p)} \\ C_c A_c^{(-p)} \end{bmatrix} \quad (7)$$

and

$$L = \begin{bmatrix} I \\ 0 \end{bmatrix}, \quad (8)$$

where the dagger sign in equation (6) designates, that the Moore-Penrose pseudo-inverse is applied to H_p . The direct transmission term D_c is assumed to be a constant, since the 'feedthrough' is assumed to be non-changing and thus not affected from the system properties if damage occurs. The change in transfer function is then proportional to the change in $R(s)$, i.e.,

$$\Delta G(s) \propto \Delta R(s) = R_d(s) - R_u(s). \quad (9)$$

The SDDL. V.s are found from the quasi-null space of $\Delta R(s)^T$ by singular value decomposition (SVD), hence yielding

$$\Delta R(s)^T = U \Sigma V^T, \quad (10)$$

in which each of the singular values contained in Σ has a corresponding left singular vector in U and a right singular vector in V . The right singular vector associated with the smallest singular value is used as pseudo-loads.

The damage localization is not efficient for all s -values of the quasi-null space of $\Delta R(s)$. Proper ones are selected on the basis of the response characteristics of the system. This information is available when solving an eigenvalue problem of the state matrix. Only the s -value(s) near the poles of the system are selected for the $\Delta R(s)$, hereby introducing a modal truncation of the system. The applied s -values are increased by 1% since studies in context of this paper confirm that the value must be slightly different from the poles of the system, as stated in [5]. A more robust selection may exist and the selection is further discussed by the authors in [9].

5. Finite element model

The pseudo-loads obtained in section 4 are applied to the finite element (FE) model of the blade, in which elements containing stresses approaching zero are potentially damaged according to the (-)DLV approach. The model is based on an approximated 3D CAD geometry and is discretized by equally sized first order shell elements. The FE model is fixed at the blade root, i.e., all displacements and rotations are equal to zero, in order to simulate the clamping mechanism from the experimental setup shown in figure 1. It is calibrated against the first four experimental natural eigenfrequencies and mode shapes obtained from operational modal analysis (OMA) of the undamaged structure, see table 1. The bolts and accelerometers are not included in the model; however, the increased mass is taken into consideration by calibrating the density of the material.

Table 1. Comparison of eigenfrequencies between OMA and calibrated FE model

	Description	OMA [Hz]	Calibrated FE model [Hz]
Mode 1	1 st flapwise bending	15.9	16.0
Mode 2	1 st edgewise bending	none ^a	48.3
Mode 3	2 nd flapwise bending	87.9	88.2
Mode 4	1 st torsional	109.0	109.2
Mode 5	3 rd flapwise bending	183.3	182.8

^a was not found during the experiment.

As previously mentioned, the accelerations are measured perpendicular to the surface, which consequently defines the direction of the applied pseudo-loads. The local coordinate systems depicted in figure 3 illustrate the perpendicular direction, namely the z-axis, for each of the 14 accelerometer positions. The pseudo-loads are applied over an area corresponding to the size of the accelerometers in order to avoid stress disturbance at the specific positions.

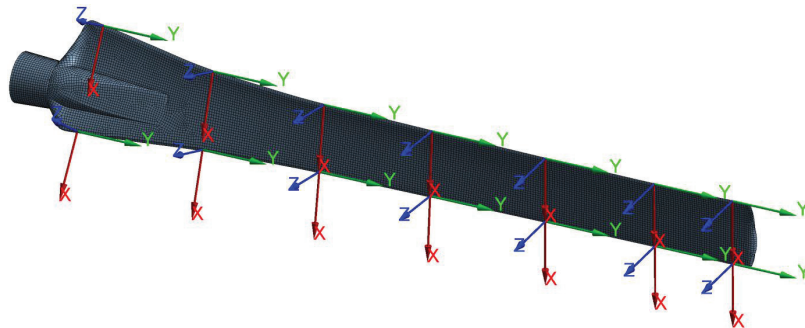


Figure 3. Discretized FE model of the blade and local coordinate systems corresponding to the orientation of the 14 accelerometers.

In the post-processing, the elemental mean von Mises stresses are chosen for locating the damaged area, since this particular stress type contains information from all stress components and is thereby applicable for different load cases, e.g., shearing and bending.

6. Summary of methodological process

A summary of the steps in the damage localization process presented in this paper is outlined in order to make a clear overview of the method before presenting the results.

- Preparation:
 - Collect reference measurements from a healthy state.
 - Perform a system identification of the reference measurements in order to estimate $R_{ii}(s)$.
 - Calibrate an FE model based on experimental modal parameters obtained using OMA.

- Damage localization:

- Perform system identification of the current measurements in order to estimate $R_d(s)$.
- Perform SVD on $\Delta R(s)^T$ for a proper s -value in order to estimate the SDDL V .
- Apply the SDDL V as static pseudo-loads to the calibrated FE model and compute stresses, e.g., von Mises stresses.
- The stresses approaching zero are identifying damaged location(s).

7. Results

By examining the SDDL V -induced stress fields for the two analysed cases, it is generally found that the global x-directional location of the areas of damage are estimated accurately and consistently, whereas the y-directional location can vary depending on the specific SDDL V applied.

The system identification of the experiments reveals that the poles corresponding to the 2nd and 3rd flapwise bending modes are the most excited and consequently only poles associated with these modes are used to estimate the SDDL V . The s -value used for determination of the SDDL V is taken as the value of the current pole increased by 1 %, as described in section 4.

In figure 4, the stress field from one SDDL V is presented for Damage 1. Here, the damage is located between 560-680 mm from the root at the leading edge, see figure 2. The stress field in figure 4 approaches zero stress in the damaged area, but also at the root and at the tip.

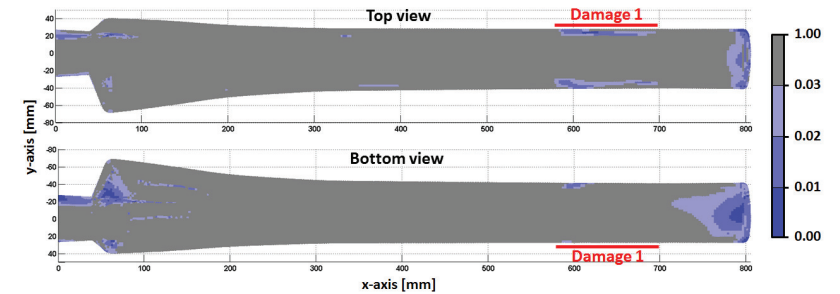


Figure 4. Stress field illustrating the normalized elemental mean von Mises stress for one SDDL V showing the appearance of Damage 1.

These disturbances and lack of precision for localization in the y-direction would most likely disappear if more sensors were used for monitoring the vibrations. The amount and location of this noise are varying for all SDDL V s, but the noise often appears at the tip and root of the blade. The disturbance at the root is understandable, as the geometry is varying more in this area and the number of sensors is small. At the tip, it is clear that noise will appear since the area from sensor 1 and 2 to the end of the blade is only affected a little by the loads applied to the structure.

Examination of SDDL V s for Damage 2 has confirmed many of the observations from Damage 1. Some SDDL V s locate the damage clearly, while others contain mostly noise. Damage 2 is located 180-300 mm from the root at the trailing edge, which defines the maximum damage size based on the same conditions as described for Damage 1. One stress field for Damage 2 is illustrated in figure 5, where the damage is clearly localized, albeit with disturbances at the root and at the tip. In some situations it is hard to distinguish between actual damage and disturbances when observing the stress field for a single SDDL V . However, examination of several SDDL V s has revealed that the damaged location is the only area in which the stresses always approach zero. An informative overview of examined SDDL V s from different operational experiments is listed in table 2. The table, which is

based on 25 experiments for each of the two damage scenarios, shows consistency in localization of the damage, even when the disturbance is changing.

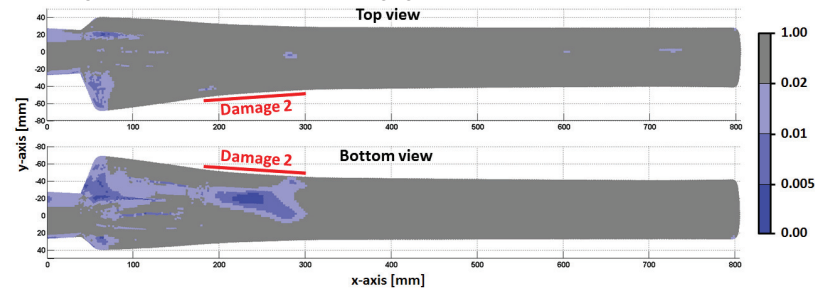


Figure 5. Stress field illustrating the normalized elemental mean von Mises stress for one SDDL V showing the appearance of Damage 2.

Table 2. SDDL V-based damage localization results for two damage types.

	Experiments	Localized			Noise root			Noise tip		
		Yes	No		High	Low	None	High	Low	None
Damage 1	25	23	2	10	8	7	10	3	12	
Damage 2	25	25	0	8	10	7	13	0	12	

A clear explanation of the varying precision of the SDDL Vs throughout the examination of the two areas of damage has not been observed. However, it has been observed that SDDL Vs based on s -values corresponding to the second flapwise bending mode and the third flapwise bending mode yield less stress disturbance than those for the remaining identified blade modes for Damage 1 and Damage 2, respectively. It has been noticed during OMA, that these two modes are excited significantly better than other higher modes.

From the experiments visualized in figure 4 and figure 5 and the results listed in table 2, it is clear that the stresses in the damaged areas approach zero, while the zero stresses elsewhere occur rather randomly. This observation suggests that one way of reducing the level of disturbance, in order to separate damages from noise, is to apply a statistical evaluation on a large set of stress fields obtained from different SDDL Vs. This is treated in [9].

8. Conclusion

The presented paper deals with localization of damage in a residential-sized wind turbine blade by use of the SDDL V method. The method employs the vectors from the quasi-null space of the damage-induced change in transfer function matrix as static pseudo-loads, which are applied to a known model of the undamaged system. The damage is then, suggestively, found at locations where the stresses are approaching zero.

The SDDL V method is demonstrated as capable of locating different areas of damage on both the leading and trailing edges of the blade. The stress field generally approaches zero in the location of the damage. However, noise is, in most cases, present, making it difficult to obtain unambiguous localization. The disturbances primarily appear at the tip and at the root of the blade; thus a way to reduce these noise contributions could be to apply a statistical approach in which several SDDL V-induced stress fields are evaluated in a combined manner. This is a part of future research activities.

Further future research activities will deal with the selection of s -value(s). In the present study, it has been set to be a 1 % increment of the s -value corresponding to the consistently identified pole. This procedure has been chosen somewhat randomly, and it could therefore be an interesting study to apply different s -values around the pole of interest in order to see, if any general approach can be established for the choice of s -values, hereby increasing the reliability and robustness of the SDDL V method.

9. Acknowledgement

The experimental part of the project was supported by the EUDP (Danish Energy Technology Development and Demonstration Programme) grant 64011-0084 "Predictive Structure Health monitoring of Wind Turbines". The authors also acknowledge Robert Flemming Mikkelsen who provided the blade for the experiments.

10. References

- [1] Ciang C C *et al* 2008 Structural health monitoring for a wind turbine system a review of damage detection methods *Meas. Sci. Technol.* **19** 122001
- [2] Rytter A 1993 Vibration based inspection of civil engineering structures Ph.D. Thesis Aalborg University Denmark
- [3] Farrar C R *et al* 2001 Vibration-based structural damage identification *Philosophical Transactions: Mathematical, Physical and Engineering Sciences* **359** 131-149
- [4] Bernal D 2002 Load vectors for damage localization *J. Eng. Mech.* **128** 7-14
- [5] Bernal D 2007 Damage localization from the null space of the transfer matrix *AIAA Journal* **45** 374-381
- [6] Bernal D 2010 Load vectors for damage location in systems identified from operational loads *J. Eng. Mech.* **136** 31-39
- [7] Bottoli F and Pignatti L 2001 Design and processing of structural components in biocomposite materials rotor blade for wind turbine cars M.Sc. Thesis Risø DTU
- [8] Van Overschee P and Moor B L R 1996 Subspace identification for linear systems theory implementation applications Kluwer academic publishers
- [9] Hansen L M *et al* 2015 Statistical evaluation of characteristic SDDL V-induced stress resultants to discriminate between damaged and undamaged elements *Submitted to 11th International Conference on Damage Assessment of Structures*

Damage assessment for wind turbine blades based on a multivariate statistical approach

David García ¹, Dmitri Tcherniak ² and Irina Trendafilova ¹

¹Mechanical & Aerospace Engineering, University of Strathclyde, 75 Montrose street, G11XJ, Glasgow, UK

²Bruel & Kjaer Sound & Vibration Measurement A/S, Skodsborgvej 307, Nærum, Denmark

E-mail: david.garcia@strath.ac.uk

Abstract. This paper presents a vibration based structural health monitoring methodology for damage assessment on wind turbine blades made of composite laminates. Normally, wind turbine blades are manufactured by two half shells made by composite laminates which are glued together. This connection must be carefully controlled due to its high probability to disbond which might result in collapse of the whole structure. The delamination between both parts must be monitored not only for detection but also for localisation and severity determination. This investigation consists in a real time monitoring methodology which is based on singular spectrum analysis (SSA) for damage and delamination detection. SSA is able to decompose the vibratory response in a certain number of components based on their covariance distribution. These components, known as Principal Components (PCs), contain information about of the oscillatory patterns of the vibratory response. The PCs are used to create a new space where the data can be projected for better visualization and interpretation. The method suggested is applied herein for a wind turbine blade where the free-vibration responses were recorded and processed by the methodology. Damage for different scenarios *viz* different sizes and locations was introduced on the blade. The results demonstrate a clear damage detection and localization for all damage scenarios and for the different sizes.

1. Introduction

Vibration-based Structural Health Monitoring (VSHM) has been widely used for damage assessment in a multitude of engineering structures based on the features of the vibration response measured along the structure [1, 2]. Nowadays, VSHM became a trend in the future techniques for monitoring the health of modern civil engineering and aerospace engineering among many others sectors. Indeed, the growth of the off-shore wind turbines place VSHM at the forefront of the contemporary research. The visual inspections of these structures are dangerous, expensive and it might requires a tedious planning, which can be particular and different for each case. The idea of develop an on-line remote system to monitor the health of the structure is the great interest for these structures.

Although failure can happen in any structural component of the wind turbine, one of the most likely parts are the turbine blades [3]. One of the most common failure mechanism in turbine occurs in the glued interface between the two shell parts of the blade. This failure is relative small compare with the total dimension of the blade and it can growth until collapse the entire part. Therefore, it is very important to detect, control and localise this kind of failures.

VSHM can be divided in two groups: model base methodologies [4] and non-model based methodologies [5]. Model based methodologies requires the existence of a model which is able to describe the behaviour of the system. However, the second group is based on pure data-driven techniques to create a reference system space where compare the changes that happen in the system.

Thus the aim of this study is to apply a data-driven technique based on Singular Spectrum Analysis (SSA). This technique is able to separate the stationary and non-stationary components from a vibratory response [6]. SSA divides the data signal in blocks with the same mean and variance over the time. Those blocks called Principal Components (PCs) are used to reduce the dimension of the system by considering the most relevant for each case of study. The projection of the reconstructed signals based on the importance of the PCs is used as a feature for damage detection and localization [7].

The papers is organized as follows: the first sections describe the methodology implemented and the following sections describe the basis and results of the application case.

2. Stochastic subspace approach for damage assessment

The stochastic subspace approach presented in this paper is an output-only measurement damage assessment method. The methodology is performed to compare two data sets: one from the undamaged system which is considered as baseline (reference data) and another from the damage system (observation data). The approach is based on Singular Spectrum Analysis (SSA) which is an extension of Principal Component Analysis able to decompose and compress the non-independent values such as time series in their covariance distribution. Stochastic subspace methods are efficient tools for system identification and hence for damage assessment [8, 9]. The projection of the observation data onto the new space reduces the distances between elements from the same system/category and on the same time the distances from different systems/categories increase.

2.1. Step 1: Baseline covariance subspace model

The discrete time-acceleration measurements taken from the undamaged system are considered as a reference data to create the new subspace.

The time-acceleration signals are represented in the frequency domain. The amplitudes values of the frequency spectrum are arranged into a vector as $\mathbf{z} = (z_1, z_2, \dots, z_N)$. The new vector is embedding in a Hankel matrix form as bellow

$$\tilde{\mathbf{Z}}^i = \begin{pmatrix} z_1^i & z_2^i & z_3^i & \dots & z_w^i & \dots & z_W^i \\ z_2^i & z_3^i & z_4^i & \dots & z_{w+1}^i & \dots & z_{W+1}^i \\ z_3^i & z_4^i & z_5^i & \dots & z_{w+2}^i & \dots & z_{W+2}^i \\ \vdots & \vdots & \vdots & \dots & \vdots & \dots & \vdots \\ z_4^i & z_5^i & z_6^i & \dots & z_{w+3}^i & \dots & \vdots \\ z_5^i & z_6^i & \vdots & \dots & \vdots & \dots & z_N^i \\ z_6^i & \vdots & \vdots & \dots & z_N^i & \dots & 0 \\ \vdots & \vdots & z_N^i & \dots & 0 & \dots & 0 \\ \vdots & z_N^i & 0 & \dots & 0 & \dots & 0 \\ z_N^i & 0 & 0 & \dots & 0 & \dots & 0 \end{pmatrix} \quad (1)$$

where W is the window length and $i = 1 \dots M$ the number of realisations considered to build the new subspace. Each M realisation is performed in the same Hankel matrix form. The group of embedding matrices constructs a large matrix which contains the information about the oscillatory patterns of the undamaged system as $\tilde{\mathbf{Z}} = (\tilde{\mathbf{Z}}^1, \tilde{\mathbf{Z}}^2, \dots, \tilde{\mathbf{Z}}^M)$. The computation

of the covariance matrix of $\tilde{\mathbf{Z}}$ distributes the information contained in the dynamics of the undamaged system in vectors with the same mean and variance over the frequency spectrum. These vectors are namely as Empirical Orthogonal Functions (EOFs).

The EOFs are obtained by the eigen-decomposition of the covariance matrix $\mathbf{C}_{\tilde{\mathbf{Z}}}$. The eigenvalues λ_k are then ordered in the diagonal matrix $\mathbf{\Lambda}_{\tilde{\mathbf{Z}}}$ in decreasing order and the matrix $\mathbf{E}_{\tilde{\mathbf{Z}}}$ contains their corresponding eigenvectors ρ_k written as columns.

$$\mathbf{E}'_{\tilde{\mathbf{Z}}} \mathbf{C}_{\tilde{\mathbf{Z}}} \mathbf{E}_{\tilde{\mathbf{Z}}} = \mathbf{\Lambda}_{\tilde{\mathbf{Z}}} \quad (2)$$

The EOFs are considered as the basis for the new subspace. The projection of the reference data onto the new basis yields the Principal Components (PCs) as

$$\mathbf{A} = \tilde{\mathbf{Z}} \mathbf{E}_{\tilde{\mathbf{Z}}} \quad (3)$$

The dynamic response is then distributed in $W \times M$ number of PCs placed into the matrix \mathbf{A} . The PCs are allocated in the matrix \mathbf{A} in decreasing order from the ones which contain more percent of the total variance to the components with the lowest percent of variance.

The dynamic response is then reconstructed by the projection of the PCs onto the EOFs. For a given set of indices \mathcal{K} corresponding to the set of PCs contained in \mathbf{A} , the Reconstructed Components (RCs) are obtained as is shown in the equation below

$$R_{m,n}^k = \frac{1}{W} \sum_{w=1}^W A_{n-w}^k E_{m,w}^k \quad (4)$$

where k -eigenvectors give the k^{th} RC at n -frequency between $n = 1 \dots N$ for each m -realisation ($m = 1 \dots M$) which was embedded in a w -lagged vectors with the maximum W -length. The RCs are placed in the \mathbf{R} matrix.

The RCs are the new reconstructed signals based on the percent of variance contained in the PCs used in their reconstruction. Each RC contains different variance of the total reference signal (original signal). Therefore, the RCs can be used separately and independently for the damage assessment methodology.

2.2. Step 2: Subspace projection. Damage index

The RCs are well separated signals reconstructed by the components which contain the same mean and variance over the whole frequency spectrum [10]. Therefore, the new subspace allows us to project the data from the damaged systems (observation data) onto the new subspace based on the undamaged system. The representation of the data onto the new space is performed by using an inner-product between the RCs and the observation data. This projection is able to characterise the vibratory response into a single point as

$$T = \langle \mathbf{O}, \mathbf{R} \rangle \quad (5)$$

where \mathbf{O} is the observation data matrix and the matrix \mathbf{R} is the set of RCs, which correspond to the undamaged system (reference data).

2.3. Step 3: Dimensionality magnitude estimation

The data obtained in the projection onto the new space can be utilised as damage index because it contains the information of the dynamic response. The damage index T is a vector which contains the inner product of the observation data in each RCs. As mention in the previous sections, each RC contains a certain percent of variance from the signals of the reference data. The first RCs contains more variance than the rest of RCs.

Computing the Mahalanobis distance (MD) between the projection of the observation data \mathbf{T}_0 and the projection of the reference data \mathbf{T}_z onto the new space as the following equation,

$$\mathbf{D}_M(T_z) = \sqrt{(\mathbf{T}_0 - \mu_z)^T \mathbf{S}_z^{-1} (\mathbf{T}_0 - \mu_z)} \quad (6)$$

provides a magnitude used for system identification and hence for damage assessment. $\mathbf{D}_M(T_z)$ is the Mahalanobis distance to the reference data set \mathbf{T}_z , \mathbf{T}_0 is the observation data, μ_z is the means of the \mathbf{T}_z and \mathbf{S}_z is the standard deviation of \mathbf{T}_z .

Theoretically, the dimension of the \mathbf{D}_M can be as much as the dimension of the projection vector T . However, the dimension of \mathbf{D}_M is best established by inspecting results from the PCs decomposition of the reference system.

3. Application for a wind turbine blade

3.1. Description of the experiment

For testing different damage detection and localization algorithms, a dedicated test setup was created. The test object is a 80 cm long rotor blade, which was created in the frame of DTU Wind Car project at Wind Energy department of Technical University of Denmark. The blade consists of two parts: the pressure and suction sides are manufactured separately from composite materials ([11] details the blade design and implementation). In Wind Car projects, the parts are glued together, which very much resembles the manufacturing process of real wind turbine blades. For the described test setup, the parts were squeezed together by means of a big number of small bolts, placed along the leading and trailing edges of the blade approximately 25 mm from each other. This solution greatly simplifies introducing a damage into the blade: one shall simply loose some of the bolts; this way, it is easy to control damage location and size. For damage "repair", the loosen bolts need to be re-tightened. This approach allows us modelling only one type of damage: leading and trailing edge de-bonding, which are quite common for many types of real blades. However, there are other types of damages, which cannot be modelled with the current setup.

For the experiment, the blade was clamped from the root end, in a similar way as it is supposed to be mounted on the rotor hub (Figure 1(a)). During the tests, the blade was artificially excited by a small electro-mechanical actuator mounted close to the root. The actuator is driven by a signal generator. This setup enables periodic highly repeatable force impulses being introduced into the blade structure. The response due to the actuator strikes was being measured by an array of accelerometers. Fifteen B&K Type 4507 B 4 monoaxial accelerometers were used, seven were mounted along the leading edge, another seven along the trailing edge, and one in a vicinity of the actuator (Figure 1(b)). The data acquisition was conducted using B&K Pulse LAN-Xi modules Type 3053 - B - 120 and 3160 - A - 042, the latter also includes the signal generator. In total, 16 channels were recorded: 15 acceleration signals and the driving signal from the signal generator, the latter to facilitate triggering during the post-processing.

3.2. Data collection

The most of damage detection and localization algorithms heavily rely on statistics in order to improve the robustness and detection rate and minimize the number of false alarms. The described algorithm belongs to the class of unsupervised learning, i.e. the algorithm is trained on healthy state (or also called reference state) of the test object, and the damage state is associated with a deviation from the normal state. First, the statistics for the reference state is collected: when all bolts are tightened, a series of approximately hundred actuator hits is recorded. Then a damage was introduced and expanded. The presented study uses the measurements from three damages: Damage 1 leading edge tip section; Damage 2 trailing edge middle section; Damage 3 leading edge root section. All three damages were introduced following the same scenario: first



(a) Disposition of the bolts on the blade and blade support



(b) Distribution of the accelerometers along the blade

Figure 1. Experiment test ring for the wind turbine blade

only one bolt was loosened, and a series of new measurements (corresponding to about 60 hits) is conducted. Then a neighboring bolt was loosen, which modeled damage progression. Finally, the third bolt was untightened. After the state corresponding to the biggest damage was measured (namely, three loosened bolts for Damage 1 and Damage 2 cases and four bolts for Damage 3 case), all bolts were re-tightened, thus the structure was brought to the undamaged state, again. We did not tested the cases with more than one damage. It is important to note that, when loosen, the bolts were not removed from the blade, thus the total mass of the structure kept unchanged. The soft rubber washers keep the bolts fixed in the holes, thus preventing the bolt rattling. Doing this, we tried to avoid any possible side effects of loosening the bolts, which the algorithm can confuse with the changes in local structural stiffness, which we are trying to detect.

3.3. Damage detection

The discrete time-acceleration measurements (free-decay responses), from the undamaged blade, were recorded and processed by the methodology explained in §2. The new subspace based on the undamaged blade was used as reference state where the vibratory responses measured from the different damage locations and sizes can be compared. Ten signals were used to build the new subspace and the window length was selected as $W = 10$. The reason to choose this window length follows similar considerations than [12]. The statistical model was created by using only the undamaged responses for one sensor. The signals from the damaged blades were recorded form the same sensor and consequently projected onto the new subspace. This procedure was separately repeated for each sensor.

Figure 2 represents the projection of undamaged and damaged responses characterised in a single point onto the new subspace. Each damage location was studied separately. For the case of Damage 1 (damage located on the tip of the blade) and Damage 2 (damage located on the middle of the leading edge) can clearly be observed that the values cluster within groups of the same

category. The distances from elements of the same category reduces their distances meanwhile elements from different categories increase the distances from the other categories groups (see Figure2(a) and 2(b)). Therefore, the detection between undamaged and damaged blades is achieved as well as the detection between different damage sizes. However, the clustering effect in the case of the Damage 3 (damage located on the trailing edge close to the support) does not clearly differentiate between different damage sizes. Although, the detection between damaged and undamaged is clearly achieved (see Figure2(c)).

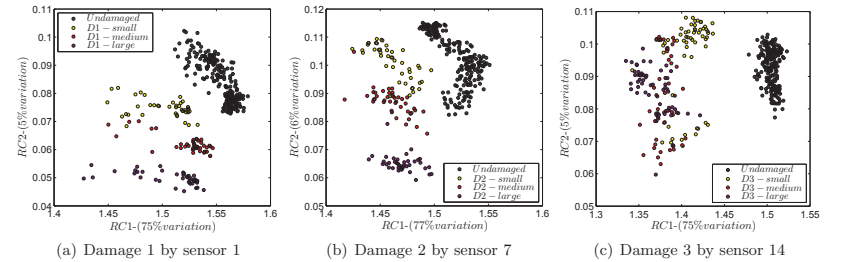


Figure 2. Projection of all damages location and sizes (small, medium and large) onto the new sub space based on undamaged structure.

In order to quantify the results obtained in the projection figures above, the MD was computed to measure the distances between undamaged elements to the different damages locations and sizes. Figure 3 shows separately the MD for each damage location. It can be observed within the three damage locations that the damaged was successfully detected. Also, the progression of the damaged is well observed even for the case of Damage 3 (Figure 3(c)) where the cluster classification in Figure 2(c) was not very well achieved. Figure 3(a) and 3(b) demonstrate that as much as the damage increases the distance from the undamaged state also increase. Moreover, the distance between different sizes of the damages is also distinguishable. For the three cases the damage progression is perfectly described.

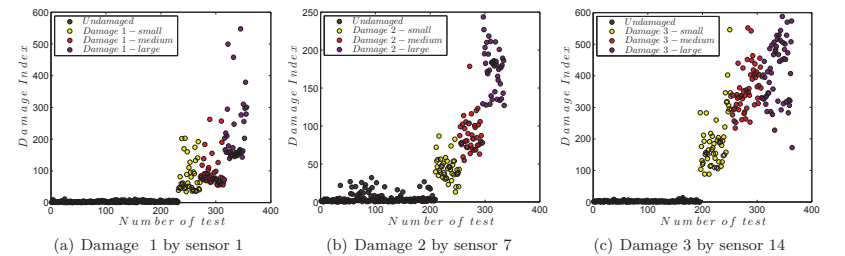


Figure 3. Mahalanobis distance from the undamaged scenario to different damage sizes (small, medium and large) for each damage location.

3.4. Damage localization

Other important aspect to consider for VSHM is the localization of the damage along the blade. The damage index described in the previous sections and the localisation of the sensors along the blade are correlated to determinate a potential location of the damage. The sensors which are located close to the damage are more prone to detect such damage [13]. Therefore, the sensors which obtain larger value of MD index indicates that damage occurs close to the region where such sensor is located.

Figure 4(a) shows the sensitivity of the sensors on the Damage 1. It can be observed that the largest values of the MD occurs between sensors 1-5. These sensors are located around the area close to the tip of the blade which is the region where Damage 1 was performed. Similarly, Figure 4(b) represents the sensitivity to the Damage 2. It can be observed that although damage 2 occurs between sensor 5 and 7, the sensors around the area are more sensitive to damage. Finally, Figure 4(c) shows clearly the sensitivity of the sensor 12 on the Damage 3. The area where Damage 3 occurs is exactly in this position. As a general comment, the growth of the damage, in all the damages scenarios, is clearly observed in all sensor of the structure.

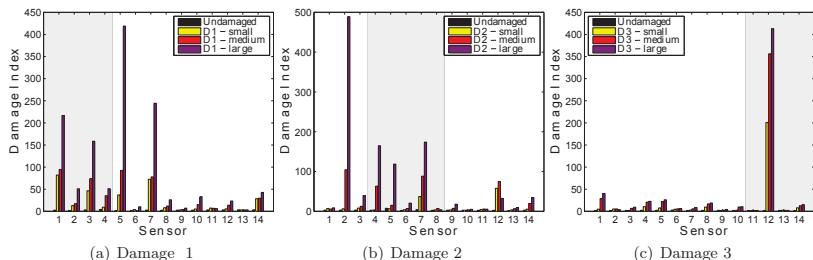


Figure 4. Mahalanobis distance for each damage location and size corresponding to each sensor. The grey region involves the sensors which are closer to the damage.

4. Conclusion

The study presented in this paper is focused of using a multivariate signal processing technique for damage assessment in turbine blades. The experimental lab data on a turbine blade was used to evaluate the effectiveness of the methodology for damage detection and localization. The damage detection is fruitfully achieved for the different damages scenarios. The methodology is also able to monitor the progression of the damage being clearly detected the different sizes introduced during the experimental test procedure. The correlation of the damage index and the location of the sensors along the blade provides a high potential for damage localization. The damages were approximately located in the regions where each damage was performed. Further studies in this direction are extremely recommend due to the successful results obtained. It is also important to pointed out that the test data used in this study is focus on the low frequency damage data. As a conclusion, the methodology clearly present a high potential for on-line damage assessment in wind turbine blades.

Acknowledgments

The experimental part of the project was supported by the EUDP (Danish Energy Technology Development and Demonstration Programme) grant 64011 – 0084 ”Predictive Structure Health

monitoring of Wind Turbines”. The authors also acknowledge Robert Flemming Mikkelsen who provided the blade for the experiments.

References

- [1] Montalvao, Diogo and Maia, Nuno Manuel Mendes and Ribeiro, António Manuel Relógio, 2006. *A review of vibration-based structural health monitoring with special emphasis on composite materials*. The Shock and Vibration Digest, 38(4):295324.
- [2] Zou, Y and Tong, LPSG and Steven, GP, 2000. *Vibration-based model-dependent damage (delamination) identification and health monitoring for composite structuresa review*. Journal of Sound and vibration.
- [3] M. M. Khan, M. T. Iqbal, and F. Khan, 2005. *Reliability and condition monitoring of a wind turbine*. Proceedings of 18th Annual Canadian Conference on Electrical and Computer Engineering.
- [4] Jaishi, Bijaya and Ren, Wei-Xin, 2006. *Damage detection by finite element model updating using modal flexibility residual*. Journal of sound and vibration, 290(1):369-387
- [5] S.D. Fassois and J.S. Sakellariou, 2007. *Time series methods for fault detection and identification in vibrating structures*. The Royal Society Philosophical Transactions: Mathematical, Physical and Engineering Sciences, 365:411448.
- [6] Schölkopf, Bernhard and Smola, Alexander and Müller, Klaus-Robert, 1998. *Nonlinear component analysis as a kernel eigenvalue problem*. Neural computation, 10(5):1299-1319.
- [7] Garcia, David and Trendafilova, Irina, 2014. *A multivariate data analysis approach towards vibration analysis and vibration-based damage assessment: Application for delamination detection in a composite beam*. Journal of Sound and Vibration, 333(25):7036-7050.
- [8] Marin, Luciano and Döhler, Michael and Bernal, Dionisio and Mevel, Laurent, 2014. *Robust statistical damage localization with stochastic load vectors*. Structural Control and Health Monitoring.
- [9] Kopsaftopoulos, FP and Fassois, SD, 2013. *A functional model based statistical time series method for vibration based damage detection, localization, and magnitude estimation*. Mechanical Systems and Signal Processing, 39:143161.
- [10] Baktashmotlagh, Mahsa and Harandi, Mehrtash and Bigdeli, Abbas and Lovell, Brian and Salzmann, Mathieu, 2013. *Non-Linear Stationary Subspace Analysis with Application to Video Classification*. Proceedings of The 30th International Conference on Machine Learning, p.450-458.
- [11] Bottoli F and Pignatti L, 2001 *Design and processing of structural components in biocomposite materials rotor blade for wind turbine cars M.Sc.Thesis Ris DTU*
- [12] Garcia, D and Trendafilova, I, 2014. *Singular Spectrum Analysis for identifying structural nonlinearity using free-decay responses. Application for delamination detection and diagnosis in composite laminates*. 26th International Conference on Noise and Vibration Engineering, Leuven, Belgium.
- [13] Liu, Gang and Mao, Zhu and Todd, Michael and Huang, Zongming, 2014. *Localization of nonlinear damage using state-space-based predictions under stochastic excitation*. Smart Materials and Structures, 23(2):25-26.

Blade Failure Catalogue

Version 2.0

Prepared by: Andrei Buliga

Approved by: Find Møhlholt Jensen

21 August 2014

Contents

Terms and definitions	2
Introduction	4
1 Surface damages; erosion and coating	5
2 Lightning strikes	6
3 Structural cracks	7
3.1 Longitudinal cracks	7
3.2 Transversal cracks	8
3.3 Delamination	9
4 Manufacturing defects	10
4.1 Wrinkles.....	10
4.2 Core material issues	10
4.3 Debonding – Adhesive failure	11
5 Broken blades.....	13
6 Miscellaneous damages	14
6.1 Foreign materials inside the blades.....	14
6.2 Physical impact with foreign objects	15
6.3 Transportation damages.....	15
7 Appendix A: Expanded examples of damages observed in the field.....	16
7.1 Surface damages; erosion and coating.....	16
7.2 Lighting protection	24
7.3 Structural cracks	26
7.4 Longitudinal cracks.....	26
7.5 Transverse cracks.....	30
7.6 Wrinkles.....	36
7.7 Bonding issues.....	36
7.8 Discontinuities on the sandwich, waves, air inclusions.....	37
7.8.1 Miscellaneous	37
8 Appendix B - Guide2Defect Database	39

Together, we make your blade stronger
© Bladena

Bladena
Sct. Hansgade 9^o
DK-4100 Ringsted
www.bladena.com

Page 1 of 40

Terms and definitions

Blade nomenclature:

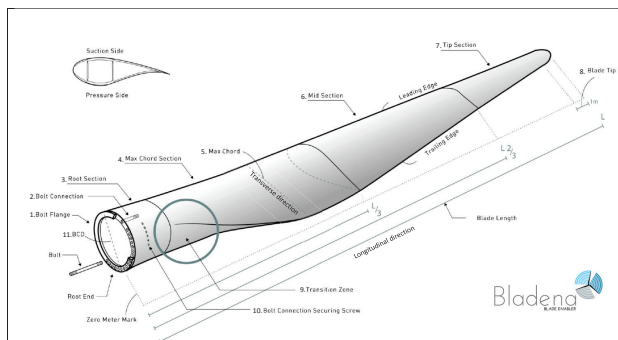


Figure 1: Blade nomenclature

1. Bolt flange
The steel flange placed at the root end towards the hub.
2. Bolt connection
The steel bushing inserting into the root end into the root end in a circular pattern, and used as a threaded connection for the bolts.
3. Root section
The cylindrical section of the blade at the root end towards the Blade tip.
4. Max chord section
The section of the blade between the Root Section and the 1/3 of the total Blade Length.
5. Max chord
The longest distance between the two chord wise extreme points (viz. Leading Edge and Trailing Edge Extreme Point respectively) measured on the chord wise center line along the Blade center line length wise.
6. Mid-section
The section of the blade between Max Chord Section and 2/3 of the blade length.
7. Tip section
The section of the blade between mid-section and Blade Tip.
8. Blade tip
The tip of the blade in the opposite direction of the Root End defined at the last meter of the blade.

Together, we make your blade stronger
© Bladena

Bladena
Sct. Hansgade 9^o
DK-4100 Ringsted
www.bladena.com

Page 2 of 40

9. Transition zone
The flat back at the root zone on blades, where the transition from round to profiled is done by use of third surface.
10. Bolt connection securing screw
Screw along the circumference close to the root end and used to secure the bolt in the bolt connection. Used in the so-called IKEA bolt connection.
11. BCD
Bolt Circle Diameter - the diameter between centers of opposite bolts in the root end.

The term wrinkles refers to the deflections in the orientation of the fibers.

Abbreviations used:

TE	Trailing edge
LE	Leading edge
PS	Pressure side
SS	Suction side

Damages nomenclature:

The blade damages themselves can be prioritized when it comes to the impact they have on the wind turbine blade itself. One suggested categorization can be:

1. Visual damage (cosmetic). When this is seen there is no need for immediate action.
2. Relatively low damage (not serious). Reparation task should be performed during the next planned inspection of the turbine.
3. High risk damage without the need to stop the turbine. This particular damage should be kept under surveillance and repaired as soon as possible to prevent further damage of the turbine. This category has a high risk and it might damage other areas of the blade.
4. Very serious damage. Immediate stop of the turbine is required and damage repaired.

Together, we make your blade stronger
© Bladena

Bladena
Sct. Hansgade 9^o
DK-4100 Ringsted
www.bladena.com

Page 3 of 40

Introduction

The industry is facing a huge challenge regarding operation and maintenance costs on wind turbine generators. One of the main areas of interest is blades, especially for offshore installed turbines.

During blade inspections more and more damages are seen on wind turbine blades in operation. They vary in size, position, and type from site to site and from turbine type to turbine type.

As a part of the EUDP Project Predictive Structural Health Monitoring (PHM) system led by Brüel & Kjær, Bladena has started the process of categorizing blade damages, more specific to divide them in relevant groups. It is of key importance to have a clear understanding of the damages observed on the field and their location on blades. This is the second version of the document showing one way of structuring the observed damages.

The tool used in this process is called Guide2Defect Database. It is an online database that categorizes blade failures. The data can provide relevant statistical insights regarding damage trends based on inspection reports. The tool is flexible and is able to accommodate each user requests. Further information about Guide2Defect Database can be found in Appendix B.

The aim of this document is to create a framework for future discussions and to inform regarding the issues seen on the wind turbine blades in operation. This is relevant because there are differences between what it is seen in the field and what it is seen during full scale test. Furthermore, having a strong foundation for understanding the observed damages, a trend might be established. Even more, data regarding the severity of damages, the location of them on blades, their size, etc. can be used to build relevant statistics that, together with a health monitoring system, can ultimately help to bring down the maintenance cost and downtime and reduce the Cost of Energy (CoE).

The way Bladena together with partners proposes to divide the damages is presented in the following chapters:

- Surface damages, erosion and coating
- Lighting protection
- Structural cracks
- Manufacturing defects
- Broken blades
- Miscellaneous
- Appendix

1 Surface damages; erosion and coating

Erosion is a physical phenomenon specific to materials exposed to elements. For wind turbine blades it is accelerated due to the rotation of blades in operation. Even though the blades are protected against erosion and industry standards coating materials today are high, the blades do get erosion after a certain time. This will expose the laminate to the harsh environmental wind conditions making the blade more vulnerable to elements.

This phenomenon is seen especially towards the tip of the blades where the flow has maximum velocity over the blade surface, see Figure 2a and Figure 2b. There are different options to slow down the erosion, either with the helicopter tape or special painting. This procedure is used in the leading edge area of the blades. However, after a relative short amount of time, this will get degraded as well, see Figure 2a.

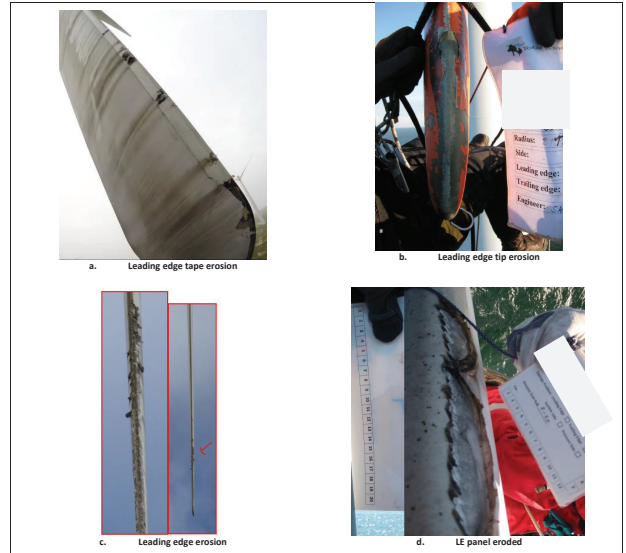


Figure 2: Surface damages due to erosion.

2 Lightning strikes

Wind turbines and wind turbine blades are hit by lightning in their lifetime and sometimes this will cause damages to the blades. The blades have installed a lightning system that will take the lightning energy and transport it to the ground. In most cases this system is formed by a conductor in each blade and lightning receptors, several per blade. Depending on the lightning, the receptors and the area around the receptors is subjected to intense energy.

In most cases the lightning strikes the tip of the blades, see Figure 3a. Even with the installed protection due to the high energy in many cases the blade itself is affected. This can be local, Figure 3b or global, Figure 3c.



Figure 3: Blade damages caused by lightning strikes

3 Structural cracks

This chapter covers the observed damages whose root comes from either the manufacturing process or structural design flaws. The cracks are divided into:

3.1 Longitudinal cracks

When referring to cracks, coating and erosion is not taken into consideration. A crack might appear as a coating failure, however when closely observed, a blade crack will appear in the form of thin lines along the blade shells.

Longitudinal cracks are considered the cracks seen in the longitudinal direction of blades.

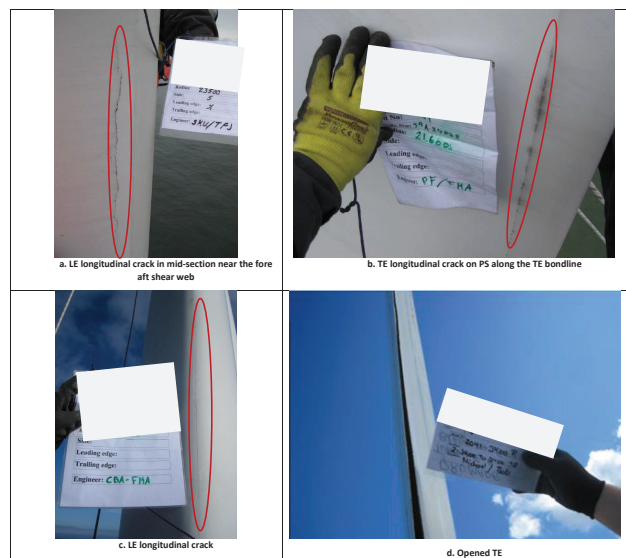


Figure 4: Longitudinal cracks

A very common place where longitudinal cracks are found is in the TE, see figure below.



Figure 5: Longitudinal cracks found in TE

3.2 Transversal cracks

For blades in operation, if a transverse crack of the core material occurs, a 2nd phase of the crack is expected to develop, in the form of a longitudinal crack as seen in Figure 6b and Figure 6d.

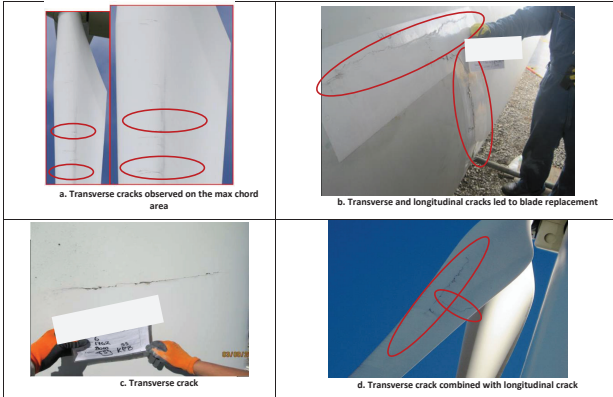


Figure 6: Transverse cracks observed on wind turbine blades in operation

3.3 Delamination

Delamination of composite materials is a failure mechanism that refers to the separation of the composite layers.

The main cause is the weakening of the bonds holding the layers together, often meaning that the adhesive between the glass fibre layers begins to break down. Since this happens inside the composite material, the blade won't necessarily show any signs of wear, making its breakdown unexpected.

However due to the delamination process the blade can show signs of this failure mode in the form cracks observed on the exterior, as it can be seen in Figure 7.



Figure 7: Observed cracks due to delamination

In some cases delamination can lead to the full separation of pressure side and suction side of the trailing edge shells as it can be seen in Figure 8.

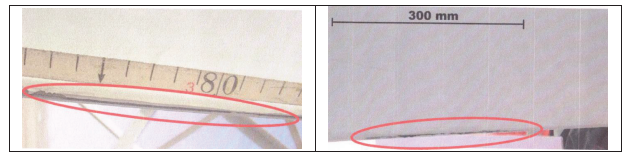


Figure 8: Delamination along the trailing edge of a wind turbine blade

4 Manufacturing defects

4.1 Wrinkles

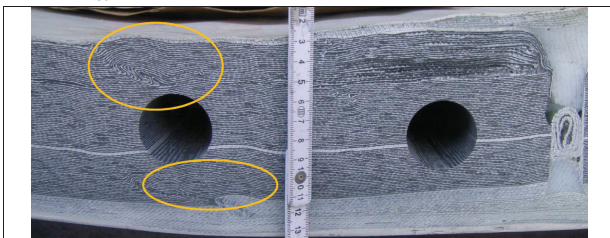


Figure 9: Flange of a 55m blade. Left: wrinkles observed in the laminate



The wrinkles themselves can be categorized by their condition from superficial wrinkles (repairable) defects to irreparable ones.

4.2 Core material issues

It is known that sometimes during the manufacturing process there can be flaws in the making of the sandwich panels. The sandwich material can be made from multiple sheets of core material during this process. In the case where balsa wood is being used it is difficult to make a "perfect" connection of the Balsa plates. Figure 10 shows an example where the core material (balsa wood) has been misplaced after the infusion process.

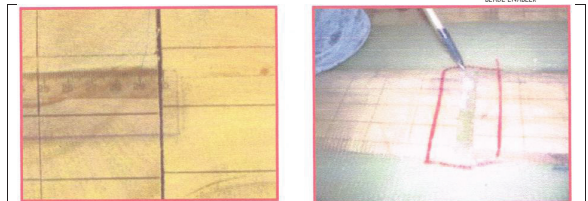


Figure 10: Misplacement of core material after infusion

Furthermore, when the core panels are joined together, an adhesive (resin) is used. The area of the core material where the join process is performed will have a different structural behaviour under operation conditions than the area where "isotropic" core material is considered to be.

During the manufacturing process if the core material (balsa wood in this case) has been dimensioned incorrectly, the core will require additional work, meaning a resizing process using in most cases a utility knife, see Figure 11.



Figure 11: Transversal cut in glass layers that might lead to transversal crack in blades

4.3 Debonding – Adhesive failure

The debonding process refers to the process where blade parts joined together by adhesive materials are separated. Figure 12 shows one of the wind turbine spars being separated from the structure where it was supposed to be bonded to. In this case, this is a major flaw since the spar is the main structural component carrying the loads in the flapwise direction.



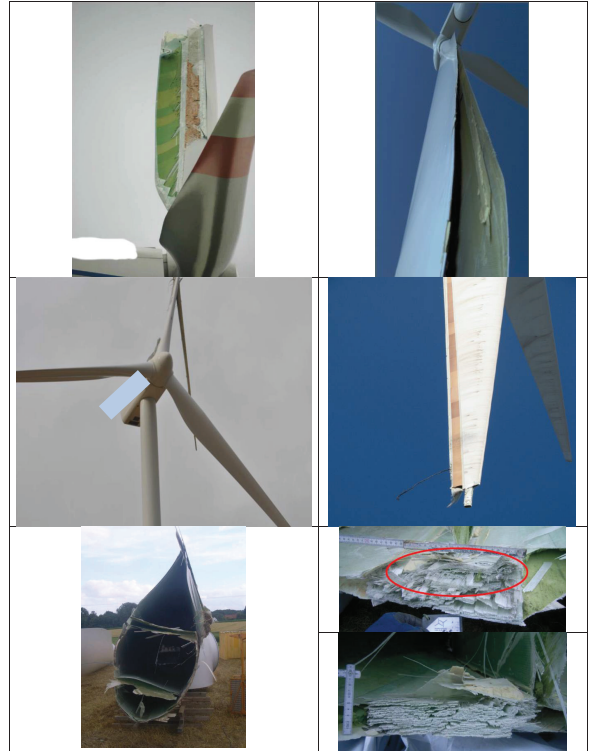
Figure 12: Spar debonding inside the blade

Sometimes during the manufacturing process insufficient bonding paste is used when bonding the different components together. This can lead to catastrophic failure since in many cases the structural carrying system is not "connected" properly with the load introduction part (shells). Figure 13 shows such an example where lack of bonding material is seen between a load carrying box and the aerodynamically shaped shells.



Figure 13: Insufficient bonding material found between the load carrying box and blade shell.

5 Broken blades



6 Miscellaneous damages

6.1 Foreign materials inside the blades



Figure 14: Separated glue rolling inside the blade

In Figure 14 parts of the excess glue got separated. This particular damage has no impact on the blade health. However when the turbine is in operation it makes a curious sound.



Figure 15: Loose blade lid inside the blade

In Figure 15 the blade lid felt into the blade and got stuck. There might be implications on the structural integrity of the blade since the lid acts now as a structural element. Furthermore it may add concentrated force in certain areas these further causing other issues.

6.2 Physical impact with foreign objects

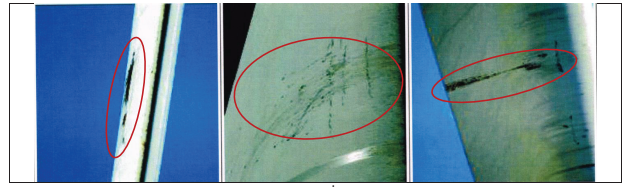


Figure 16: Bird impact: a. Impact produced a large crack in the panels; b. Damaged paint and first layer of the shell fiber; c. Small scratches in the shell

6.3 Transportation damages

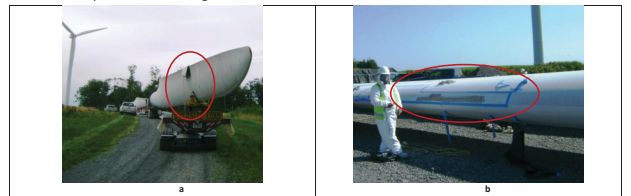
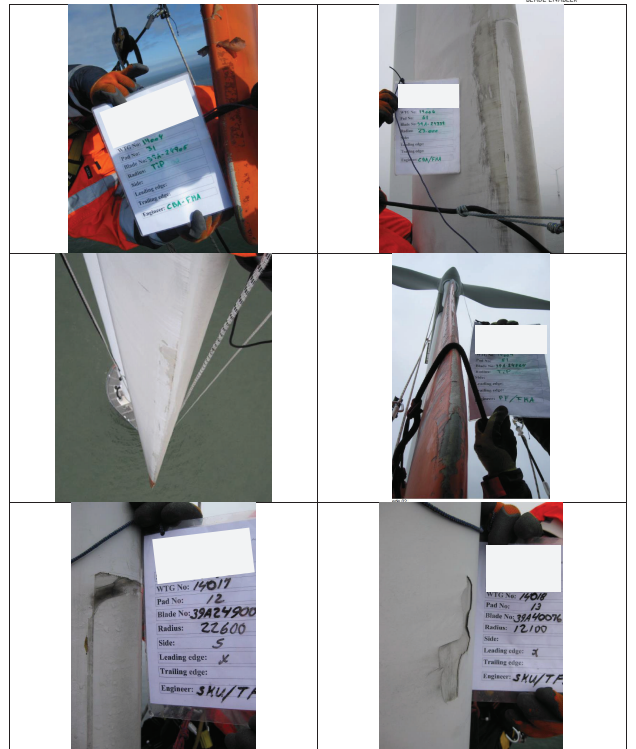
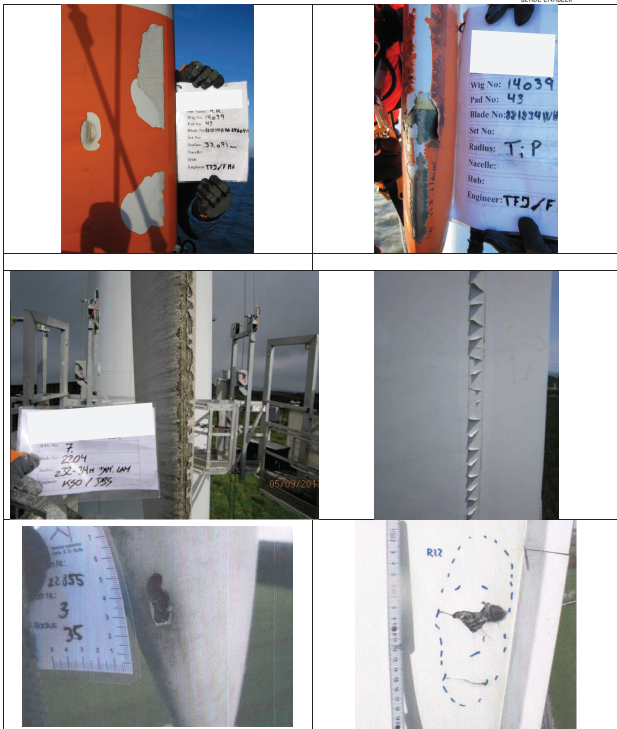
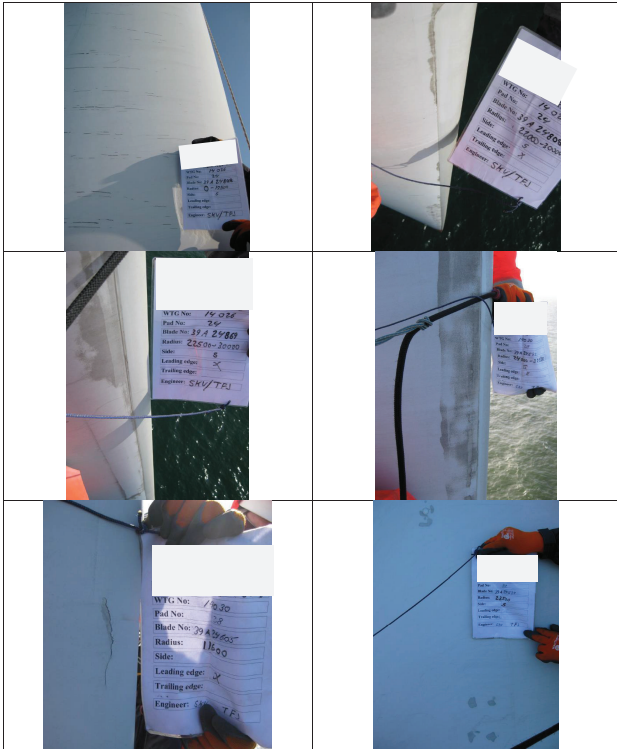


Figure 17: Transportation damages seen on blades: a. Trucking blades to site; b. Typical shipping damage. The area where the blade has been anchored to the truck shows damages.

7 Appendix A: Expanded examples of damages observed in the field

7.1 Surface damages; erosion and coating





7.2 Lighting protection



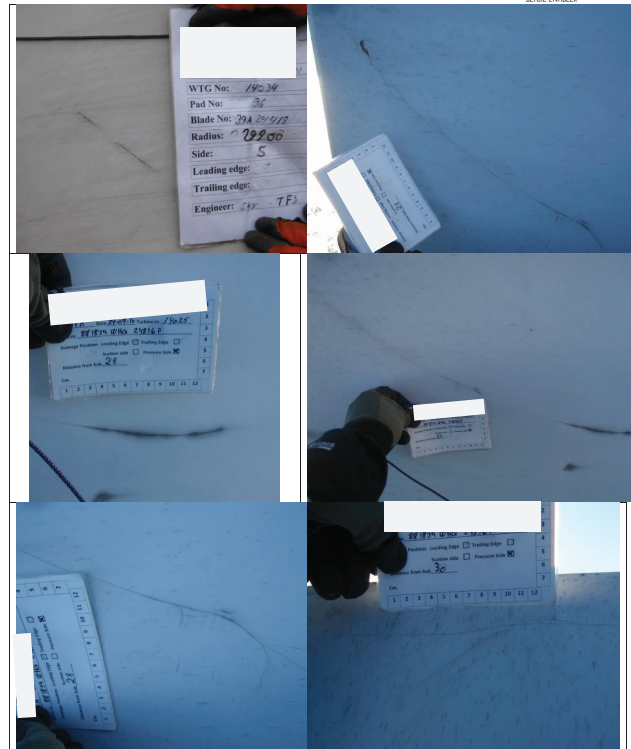
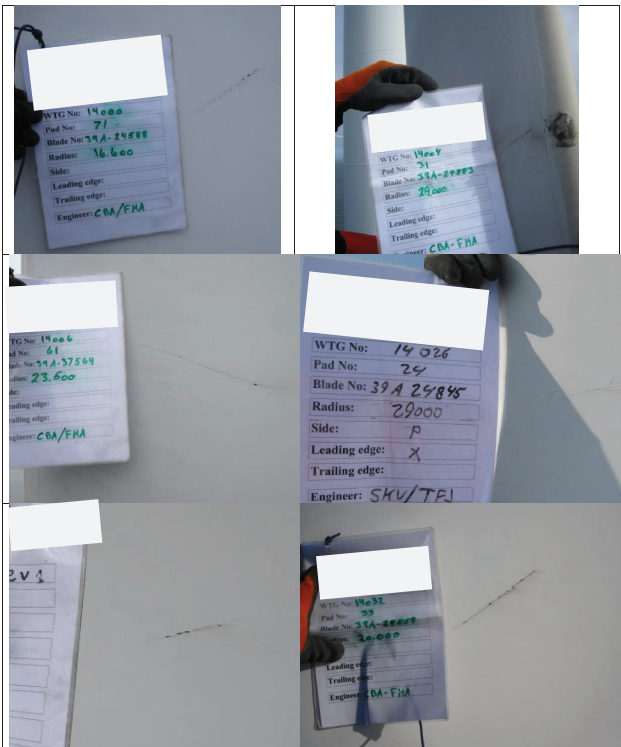
7.3 Structural cracks

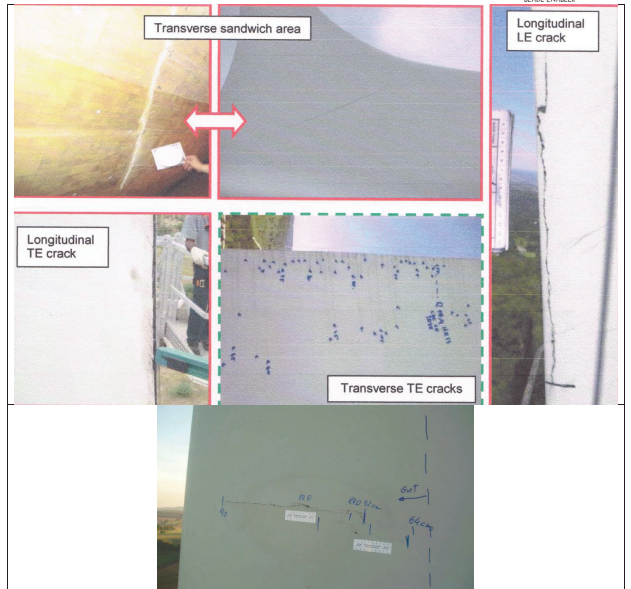
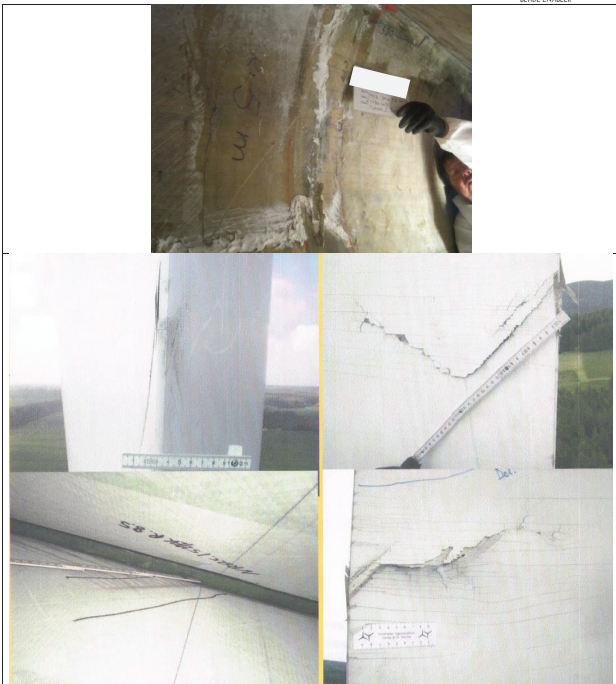
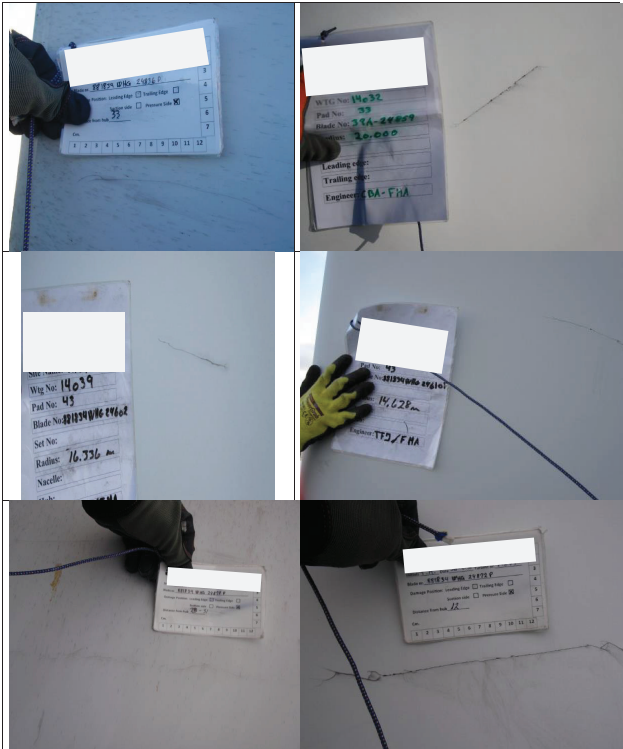
7.4 Longitudinal cracks





7.5 Transverse cracks





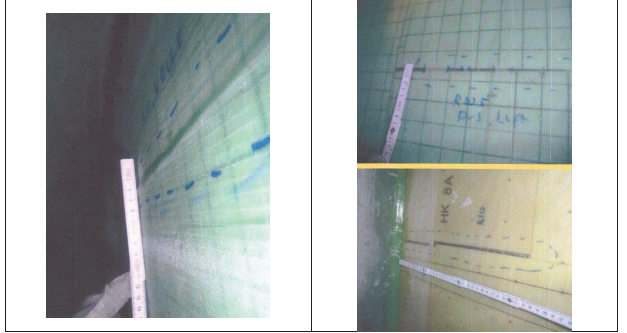
7.6 Wrinkles



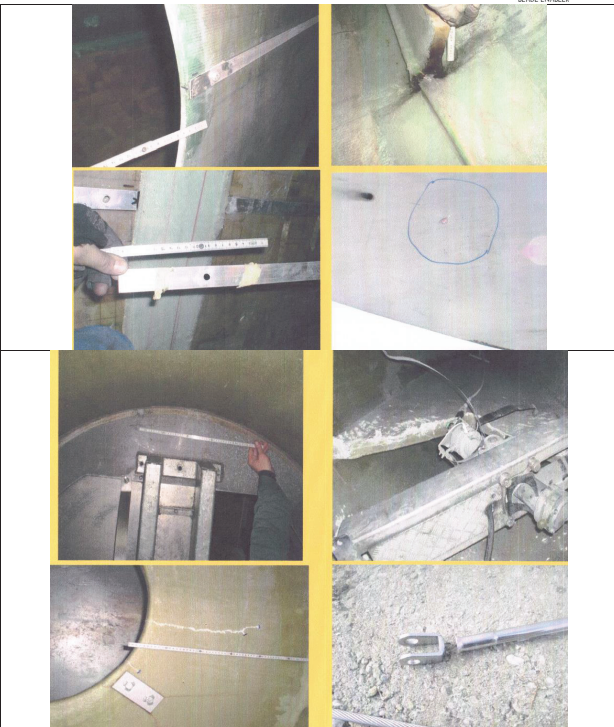
7.7 Bonding issues



7.8 Discontinuities on the sandwich, waves, air inclusions



7.8.1 Miscellaneous



8 Appendix B - Guide2Defect Database

Guide2Defect is a web based application which categorizes and describes identified defects on blades for wind turbine generators. The purpose of the Guide2Defect Database is to:

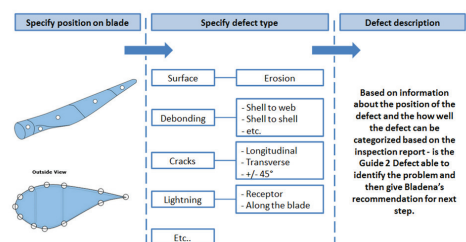
- Provide users with an easy and quick access to a relevant descriptive framework covering the vast majority of observed defects on blades for Wind Turbine Generators, categorize those, evaluate them on a generic level and finally provide an easy to communicate and understandable information sheet on the defect in question.
- Acquire statistical data to support the above and generate relevant analysed data for intelligent planning and design.

The core program has been developed and the functional testing of the program has been completed with success. Next step is build up a data population sized to test the structure and provide some a level of information, which can be evaluated.

Guide2Defect is built as follows:

- Data based driven customized software programmed on a standard platform.
- Web based – available on all relevant platforms: PC, tablet and smart phone.
- Standard dash board for walk-in users.
- Customized dash board with pre-loaded data and reports for subscribers.
- Defect tree leads the user by simple choices to a description of the defect and a detailed descriptive report.
- Uses pre-defined descriptive framework to ensure consistency, but customized frame work can be prepared.
- Access in controlled – registered users only.

The Guide2Defect methodology can be summarized below:



The participating owners will very quickly get an efficient tool based on comprehensive consolidated data to monitor, manage, predict and cost defects on blades; plan future maintenance and inspection regimes and evaluate future suppliers.

Due to the structure of the system, the reliability of the data will grow with the population. With inputs from several owners and our service partners, the owners will get access to a volume of relevant data many times higher than their own installed base.

A screenshot from the web based GUI is presented below.



Algorithms

SIMPLIFY AND PREDICT

blade maintenance



Getting to work offshore to inspect blades has at times required an expensive air transport service. Automated-blade monitoring may eliminate such costly transport.

Dmitri Tcherniak

PhD, Research Engineer / Brüel & Kjær

Jens J. Hansen

Global Key Account Manager

The associated cost of maintaining and repairing blades is an issue for wind-farm operators, and so far no remote inspection method has offered a viable solution. The best answer could lie in sophisticated algorithms using vibration measurement.

Since September 2011, an Energy Technology Development and Demonstration Program (EUDP) project has been underway to develop a practical way to detect, localize, and predict damage to wind-turbine blades. One reason this is important is because reducing the costs associated with wind energy is essential to staying competitive and attracting investors. The industry faces various challenges in this regard, especially as turbines and blades increase in size. Offshore wind farms face even

more challenges which include new materials and designs, and transportation issues due to sheer size.

As the wind industry grows, so has understanding of the stresses and strain turbines endure over prolonged exposure to nature. A wind turbine is made of thousands of components integrated into a finely balanced piece of engineering.



Technicians from Total Wind Blades ApS inspect a turbine blade.

thorough yearly inspection, the operator reduces the risk of a catastrophic failure by addressing issues and taking action before damage becomes a serious problem resulting in costly repairs and lost revenue.

Blade damage is usually due to wear and tear from natural elements, or manufacturing defects and transportation mishaps. Most damage appears in the form of cracks and delamination. Over time, sand, ice, rain, sun and lightning strikes have serious adverse effects on a blade's leading edge and structure. Worse still for offshore installations, salt crystals are a major cause of erosion and cause moisture diffusion within the blade structure. As a result, routine inspections and ongoing maintenance are not simply a luxury—they are a necessity.

Shortcomings of manual inspection

The wind industry is growing fast. Turbines and blades have increased in size and numbers, and as a result, the industry demands greater equipment reliability. Consequently, wind-farm operators and OEMs have been searching for a condition-monitoring system capable of detecting adverse conditions and predicting failures, to help minimize risks and prioritize repairs. Currently, there is no real-time health overview of blade fleets. For many operators, manual inspection continues as the method of choice to determine blade health. However, for many reasons this is not an effective solution. Manual inspection involves a hands-on, visual check of the rotor blades that must be conducted by qualified technicians hanging

Any defect can result in a significant drop in performance leading to costly structural failures, safety issues and system downtime. Even though some parts of a wind turbine are monitored, such as the gearbox and main bearing, there is currently no viable means to check the integrity of the blades beyond expensive manual inspections, typically once a year. OEMs and major industry operators such as DONG Energy, EON and Vattenfall are researching this, but so far ideas to automate the process have been met with limited success. The EUDP initiated a project with Vattenfall, DTU Wind Energy and DTU Compute, Bladerna, Total Wind and Brüel & Kjær to find a solution.

The EUDP partners and the skills and qualifications they provided include:

- Vattenfall, Bladerna and Total Wind: Overall problem formulation, blade expertise, maintenance expertise
- Total Wind: Damage repair
- DTU Wind Energy: Mathematical modeling, and access to a test wind turbine and test facilities
- DTU Compute: Statistical models, decision-making algorithm, and changes in noise and environmental conditions
- Brüel & Kjær: Overall project design and management, measurement equipment, long-term monitoring, damage detection algorithms, and prototype design and implementation

WHAT IS THE EUDP?

The EUDP is a Danish organization that supports the development of energy technologies that create growth, secure supply and let Denmark become independent of fossil fuels. With a budget of roughly €250 million each year, the EUDP has been instrumental in helping Danish businesses create world-leading solutions to aid local and global energy issues. These advances ultimately help worldwide wind-energy industries work together and learn from each other.

Blade maintenance – a necessity, not a luxury

Even though they are intended to last for 20 years, damaged or faulty wind-turbine blades can reduce overall productivity and must be repaired. By carrying out a

from ropes or using special platforms.

In both cases, the methods require well-trained specialists in both blade engineering and rope climbing to spot damage with the naked eye.

This means the inspection process is limited to the surface of the rotor blade or tapping the blade to get an idea of its structural integrity, both of which are widely open to human error. Furthermore, each blade has to be checked individually, which is time consuming, costly and dependent on weather conditions. Unfortunately, damage can always occur soon after an inspection.

What's more, this maintenance can cause an exceptional amount of downtime. During inspections, the wind turbine has to be withdrawn from service and the process can only be performed under certain conditions, such as wind speeds of less than 10 m/s, by industrial climbers in groups of three, due to safety rules. These issues are magnified offshore where wind farms are considerably larger and the use of lifts and platforms is difficult due to the swell of the sea. The marine environment makes working conditions psychologically and physically stressful. Turbines can be up to 20 km

from land, so the timeframe for working on location is limited, and most workers must be transported by boat or helicopter.

Taking up the automation challenge

As a result, a variety of automated methods and technologies, such as structural health monitoring (SHM), have been tried and tested in an attempt to find a better approach. SHM is a relatively new field and there are only a few projects running in other industries, such as monitoring bridges and buildings in seismic areas. A few SHM techniques have been adapted for wind turbines with

limited success, including strain gauges, acoustics, lasers and thermography.

Working together, the teams behind the EUDP project developed a novel approach to the blade inspection issue. This led to a potentially effective SHM solution for wind-turbine blades that also has considerable potential beyond the wind industry. The approach is based on the premise that any structural change to the wind-turbine blade, such as damage, will cause a vibration pattern that deviates from normal. This results in unusual

was developed with greater sensitivity. In this new method, mechanical energy is introduced into the blade by means of an electro-mechanical actuator and the resulting vibrations are measured using accelerometers placed along the blade. This technique proved so effective it allows detecting a crack or delamination as small as 20-cm long on a 34-m blade, even in the presence of environmental noise. Algorithms form the heart of the new method. To distinguish between actual damage and merely the effects of

environmental noise, these algorithms are based on statistics collected from hundreds of careful measurements taken when the blade was in an undamaged state, during as many different weather and operating conditions as possible, a process known as model training.

will provide the owner or operator with the unique ability to get a daily updated overview of the health of its asset, and constantly assess which blades need maintenance and when. This results in the ability to optimize a scheduled-maintenance program that decreases the cost of energy because:

- In-time inspections and repair happen before a problem worsens.
- The ability to optimize schedules in both peak and off-peak seasons.
- Technicians arrive ready to inspect blades with identified problems.
- Crane and vessels are mobilized and ready for multiple inspections and so on.
- The company database receives a report, documentation and complete maintenance record, which improves the knowledge and understanding of the fleet health.
- A daily detailed assessment view provides insight and ability to react to changes in health before damage compounds and becomes catastrophic.



The 34 m wind turbine blade (top) is in the test facility at DTU's Wind Energy department's test facilities at Roskilde. A triaxial accelerometer (bottom) is mounted on the leading edge of a blade.



Working toward an intelligent, accurate solution

This method points the way to a future solution that will let vibration data be gathered, pre-processed and

vibrations that can be detected and measured by sensors on the blade. Any deviation from the norm would suggest that damage has indeed occurred.

Initially, operational modal analysis appeared an excellent tool for measuring these changes. However, tests showed that the process was not sensitive enough to detect and identify where the damage had occurred, so an alternative method

transmitted wirelessly to the cloud, which allows for quick data transfer, storage and processing. Based on advanced algorithms, several levels of analysis take place in the cloud, and when damage is detected, a report is issued to the wind-farm operator via a Web-based interface that details which turbine blade is affected and to what extent.

To optimize inspections and maintenance schedules, blade-health

INSIDE THE ALGORITHM

The algorithm that determines whether or not the blade is damaged compares the current vibration pattern against those of an undamaged blade. If the results are the same, all is well and we can be sure that the blade is fine. In contrast, if the measured states differ, we can suspect that damage has occurred and the blade is in need of closer inspection and repair.

women of wind of ENERGY



TO OUR MEMBERS,
VOLUNTEERS AND
CORPORATE SPONSORS

THANK YOU!

Our 2014 successes were made possible by you!



WoWE 2014 Rudd Mayer Fellows (L-R): Michelle Montague (WoWE Board), Kalie Brunton, Tanzila Ahmed, Alie Brown, Kaitlyn Bunker, Melissa Showers, Huiyi Zhang, Kristen Graf (WoWE Staff)



Spring 2014 WoWE Board Meeting (Back Row L-R): Trudy Forsyth, Karen Conover, Jan Blomstrann, Michelle Montague, Jennifer and Julia Daiger (Front Row L-R): Kristen Graf, Lisa Daniels, Suzanne Tegen

Your company can be part of this great effort!
Email giving@womenofwindenergy.org for more information

Thank you to our lead sponsors!



A step further

Typically, damages are categorized according to industry guidelines which determine the necessary follow-up. For example, in one category repairs must be immediate, while in another, repairs are ok within a three or six-month period. For the operator to categorize the detected damage and make a decision regarding follow up, he must know where on the blade the damage is located, and if it is progressing or stabilized. In effect, the new method constantly monitors the overall health of the blades and alerts the operator when a fault occurs, letting them prioritize repairs and schedule maintenance before it becomes a serious problem.

Currently, the algorithm provides a general damage location. The next stage of the project is to develop more advanced localization algorithms that can deduce exactly where the damage has occurred, even in its inner substructure. When done, this will help to give a more detailed overview of the blade's health and let operators develop a repair and maintenance strategy in a cost-efficient way.

Healthy blades, happy operators

The outcome of the project represents a step forward for the industry and offers an invaluable new technique that will help operators maintain wind turbines at far lower costs and with improved reliability and efficiency. The solution fits all the criteria for an ideal SHM system, which is able to detect, locate and immediately alert the owner of damages in the blades. The system can be incorporated in new blades or retrofitted into existing ones.

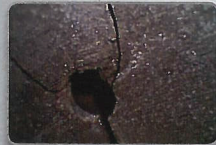
At this stage the project has produced a working prototype that is currently being tested on a real turbine. Further testing and development is required with an OEM or owner to make the working prototype into a commercial application. 

Hawkeye® V2 Videoscope

Fast, Reliable, Affordable, Visual Inspection



90° Prism & Close-Focus tips available!



Using the Close-Focus tip, fine cracks are detected inside a combustion chamber.

- Sharp, Clear Photos & Video
- Large 5-inch LCD Monitor
- Easy-to-Use Controls
- Annotation Feature
- Rugged Tungsten Sheath
- Quality Construction
- Precise 4-Way Articulation
- Starting at only \$8,995

In stock, ready for overnight delivery!

Hawkeye® V2 Video Borescopes are fully portable, finely constructed, and deliver clear, bright high resolution photos and video! The 5" LCD monitor allows comfortable viewing, and intuitive, easy-to-use controls provide photo and video capture at the touch of a button! V2's have a wide, 4-way articulation range, and are small, lightweight, and priced starting at only \$8995. V2's are available in both 4 and 6 mm diameters. Optional 90° Prism or Close-Focus adapter tips.

Made in USA


VIDEO BORESCOPES
gradientlens.com/V2

Gradient Lens Corporation*

800.536.0790

TRY
BEFORE
YOU BUY!

